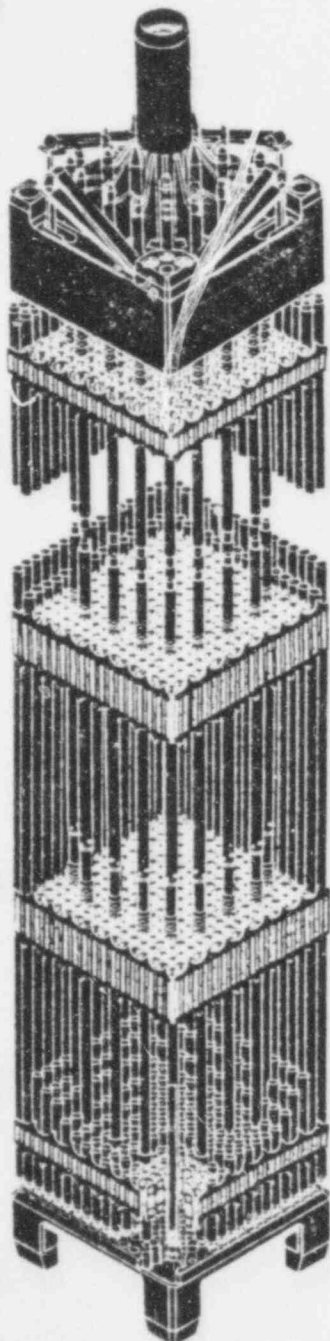


# REFERENCE CORE REPORT

## 17x17

### OPTIMIZED FUEL ASSEMBLY

### VOLUME 1



**Westinghouse  
Nuclear  
Energy  
Systems**

008010471

612-003

612 004

## FOREWORD

This Topical Report (WCAP-9500) serves as a reference core design report for those Westinghouse Pressurized Water Reactors which employ a new fuel assembly design herein referred to as the Optimized Fuel Assembly (OFA) design.

The Optimized Fuel Assembly design presented here consists of a 17x17 array of fuel rods having a reduced diameter relative to the presently licensed 17x17 design. It also employs the use of Zircaloy spacer grids in all positions except the top and bottom grids, which will continue to be of Inconel. These design changes result in an improved water-to-uranium ratio and reduced parasitic neutron absorption, which aid in neutron economy and allow for more efficient use of the fuel. The 17x17 OFA design will be generally available for use in all three and four loop plants, including those now under construction.

This report presents the information contained in Chapters 4, 15, and 16 of a typical Safety Analysis Report, and is in conformance with the requirements of Regulatory Guide 1.70 "Standard Format and Content of Safety Analysis Reports for Nuclear Power Plants," November 1978, Revision 3. Places in the text where references are given to sections other than 4, 15, or 16 (e.g., Chapter 5) are for use when plant specifics have been included in the form of other chapters of a particular SAR. The design improvements of the OFA will also be used in reload regions. Therefore, a description of the methodology to be applied to analyze cores containing combinations of fuel assemblies of standard and OFA design has been included in a section designated as "Chapter 18". The methodology described applies not only to 3 and 4 loop 17x17 plants but generically for plants having other standard arrays (e.g. 14x14, 15x15 and 16x16). In these cases the two significant design features of OFA may be applied together as with 17x17 or independently based upon the economics involved.

In the preparation of this report, two types of four loop Westinghouse plants were studied and are documented to enhance the applicability of this document in future licensing efforts.

Plant A - is a typical four loop, 12 foot core with non Upper Head Injection (UHI) Emergency Core Cooling System (ECCS) and incorporating the Integrated Control and Protection System (IPS). This plant representation appears on white paper in the text.

Plant B - is a typical four loop, 12 foot core incorporating a conventional control and protection system with a UHI, ECCS. Those white pages of the text affected by the Specific Plant B features are to be superceded by a corresponding blue page.

While other plant types are not documented herein (e.g. three loop) the mechanical design is applicable to all 17x17 12 foot core Westinghouse PWR's. Appropriate nuclear, thermal-hydraulic, and safety analysis information will be provided as part of plant specific applications.

Duplicate text and figures are provided where appropriate to facilitate separation of Plant A and B material. Chapter 4 has interspersed white and blue pages, while Chapters 15 & 16 have two complete chapters each; one white, one blue.

The major differences in Plant A and B are the IPS vs conventional control and protection system, and UHI vs Non-UHI (for ECCS analysis). It is instructive to note that the IPS does not impact on the ECCS analysis, and vice versa. For example it is possible to use this document for a UHI plant with the IPS. The new document would consist of white pages, except for Section 15.6.5 which would require blue pages. (Some minor modification to Chapter 16, "Technical Specifications" may be required, but it would be largely a question of plant specific information).

Two topical reports are to be used to aid in the regulatory review process for applications containing optimized fuel:

1. A previously submitted topical, WCAP-9401 (Proprietary), (also represented by a Non-Proprietary version, WCAP-9402) "Verification Testing and Analyses of the 17x17 Optimized Fuel Assembly", documents the results of the tests and analyses performed by Westinghouse to verify design adequacy of the new 17x17 OFA. (Note: The structural analysis of fuel grids in WCAP-9401 demonstrates that LOCA and seismic loads do not require combination to insure adequate design margin)
2. This topical report (WCAP-9500) which describes the design and evaluation of steady state reactor performance, reactor transients, and accidents for new and reload cores.

The Topical Reports therefore provide a licensing basis for evaluating the Optimized Fuel Assembly on its own merits as well as its application to new and reload cores. Once approved they will serve as the basis for applications and amendments incorporating the OFA design features.

612 007

612 003

CHAPTER 4.0 - REACTOR

TABLE OF CONTENTS

|           |  | <u>PAGE</u> |
|-----------|--|-------------|
| 4.0       | <u>REACTOR</u>   | 4.1-1       |
| 4.1       | <u>SUMMARY DESCRIPTION</u>                             | 4.1-1       |
| 4.1.1     | REFERENCES   | 4.1-4       |
| 4.2       | <u>FUEL SYSTEM DESIGN</u>                              | 4.2-1       |
| 4.2.1     | DESIGN BASES   | 4.2-2       |
| 4.2.1.1   | Cladding   | 4.2-2       |
| 4.2.1.2   | Fuel Material  | 4.2-3       |
| 4.2.1.3   | Fuel Rod Performance                                   | 4.2-4       |
| 4.2.1.4   | Spacer Grids   | 4.2-5       |
| 4.2.1.5   | Fuel Assembly  | 4.2-6       |
| 4.2.1.6   | Core Components  | 4.2-8       |
| 4.2.1.7   | Testing, Irradiation Demonstration<br>and Surveillance | 4.2-11      |
| 4.2.2     | DESIGN DESCRIPTION                                     | 4.2-12      |
| 4.2.2.1   | Fuel Rods  | 4.2-13      |
| 4.2.2.2   | Fuel Assembly Structure                                | 4.2-14      |
| 4.2.2.2.1 | Bottom Nozzle  | 4.2-14      |
| 4.2.2.2.2 | Top Nozzle   | 4.2-14      |
| 4.2.2.2.3 | Guide and Instrument Thimbles                          | 4.2-15      |
| 4.2.2.2.4 | Grid Assemblies  | 4.2-17      |
| 4.2.2.3   | Core Components  | 4.2-17      |
| 4.2.2.3.1 | Rod Cluster Control Assembly                           | 4.2-17      |
| 4.2.2.3.2 | Burnable Poison Assembly                               | 4.2-19      |
| 4.2.2.3.3 | Neutron Source Assembly                                | 4.2-20      |
| 4.2.2.3.4 | Thimble Plug Assembly                                  | 4.2-21      |

TABLE OF CONTENTS (Cont'd)

|         | <u>PAGE</u>   |        |
|---------|---|--------|
| 4.2.3   | DESIGN EVALUATION   | 4.2-22 |
| 4.2.3.1 | Cladding  | 4.2-22 |
| 4.2.3.2 | Fuel Materials Consideration                              | 4.2-28 |
| 4.2.3.3 | Fuel Rod Performance                                      | 4.2-29 |
| 4.2.3.4 | Spacer Grids  | 4.2-36 |
| 4.2.3.5 | Fuel Assembly   | 4.2-37 |
| 4.2.3.6 | Reactivity Control Assembly and Burnable<br>Poison Rods   | 4.2-38 |
| 4.2.4   | TESTING AND INSPECTION PLAN                               | 4.2-41 |
| 4.2.4.1 | Quality Assurance Program                                 | 4.2-41 |
| 4.2.4.2 | Quality Control   | 4.2-41 |
| 4.2.4.3 | Core Component Testing and Inspection                     | 4.2-45 |
| 4.2.4.4 | Tests and Inspections by Others                           | 4.2-47 |
| 4.2.4.5 | Onsite Inspection   | 4.2-47 |
| 4.2.5   | REFERENCES  | 4.2-47 |
| 4.3     | <u>NUCLEAR DESIGN</u>                                     | 4.3-1  |
| 4.3.1   | DESIGN BASES  | 4.3-1  |
| 4.3.1.1 | Fuel Burnup   | 4.3-2  |
| 4.3.1.2 | Negative Reactivity Feedbacks (Reactivity<br>Coefficient) | 4.3-3  |
| 4.3.1.3 | Control of Power Distribution                             | 4.3-4  |
| 4.3.1.4 | Maximum Controlled Reactivity Insertion Rate              | 4.3-5  |
| 4.3.1.5 | Shutdown Margins  | 4.3-6  |
| 4.3.1.6 | Stability   | 4.3-8  |
| 4.3.1.7 | Anticipated Transients Without Trip                       | 4.3-9  |
| 4.3.2   | DESCRIPTION   | 4.3-9  |
| 4.3.2.1 | Nuclear Design Description                                | 4.3-9  |



TABLE OF CONTENTS (Cont'd)

|  | <u>PAGE</u> |
|--|-------------|
| 4.3.2.2 Power Distributions  | 4.3-12      |
| 4.3.2.2.1 Definitions  | 4.3-12      |
| 4.3.2.2.2 Radial Power Distributions   | 4.3-15      |
| 4.3.2.2.3 Assembly Power Distributions   | 4.3-16      |
| 4.3.2.2.4 Axial Power Distributions  | 4.3-16      |
| 4.3.2.2.5 Local Power Peaking  | 4.3-18      |
| 4.3.2.2.6 Limiting Power Distributions   | 4.3-19      |
| 4.3.2.2.7 Experimental Verification of Power<br>Distribution Analysis          | 4.3-28      |
| 4.3.2.2.8 Testing  | 4.3-30      |
| 4.3.2.2.9 Monitoring Instrumentation   | 4.3-30      |
| 4.3.2.3 Reactivity Coefficients  | 4.3-31      |
| 4.3.2.3.1 Fuel Temperature (Doppler) Coefficient                               | 4.3-32      |
| 4.3.2.3.2 Moderator Coefficients   | 4.3-33      |
| 4.3.2.3.3 Power Coefficients   | 4.3-35      |
| 4.3.2.3.4 Comparison of Calculated and Experimental<br>Reactivity Coefficients | 4.3-36      |
| 4.3.2.3.5 Reactivity Coefficients Used in Transient<br>Analysis                | 4.3-36      |
| 4.3.2.4 Control Requirements   | 4.3-37      |
| 4.3.2.4.1 Doppler  | 4.3-38      |
| 4.3.2.4.2 Variable Average Moderator Temperature                               | 4.3-38      |
| 4.3.2.4.3 Redistribution   | 4.3-38      |
| 4.3.2.4.4 Void Content   | 4.3-39      |
| 4.3.2.4.5 Rod Insertion Allowance  | 4.3-39      |
| 4.3.2.4.6 Burnup   | 4.3-39      |
| 4.3.2.4.7 Xenon and Samarium Poisoning   | 4.3-40      |
| 4.3.2.4.8 pH Effects   | 4.3-40      |
| 4.3.2.4.9 Experimental Confirmation  | 4.3-40      |
| 4.3.2.4.10 Control   | 4.3-40      |
| 4.3.2.4.11 Chemical Poisoning  | 4.3-41      |

TABLE OF CONTENTS (Cont'd)

|   | <u>PAGE</u> |
|---|-------------|
| 4.3.2.4.12 Rod Cluster Control Assemblies   | 4.3-41      |
| 4.3.2.4.13 Reactor Coolant Temperature  | 4.3-42      |
| 4.3.2.4.14 Burnable Poison Rods   | 4.3-43      |
| 4.3.2.4.15 Peak Xenon Startup   | 4.3-44      |
| 4.3.2.4.16 Load Follow Control and Xenon Control  | 4.3-44      |
| 4.3.2.4.17 Burnup   | 4.3-44      |
| 4.3.2.5 Control Rod Patterns and Reactivity Worth   | 4.3-45      |
| 4.3.2.6 Criticality of the Reactor During Refueling<br>and Criticality of Fuel Assemblies | 4.3-47      |
| 4.3.2.7 Stability   | 4.3-50      |
| 4.3.2.7.1 Introduction  | 4.3-50      |
| 4.3.2.7.2 Stability Index   | 4.3-51      |
| 4.3.2.7.3 Prediction of the Core Stability  | 4.3-51      |
| 4.3.2.7.4 Stability Measurements  | 4.3-52      |
| 4.3.2.7.5 Comparison of Calculations with Measurement                                     | 4.3-54      |
| 4.3.2.7.6 Stability Control and Protection  | 4.3-55      |
| 4.3.2.8 Vessel Irradiation  | 4.3-56      |
| 4.3.3 ANALYTICAL METHODS  | 4.3-57      |
| 4.3.3.1 Fuel Temperature (Doppler) Calculations   | 4.3-58      |
| 4.3.3.2 Macroscopic Group Constants   | 4.3-59      |
| 4.3.3.3 Spatial Few-Group Diffusion Calculations  | 4.3-61      |
| 4.3.4 CHANGES   | 4.3-62      |
| 4.3.5 REFERENCES  | 4.3-63      |
| <br>  |             |
| 4.4 <u>THERMAL AND HYDRAULIC DESIGN</u>   | 4.4-1       |
| <br>  |             |
| 4.4.1 DESIGN BASES  | 4.4-1       |
| 4.4.1.1 Departure from Nucleate Boiling Design Basis                                      | 4.4-1       |
| 4.4.1.2 Fuel Temperature Design Basis   | 4.4-3       |
| 4.4.1.3 Core Flow Design Basis  | 4.4-4       |

TABLE OF CONTENTS (Cont'd)

|  | <u>PAGE</u> |
|--|-------------|
| 4.3.2.2 Power Distribution   | 4.3-12      |
| 4.3.2.2.1 Definitions  | 4.3-12      |
| 4.3.2.2.2 Radial Power Distributions   | 4.3-15      |
| 4.3.2.2.3 Assembly Power Distributions   | 4.3-16      |
| 4.3.2.2.4 Axial Power Distributions  | 4.3-16      |
| 4.3.2.2.5 Local Power Peaking  | 4.3-18      |
| 4.3.2.2.6 Limiting Power Distributions   | 4.3-19      |
| 4.3.2.2.7 Experimental Verification of Power<br>Distribution Analysis          | 4.3-27      |
| 4.3.2.2.8 Testing  | 4.3-30      |
| 4.3.2.2.9 Monitoring Instrumentation   | 4.3-30      |
| 4.3.2.3 Reactivity Coefficients  | 4.3-31      |
| 4.3.2.3.1 Fuel Temperature (Doppler) Coefficient                               | 4.3-32      |
| 4.3.2.3.2 Moderator Coefficients   | 4.3-33      |
| 4.3.2.3.3 Power Coefficient  | 4.3-35      |
| 4.3.2.3.4 Comparison of Calculated and Experimental<br>Reactivity Coefficients | 4.3-36      |
| 4.3.2.3.5 Reactivity Coefficients Used in Transient<br>Analysis                | 4.3-36      |
| 4.3.2.4 Control Requirements   | 4.3-37      |
| 4.3.2.4.1 Doppler  | 4.3-38      |
| 4.3.2.4.2 Variable Average Moderator Temperature                               | 4.3-38      |
| 4.3.2.4.3 Redistribution   | 4.3-38      |
| 4.3.2.4.4 Void Content   | 4.3-39      |
| 4.3.2.4.5 Rod Insertion Allowance  | 4.3-39      |
| 4.3.2.4.6 Burnup   | 4.3-39      |
| 4.3.2.4.7 Xenon and Samarium Poisoning   | 4.3-40      |
| 4.3.2.4.8 pH Effects   | 4.3-40      |
| 4.3.2.4.9 Experimental Confirmation  | 4.3-40      |
| 4.3.2.4.10 Control   | 4.3-40      |
| 4.3.2.4.11 Chemical Poisoning  | 4.3-41      |

TABLE OF CONTENTS (Cont'd)

|           | <u>PAGE</u>   |        |
|-----------|---|--------|
| 4.4.1.4   | Hydrodynamic Scability Design Basis   | 4.4-5  |
| 4.4.1.5   | Other Considerations  | 4.4-5  |
| 4.4.2     | DESCRIPTION   | 4.4-5  |
| 4.4.2.1   | Summary Comparison  | 4.4-5  |
| 4.4.2.2   | Critical Heat Flux Ratio or Departure<br>from Nucleate Boiling Ratio and Mixing<br>Technology | 4.4-7  |
| 4.4.2.2.1 | Departure from Nucleate Boiling Technology  | 4.4-7  |
| 4.4.2.2.2 | Definition of Departure from Nucleate<br>Boiling Ratio  | 4.4-8  |
| 4.4.2.2.3 | Mixing Technology   | 4.4-9  |
| 4.4.2.2.4 | Hot Channel Factors   | 4.4-11 |
| 4.4.2.3   | Linear Heat Generation Rate   | 4.4-13 |
| 4.4.2.4   | Void Fraction Distribution  | 4.4-13 |
| 4.4.2.5   | Core Coolant Flow Distribution  | 4.4-13 |
| 4.4.2.5   | Core Pressure Drops and Hydraulic Loads   | 4.4-13 |
| 4.4.2.6.1 | Core Pressure Drops   | 4.4-13 |
| 4.4.2.6.2 | Hydraulic Loads   | 4.4-14 |
| 4.4.2.7   | Correlation and Physical Data   | 4.4-15 |
| 4.4.2.7.1 | Surface Heat Transfer Coefficient   | 4.4-15 |
| 4.4.2.7.2 | Total Core and Vessel Pressure Drop   | 4.4-16 |
| 4.4.2.7.3 | Void Fraction Correlation   | 4.4-18 |
| 4.4.2.8   | Thermal Effects of Operational Transients   | 4.4-18 |
| 4.4.2.9   | Uncertainties in Estimates  | 4.4-19 |
| 4.4.2.9.1 | Uncertainties in Fuel and Cladding Temperatures   | 4.4-19 |
| 4.4.2.9.2 | Uncertainties in Pressure Drops   | 4.4-20 |
| 4.4.2.9.3 | Uncertainties Due to Inlet Flow Maldistribution   | 4.4-20 |
| 4.4.2.9.4 | Uncertainty in DNB Correlation  | 4.4-20 |
| 4.4.2.9.5 | Uncertainties in DNBR Calculations  | 4.4-20 |
| 4.4.2.9.6 | Uncertainties in Flow Rates   | 4.4-21 |
| 4.4.2.9.7 | Uncertainties in Hydraulic Loads  | 4.4-22 |

TABLE OF CONTENTS (Cont'd)

|            | <u>PAGE</u>  |        |
|------------|--|--------|
| 4.4.2.9.8  | Uncertainty in Mixing Coefficient  | 4.4-22 |
| 4.4.2.10   | Flux Tilt Considerations   | 4.4-23 |
| 4.4.2.11   | Fuel and Cladding Temperature  | 4.4-24 |
| 4.4.2.11.1 | UO <sub>2</sub> Thermal Conductivity   | 4.4-25 |
| 4.4.2.11.2 | Radial Power Distribution in UO <sub>2</sub> Fuel Rods                           | 4.4-26 |
| 4.4.2.11.3 | Gap Conductance  | 4.4-26 |
| 4.4.2.11.4 | Surface Heat Transfer Coefficients   | 4.4-27 |
| 4.4.2.11.5 | Fuel Cladding Temperature  | 4.4-28 |
| 4.4.2.11.6 | Treatment of Peaking Factors   | 4.4-28 |
| 4.4.3      | DESCRIPTION OF THE THERMAL AND HYDRAULIC<br>DESIGN OF THE REACTOR COOLANT SYSTEM | 4.4-29 |
| 4.4.3.1    | Plant Configuration Data   | 4.4-29 |
| 4.4.3.2    | Operating Restrictions on Pumps  | 4.4-30 |
| 4.4.3.3    | Power-Flow Operating Map (BWR)   | 4.4-30 |
| 4.4.3.4    | Temperature-Power Operating Map  | 4.4-30 |
| 4.4.3.5    | Load Following Characteristics   | 4.4-30 |
| 4.4.3.6    | Thermal and Hydraulic Characteristics<br>Summary Table                           | 4.4-31 |
| 4.4.4      | EVALUATION   | 4.4-31 |
| 4.4.4.1    | Critical Heat Flux   | 4.4-31 |
| 4.4.4.2    | Core Hydraulics  | 4.4-31 |
| 4.4.4.2.1  | Flow Paths Considered in Core Pressure Drop<br>and Thermal Design                | 4.4-31 |
| 4.4.4.2.2  | Inlet Flow Distributions   | 4.4-32 |
| 4.4.4.2.3  | Empirical Friction Factor Correlations   | 4.4-33 |
| 4.4.4.3    | Influence of Power Distribution  | 4.4-34 |
| 4.4.4.3.1  | Nuclear Enthalpy Rise Hot Channel<br>Factor $F_{\Delta H}^N$                     | 4.4-34 |
| 4.4.4.3.2  | Axial Heat Flux Distributions  | 4.4-36 |
| 4.4.4.4    | Core Thermal Response  | 4.4-37 |
| 4.4.4.5    | Analytical Techniques  | 4.4-38 |

TABLE OF CONTENTS (Cont'd)

|            | <u>PAGE</u>  |        |
|------------|--|--------|
| 4.4.2.9.8  | Uncertainty in Mixing Coefficient  | 4.4-22 |
| 4.4.2.10   | Flux Tilt Considerations   | 4.4-23 |
| 4.4.2.11   | Fuel and Cladding Temperature  | 4.4-24 |
| 4.4.2.11.1 | UO <sub>2</sub> Thermal Conductivity   | 4.4-25 |
| 4.4.2.11.2 | Radial Power Distribution in UO <sub>2</sub> Fuel Rods                           | 4.4-26 |
| 4.4.2.11.3 | Gap Conductance  | 4.4-26 |
| 4.4.2.11.4 | Surface Heat Transfer Coefficients   | 4.4-27 |
| 4.4.2.11.5 | Fuel Cladding Temperature  | 4.4-28 |
| 4.4.2.11.6 | Treatment of Peaking Factors   | 4.4-28 |
| 4.4.3      | DESCRIPTION OF THE THERMAL AND HYDRAULIC<br>DESIGN OF THE REACTOR COOLANT SYSTEM | 4.4-29 |
| 4.4.3.1    | Plant Configuration Data   | 4.4-29 |
| 4.4.3.2    | Operating Restrictions on Pumps  | 4.4-30 |
| 4.4.3.3    | Power-Flow Operating Map (BWR)   | 4.4-30 |
| 4.4.3.4    | Temperature-Power Operating Map  | 4.4-30 |
| 4.4.3.5    | Load Following Characteristics   | 4.4-30 |
| 4.4.3.6    | Thermal and Hydraulic Characteristics<br>Summary Table                           | 4.4-31 |
| 4.4.4      | EVALUATION   | 4.4-31 |
| 4.4.4.1    | Critical Heat Flux   | 4.4-31 |
| 4.4.4.2    | Core Hydraulics  | 4.4-31 |
| 4.4.4.2.1  | Flow Paths Considered in Core Pressure Drop<br>and Thermal Design                | 4.4-31 |
| 4.4.4.2.2  | Inlet Flow Distributions   | 4.4-32 |
| 4.4.4.2.3  | Empirical Friction Factor Correlations   | 4.4-33 |
| 4.4.4.3    | Influence of Power Distribution  | 4.4-34 |
| 4.4.4.3.1  | Nuclear Enthalpy Rise Hot Channel<br>Factor $F_{\Delta H}^N$                     | 4.4-34 |
| 4.4.4.3.2  | Axial Heat Flux Distributions  | 4.4-35 |
| 4.4.4.4    | Core Thermal Response  | 4.4-36 |
| 4.4.4.5    | Analytical Techniques  | 4.4-38 |

TABLE OF CONTENTS (Cont'd)

|           |   | <u>PAGE</u> |
|-----------|---|-------------|
| 4.4.4.5.1 | Core Analysis   | 4.4-38      |
| 4.4.4.5.2 | Steady-State Analysis   | 4.4-38      |
| 4.4.4.5.3 | Experimental Verification   | 4.4-39      |
| 4.4.4.5.4 | Transient Analysis  | 4.4-39      |
| 4.4.4.6   | Hydrodynamic and Flow Power Coupled Instability                                 | 4.4-40      |
| 4.4.4.7   | Fuel Rod Behavior Effects from Coolant Flow<br>Blockage                         | 4.4-43      |
| 4.4.5     | TESTING AND VERIFICATION  | 4.4-45      |
| 4.4.5.1   | Tests Prior to Initial Criticality  | 4.4-45      |
| 4.4.5.2   | Initial Power and Plant Operation   | 4.4-45      |
| 4.4.5.3   | Component and Fuel Inspection   | 4.4-45      |
| 4.4.6     | INSTRUMENTATION REQUIREMENTS  | 4.4-45      |
| 4.4.6.1   | Incore Instrumentation  | 4.4-45      |
| 4.4.6.2   | Overtemperature and Overpower $\Delta T$ Instrumentation                        | 4.4-46      |
| 4.4.6.3   | Instrumentation to Limit Maximum Power Output                                   | 4.4-47      |
| 4.4.7     | REFERENCES  | 4.4-49      |
| 4.5       | <u>REACTOR MATERIALS</u>  | 4.5-1       |
| 4.5.1     | CONTROL ROD SYSTEM STRUCTURAL MATERIALS   | 4.5-1       |
| 4.5.1.1   | Materials Specifications  | 4.5-1       |
| 4.5.1.2   | Austenitic Stainless Steel Components   | 4.5-3       |
| 4.5.1.3   | Other Materials   | 4.5-5       |
| 4.5.2     | REACTOR INTERNALS MATERIALS   | 4.5-6       |
| 4.5.2.1   | Materials Specification   | 4.5-6       |
| 4.5.2.2   | Controls on Welding   | 4.5-7       |
| 4.5.2.3   | Nondestructive Examination of Wrought Seamless<br>Tubular Products and Fittings | 4.5-7       |
| 4.5.2.4   | Fabrication and Processing of Austenitic<br>Stainless Steel Components          | 4.5-7       |
| 4.5.2.5   | Contamination Protection and Cleaning of<br>Austenitic Stainless Steel          | 4.5-7       |

TABLE OF CONTENTS (Cont'd)

|       |   | <u>PAGE</u> |
|-------|---|-------------|
| 4.6   | <u>FUNCTIONAL DESIGN OR REACTIVITY CONTROL SYSTEMS</u>        | 4.6-1       |
| 4.6.1 | INFORMATION FOR CONTROL ROD DRIVE SYSTEM (CRDS)               | 4.6-1       |
| 4.6.2 | EVALUATION OF THE CRDS  | 4.6-1       |
| 4.6.3 | TESTING AND VERIFICATION OF THE CRDS                          | 4.6-2       |
| 4.6.4 | INFORMATION FOR COMBINED PERFORMANCE OF<br>REACTIVITY SYSTEMS | 4.6-2       |
| 4.6.5 | EVALUATION OF COMBINED PERFORMANCE                            | 4.6-3       |
| 4.6.6 | REFERENCES  | 4.6-3       |



CHAPTER 4.0 - REACTOR

LIST OF TABLES

| <u>NUMBER</u> | <u>TITLE</u>  | <u>PAGE</u> |
|---------------|---|-------------|
| 4.1-1         | Reactor Design Comparison Table   | 4.1-5       |
| 4.1-2         | Analytical Techniques in Core Design  | 4.1-11      |
| 4.1-3         | Design Loading Conditions Considered<br>for Reactor Core Components                 | 4.1-13      |
| 4.3-1         | Reactor Core Description (First Cycle)  | 4.3-68      |
| 4.3-2         | Nuclear Design Parameters (First Cycle)   | 4.3-71      |
| 4.3-3         | Reactivity Requirements for Rod Cluster<br>Control Assemblies                       | 4.3-74      |
| 4.3-4         | Benchmark Critical Experiments  | 4.3-75      |
| 4.3-5         | Axial Stability Index Pressurized Water<br>Reactor Core With a 12-Foot Height       | 4.3-76      |
| 4.3-6         | Typical Neutron Flux Levels ( $n/cm^2$ -sec)<br>at Full Power                       | 4.3-77      |
| 4.3-7         | Comparison of Measured and Calculated<br>Doppler Defects                            | 4.3-78      |
| 4.3-8         | Saxton Core II Isotopics Rod MY, Axial Zone 6                                       | 4.3-79      |
| 4.3-9         | Critical Boron Concentrations, HZP, BOL   | 4.3-80      |
| 4.3-10        | Comparison of Measured and Calculated Rod Worth                                     | 4.3-81      |
| 4.3-11        | Comparison of Measured and Calculated Moderator<br>Coefficients at HZP, BOL         | 4.3-82      |
| 4.4-1         | Thermal and Hydraulic Comparison Table  | 4.4-58      |
| 4.4-2         | Thermal-Hydraulic Design Parameters for<br>One of Four Coolant Loops Out of Service | 4.4-61      |
| 4.4-3         | Void Fractions at Nominal Reactor Conditions<br>With Design Hot Channel Factors     | 4.4-62      |

612 019

CHAPTER 4.0 - REACTOR  
LIST OF FIGURES

| <u>NUMBER</u> | <u>TITLE</u>  |
|---------------|---|
| 4.2-1         | 17x17 Optimized Fuel Assembly Cross Section   |
| 4.2-2         | 17x17 Optimized Fuel Assembly Outline   |
| 4.2-3         | Fuel Rod Schematic  |
| 4.2-4         | Plan View of Mid Grid to guide Thimble Joint (Bottom View)  |
| 4.2-5         | Elevation View of Mid Grid to Guide Thimble Joint   |
| 4.2-6         | Top Grid to Guide Thimble and Top Nozzle Attachment   |
| 4.2-7         | Guide Thimble to Bottom Grid and Nozzle Joint   |
| 4.2-8         | Rod Cluster Control and Drive Rod   |
| 4.2-9         | Rod Cluster Control Assembly Outline  |
| 4.2-10        | Absorber Rod. All Ag-In-Cd Design   |
| 4.2-11        | Hybrid B <sub>4</sub> C Absorber Rod  |
| 4.2-12        | Composite Core Component Rods and Assembly Outline  |
| 4.3-1         | Fuel Loading Arrangement  |
| 4.3-2         | Production and Consumption of Higher Isotopes   |
| 4.3-3         | Boron Concentration vs. First Cycle Burnup With and Without Burnable Poison Rods  |
| 4.3-4         | Burnable Poison Rod Arrangement Within an Assembly  |
| 4.3-5         | Burnable Poison Loading Pattern (Typical)   |
| 4.3-6         | Normalized Power Density Distribution Near Beginning of Life, Unrodded Core, Hot Full Power, No Xenon                   |
| 4.3-7         | Normalized Power Density Distribution Near Beginning of Life, Unrodded Core, Hot Full Power, Equilibrium Xenon          |
| 4.3-8         | Normalized Power Density Distribution Near Beginning of Life, Group D at 28% Inserted Hot Full Power, Equilibrium Xenon |
| 4.3-9         | Normalized Power Density Distribution Near Middle of Life, Unrodded Core, Hot Full Power, Equilibrium Xenon             |
| 4.3-10        | Normalized Power Density Distribution Near End of Life, Unrodded Core, Hot Full Power, Equilibrium Xenon                |

LIST OF FIGURES (Cont'd)

| <u>NUMBER</u> | <u>TITLE</u>   |
|---------------|--|
| 4.3-11        | Normalized Power Density Distribution Near End of Life, Group D at 28% Inserted Hot Full Power, Equilibrium Xenon                        |
| 4.3-12        | Rodwise Power Distribution in a Typical Assembly (Assembly G-9) Near Beginning of Life, Hot Full Power, Equilibrium Xenon, Unrodded Core |
| 4.3-13        | Rodwise Power Distribution in a Typical Assembly (Assembly G-9) Near End of Life, Hot Full Power, Equilibrium Xenon, Unrodded Core       |
| 4.3-14        | Typical Axial Power Shapes Occurring at Beginning of Life  |
| 4.3-15        | Typical Axial Power Shapes Occurring at Middle of Life   |
| 4.3-16        | Typical Axial Power Shapes Occurring at End of Life  |
| 4.3-17        | Comparison of Assembly Axial Power Distribution With Core Average Axial Distribution Bank Slightly Inserted                              |
| 4.3-18        | Flow Chart for Determining Spike Model   |
| 4.3-19        | Predicted Power Spike Due to Single Non-Flattened Gap in the Adjacent Fuel   |
| 4.3-20        | Power Spike Factor as a Function of Axial Position   |
| 4.3-21        | Maximum $F_Q$ x Power vs. Axial Height During Normal Operation   |
| 4.3-22        | Peak Linear Power During Control Rod Malfunction Overpower Transients  |
| 4.3-23        | Peak Linear Power During Boration/Dilution Overpower Transients  |
| 4.3-24        | Typical Comparison Between Calculated and Measured Relative Fuel Assembly Power Distribution   |
| 4.3-25        | Comparison of Calculated and Measured Axial Shape  |
| 4.3-26        | Comparison of Calculated and Measured Peaking Factors, $(F_Q \times P_{REL})_{MAX}$ Envelope as a Function of Core Height                |
| 4.3-27        | Doppler Temperature Coefficient at BOL and EOL Cycle 1   |
| 4.3-28        | Doppler - Only Power Coefficient - BOL, EOL, Cycle 1   |
| 4.3-29        | Doppler - Only Power Defect - BOL, EOL, Cycle 1  |
| 4.3-30        | Moderator Temperature Coefficient - BOL, Cycle 1, No Rods  |
| 4.3-31        | Moderator Temperature Coefficient - EOL, Cycle 1   |

LIST OF FIGURES (Cont'd)

| <u>NUMBER</u> | <u>TITLE</u>  |
|---------------|---|
| 4.3-32        | Moderator Temperature Coefficient as a Function of Boron Concentration - BOL Cycle 1, No Rods             |
| 4.4-33        | Hot Full Power Temperature Coefficient During Cycle 1 for the Critical Boron Concentration                |
| 4.3-34        | Total Power Coefficient - BOL, EOL, Cycle 1   |
| 4.3-35        | Total Power Defect BOL, EOL, Cycle 1  |
| 4.3-36        | Rod Cluster Control Assembly Pattern  |
| 4.3-37        | Accidental Simultaneous Withdrawal of Two Control Banks, EOL, HZP Banks and B Moving in the Same Plane    |
| 4.3-38        | Design-Trip Curve   |
| 4.3-39        | Normalized Rod Worth vs. Percent Insertion - All Rods but One   |
| 4.3-40        | Axial Offset vs. Time PWR Core With a 12-Ft Height and 121 Assemblies                                     |
| 4.3-41        | XY Xenon Test Thermocouple Response Quadrant Tilt Difference vs. Time                                     |
| 4.3-42        | Calculated and Measured Doppler Defect and Coefficients at BOL Two-Loop Plant, 121 Assemblies, 12-Ft Core |
| 4.3-43        | Comparison of Calculated and Measured Boron Concentration for 2-Loop Plant, 121 Assemblies, 12-Ft Core    |
| 4.3-44        | Comparison of Calculated and Measured $C_B$ 3-Loop Plant, 157 Assemblies, 12-Ft Core                      |
| 4.3-45        | Comparison of Calculated and Measured $C_B$ 4-Loop Plant, 193 Assemblies, 12-Ft Core                      |
| 4.3-46        | Typical Nuclear Enthalpy Rise Limits for the First Cycle, Without Nuclear Uncertainty Allowance           |
| 4.4-1         | Improved Thermal Design Procedure Illustration  |
| 4.4-2         | Measured vs. Predicted Critical Heat Flux-WRB-1 Correlation   |
| 4.4-3         | TDC vs. Reynolds Number for 26" Grid Spacing  |
| 4.4-4         | Normalized Radial Flow and Enthalpy Rise Distribution at 4-Ft Elevation                                   |

LIST OF FIGURES (Cont'd)

| <u>NUMBER</u> | <u>TITLE</u>  |
|---------------|---|
| 4.3-32        | Moderator Temperature Coefficient as a Function of Boron Concentration - BOL Cycle 1, No Rods             |
| 4.4-33        | Hot Full Power Temperature Coefficient During Cycle 1 for the Critical Boron Concentration                |
| 4.3-34        | Total Power Coefficient - BOL, EOL, Cycle 1   |
| 4.3-35        | Total Power Defect BOL, EOL, Cycle 1  |
| 4.3-36        | Rod Cluster Control Assembly Pattern  |
| 4.3-37        | Accidental Simultaneous Withdrawal of Two Control Banks, EOL, HZP Banks and B Moving in the Same Plane    |
| 4.3-38        | Design-Trip Curve   |
| 4.3-39        | Normalized Rod Worth vs. Percent Insertion - All Rods but One   |
| 4.3-40        | Axial Offset vs. Time PWR Core With a 12-Ft Height and 121 Assemblies                                     |
| 4.3-41        | XY Xenon Test Thermocouple Response Quadrant Tilt Difference vs. Time                                     |
| 4.3-42        | Calculated and Measured Doppler Defect and Coefficients at BOL Two-Loop Plant, 121 Assemblies, 12-Ft Core |
| 4.3-43        | Comparison of Calculated and Measured Boron Concentration for 2-Loop Plant, 121 Assemblies, 12-Ft Core    |
| 4.3-44        | Comparison of Calculated and Measured $C_B$ 3-Loop Plant, 157 Assemblies, 12-Ft Core                      |
| 4.3-45        | Comparison of Calculated and Measured $C_B$ 4-Loop Plant, 193 Assemblies, 12-Ft Core                      |
| 4.4-1         | Improved Thermal Design Procedure Illustration  |
| 4.4-2         | Measured vs. Predicted Critical Heat Flux-WRB-1 Correlation   |
| 4.4-3         | TDC vs. Reynolds Number for 26" Grid Spacing  |
| 4.4-4         | Normalized Radial Flow and Enthalpy Rise Distribution at 4-Ft Elevation                                   |

LIST OF FIGURES (Cont'd)

| <u>NUMBER</u> | <u>TITLE</u>   |
|---------------|--|
| 4.4-5         | Normalized Radial Flow and Enthalpy Rise Distribution at 8-Ft Elevation    |
| 4.4-6         | Normalized Radial Flow and Enthalpy Rise Distribution at 12-Ft Elevation   |
| 4.4-7         | Void Fraction vs. Thermodynamic Quality $H-H_{SAT}/H_g-H_{SAT}$            |
| 4.4-8         | Thermal Conductivity of $UO_2$ (Data Corrected to 95% Theoretical Density) |
| 4.4-9         | Reactor Coolant System Temperature Percent Power Map                       |
| 4.4-10        | Distribution of Incore Instrumentation                                     |

LIST OF FIGURES (Cont'd)

| <u>NUMBER</u> | <u>TITLE</u>   |
|---------------|--|
| 4.4-5         | Normalized Radial Flow and Enthalpy Rise Distribution at 8-Ft Elevation  |
| 4.4-6         | Normalized Radial Flow and Enthalpy Rise Distribution at 12-Ft Elevation   |
| 4.4-7         | Void Fraction vs. Thermodynamic Quality $H-H_{SAT}/H_g-H_{SAT}$  |
| 4.4-8         | Thermal Conductivity of $UO_2$ (Data Corrected to 95% Theoretical Density)   |
| 4.4-9         | Reactor Coolant System Temperature Percent Power Map   |
| 4.4-10        | Distribution of Incore Instrumentation   |
| 4.4-11        | 100% Power Shapes Evaluated at Conditions Representative of Loss of Flow All Shapes Evaluated with $F_{\Delta H}^N = 1.49$ |

612 026



## 4.0 REACTOR

### 4.1 SUMMARY DESCRIPTION

This chapter describes (1) the mechanical components of the reactor and reactor core including the fuel rods and fuel assemblies, (2) the nuclear design, and (3) the thermal-hydraulic design.

The reactor core is comprised of an array of fuel assemblies which are identical in mechanical design, but different in fuel enrichment. The initial design employs three enrichments in a three-region core, whereas more enrichments may be employed for a particular refueling scheme. Fuel cycle times of 6 months to 18 months are possible and may be employed with the core described herein.

The core is cooled and moderated by light water at a pressure of 2250 psia in the Reactor Coolant System. The moderator coolant contains boron as a neutron poison. The concentration of boron in the coolant is varied as required to control relatively slow reactivity changes including the effects of fuel burnup. Additional boron, in the form of burnable poison rods, is employed to establish the desired initial reactivity as discussed in Subsection 4.2.2.3.

Two hundred and sixty-four fuel rods are mechanically joined in a square array to form a fuel assembly. The fuel rods are supported at intervals along their length by grid assemblies which maintain the lateral spacing between the rods throughout the design life of the assembly. The top and bottom grids are made of Inconel and the intermediate grids are made of Zircaloy. The grid assemblies consist of an "egg-crate" arrangement of interlocked straps. The straps contain spring fingers and dimples for fuel rod support as well as coolant mixing vanes. The fuel rods consist of slightly enriched uranium dioxide ceramic cylindrical pellets contained in slightly cold worked Zircaloy-4 tubing which is plugged and seal welded at the ends to encapsulate the fuel. All fuel rods are pressurized with helium during fabrication to reduce stresses and strains, and to increase fatigue life.

The center position in the assembly is reserved for use by the incore instrumentation, while the remaining 24 positions in the array are equipped with guide thimbles joined to the grids and the top and bottom nozzles. Depending upon the position of the assembly in the core, the guide thimbles are used as core locations for rod cluster control assemblies (RCCA's), neutron source assemblies, and burnable poison assemblies. Otherwise, the guide thimbles are fitted with plugging devices to limit bypass flow.

The bottom nozzle is a box-like structure which serves as the bottom structural element of the fuel assembly and directs the coolant flow distribution to the assembly.

The top nozzle functions as the upper structural element of the fuel assembly in addition to providing a partial protective housing of the RCCA or other components.

The RCCA's each consist of a group of individual absorber rods fastened at the top end to a common hub or spider assembly, containing full length absorber material to control the reactivity of the core under operating conditions.

The nuclear design analyses and evaluations establish physical locations for control rods, burnable poison rods, and physical parameters such as fuel enrichments and boron concentration in the coolant. The nuclear design evaluation established that the reactor core has inherent characteristics which together with corrective actions of the reactor control and protective systems provide adequate reactivity control even if the highest reactivity worth RCCA is stuck in the fully withdrawn position.

The design also provides for inherent stability against diametral and azimuthal power oscillations and for control of induced axial power oscillation through the use of control rods.

612-128

The thermal-hydraulic design analyses and evaluations establish coolant flow parameters which assure that adequate heat transfer is provided between the fuel cladding and the reactor coolant. The thermal design takes into account local variations in dimensions, power generation, flow distribution, and mixing. The mixing vanes incorporated in the fuel assembly spacer grid design induce additional flow mixing between the various flow channels within a fuel assembly as well as between adjacent assemblies. Instrumentation is provided in and out of the core to monitor the nuclear, thermal-hydraulic, and mechanical performance of the reactor and to provide inputs to automatic control functions.

Table 4.1-1 presents a comparison of the principal nuclear, thermal-hydraulic and mechanical design parameters between the Byron/Braidwood units and the Optimized Fuel Assembly. The effects of fuel densification were evaluated with the methods described in Reference[1]. The analytical techniques employed in the core design are tabulated in Table 4.1-2. The loading conditions considered in general for the core internals and components are tabulated in Table 4.1-3. Specific or limiting loads considered for design purposes of the various components are listed as follows: fuel assemblies in Subsection 4.2.1.1.2, neutron absorber rods, burnable poison rods, neutron source rods and thimble plug assemblies in Subsection 4.2.1.6.

#### 4.1.1 REFERENCES

1. Heilman, J. M., (Ed.), "Fuel Densification Experimental Results and Model for Reactor Operation," WCAP-8218-P-A, March 1975 (Proprietary) and WCAP-8219-A, March 1975.
2. Beaumont, M. D., Skaritka, J. (Editors), "Verification Testing and Analyses of the 17x17 Optimized Fuel Assembly," WCAP-9401 (Proprietary) and WCAP-9402, March 1979.

The thermal-hydraulic design analyses and evaluations establish coolant flow parameters which assure that adequate heat transfer is provided between the fuel cladding and the reactor coolant. The thermal design takes into account local variations in dimensions, power generation, flow distribution, and mixing. The mixing vanes incorporated in the fuel assembly spacer grid design induce additional flow mixing between the various flow channels within fuel assembly as well as between adjacent assemblies. Instrumentation is provided in and out of the core to monitor the nuclear, thermal-hydraulic, and mechanical performance of the reactor and to provide inputs to automatic control functions.

Table 4.1-1 presents a comparison of the principal nuclear, thermal-hydraulic and mechanical design parameters between the W. B. McGuire units and Optimized Fuel Assembly. The effects of fuel densification were evaluated with the methods described in Reference [1]. The analytical techniques employed in the core design are tabulated in Table 4.1-2. The loading conditions considered in general for the core internals and components are tabulated in Table 4.1-3. Specific or limiting loads considered for design purposes of the various components are listed as follows: fuel assemblies in Subsection 4.2.1.1.2, neutron absorber rods, burnable poison rods, neutron source rods and thimble plug assemblies in Subsection 4.2.1.6.

612 031

REACTOR DESIGN COMPARISON TABLE

| <u>THERMAL AND HYDRAULIC DESIGN PARAMETERS</u>                 | <u>BYRON AND BRAIDWOOD<br/>UNITS 1 and 2</u> | <u>OPTIMIZED FUEL<br/>ASSEMBLY</u> |
|--|--|------------------------------------|
| 1. Reactor Core Heat Output, (100%), $MW_t$                    | 3411   | 3411                               |
| 2. Reactor Core Heat Output, $10^6$ Btu/hr                     | 11641  | 11641.7                            |
| 3. Heat Generated in Fuel, %                                   | 97.4   | 97.4                               |
| 4. System Pressure, Nominal, psia <sup>(1)</sup>               | 2250   | 2280                               |
| 5. System Pressure, Minimum Steady State, psia <sup>(1)</sup>  | 2220   | 2250                               |
| 6. Minimum DNBR at Nominal Conditions                          |  |                                    |
| Typical Flow Channel   | 2.09   | 2.43                               |
| Thimble (Cold Wall) Flow Channel                               | 1.74   | 2.29                               |
| 7. Minimum DNBR for Design Transients                          |  |                                    |
| Typical Flow Channel   | $\geq 1.30$                                  | $> 1.85$                           |
| Thimble Flow Channel   | $\geq 1.30$                                  | $> 1.82$                           |
| 8. DNB Correlation   | "P" (W-3 with Modified<br>Spacer Factor)     | WRB-1                              |
| <u>COOLANT FLOW</u>  |  |                                    |
| 9. Total Thermal Flow Rate, $10^6$ $lb_m/hr$                   | 138.6  | 143.5                              |
| 10. Effective Flow Rate for Heat Transfer,<br>$10^6$ $lb_m/hr$ | 132.4  | 137.3                              |
| 11. Effective Flow Area for Heat Transfer, $ft^2$              | 51.1   | 54.1                               |
| 12. Average Velocity Along Fuel Rods, ft/sec                   | 16.4   | 16.1                               |
| 13. Average Mass Velocity, $10^6$ $lb_m/hr-ft^2$               | 2.59   | 2.54                               |

(1) Values used for thermal hydraulic core analysis

4.1-5

612  
052

TABLE 4.1-1 (Cont'd)

| <u>THERMAL AND HYDRAULIC DESIGN PARAMETERS</u>  | <u>BYRON AND BRAIDWOOD<br/>UNITS 1 and 2</u> | <u>OPTIMIZED FUEL<br/>ASSEMBLY</u> |
|---|--|------------------------------------|
| <u>COOLANT TEMPERATURE, °F</u>  |  |                                    |
| 14. Nominal Inlet   | 556.9  | 562.5                              |
| 15. Average Rise in Vessel  | 61.1   | 58.3                               |
| 16. Average Rise in Core  | 63.6   | 60.6                               |
| 17. Average in Core   | 590.4  | 594.4                              |
| 18. Average in Vessel   | 587.4  | 593.1                              |
| <u>HEAT TRANSFER</u>  |  |                                    |
| 19. Active Heat Transfer, Surface Area, ft <sup>2</sup>   | 59,700                                       | 57,500                             |
| 20. Average Heat Flux, Btu/hr-ft <sup>2</sup>   | 189,800                                      | 197,200                            |
| 21. Maximum Heat Flux for Normal Operation,<br>Btu/hr-ft <sup>2</sup>   | 440,300                                      | 457,500                            |
| 22. Average Linear Power, kW/ft   | 5.44   | 5.44                               |
| 23. Peak Linear Power for Normal Operation,<br>kW/ft(*)   | 12.6   | 12.6                               |
| 24. Peak Linear Power Resulting from Overpower<br>Transients/Operator Errors (assuming a<br>maximum overpower of 118%), kW/ft(**) | 18.0   | 18.0                               |
| 25. Peak Linear Power for Prevention of<br>Centerline Melt, kW/ft(***)  | >18.0  | >18.0                              |

\* This limit is associated with the value of  $F_Q = 2.32$

\*\* See Subsection 4.3.2.2.6

\*\*\* See Subsection 4.4.2.11.6.

4.1-6

612 033

TABLE 1 (Cont'd)

| <u>THERMAL AND HYDRAULIC DESIGN PARAMETERS</u>                         | <u>BYRON AND BRAIDWOOD<br/>UNITS 1 and 2</u> | <u>OPTIMIZED FUEL<br/>ASSEMBLY</u> |
|--|--|------------------------------------|
| 26. Power Density, kW per Liter of Core <sup>(+)</sup>                 | 104.5  | 104.5                              |
| 27. Specific Power, kW per kg Uranium                                  | 38.4   | 41.8                               |
| <u>FUEL CENTRAL TEMPERATURE</u>  |  |                                    |
| 28. Peak at Peak Linear Power for Prevention<br>of Centerline Melt, °F | 4700   | 4700                               |
| 29. Pressure Drop <sup>(++)</sup>                                      |  |                                    |
| Across Core, psi   | 26.9 <sub>-2.7</sub> <sup>(+++)</sup>        | 26.2 <sub>-2.6</sub>               |
| Across Vessel, Including Nozzle psi                                    | 47.4 <sub>-4.7</sub> <sup>(+++)</sup>        | 46.4 <sub>-4.6</sub>               |
| <u>CORE MECHANICAL DESIGN PARAMETERS</u>                               |  |                                    |
| 30. Design   | RCC Canless<br>17 x 17                       | RCC Canless<br>17 x 17             |
| 31. Number of Fuel Assemblies  | 193  | 193                                |
| 32. UO <sub>2</sub> Rods per Assembly                                  | 264  | 264                                |
| 33. Rod Pitch, in.   | 0.496  | 0.496                              |
| 34. Overall Dimensions, in.  | 8.426 x 8.426                                | 8.426 x 8.426                      |
| 35. Fuel Weight (as UO <sub>2</sub> ), lb                              | 222,739                                      | 204,236                            |
| 36. Clad Weight, lb  | 50,913                                       | 43,376                             |

+ Based on cold dimensions and 95% of theoretical density fuel

++ Based on best estimate reactor flow rate as discussed in Section 5.1

+++ Pressure drops revised based on results from Reference 2.

4.1-7

612 034



TABLE 4.1-1 (Cont'd)

| <u>THERMAL AND HYDRAULIC DESIGN PARAMETERS</u> | <u>BYRON AND BRAIDWOOD<br/>UNITS 1 and 2</u> | <u>OPTIMIZED FUEL<br/>ASSEMBLY</u>                          |
|--|--|---|
| 37. Number of Grids per Assembly               | 8 - Type R                                   | 2-Type R, 6-Type Z  |
| 38. Composition of Grids                       | Inconel 718                                  | 2 End Grids<br>Inconel 718                                  |
| 39. Loading Technique                          | 3 Region Nonuniform                          | 6 Intermediate<br>Grids - Zircaloy 4<br>3 Region Nonuniform |
| <u>CORE MECHANICAL DESIGN PARAMETERS</u>       |  |   |
| <u>FUEL RODS</u>                               |  |   |
| 40. Number                                     | 50,952                                       | 50,952  |
| 41. Outside Diameter, in.                      | 0.374  | 0.360   |
| 42. Diametral Gap, in.                         | 0.0065                                       | 0.0062  |
| 43. Cladding Thickness, in.                    | 0.0225                                       | 0.0225  |
| 44. Cladding Material                          | Zircaloy-4                                   | Zircaloy-4  |
| <u>FUEL PELLETS</u>                            |  |   |
| 45. Material                                   | UO <sub>2</sub> Sintered                     | UO <sub>2</sub> Sintered                                    |
| 46. Density (% of Theoretical)                 | 95   | 95  |
| 47. Diameter, in.                              | 0.3225                                       | 0.3088  |
| 48. Length, in.                                | 0.530  | 0.507   |

4.1-8

612 035

TABLE 1 (Cont'd)

| <u>CORE MECHANICAL DESIGN PARAMETERS</u>            | <u>BYRON AND BRAIDWOOD<br/>UNITS 1 and 2</u> | <u>OPTIMIZED FUEL<br/>ASSEMBLY</u>    |
|---|--|---------------------------------------|
| <u>ROD CLUSTER CONTROL ASSEMBLIES</u>               |  |                                       |
| 49. Neutron Absorber                                | Ag-In-Cd                                     | B <sub>4</sub> C (with Ag-In-Cd tips) |
| 50. Cladding Material                               | Type 304<br>SS-Cold Worked                   | Type 304 SS-Cold<br>Cold Worked       |
| 51. Cladding Thickness, in.                         | 0.0185                                       | 0.0385                                |
| 52. Number of Clusters                              | 53   | 53                                    |
| 53. Number of Absorber Rods per Cluster             | 24   | 24                                    |
| <u>CORE STRUCTURE</u>                               |  |                                       |
| 54. Core Barrel, ID/OD, in.                         | 144.0/152.5                                  | 148.0/152.5                           |
| 55. Thermal Shield                                  | Neutron Pad Design                           | Neutron Pad Design                    |
| <u>STRUCTURE CHARACTERISTICS</u>                    |  |                                       |
| 56. Core Diameter, in. (Equivalent)                 | 132.7  | 132.7                                 |
| 57. Core Height, in. (Active Fuel, Cold Dimensions) | 144  | 144                                   |
| <u>REFLECTOR THICKNESS AND COMPOSITION</u>          |  |                                       |
| 58. Top - Water plus Steel, in.                     | ~10  | ~10                                   |

4.1-9

612 036

TABLE 4.1-1 (Cont'd)

| <u>CORE MECHANICAL DESIGN PARAMETERS</u>                                   | <u>BYRON AND BRAIDWOOD<br/>UNITS 1 and 2</u> | <u>OPTIMIZED FUEL<br/>ASSEMBLY</u> |
|--|--|------------------------------------|
| <u>REFLECTOR THICKNESS AND COMPOSITION</u>                                 |  |                                    |
| 59. Bottom - Water plus Steel, in.   | ~10  | ~10                                |
| 60. Side - Water plus Steel, in.   | ~15  | ~15                                |
| 61. H <sub>2</sub> O/U Molecular Ratio, Cell (Cold)                        | 2.43   | 2.73                               |
| 62. H <sub>2</sub> O/U Molecular Ratio, Core Average,<br>Cold (first core) | 2.78   | 3.16                               |
| <u>FEED ENRICHMENT, W/O</u>  |  |                                    |
| 63. Region 1   | 2.10   | 2.10                               |
| 64. Region 2   | 2.60   | 2.60                               |
| 65. Region 3   | 2.10   | 3.10                               |

4.1-10

612 037

REACTOR DESIGN COMPARISON TABLE

| <u>THERMAL AND HYDRAULIC DESIGN PARAMETERS</u>                                    | <u>W. B. McGUIRE<br/>UNITS 1 and 2</u>   | <u>OPTIMIZED FUEL<br/>ASSEMBLY</u> |
|---|--|------------------------------------|
| 1. Reactor Core Heat Output, (100%), MW <sub>t</sub>                              | 3411                                     | 3411                               |
| 2. Reactor Core Heat Output, 10 <sup>6</sup> Btu/hr                               | 11641.7                                  | 11641.7                            |
| 3. Heat Generated in Fuel, %  | 97.4                                     | 97.4                               |
| 4. System Pressure, Nominal, psia <sup>(1)</sup>                                  | 2250                                     | 2280                               |
| 5. System Pressure, Minimum Steady State, psia <sup>(1)</sup>                     | 2220                                     | 2250                               |
| 6. Minimum DNBR at Nominal Conditions   |  |                                    |
| Typical Flow Channel  | 2.05                                     | 2.4                                |
| Thimble (Cold Wall) Flow Channel  | 1.72                                     | 2.26                               |
| 7. Minimum DNBR for Design Transients   |  |                                    |
| Typical Flow Channel  | >1.3                                     | >1.49                              |
| Thimble Flow Channel  | >1.3                                     | >1.47                              |
| 8. DNB Correlation  | "R" (W-3 with Modified<br>Spacer Factor) | WRB-1                              |
| <br><u>COOLANT FLOW</u>   |  |                                    |
| 9. Total Thermal Flow Rate, 10 <sup>6</sup> lb <sub>m</sub> /hr                   | 144.7                                    | 143.3                              |
| 10. Effective Flow Rate for Heat Transfer,<br>10 <sup>6</sup> lb <sub>m</sub> /hr | 133.9                                    | 134.7                              |
| 11. Effective Flow Area for Heat Transfer, ft <sup>2</sup>                        | 51.1                                     | 54.1                               |
| 12. Average Velocity Along Fuel Rods, ft/sec                                      | 16.6                                     | 15.8                               |
| 13. Average Mass Velocity, 10 <sup>6</sup> lb <sub>m</sub> /hr-ft <sup>2</sup>    | 2.62                                     | 2.49                               |

(1) Values used for thermal hydraulic core analysis

4.1-5

612 038

PL 111

TABLE 4.1-1 (Cont'd)

| <u>THERMAL AND HYDRAULIC DESIGN PARAMETERS</u>  | <u>W. B. McGUIRE</u><br><u>UNITS 1 and 2</u> | <u>OPTIMIZED FUEL</u><br><u>ASSEMBLY</u> |
|---|--|--|
| <u>COOLANT TEMPERATURE, °F</u>  |  |  |
| 14. Nominal Inlet   | 559.1  | 561.6                                    |
| 15. Average Rise in Vessel  | 58.4   | 58.5                                     |
| 16. Average Rise in Core  | 62.5   | 61.8                                     |
| 17. Average in Core   | 590.4  | 594.2                                    |
| 18. Average in Vessel   | 588.3  | 592.3                                    |
| <u>HEAT TRANSFER</u>  |  |  |
| 19. Active Heat Transfer, Surface Area, ft <sup>2</sup>   | 59,700                                       | 57,500                                   |
| 20. Average Heat Flux, Btu/hr-ft <sup>2</sup>   | 189,800                                      | 197,200                                  |
| 21. Maximum Heat Flux for Normal Operation,<br>Btu/hr-ft <sup>2</sup>   | 440,300                                      | 457,500                                  |
| 22. Average Linear Power, kW/ft   | 5.44   | 5.44                                     |
| 23. Peak Linear Power for Normal Operation,<br>kW/ft(*)   | 12.6   | 12.6                                     |
| 24. Peak Linear Power Resulting from Overpower<br>Transients/Operator Errors (assuming a<br>maximum overpower of 118%), kW/ft(**) | 18.0   | 18.0                                     |
| 25. Peak Linear Power for Prevention of<br>Centerline Melt, kW/ft(***)  | >18.0  | >18.0                                    |

\* This limit is associated with the value of  $F_Q = 2.32$

\*\* See Subsection 4.3.2.2.6

\*\*\* See Subsection 4.4.2.11.6.

4.1-6

612 039

BLUE

TABLE -1 (Cont'd)

| <u>THERMAL AND HYDRAULIC DESIGN PARAMETERS</u>                         | W. B. McGUIRE<br><u>UNITS 1 and 2</u> | <u>OPTIMIZED FUEL<br/>ASSEMBLY</u> |
|--|---------------------------------------|------------------------------------|
| 26. Power Density, kW per Liter of Core <sup>(+)</sup>                 | 104.5                                 | 104.5                              |
| 27. Specific Power, kW per kg Uranium                                  | 38.4                                  | 41.8                               |
| <u>FUEL CENTRAL TEMPERATURE</u>  |                                       |                                    |
| 28. Peak at Peak Linear Power for Prevention<br>of Centerline Melt, °F | 4700                                  | 4700                               |
| 29. Pressure Drop <sup>(++)</sup>                                      |                                       |                                    |
| Across Core, psi   | 25.9±2.6 <sup>(+++)</sup>             | 25.7±2.6                           |
| Across Vessel, Including Nozzle psi                                    | 46.3±4.6 <sup>(+++)</sup>             | 45.7±4.6                           |
| <u>CORE MECHANICAL DESIGN PARAMETERS</u>                               |                                       |                                    |
| 30. Design   | RCC Canless<br>17 x 17                | RCC Canless<br>17 x 17             |
| 31. Number of Fuel Assemblies  | 193                                   | 193                                |
| 32. UO <sub>2</sub> Rods per Assembly                                  | 264                                   | 264                                |
| 33. Rod Pitch, in.   | 0.496                                 | 0.496                              |
| 34. Overall Dimensions, in.  | 8.426 x 8.426                         | 8.426 x 8.426                      |
| 35. Fuel Weight (as UO <sub>2</sub> ), lb                              | 222,739                               | 204,236                            |
| 36. Clad Weight, lb  | 50,913                                | 43,376                             |

+ Based on cold dimensions and 95% of theoretical density fuel

++ Based on best estimate reactor flow rate as discussed in Section 5.1

+++ Pressure drops revised based on results from Reference 2.

4.1-7

612 040

BLUE

TABLE 4.1-1 (Cont'd)

THERMAL AND HYDRAULIC DESIGN PARAMETERS

W. B. McGUIRE

OPTIMIZED FUEL ASSEMBLY

UNITS 1 and 2

- 37. Number of Grids per Assembly
- 38. Composition of Grids

8 - Type R  
Inconel 718

2-Type R, 6-Type Z  
2 End Grids -  
Inconel 718  
6 Intermediate  
Grids - Zircaloy 4  
3 Region Nonuniform

- 39. Loading Technique

3 Region Nonuniform

CORE MECHANICAL DESIGN PARAMETERS

FUEL RODS

- 40. Number
- 41. Outside Diameter, in.
- 42. Diametral Gap, in.
- 43. Cladding Thickness, in.
- 44. Cladding Material

50,952  
0.374  
0.0065  
0.0225  
Zircaloy-4

50,952  
0.360  
0.0062  
0.0225  
Zircaloy-4

FUEL PELLETS

- 45. Material
- 46. Density (% of Theoretical)
- 47. Diameter, in.
- 48. Length, in.

UO<sub>2</sub> Sintered  
95  
0.3225  
0.530

UO<sub>2</sub> Sintered  
95  
0.3088  
0.507

4.1-8

612  
041

BLUE

TABLE 4.1-1 (Cont'd)

| <u>CORE MECHANICAL DESIGN PARAMETERS</u>            | W. B. McGUIRE<br><u>UNITS 1 and 2</u> | <u>OPTIMIZED FUEL<br/>ASSEMBLY</u>    |
|---|---------------------------------------|---------------------------------------|
| <u>ROD CLUSTER CONTROL ASSEMBLIES</u>               |                                       |                                       |
| 49. Neutron Absorber                                | Ag-In-Cd                              | B <sub>4</sub> C (with Ag-In-Cd tips) |
| 50. Cladding Material                               | Type 304<br>SS-Cold Worked            | Type 304 SS-Cold<br>Cold Worked       |
| 51. Cladding Thickness, in.                         | 0.0135                                | 0.0385                                |
| 52. Number of Clusters                              | 53                                    | 53                                    |
| 53. Number of Absorber Rods per Cluster             | 24                                    | 24                                    |
| <u>CORE STRUCTURE</u>                               |                                       |                                       |
| 54. Core Barrel, ID/OD, in.                         | 148.0/152.5                           | 148.0/152.5                           |
| 55. Thermal Shield                                  | Neutron Pad Design                    | Neutron Pad Design                    |
| <u>STRUCTURE CHARACTERISTICS</u>                    |                                       |                                       |
| 56. Core Diameter, in. (Equivalent)                 | 132.7                                 | 132.7                                 |
| 57. Core Height, in. (Active Fuel, Cold Dimensions) | 144                                   | 144                                   |
| <u>REFLECTOR THICKNESS AND COMPOSITION</u>          |                                       |                                       |
| 58. Top - Water plus Steel, in.                     | ~10                                   | ~10                                   |

4.1-9

612

042

BLUE



TABLE 4.1-1 (Cont'd)

CORE MECHANICAL DESIGN PARAMETERSW. B. MCGUIRE  
UNITS 1 and 2OPTIMIZED FUEL  
ASSEMBLYREFLECTOR THICKNESS AND COMPOSITION

|  |      |      |
|--|------|------|
| 59. Bottom - Water plus Steel, in.   | ~10  | ~10  |
| 60. Side - Water plus Steel, in.   | ~15  | ~15  |
| 61. H <sub>2</sub> O/U Molecular Ratio, Cell (Cold)                        | 2.43 | 2.73 |
| 62. H <sub>2</sub> O/U Molecular Ratio, Core Average,<br>Cold (first core) | 2.78 | 3.16 |

FEED ENRICHMENT, W/O

|              |      |      |
|--------------|------|------|
| 63. Region 1 | 2.10 | 2.10 |
| 64. Region 2 | 2.60 | 2.60 |
| 65. Region 3 | 3.10 | 3.10 |

4.1-10

612  
043

BLUE

ANALYTICAL TECHNIQUES IN CORE DESIGN

| <u>ANALYSIS</u>   | <u>TECHNIQUE</u>  | <u>COMPUTER CODE</u>   | <u>SECTION REFERENCED</u>                            |
|---|---|--|--|
| Fuel Rod Design   |   |  |  |
| Fuel Performance Characteristics (temperature, internal pressure cladding stress, etc.)                                     | Semiempirical thermal Model<br>Model of fuel rod with consideration of fuel density changes, heat transfer, fission gas release, etc. | Westinghouse fuel rod design model                               | 4.2.1.1<br>4.2.3.2<br>4.2.3.3<br>4.3.3.1<br>4.4.2.11 |
| Nuclear Design  |   |  |  |
| 1. Cross Sections and Group Constants   | Microscopic data<br>Macroscopic constants for homogenized core regions<br>Group constants for control rods with self-shielding        | Modified ENDF/B library<br>LEOPARD/CINDER type<br><br>HAMMER-AIM | 4.3.3.2<br>4.3.3.2<br><br>4.3.3.2                    |
| 2. X-Y Power Distributions, Fuel Depletion, Critical Boron Concentrations, X-Y Xenon Distributions, Reactivity Coefficients | 2-D and 3-D, 2-Group Diffusion Theory<br><br>Nodal Code   | TURTLE<br><br>PALADON  | 4.3.3.3  |

4.1-11

6/2 OAA

TABLE 4.1-2 (Cont'd)

| <u>ANALYSIS</u>   | <u>TECHNIQUE</u>  | <u>COMPUTER CODE</u>            | <u>SECTION REFERENCED</u> |
|---|---|---------------------------------|---------------------------|
| 3. Axial Power Distributions Control Rod Worths, and Axial Xenon Distribution | 1-D, 2-Group Diffusion Theory   | PANDA                           | 4.3.3.3.                  |
|   | 2D and 3D 2-Group Model Analysis Code   | PALADON                         |                           |
| 4. Fuel Rod Power   | Integral Transport Theory   | LASER                           | 4.3.3.1.                  |
| Effective Resonance Temperature   | Monte Carlo Weighting Function  | REPAD                           |                           |
| 5. Criticality of Reactor and Fuel Assemblies                                 | 1-D, Multi-group Transport Theory<br>3-D Monte Carlo  | AMPX SYSTEM of Codes<br>KENO-IV | 4.3.2.6                   |
| Thermal-Hydraulic Design  |   |                                 |                           |
| 1. Steady-state   | Subchannel analysis of local fluid conditions in rod bundles, including inertial and crossflow resistance terms, solution progresses from core-wide to hot assembly to hot channel                          | THINC-IV                        | 4.4.4.5                   |
| 2. Transient Departure from Nucleat Boiling Analysis                          | Subchannel analysis of local fluid conditions in rod bundles during transients by including accumulation terms in conservation equations; solution progresses from core-wide to hot assembly to hot channel | THINC-I (THINC-III)             | 4.4.4.5.4                 |

4.1-12

612

045

TABLE 4.1-3

DESIGN LOADING CONDITIONS CONSIDERED FOR REACTOR CORE COMPONENTS

1. Fuel Assembly Weight
2. Fuel Assembly Spring Forces
3. Internals Weight
4. Control Rod Trip (equivalent static load)
5. Differential Pressure
6. Spring Preloads
7. Coolant Flow Forces (static)
8. Temperature Gradients
9. Differences in Thermal Expansion
  - a. Due to temperature differences
  - b. Due to expansion of different materials
10. Interference Between Components
11. Vibration (mechanically or hydraulically induced)
12. One or More Loops Out of Service
13. All Operational Transients Listed in Table 5.2-1
14. Pump Overspeed
15. Seismic Loads (operation basis earthquake and safe shutdown earthquake)
16. Blowdown Forces (due to cold and hot leg break)

612 047

## 4.2 FUEL SYSTEM DESIGN

The plant design conditions are divided into four categories in accordance with their anticipated frequency of occurrence and risk to the public: Condition I - Normal Operation; Condition II - Incidents of Moderate Frequency; Condition III - Infrequent Incidents; Condition IV - Limiting Faults. The bases and description of plant operation and events involving each Condition are given in the Accident Analysis Chapter 15.0.

The reactor is designed so that its components meet the following performance and safety criteria:

1. The mechanical design of the reactor core components and their physical arrangement, together with corrective actions of the reactor control, protection, and emergency cooling systems (when applicable) assure that:
  - a. Fuel damage\* is not expected during Condition I and Condition II events. It is not possible, however, to preclude a very small number of rod failures. These are within the capability of the plant cleanup system and are consistent with plant design bases. The number of rod failures is small enough such that the dose limits given in 10 CFR 100 will not be exceeded.
  - b. The reactor can be brought to a safe state following a Condition III event with only a small fraction of fuel rods damaged.\* The extent of fuel damage might preclude immediate resumption of operation.
  - c. The reactor can be brought to a safe state and the core can be kept subcritical with acceptable heat transfer geometry following transients arising from Condition IV events.

\* Fuel damage as used here is defined as penetration of the fission product barrier (i.e., the fuel rod clad).

2. The fuel assemblies are designed to withstand loads induced during shipping, handling, and core loading without exceeding the criteria of Subsection 4.2.1.5.
3. The fuel assemblies are designed to accept control rod insertions in order to provide the required reactivity control for power operations and reactivity shutdown conditions (if in such core locations).
4. All fuel assemblies have provisions for the insertion of incore instrumentation necessary for plant operation (if in such core locations).
5. The reactor internals in conjunction with the fuel assemblies and incore control components direct coolant through the core. This achieves acceptable flow distribution and restricts bypass flow so that the heat transfer performance requirements can be met for all modes of operation.

#### 4.2.1 DESIGN BASES

The fuel rod and fuel assembly design bases are established to satisfy the general performance and safety criteria presented in this section.

Design values for the properties of the materials which comprise the fuel rod, fuel assembly and incore control components are given in Reference [2].

##### 4.2.1.1 Cladding

###### 1. Material and Mechanical Properties

Zircaloy-4 combines low absorption cross section; high corrosion resistance to coolant, fuel and fission products; high strength and ductility at operating temperatures; and high reliability. Reference [1] documents the operating experience with Zircaloy-4 as a clad material, and Reference [2] provides its mechanical properties with due consideration of temperature and irradiation effects.

612 049

## 2. Stress-Strain Limits

Cladding Stress - The von Mises criterion is used to calculate the effective stresses. The cladding stresses under Condition I and II events are less than the Zircaloy 0.2% offset yield stress, with due consideration of temperature and irradiation effects. While the cladding has some capability for accommodating plastic strain, the yield stress has been accepted as a conservative design basis.

Cladding Tensile Strain - The total tensile creep strain is less than 1% from the unirradiated condition. The elastic tensile strain during a transient is less than 1% from the pre-transient value. This limit is consistent with proven practice.

## 3. Vibration and Fatigue

Strain Fatigue - The cumulative strain fatigue cycles are less than the design strain fatigue life. This basis is consistent with proven practice.

Vibration - Potential for fretting wear of the clad surface exists due to flow induced vibrations. This condition is taken into account in the design of the fuel rod support system. The clad wear depth is limited to acceptable values by the grid support dimple and spring design.

## 4. Chemical Properties of the Cladding - This is discussed in Reference [2].

### 4.2.1.2 Fuel Material

#### 1. Thermal Physical Properties

The thermal-physical properties of  $UO_2$  are described in Reference [2] with due consideration of temperature and irradiation effects.

Fuel Pellet Temperatures - The center temperature of the hottest pellet is below the melting temperature of the  $UO_2$  [melting point



of 2805°C (Reference 2) unirradiated and decreasing by 32°C per 10,000 MWD/MTU. While a limited amount of center melting can be tolerated, the design conservatively precludes center melting. A calculated fuel centerline temperature of 4700°F has been selected as an overpower limit to assure no fuel melting. This provides sufficient margin for uncertainties as described in Subsection 4.4.2.9.

Fuel Pellet Density - The nominal design density of the fuel is 95% of theoretical.

## 2. Fuel Densification and Fission Product Swelling

The design bases and models used for fuel densification and swelling are provided in References [3 and 4].

## 3. Chemical Properties

Reference [2] provides the basis for justifying that no adverse chemical interactions occur between the fuel and its adjacent material.

### 4.2.1.3 Fuel Rod Performance

The detailed fuel rod design establishes such parameters as pellet size and density, cladding-pellet diametral gap, gas plenum size, and helium pre-pressurization level. The design also considers effects such as fuel density changes, fission gas release, cladding creep, and other physical properties which vary with burnup. The integrity of the fuel rods is ensured by designing to prevent excessive fuel temperatures, excessive internal rod gas pressures due to fission gas releases, and excessive cladding stresses and strains. This is achieved by designing the fuel rods to satisfy the conservative design bases in the following subsections during Condition I and Condition II events over the fuel lifetime. For each design basis, the performance of the limiting fuel rod must not exceed the limits specified.

612 051

1. Fuel Rod Models

The basic fuel rod models and the ability to predict operating characteristics are given in Reference [4] and the Design Evaluation Subsection 4.2.3.

2. Mechanical Design Limits

Cladding collapse shall be precluded during the fuel rod design lifetime. The models described in Reference [5] are used for this evaluation.

The rod internal gas pressure shall remain below the value which causes the fuel-cladding diametral gap to increase due to outward cladding creep during steady-state operation.

Rod pressure is also limited such that extensive D.  $\delta$  propagation shall not occur during normal operation and accident events (Reference 12).

4.2.1.4 Spacer Grids

1. Material Properties and Mechanical Design Limits

Two types of spacer grids are used in each fuel assembly. The top and bottom grids are made of Inconel 718. The others are made of Zircaloy-4.

Lateral loads resulting from a seismic or LOCA event will not cause unacceptably high plastic grid deformation. Each fuel assembly's geometry will be maintained such that the fuel rods remain in an array amenable to cooling. The behavior of the grids under loading has been studied experimentally.

612 052

## 2. Vibration and Fatigue

The grids provide sufficient fuel rod support to limit fuel rod vibration and maintain cladding fretting wear to within acceptable limits.

### 4.2.1.5 Fuel Assembly

#### 1. Structural Design

As previously discussed in Subsection 4.2.1, the structural integrity of the fuel assemblies is assured by setting design limits on stresses and deformations due to various nonoperational, operational and accident loads. These limits are applied to the design and evaluation of the top and bottom nozzles, guide thimbles, grids, and the thimble joints.

The design bases for evaluating the structural integrity of the fuel assemblies are:

- a. Nonoperational - 6 g loading with dimensional stability.
- b. Normal and abnormal loads for Conditions I and II - the fuel assembly component structural design criteria are established for the two primary material categories, namely austenitic steels and Zircaloy. The stress categories and strength theory presented in the ASME Boiler and Pressure Vessel Code, Section III, are used as a general guide.

For austenitic steel structural components, Tresca criterion is used to determine the stress intensities. The design stress intensity value,  $S_m$ , is given by the lowest of the following:

- One-third of the specified minimum tensile strength or 2/3 of the specified minimum yield strength at room temperature.

612 053

- One-third of the tensile strength or 90% of the yield strength at operating temperature, but not to exceed 2/3 of the specified minimum yield strength at room temperature.

The stress intensity limits are given below. All stress nomenclature is per the ASME Boiler and Pressure Vessel Code, Section III.

#### Stress Intensity Limits

| <u>Categories</u>                                      | <u>Limits</u> |
|--|---------------|
| General Primary Membrane Stress Intensity              | $S_m$         |
| Local Primary Membrane Stress Intensity                | $1.5 S_m$     |
| Primary Membrane plus Primary Bending Stress Intensity | $1.5 S_m$     |
| Total Primary plus Secondary Stress Intensity Range    | $3.0 S_m$     |

The Zircaloy structural components, which consist of guide thimbles, inner six grids and fuel tubes are in turn subdivided into two categories because of material differences and functional requirements. The fuel tube and grid design criteria are covered separately in Subsections 4.2.1.1 and 4.2.1.4, respectively. For the guide thimble design, the stress intensities, the design stress intensities and the stress intensity limits are calculated using the same methods as for the austenitic steel structural components. For conservative purposes the unirradiated properties of Zircaloy are used.

- c. Abnormal loads during Conditions III or IV - worst case represented by seismic loads, or blowdown loads during a LOCA event.
- Deflections or failures of components cannot interfere with the reactor shutdown or emergency cooling of the fuel rods.

The fuel assembly structural component stresses under faulted conditions are evaluated using primarily the methods outlined in Appendix F of the ASME Boiler and Pressure Vessel Code, Section III.

For the austenitic steel fuel assembly components, the stress intensity and the design stress intensity value,  $S_m$  are defined in accordance with the rules described in the previous section for normal operating conditions. Since the current analytical methods utilize elastic analysis, the stress intensity limits are defined as the smaller value of  $2.4 S_m$  or  $0.70 S_u$  for primary membrane and  $3.6 S_m$  or  $1.05 S_u$  for primary membrane plus primary bending.

For the Zircaloy components the stress intensities are defined in accordance with the rules described in the previous section for normal operating conditions, and the design stress intensity values,  $S_m$ , are set at two-thirds of the material yield strength,  $S_y$ , at reactor operating temperature. This results in Zircaloy stress intensity limits being the smaller of  $1.6 S_y$  or  $0.70 S_u$  for primary membrane and  $2.4 S_y$  or  $1.05 S_u$  for primary membrane plus bending. For conservative purposes, the Zircaloy unirradiated properties are used to define the stress limits.

## 2. Thermal-hydraulic Design

This topic is covered in Section 4.4.

### 4.2.1.6 Core Components

The core components consist of the rod cluster control assemblies (RCCAs), the primary and secondary source assemblies, the thimble plug assemblies and the burnable poison assemblies. A description of these components is provided in Section 4.2.2.

612 055

### 1. Thermal-Physical Properties of the Absorber Material

The absorber material for the RCCA is either all Ag-In-Cd, or B<sub>4</sub>C pellets with Ag-In-Cd alloy slugs. The thermal-physical properties of Ag-In-Cd are described in Reference [2], and B<sub>4</sub>C properties are described in References [2 and 13]. The absorber material temperature shall not exceed its melting temperature (1454<sup>o</sup>F for Ag-In-Cd and 4400<sup>o</sup>F for B<sub>4</sub>C if used).

The burnable poison material is borosilicate glass. The thermal-physical properties of the borosilicate glass are described in Reference [2]. The burnable poison rods are designed so that the borosilicate glass temperature is below its minimum softening temperature of 1492<sup>o</sup>F (for reference 12.5 weight percent boron). The softening temperature is defined in accordance with ASTM C 338. In addition, the structural elements are designed to prevent excessive slumping.

### 2. Compatibility of the Absorber and Cladding Materials

The control rod and burnable poison rod cladding is cold drawn type 304 stainless steel tubing. Extensive in-reactor experience and available quantitative information shows that reaction rates between 304 stainless steel and water, or any contacting metals is negligible at operational temperatures (References 2 and 13).

### 3. Cladding Stress-Strain Limits

For Conditions I and II the stress categories and strength theory presented in the ASME Boiler and Pressure Vessel Code Section III, subsection NG-3000, are used as a general guide. The Code methodology is applied, as with fuel assembly structural design, where possible. For Conditions III and IV code stresses are not limiting. Failures of the burnable poison rods during these conditions must not interfere with reactor shutdown or cooling of the fuel rods.

612 056

The deformation or failure of the control rod cladding must not prevent reactor shutdown or cooling of the fuel rods. A breach in the cladding does not result in serious consequences because the Ag-In-Cd material is relatively inert, and for the  $B_4C$  material it would take months for a significant loss of highly irradiated  $B_4C$  to occur and years for slightly irradiated  $B_4C$  (Reference 13). The mechanical design bases for the control rods are consistent with the loading conditions of the ASME Boiler and Pressure Vessel Code, Section III:

- a. External pressure equal to the Reactor Coolant System operating pressure with appropriate allowance for overpressure transients.
- b. Wear allowance equivalent to 1000 full power reactor trips.
- c. Bending of the rod due to a misalignment in the guide tube.
- d. Forces imposed on the rods during rod drop.
- e. Loads imposed by the accelerations of the control rod drive mechanism.
- f. Radiation exposure during maximum core life.
- g. Temperature effects from room to operating conditions.

The burnable poison assemblies, thimble plug assemblies and source assemblies are static core components. The mechanical design of these components satisfies the following:

- a. Accommodate the differential thermal expansion between the fuel assembly and the core internals.
- b. Maintain positive contact with the fuel assembly and the core internals.

The design evaluation of the core components is discussed in Section 4.2.3.6.

#### 4. Irradiated Behavior of Absorber Material

Operating experience and testing evaluation of the effects of irradiation upon the properties of Ag-In-Cd have shown that in-pile corrosion behavior is similar to out-of-pile behavior and that, for low oxygen content water, corrosion rates are low (Reference 2).

The major differences between irradiated  $B_4C$  and irradiated Ag-In-Cd are irradiation swelling, solubility of highly irradiated  $B_4C$  in the reactor coolant, and gaseous product release.

All of these material properties for  $B_4C$  are appropriately accommodated into the hybrid control rod design (Reference 13).

##### 4.2.1.7 Testing, Irradiation Demonstration and Surveillance

An extensive testing program has been conducted to verify the adequacy of the predicted fuel performance and the design bases. Reference [7], provides a description of the tests performed and a summary of the results.

In addition, an in-plant irradiation demonstration program is in progress. The objectives of this program are to confirm the adequacy of the design and obtain early performance information. Demonstration assemblies will be inserted in operating reactors and will be subjected to normal operating conditions for a planned three cycles of operation.

On-site examination of the demonstration assemblies is possible during refueling outages. These examinations will be planned and scheduled in cooperation with the utility or utilities involved. The scope of these examinations will be chosen as necessary based upon assembly performance. The assemblies are of the removable rod type to permit as detailed an examination as required.

612 058



Upon completion of post-irradiation examinations, the results will be evaluated to assess the performance of the improved fuel assembly and the predicted irradiation effects which were assumed in the design.

Performance of the fuel is indirectly monitored by measurement of the activity of the primary coolant for compliance with Technical Specification values.

A surveillance program (if required) for the improved fuel design could involve visual examination (e.g. television and/or binocular scanning) of selected fuel assemblies from the first plant (or plants) to use a region or core of the design. These programs can be further defined, if necessary, based upon the results of the demonstration program, and the needs and desires of the particular customers involved.

Removable rod type optimized fuel assemblies are not planned for insertion in the initial cores using this improved design.

#### 4.2.2 DESIGN DESCRIPTION

The fuel assembly, fuel rod, and core component design data are given in Table 4.3-1.

Each fuel assembly consists of 264 fuel rods, 24 guide thimble tubes and 1 instrumentation thimble tube are arranged within a supporting structure. The instrumentation thimble is located in the center position and provides a channel for insertion of an incore neutron detector, if the fuel assembly is located in an instrumented core position. The guide thimbles provide channels for insertion of either a rod cluster control assembly, a neutron source assembly, a burnable poison assembly or a thimble plug assembly, depending on the position of the particular fuel assembly in the core. Figure 4.2-1 shows a cross-section of the fuel assembly array, and Figure 4.2-2 shows a fuel assembly full length view. The fuel rods are loaded into the fuel assembly structure so that there is clearance between the fuel rod ends and the top and bottom nozzles.

Each fuel assembly is installed vertically in the reactor vessel and stands upright on the lower core plate, which is fitted with alignment pins to locate and orient the assembly. After all fuel assemblies are set in place, the upper support structure is installed. Alignment pins, built into the upper core plate, engage and locate the upper ends of the fuel assemblies. The upper core plate then bears downward against the holddown springs on the top nozzle of each fuel assembly to hold the fuel assemblies in place.

Visual confirmation of the orientation of the fuel assemblies within the core is provided by an engraved identification number on a corner clamp on the top nozzle, and an indexing hole in the opposite corner clamp.

#### 4.2.2.1 Fuel Rods

The fuel rods consist of uranium dioxide ceramic pellets contained in slightly cold worked Zircaloy-4 tubing which is plugged and seal welded at the ends to encapsulate the fuel. A schematic of the fuel rod is shown in Figure 4.2-3. The fuel pellets are right circular cylinders consisting of slightly enriched uranium dioxide powder which has been compacted by cold pressing and then sintered to the required density. The ends of each pellet are dished slightly to allow greater axial expansion at the center of the pellets.

Void volume and clearances are provided within the rods to accommodate fission gases released from the fuel, differential thermal expansion between the cladding and the fuel, and fuel density changes during irradiation, thus, avoiding overstressing of the cladding or seal welds. Shifting of the fuel within the cladding during handling or shipping prior to core loading is prevented by a stainless steel helical spring which bears on top of the fuel. At assembly the pellets are stacked in the cladding to the required fuel height, the spring is then inserted into the top end of the fuel tube and the end plugs pressed into the ends of the tube and welded. All fuel rods are internally pressurized with helium during the welding process in order to minimize compressive cladding stresses and prevent cladding flattening due to coolant operating pressures.

612 060

#### 4.2.2.2 Fuel Assembly Structure

The fuel assembly structure consists of a bottom nozzle, top nozzle, guide and instrument thimbles, and grids, as shown in Figure 4.2-2.

##### 4.2.2.2.1 Bottom Nozzle

The bottom nozzle serves as the bottom structural element of the fuel assembly and directs the coolant flow distribution to the assembly. The square nozzle is fabricated from Type 304 stainless steel and consists of a perforated plate and four angle legs with bearing plates as shown in Figure 4.2-2. The legs form a plenum for the inlet coolant flow to the fuel assembly. The plate also prevents accidental downward ejection of the fuel rods from the fuel assembly. The bottom nozzle is fastened to the fuel assembly guide thimbles by weld-locked screws which penetrate through the nozzle and mate with a threaded plug in each guide thimble.

Coolant flows from the plenum in the bottom nozzle upward through the penetrations in the plate to the channels between the fuel rods. The penetrations in the plate are positioned between the rows of the fuel rods.

Axial loads (holddown) imposed on the fuel assembly and the weight of the fuel assembly are transmitted through the bottom nozzle to the lower core plate. Indexing and positioning of the fuel assembly is controlled by alignment holes in two diagonally opposite bearing plates which mate with locating pins in the lower core plate. Lateral loads on the fuel assembly are transmitted to the lower core plate through the locating pins.

##### 4.2.2.2.2 Top Nozzle

The top nozzle assembly functions as the upper structural element of the fuel assembly and provides a partial protective housing for the rod cluster control assembly or other core components. It consists of an

612 061

adapter plate, enclosure, top plate, and pads. Holddown springs mounted on the top nozzle as shown in Figure 4.2-2. The springs and bolts are made of Inconel-718, whereas the top nozzle is made of Type 304 stainless steel.

The square adapter plate is provided with round penetrations and semi-circular ended slots to permit the flow of coolant upward through the top nozzle. Other round holes are provided to accept sleeves which are welded to the adapter plate and mechanically attached to the thimble tubes. The ligaments in the plate cover the tops of the fuel rods and prevent their upward ejection from the fuel assembly. The enclosure is a box-like structure which sets the distance between the adapter plate and the top plate. The top plate has a large square hole in the center to permit access for the control rods and the control rod spiders.

Holddown springs are mounted on the top plate and are fastened in place by bolts and clamps located at two diagonally opposite corners. On the other two corners integral pads are positioned which contain alignment holes for locating the upper end of the fuel assembly.

#### 4.2.2.2.3 Guide and Instrument Thimbles

The guide thimbles are structural members which also provide channels for the neutron absorber rods, burnable poison rods, neutron source, or thimble plug assemblies. Each thimble is fabricated from Zircaloy-4 tubing having two different diameters. The tube diameter at the top section provides the annular area necessary to permit rapid control rod insertion during a reactor trip. The lower portion of the guide thimble is swaged to a smaller diameter to reduce diametral clearances and produce a dashpot action near the end of the control rod travel during normal trip operation. Holes are provided on the thimble tube above the dashpot to reduce the rod drop time. The dashpot is closed at the bottom by means of an end plug which is provided with a small flow port to avoid fluid stagnation in the dashpot volume during normal operation. The top end of the guide thimble is fastened to a tubular sleeve by three expansion swages. The sleeve fits into and is welded to the

612 062

top nozzle adapter plate. The lower end of the guide thimble is fitted with an end plug which is then fastened into the bottom nozzle by a welded screw.

Each grid is fastened to the guide thimble assemblies to create an integrated structure. The fastening technique depicted in Figure 4.2-4 and 4.2-5 is used for all but the top and bottom grids in a fuel assembly.

An expanding tool is inserted into the inner diameter of the Zircaloy thimble tube at the elevation of Zircaloy sleeves that have been welded into the inner six Zircaloy grid assemblies. The four lobed tool forces the thimble and sleeve outward to a predetermined diameter, thus joining the two components.

The top grid to thimble attachment is shown in Figure 4.2-6. The stainless steel sleeves are brazed into the Inconel grid assembly. The Zircaloy guide thimbles are fastened to the long sleeves by expanding the two members as shown by Figure 4.2-6. Finally, top ends of the sleeves are welded to the top nozzle adapter plate as shown in Figure 4.2-6.

The bottom grid assembly is joined to the assembly as shown in Figure 4.2-7. The stainless steel insert is spotwelded to the bottom grid and later captured between the guide thimble end plug and the bottom nozzle by means of a stainless steel thimble screw.

The described methods of grid fastening are standard and have been used successfully since the introduction of Zircaloy guide thimbles in 1969.

The central instrumentation thimble of each fuel assembly is constrained by seating in counterbores in each nozzle. This tube is a constant diameter and guides the incore neutron detectors. This thimble is expanded at the top and mid-grids in the same manner as the previously discussed expansion of the guide thimbles to the grids.

#### 4.2.2.2.4 Grid Assemblies

The fuel rods, as shown in Figure 4.2-2, are supported at intervals along their length by grid assemblies which maintain the lateral spacing between the rods. Each fuel rod is supported within each grid by the combination of support dimples and springs. The magnitude of the grid restraining force on the fuel rod is set high enough to minimize possible fretting, without overstressing the cladding at the points of contact between the grids and fuel rods. The grid assemblies also allow axial thermal expansion of the fuel rods without imposing restraint sufficient to develop buckling or distortion of the fuel rods.

Two types of grid assemblies are used in each fuel assembly. Both types consist of individual slotted straps interlocked in an "egg-crate" arrangement. The straps contain spring fingers, support dimples and mixing vanes. One type, used in the high flux region of the fuel assemblies, consists of Zircaloy straps arranged as described above and permanently joined by welding at their points of intersection. This material is primarily chosen for its low neutron absorption properties. The internal straps include mixing vanes which project into the coolant stream and promote mixing of the coolant. The other grid type, located at the ends of the fuel assemblies, does not include mixing vanes on the internal straps. The material of these grid assemblies is Inconel-718, chosen because of its corrosion resistance and high strength. Joining of the individual straps is achieved by brazing at the points of intersection. The outside straps on all grids contain mixing vanes which, in addition to their mixing function, aid in guiding the grids and fuel assemblies past projecting surfaces during handling or during loading and unloading of the core.

#### 4.2.2.3 Core Components

##### 4.2.2.3.1 Rod Cluster Control Assembly

The rod cluster control assemblies are used for shutdown and control purposes to offset fast reactivity changes. Figure 4.2-8 illustrates

the rod cluster control assembly location in the reactor relative to the interfacing fuel assemblies and guide tube assemblies.

A rod cluster control assembly is comprised of a group of individual neutron absorber rods fastened at the top end to a common spider assembly, as illustrated in Figure 4.2-9.

The absorber materials used in the control rod design are either 1) all Ag-In-Cd alloy rods, or 2) boron carbide pellets and Ag-In-Cd alloy slugs. The absorber materials are essentially "black" to thermal neutrons and have sufficient additional resonance absorption to significantly increase their worth. For the all Ag-In-Cd design, the alloy is in the form of extruded rods which are sealed in cold-worked type 304 stainless steel tubes to prevent the absorber material from coming in direct contact with the coolant (Figure 4.2-10). For the  $B_4C$  hybrid design, the  $B_4C$  pellets are stacked on top of the extruded Ag-In-Cd rods, and the absorber materials are sealed in cold-worked stainless steel tubes (Figure 4.2-11). Sufficient diametral and end clearance is provided to accommodate relative thermal expansions and material swelling, as shown in Section 4.2.3.6.

The bottom end plugs are bullet-nosed to reduce the hydraulic drag during reactor trip and to guide smoothly into the dashpot section of the fuel assembly guide thimbles.

The spider assembly is in the form of a central hub with radial vanes supporting fingers from which the absorber rods are suspended. Handling detents and detents for connection to the drive rod assembly are machined into the upper end of the hub. A coil spring inside the spider body absorbs the impact energy at the end of a trip insertion. The radial vanes are joined to the hub by welding and brazing, and the fingers are joined to the vanes by brazing. A centerpost which holds the spring and its retainer is threaded into the hub within the skirt and welded to prevent loosening in service. All components of the spider assembly are made from Types 304 and 308 stainless steel except

612 065

for the retainer which is of 17-4 pH material and the springs which are Inconel-718 alloy.

The absorber rods are fastened securely to the spider. The rods are first threaded into the spider fingers and then pinned to maintain joint tightness, after which the pins are welded in place. The end plug below the pin position is designed with a reduced section to permit flexing of the rods to correct for small misalignments.

The overall length is such that when the assembly is withdrawn through its full travel the tips of the absorber rods remain engaged in the guide thimbles so that alignment between rods and thimbles is always maintained. Since the rods are long and slender, they are relatively free to conform to any small misalignments with the guide thimble.

#### 4.2.2.3.2 Burnable Poison Assembly

Each burnable poison assembly consists of burnable poison rods attached to a holddown assembly. A burnable poison assembly is shown in the composite core component Figure 4.2-12. When needed due to nuclear considerations, burnable poison assemblies are inserted into selected thimbles within fuel assemblies.

The poison rods consist of borosilicate glass tubes contained within Type 304 stainless steel tubular cladding which is plugged and seal welded at the ends to encapsulate the glass. The glass is also supported along the length of its inside diameter by a thin wall tubular inner liner. The top end of the liner is open to permit the diffused helium to pass into the void volume and the liner extends beyond the glass. The liner is flanged at the bottom end to maintain the position of the liner with the glass.

The poison rods in each fuel assembly are grouped and attached together at the top end of the rods to a hold down assembly by a flat perforated retaining plate which fits within the fuel assembly top nozzle and rests

612 066



on the adapter plate. The retaining plate and the poison rods are held down and restrained against vertical motion through a spring pack which is attached to the plate and is compressed by the upper core plate when the reactor upper internals assembly is lowered into the reactor. This arrangement ensures that the poison rods cannot be ejected from the core by flow forces. Each rod is permanently attached to the base plate by a nut which is lock welded into place.

The cladding of the burnable poison rods is slightly cold-worked Type 304 stainless steel. All other structural materials in the assembly are Types 304 or 308 stainless steel except for the springs which are Inconel-718. The borosilicate glass tube provides sufficient boron content to meet the criteria discussed in Subsection 4.3.1.

#### 4.2.2.3.3 Neutron Source Assembly

The purpose of the neutron source assembly is to provide a base neutron level to ensure that the neutron detectors are operational and responding to core multiplication neutrons.

Both primary and secondary neutron source rods are used. The primary source rod, containing a radioactive material (either Californium or Pu-Be), spontaneously emits neutrons during initial core loading and reactor startup. After the primary source rod decays beyond the desired neutron flux level, neutrons are then supplied by the secondary source rod. The secondary source rod contains a stable material (Sb-Be), which is activated by neutron bombardment during reactor operation. The activation results in the subsequent release of neutrons. This becomes a source of neutrons during periods of low neutron flux, such as during refueling and subsequent startups.

Four source assemblies are installed in reactor core: two primary source assemblies and two secondary source assemblies. Each primary source assembly contains one primary source rod and a number of burnable poison rods. Each secondary source assembly contains a symmetrical

612 067

grouping of four secondary source rods. In both types of assemblies locations not filled with source or burnable poison rods contain a thimble plug. The source assemblies are shown in the composite Figure 4.2-12.

The source assemblies contain a holddown assembly identical to that of the burnable poison assembly. The primary and secondary source rods have the same cladding material as the absorber rods. The secondary source rods contain pellets stacked to a height of approximately 88 inches. The primary source rods contain capsules of californium (Pu-Be possible alternate) source material and alumina spacer pellets to position the source material within the cladding. The rods in each assembly are permanently fastened at the top end to a holddown assembly.

The structural members are constructed of Type 304 stainless steel except for the springs. The springs exposed to the reactor coolant are Inconel-718.

#### 4.2.2.3.4 Thimble Plug Assembly

Thimble plug assemblies limit bypass flow through the rod cluster control guide thimbles in fuel assemblies which do not contain either control rods, source rods, or burnable poison rods.

The thimble plug assembly, as shown in the composite Figure 4.2-12, consists of a flat base plate with short rods suspended from the bottom surface and a spring pack assembly. The 24 short rods, called thimble plugs, project into the upper ends of the guide thimbles to reduce the bypass flow. Each thimble plug is permanently attached to the base plate by a nut which is lock-welded to the threaded end of the plug. Similar short rods are also used on the source assemblies and burnable poison assemblies to plug the ends of all vacant fuel assembly guide thimbles. When in the core, the thimble plug assemblies interface with both the upper core plate and with the fuel assembly top nozzles by resting on the adapter plate. The spring pack is compressed by the upper core plate when the upper internals assembly is lowered into place.

612 068

All components in the thimble plug assembly, except for the springs, are constructed from Type 304 stainless steel. The springs are Inconel-718.

#### 4.2.3 DESIGN EVALUATION

The fuel assemblies, fuel rods, and incore control components are designed to satisfy the performance and safety criteria of Section 4.2, the mechanical design bases of Subsection 4.2.1, and other interfacing nuclear and thermal-hydraulic design bases specified in Section 4.3 and 4.4. Effects of Accident Conditions II, III, IV, or Anticipated Transients Without Trip on fuel integrity are presented in the Accident Analysis Chapter or supporting topical reports.

##### 4.2.3.1 Cladding

###### 1. Vibration and Wear

Fuel rod vibrations are flow induced. The effect of the vibration on the fuel assembly and individual fuel rods is minimal. The cyclic stress range associated with deflections of such small magnitude is insignificant and has no effect on the structural integrity of the fuel rod. No significant wear of the cladding or grid supports is expected during the life of the fuel assembly. Fuel vibration has been experimentally investigated as shown in Reference [7].

###### 2. Fuel Rod Internal Pressure and Cladding Stresses

The burnup dependent fission gas release model (Reference 4) is used in determining the internal gas pressures as a function of irradiation time. The fuel rod has been designed to ensure that the maximum internal pressure of the fuel rod will not exceed the value which would cause an increase in the fuel cladding diametral gap or extensive DNB propagation during normal operation.

The cladding stresses at a constant local fuel rod power are low. Compressive stresses are created by the pressure differential between the coolant pressure and the rod internal gas pressure. Because of the pre-pressurization with helium, the volume average effective stresses are always less than approximately 10,000 psi at the pressurization level used in this fuel rod design. Stresses due to the temperature gradient are not included in this average effective stress because thermal stresses are, in general, negative at the cladding inside diameter and positive at the cladding outside diameter and their contribution to the cladding volume average stress is small. Furthermore, the thermal stress decreases with time during steady-state operation due to stress relaxation. The stress due to pressure differential is highest in the minimum power rod at the beginning-of-life due to low internal gas pressure, and the thermal stress is highest in the maximum power rod due to the steep temperature gradient.

The internal gas pressure at beginning-of-life is approximately 1400 psia at operating temperature for a typical lead burnup fuel rod. The total tangential stress at the cladding inside diameter at beginning-of-life is approximately 14,400 psi compressive ( $\sqrt{13,000}$  psi due to  $\Delta P$  and  $\sqrt{1,400}$  due to  $\Delta T$ ) for a low power rod, operating at 5 kW/ft, and approximately 12,000 psi compressive ( $\sqrt{8,500}$  psi due to  $\Delta P$  and 3,500 psi due to  $\Delta T$ ) for a high power rod operating at 15 kW/ft. However, the volume average effective stress at beginning-of-life is between approximately 8,000 psi (high power rod) and approximately 10,000 psi (low power rod). These stresses are substantially below even the unirradiated cladding strength ( $\sqrt{55,500}$  psi) at a typical cladding mean operating temperature of 700<sup>0</sup>F.

Tensile stresses could be created once the cladding has come in contact with the pellet. These stresses would be induced by the fuel pellet swelling during irradiation. Fuel swelling can result in small cladding strains (< 1% for expected discharge burnups but

the associated cladding stresses are very low because of cladding creep (thermal and irradiation-induced creep). The 1% strain criterion is extremely conservative for fuel-swelling driven cladding strain because the strain rate associated with solid fission products swelling is very slow.

### 3. Materials and Chemical Evaluation

Zircaloy-4 cladding has a high corrosion resistance to the coolant, fuel and fission products. As shown in Reference [1], there is considerable PWR operating experience on the capability of Zircaloy as a cladding material. Controls on fuel fabrication specify maximum moisture levels to preclude cladding hydriding.

Metallographic examination of irradiated commercial fuel rods have shown occurrences of fuel/clad chemical interaction. Reaction layers of < 1 mil in thickness have been observed between fuel and clad at limited points around the circumference. Metallographic data indicates that this interface layer remains very thin even at high burnup. Thus, there is no indication of propagation of the layer and eventual cladding penetration.

### 4. Fretting

Cladding fretting has been experimentally investigated as shown in Reference [7]. No significant fretting of the cladding is expected during the life of the fuel assembly.

### 5. Stress Corrosion

Stress corrosion cracking is another postulated phenomenon related to fuel/clad chemical interaction. Out-of-pile tests have shown that in the presence of high cladding tensile stresses, large concentrations of selected fission products (such as iodine) can chemically attack the Zircaloy tubing and can lead to eventual cladding

cracking. Extensive post-irradiation examination has produced no in-pile evidence that this mechanism is operative in commercial fuel.

## 6. Cycling and Fatigue

A comprehensive review of the available strain-fatigue models was conducted by Westinghouse as early as 1968. This review included the Langer-O'Donnell model (Reference 8), the Yao-Munse model, and the Manson-Halford model. Upon completion of this review and using the results of the Westinghouse experimental programs discussed below, it was concluded that the approach defined by Langer-O'Donnell would be retained and the empirical factors of their correlation modified in order to conservatively bound the results of the Westinghouse testing program.

The Westinghouse testing program was subdivided into the following subprograms:

- a. A rotating bend fatigue experiment on unirradiated Zircaloy-4 specimens at room temperature and at 725<sup>0</sup>F. Both hydrided and nonhydrided Zircaloy-4 cladding were tested.
- b. A biaxial fatigue experiment in gas autoclave on unirradiated Zircaloy-4 cladding, both hydrided and nonhydrided.
- c. A fatigue test program on irradiated cladding from the CVS and Yankee Core V conducted at Battelle Memorial Institute.

The results of these test programs provided information on different cladding conditions including the effect of irradiation, of hydrogen level, and of temperature.

The design equations followed the concept for the fatigue design criterion according to the ASME Boiler and Pressure Vessel Code, Section III.

612 072

It is recognized that a possible limitation to the satisfactory behavior of the fuel rods in a reactor which is subjected to daily load follow is the failure of the cladding by low cycle strain fatigue. During their normal residence time in reactor, the fuel rods may be subjected to  $\sim 1000$  cycles with typical changes in power level from 50 to 100% of their steady-state values.

The assessment of the fatigue life of the fuel rod cladding is subject to a considerable uncertainty due to the difficulty of evaluating the strain range which results from the cyclic interaction of the fuel pellets and cladding. This difficulty arises, for example, from such highly unpredictable phenomena as pellet cracking, fragmentation, and relocation. Nevertheless, since early 1968, this particular phenomenon has been investigated analytically and experimentally. Strain fatigue tests on irradiated and nonirradiated hydrided Zr-4 claddings were performed which permitted a definition of a conservative fatigue life limit and recommendation on a methodology to treat the strain fatigue evaluation of the Westinghouse reference fuel rod designs.

It is believed that the final proof of the adequacy of a given fuel rod design to meet the load follow requirements can only come from incore experiments performed on actual reactors. Experience in load follow operation dates back to early 1970 with the load follow operation of the Saxton reactor. Successful load follow operation has been performed on reactor A (>400 load follow cycles) and reactor B (>500 load follow cycles). In both cases, there was no significant coolant activity increase that could be associated with the load follow mode of operation.

612 073

## 7. Rod Bowing

The NRC has approved a revised rod bow correlation<sup>(14)</sup> for standard 17 x 17 fuel assemblies, based upon data evaluated from 17 x 17 demonstration assemblies. The rod bow behavior of the optimized fuel assemblies is expected to be better than that of the standard 17 x 17 assemblies. The most probable causes of significant rod bow are believed to be grid and pellet-clad interaction forces. The optimized fuel assembly will have reduced grid forces (due to zircaloy grids) and a higher fuel tube thickness-to-diameter ratio (t/d) than the standard assembly, both of which are expected to decrease rod bow.

For comparison purposes, rod bow for the 17 x 17 optimized fuel assemblies is predicted based on the current conservative NRC position<sup>(15)</sup> for comparing two different designs. That is, with equivalent span lengths between grids for the standard and optimized fuel assemblies, a comparison of  $1/I$  ( $I$  = fuel rod bending moment of inertia) and initial rod-to-rod gap for each assembly type show that the fractional closure at any given burnup is essentially the same in both cases. The  $1/I$  ratio is higher for the optimized fuel assembly, but the initial rod-to-rod gap is also larger.

Thus, for a given burnup, the rod bow effects to be applied to the optimized fuel assemblies are the same as that applied to the standard 17 x 17 fuel.

## 8. Consequences of Power-Coolant Mismatch

This subject is discussed in Chapter 15.0.

612 074



## 9. Irradiation Stability of the Cladding

As shown in Reference [1], there is considerable PWR operating experience on the capability of Zircaloy as a cladding material. Extensive experience with irradiated Zircaloy-4 is summarized in Reference [2].

## 10. Creep Collapse and Creepdown

This subject and the associated irradiation stability of cladding have been evaluated using the models described in Reference [5]. It has been established that the design basis of no clad collapse during planned core life can be satisfied by limiting fuel densification, and by having a sufficiently high initial internal rod pressure.

### 4.2.3.2 Fuel Material Consideration

#### 1. Dimensional Stability of the Fuel

The mechanical design of the fuel rods accounts for the differential thermal expansion of the fuel and the cladding, and for the pellets densification effect.

#### 2. Potential for Chemical Interaction

Sintered, high density uranium dioxide fuel reacts only slightly with the cladding at core operating temperatures and pressures. In the event of cladding defects, the high resistance of uranium dioxide to attack by water protects against fuel deterioration, although limited fuel erosion can occur. The effects of water-logging on fuel behavior are discussed in Section 4.2.3.3.

612 075

### 3. Thermal Stability

As has been shown by operating experience and extensive experimental work, the thermal design parameters conservatively account for changes in the thermal performance of the fuel elements due to pellet fracture which may occur during power operation. Observations from several operating Westinghouse PWR's (Reference 6) have shown that fuel pellets can densify under irradiation to a density higher than the manufactured values. Fuel densification and subsequent settling of the fuel pellets can result in local and distributed gaps in the fuel rods. Fuel densification has been minimized by improvements in the fuel manufacturing process and by specifying a nominal 95% initial fuel density.

The evaluation of fuel densification effects and their consideration in fuel design are described in References [3 and 4].

### 4. Irradiation Stability

The treatment of fuel swelling and fission gas release are described in Reference [4].

#### 4.2.3.3 Fuel Rod Performance

The initial step in fuel rod design evaluation for a region of fuel is to determine the limiting rod(s). Limiting rods are defined as those rod(s) whose predicted performance provides the minimum margin to each of the design criteria. For a number of design criteria the limiting rod is the lead burnup rod of a fuel region. In other instances it may be the maximum power or the minimum burnup rod. For the most part, no single rod will be limiting with respect to all design criteria.

After identifying the limiting rod(s), a worst-case evaluation is made which utilizes the limiting rod design basis power history and considers the effects of model uncertainties and dimensional variations. Furthermore, to verify adherence to the design criteria, the conservative case

evaluation also considers the effects of postulated transient power increases which are achievable during operation consistent with Conditions I and II. These transient power increases can affect both rod average and local power levels. The analytical methods used in the evaluation result in performance parameters which demonstrate the fuel rod behavior. Examples of parameters considered include rod internal pressure, fuel temperature, cladding stress, and cladding strain. In fuel rod design analyses these performance parameters provide the basis for comparison between expected fuel rod behavior and the corresponding design criteria limits.

In calculating the steady-state performance of a nuclear fuel rod, the following interacting factors are considered:

1. Cladding creep and elastic deflection;
2. Pellet density changes, thermal expansion, gas release, and thermal properties as a function of temperature and fuel burnup; and
3. Internal pressure as a function of fission gas release, rod geometry, and temperature distribution.

These effects are evaluated using a fuel rod design model (Reference 4). The model modifications for time dependent fuel densification are given in References [3 and 4]. With these interacting factors considered, the model determines the fuel rod performance characteristics for a given rod geometry, power history, and axial power shape. In particular, internal gas pressure, fuel and cladding temperatures, and cladding deflections are calculated. The fuel rod is divided into several axial sections and radially into a number of annular zones. Fuel density changes are calculated separately for each segment. The effects are integrated to obtain the internal rod pressure.

The initial rod internal pressure is selected to delay fuel/clad mechanical interaction and to avoid the potential for flattened rod formation. It is limited, however, by the design criteria for the rod internal pressure given in Subsections 4.2.1.3 and 4.2.3.1.b

The gap conductance between the pellet surface and the cladding inner diameter is calculated as a function of the composition, temperature, and pressure of the gas mixture, and the gap size or contact pressure between cladding and pellet. After computing the fuel temperature for each pellet annular zone, the fractional fission gas release is assessed using an empirical model derived from experimental data (Reference 4). The total amount of gas released is based on the average fractional release within each axial and radial zone and the gas generation rate which in turn is a function of burnup. Finally, the gas released is summed over all zones and the pressure is calculated.

The code shows good agreement and fit for a variety of published and proprietary data on fission gas release, fuel temperatures, and cladding deflections (Reference 4). Included in this spectrum are variations in power, time, fuel density and geometry. In-pile fuel temperature measurement comparisons are shown in Reference[4].

a. Fuel-Cladding Mechanical Interaction

One factor in fuel element duty is potential mechanical interaction of fuel and cladding. This fuel/clad interaction produces cyclic stresses and strains in the cladding, and these in turn consume clad fatigue life. The reduction of fuel/clad interaction is therefore a goal of design. In order to achieve this goal and to enhance the cyclic operational capability of the fuel rod, the technology for using pre-pressurized fuel rods in Westinghouse PWR's has been developed.

Initially, the gap between the fuel and cladding is sufficient to prevent hard contact between the two. However, during power operation a gradual compressive creep of the cladding onto the

fuel pellet occurs due to the external pressure exerted on the rod by the coolant. Cladding compressive creep eventually results in the fuel/clad contact. During this period of fuel/clad contact, changes in power level could result in changes in cladding stresses and strains. By using pre-pressurized fuel rods to partially offset the effect of the coolant external pressure, the rate of cladding creep toward the surface of the fuel is reduced. Fuel rod pre-pressurization delays the time at which fuel/clad contact occurs and hence, significantly reduces the number and extent of cyclic stresses and strains experienced by the cladding both before and after fuel/clad contact. These factors result in an increase in the fatigue life margin of the cladding and lead to greater cladding reliability. If gaps should form in the fuel stacks, cladding flattening will be prevented by the rod pre-pressurization so that the flattening time will be greater than the fuel core life.

A two dimensional  $(r,\theta)$  finite element model has been developed to investigate the effects of radial pellet cracks on stress concentrations in the cladding. Stress concentration, herein, is defined as the difference between the maximum cladding stress in the  $\theta$ -direction and the mean cladding stress. The first case has the fuel and cladding in mechanical equilibrium and as a result the stress in the cladding is close to zero. In subsequent cases the pellet power is increased in steps and the resultant fuel thermal expansion imposes tensile stress in the cladding. In addition to uniform cladding stresses, stress concentrations develop in the cladding adjacent to radial cracks in the pellet. These radial cracks have a tendency to open during a power increase but the frictional forces between fuel and cladding oppose the opening of these cracks and result in localized increases in cladding stress. As the power is further increased, and large tensile stresses exceed the ultimate tensile strength of  $UO_2$ , additional cracks in the fuel are created which limit the magnitude of the stress concentration in the cladding.

As part of the standard fuel rod design analysis, the maximum stress concentration evaluated from finite element calculations is added to the volume average effective stress in the cladding as determined from one dimensional stress/strain calculations. The resultant cladding stress is then compared to the temperature dependent Zircaloy yield stress in order to assure that the stress/strain criteria are satisfied.

Pellet thermal expansion due to power increases is considered the only mechanism by which significant stresses and strains can be imposed on the cladding. Power increases in commercial reactors can result from fuel shuffling, reactor power escalation following extended reduced power operation, and control rod movement. In the mechanical design model, lead rods are depleted using best estimate power histories as determined by core physics calculations. During the depletion, the amount of diametral gap closure is evaluated based upon the pellet expansion-cracking model, cladding creep model, and fuel swelling model. At various times during depletion, the power is increased locally on the rod to the burnup dependent attainable power density, as determined by core physics calculations. The radial, tangential, and axial cladding stresses resulting from the power increase are combined into a volume average effective cladding stress.

The von Mises criterion is used to evaluate whether the cladding yield stress has been exceeded. The yield stress correlation is that for irradiated cladding since fuel/clad interaction occurs at high burnup. Furthermore, the effective stress is increased by an allowance, which accounts for stress concentrations in the cladding adjacent to radial cracks in the pellet, prior to the comparison with the yield stress. This allowance was evaluated using a two-dimensional  $(r,\theta)$  finite element model.

612 080

Slow transient power increases can result in large cladding strains without exceeding the cladding yield stress because of cladding creep and stress relaxation. Therefore, in addition to the yield stress criterion, a criterion on allowable cladding strain is necessary. Based upon high strain rate burst and tensile test data on irradiated tubing, 1% strain was determined to be a conservative lower limit for irradiated cladding ductility and thus adopted as a design criterion.

b. Irradiation Experience

Westinghouse fuel operational experience is presented in Reference [1]. Additional test assembly and test rod experiences are given in Section 8 and 23 of Reference [6].

c. Fuel and Cladding Temperature

The methods used for evaluation of fuel rod temperatures are presented in Subsection 4.4.2.11.

d. Water-logging

Local cladding deformations typical of water-logging\* bursts have never been observed in commercial Westinghouse fuel. Experience has shown that the small number of rods which have acquired cladding defects, regardless of primary mechanism, remain intact and do not progressively distort or restrict coolant flow. In fact such small defects are normally observed through reductions in coolant activity to be progressively

---

\* Water-logging damage of a previously defected fuel rod has occasionally been postulated as a mechanism for subsequent rupture of the cladding. Such damage has been postulated as a consequence of a power increase on a rod after water has entered such a rod through a cladding defect of appropriate size. Rupture is postulated upon power increase if the rod internal pressure increase is excessive due to insufficient venting of water to the reactor coolant.

closed upon further operation due to the buildup of zirconium oxide and other substances. Secondary failures which have been observed in defected rods are attributed to hydrogen embrittlement of the cladding. Post-irradiation examinations point to the hydriding failure mechanism rather than a waterlogging mechanism; the secondary failures occur as axial cracks in the cladding and are similar regardless of the primary failure mechanism. Such cracks do not result in flow blockage. Hence, the presence of such fuel, the quantity of which must be maintained below technical specification limits, does not in any way exacerbate the effects of any postulated transients.

Zircaloy clad fuel rods which have failed due to water-logging (Reference 9) indicate that very rapid power transients are required for fuel failure. Normal operational transients are limited to about 40 cal/gm-min. (peak rod), while the Spert tests (Reference 10) indicate that 120 cal/gm to 150 cal/gm are required to rupture the cladding even with very short transients (5.5 milli sec period).

e. Potentially Damaging Temperature Effects During Transients

The fuel rod experiences many operational transients (intentional maneuvers) during its residence in the core. A number of thermal effects must be considered when analyzing the fuel rod performance.

The cladding can be in contact with the fuel pellet at some time in the fuel lifetime. Clad-pellet interaction occurs if the fuel pellet temperature is increased after the cladding is in contact with the pellet. Clad-pellet interaction is discussed in Subsection 4.2.3.3.

The potential effects of operation with water-logged fuel are discussed in Subsection 4.2.3.3 which concluded that water-logging is not a concern during operational transients.



Clad flattening, as shown in Reference [5], has been observed in some operating power reactors. Thermal expansion (axial) of the fuel rod stack against a flattened section of cladding could cause failure of the cladding. This is no longer a concern because cladding flattening is precluded during the fuel residence in the core (see Subsection 4.2.3.1).

Potential differential thermal expansion between the fuel rods and the guide thimbles during a transient is considered in the design. Excessive bowing of the fuel rods is precluded because the grid assemblies allow axial movement of the fuel rods relative to the grids. Specifically, thermal expansion of the fuel rods is considered in the grid design so that axial loads imposed on the fuel rods during a thermal transient will not result in excessively bowed fuel rods.

f. Fuel Element Burnout and Potential Energy Release

As discussed in Subsection 4.4.2.2, the core is protected from DNB over the full range of possible operating conditions. In the extremely unlikely event that DNB should occur, the cladding temperature will rise due to the steam blanketing at the rod surface and the consequent degradation in h. t transfer. During this time there is potential for chemical reaction between the cladding and the coolant. However, because of the relatively good film boiling heat transfer following DNB, the energy release resulting from this reaction is insignificant compared to the power produced by the fuel.

g. Coolant Flow Blockage Effects on Fuel Rods

This evaluation is presented in Subsection 4.4.4.7.

4.2.3.4 Spacer Grids

The coolant flow channels are established and maintained by the structure composed of grids and guide thimbles. The lateral spacing between

fuel rods is provided and controlled by the support dimples of adjacent grid cells. Contact of the fuel rods on the dimples is maintained through the clamping force of the grid springs. Lateral motion of the fuel rods is opposed by the spring force and the internal moments generated between the spring and the support dimples. Grid testing is discussed in Reference [7].

The fuel assembly component stress levels are limited by the grid design. For example, stresses in the fuel rod due to thermal expansion and Zircaloy irradiation growth are limited by the relative motion of the rod as it slips over the grid spring and dimple surfaces.

#### 4.2.3.5 Fuel Assembly

##### 1. Loads Applied by Core Restraint System

The upper core plate bears downward against the fuel assembly top nozzle springs. The springs are designed to accommodate the differential thermal expansion and irradiation growth between the fuel assembly and the core internals.

##### 2. Analysis of Accident Loads

As shown in Reference [7], grid crushing tests and seismic and LOCA evaluations show that the fuel assembly will maintain a geometry that is capable of being cooled under the worst-case accident Condition IV event.

A prototype fuel assembly has been subjected to column loads in excess of those expected in normal service and faulted conditions (Reference 7).

No interference between control rod insertion and thimble tubes will occur during a Safe Shutdown Earthquake (SSE).

612 084

Stresses in the fuel assembly caused by tripping of the rod cluster control assembly have little influence on fatigue because of the small number of events during the life of an assembly. Assembly components and prototype fuel assemblies made from production parts have been subjected to structural tests to verify that the design bases requirements are met (Reference 7).

### 3. Loads Applied in Fuel Handling

The fuel assembly design loads for shipping have been established at 6 g's. Accelerometers are permanently placed into the shipping cask to monitor and detect fuel assembly accelerations that would exceed the criteria. Past history and experience have indicated that loads which exceed the allowable limits rarely occur. Exceeding the limits requires reinspection of the fuel assembly for damage. Tests on various fuel assembly components such as the grid assembly, sleeves, inserts and structure joints have been performed to assure that the shipping design limits do not result in impairment of fuel assembly function.

#### 4.2.3.6 Reactivity Control Assembly and Burnable Poison Rods

##### 1. Internal Pressure and Cladding Stresses During Normal, Transient and Accident Conditions

The designs of the burnable poison, source rods and  $B_4C$  absorber rods provide a sufficient cold void volume to accommodate the internal pressure increase during operation. This is not a concern for the Ag-In-Cd absorber rod because no gas is released by the absorber material.

For the burnable poison rod, the use of glass in tubular form provides a central void volume along the length of the rods. For the source rods, and the  $B_4C$  absorber rod, a void volume is provided in the cladding in order to limit the internal pressure increase until end-of-life (see Figure 4.1-12.)

The stress analysis of the burnable poison end source rods assumes 100 percent gas release to the rod void volume in addition to the initial pressure within the rod. For the  $B_4C$  control rod a 20% gas release is assumed.

During normal transient and accident conditions the void volume limits the internal pressures to values which satisfy the criteria in Section 4.2.1.6.

These limits are established not only to assure that peak stresses do not reach unacceptable values, but also limit the amplitude of the oscillatory stress component in consideration of the fatigue characteristics of the materials.

Rod, guide thimble, and dashpot flow analyses indicate that the flow is sufficient to prevent coolant boiling. Therefore, clad temperatures at which the clad material has adequate strength to resist coolant operating pressures and rod internal pressures are maintained.

## 2. Thermal Stability of the Absorber Material, Including Phase Changes and Thermal Expansion

The radial and axial temperature profiles have been determined by considering gap conductance, thermal expansion, and neutron or gamma heating of the contained material as well as gamma heating of the clad.

The maximum temperature of the absorber material was calculated to be less than  $850^{\circ}F$  for Ag-In-Cd and less than  $1200^{\circ}F$  for  $B_4C$  and occurs axially at only the highest flux region. This temperature is well below the absorber melting temperature bases of Section 4.2.1.6.a. The thermal expansion properties of the absorber material and the phase changes are discussed in Reference 2 and 13.

612 086

The maximum temperature of the borosilicate glass was calculated to be about 1300<sup>0</sup>F and takes place following the initial rise to power. As the operating cycle proceeds the glass temperature decreases for the following reasons: 1) reduction in power generation due to boron 10 depletion, 2) better gap conductance as the helium produced diffuses to the gap, and 3) external gap reduction due to borosilicate glass creep.

Sufficient diametral and end clearances have been provided in the neutron absorber, burnable poison, and source rods to accommodate the relative thermal expansions between the enclosed material and the surrounding clad and end plug.

3. Irradiation Stability of the Absorber Material, Taking into Consideration Gas Release and Swelling

The irradiation stability of the absorber material is discussed in References [2 and 13]. Irradiation produces no deleterious effects in the absorber material.

Gas release is not a concern for the absorber rod because no gas is released by the absorber material. Sufficient diametral and end clearances are provided to accommodate swelling of the absorber material.

Based on experience with borosilicate glass, and on nuclear and thermal calculations, gross swelling or cracking of the glass tubing is not expected during operation. Some minor creep of the glass at the hot spot, on the inner surface of the tube, could occur but would continue only until the glass came in contact with the inner liner. The wall thickness of the inner liner is sized to provide adequate support in the event of slumping, and to collapse locally before rupture of the exterior cladding if unexpected large volume changes, due to swelling or cracking, should occur. The ends of the inner liner are open to allow helium, which diffuses out of the glass, to occupy the central void.

612 087

#### 4. Potential for Chemical Interaction

The structural materials selected have good resistance to irradiation damage and are compatible with the reactor environment.

Corrosion of the materials exposed to the coolant is quite low and proper control of chloride and oxygen in the coolant will prevent the occurrence of stress corrosion. The potential for interference with rod cluster control movement due to possible corrosion phenomena is very low.

#### 4.2.4 TESTING AND INSPECTION PLAN

##### 4.2.4.1 Quality Assurance Program

The Quality Assurance Program Plan of the Westinghouse Nuclear Fuel Division, as summarized in Reference [11], has been developed to serve the division in planning and monitoring its activities for the design and manufacture of nuclear fuel assemblies and associated components.

The program provides for control over all activities affecting product quality, commencing with design and development and continuing through procurement, materials handling, fabrication, testing and inspection, storage, and transportation. The program also provides for the indoctrination and training of personnel and for the auditing of activities affecting product quality through a formal auditing program.

Westinghouse drawings and product, process, and material specifications identify the inspections to be performed.

##### 4.2.4.2 Quality Control

Quality control philosophy is generally based on the following inspections being performed to a 95% confidence that at least 95% of the product meets specification, unless otherwise noted.

612 083

## 1. Fuel System Components and Parts

The characteristics inspected depend upon the component parts and include dimensions, visual appearance, audits of test reports, material certification, and nondestructive examination such as X-ray and ultrasonic.

All material used is accepted and released by Quality Control.

## 2. Pellets

Inspection is performed for dimensional characteristics such as diameter, density, length, and squareness of ends. Additional visual inspections are performed for cracks, chips, and surface conditions according to approved standards.

Density is determined in terms of weight per unit length and is plotted on zone charts used in controlling the process. Chemical analyses are taken on a specified sample basis throughout pellet production.

## 3. Rod Inspection

Fuel rod, control rod, burnable poison and source rod inspection consists of the following nondestructive examination techniques and methods, as applicable.

### a. Leak Testing

Each rod is tested using a calibrated mass spectrometer with helium being the detectable gas.

### b. Enclosure Welds

All weld enclosures are X-rayed using weld correction forms. X-rays are taken in accordance with Westinghouse specifications meeting the requirements of ASTM E-142.

c. Dimensional

All fuel rods are dimensionally inspected prior to final release. The requirements include such items as length, camber, and visual appearance.

d. Plenum Dimensions

All fuel rods are inspected by fluoroscope, X-ray, or other approved methods as discussed in Subsection 4.2.4.4 to ensure proper plenum dimensions.

e. Pellet-to-Pellet Gaps

All fuel rods are inspected by fluoroscope, gamma scanning, or other methods as discussed in Subsection 4.2.4.4 to ensure that no significant gaps exist between pellets.

f. All fuel rods are active gamma scanned to verify enrichment control prior to acceptance for assembly loading.

g. Traceability

Traceability of rods and associated rod components is established by Quality Control.

4. Assemblies

Each fuel, control, burnable poison, and source rod assembly is inspected for compliance with drawing and/or specification requirements. Other core component inspection and specification requirements are given in Subsection 4.2.4.3.

5. Other Inspections

The following inspections are performed as part of the routine inspection operation:



- a. Tool and gage inspection and control including standardization to primary and/or secondary working standards. Tool inspection is performed at prescribed intervals on all serialized tools.

Complete records are kept of calibration and conditions of tools.

- b. Audits are performed of inspection activities and records to assure that prescribed methods are followed and that records are correct and properly maintained.
- c. Surveillance inspection where appropriate, and audits of outside contractors are performed to ensure conformance with specified requirements.

#### 6. Process Control

To prevent the possibility of mixing enrichments during fuel manufacture and assembly, strict enrichment segregation and other process controls are exercised.

The  $UO_2$  powder is kept in sealed containers. The contents are fully identified both by descriptive tagging and preselected color coding. A Westinghouse identification tag completely describing the contents is affixed to the containers before transfer to powder storage. Isotopic content is confirmed by analysis.

Powder withdrawal from storage can be made by only one authorized group, which directs the powder to the correct pellet production line. All pellet production lines are physically separated from each other and pellets of only a single nominal enrichment and density are produced in a given production line at any given time.

Finished pellets are placed on trays identified with the same color code as the powder containers and transferred to segregated storage racks within the confines of the pelleting area. Samples from each pellet lot are tested for isotopic content and impurity levels prior

to acceptance by Quality Control. Physical barriers prevent mixing of pellets of different nominal densities and enrichments in this storage area. Unused powder and substandard pellets are returned to storage in the original color coded containers.

Loading of pellets into the cladding is performed in isolated production lines and again only one density and enrichment is loaded on a line at a time.

A serialized traceability code is placed on each fuel tube which identifies the enrichment. The end plugs are inserted; the bottom end plug is permanently identified to the enrichment; and the end plugs are then inert welded to seal the tube. The fuel tube remains coded, and traceability identified until just prior to installation in the fuel assembly. The traceability code and end plug identification character provide a cross reference of the fuel contained in the fuel rods.

At the time of installation into an assembly, the traceability codes are removed and a matrix is generated to identify each rod in its position within a given assembly. After the fuel rods are installed, an inspector verifies that all fuel rods in an assembly carry the correct identification character describing the fuel enrichment and density for the core region being fabricated. The top nozzle is inscribed with a permanent identification number providing traceability to the fuel contained in the assembly.

Similar traceability is provided for burnable poison, source and control rods as required.

#### 4.2.4.3 Core Component Testing and Inspection

Tests and inspections are performed on each core component to verify the mechanical characteristics. In the case of the rod cluster control assembly, prototype testing has been conducted and both manufacturing test/inspections and functional testing at the plant site are performed.

612 092

During the component manufacturing phase, the following requirements apply to the core components to assure the proper functioning during reactor operation:

1. All materials are procured to specifications to attain the desired standard of quality.
2. Each spider is proof tested by applying a 5000 pound load to the spider body, so that approximately 310 pounds is applied to each vane. This proof load provides a bending moment at the spider body approximately equivalent to 1.4 times the load caused by the acceleration imposed by the control rod drives mechanism.
3. All rods are checked for integrity by the methods described in Sub-section 4.2.4.2.c.
4. To assure proper fitup with the fuel assembly, the rod cluster control, burnable poison, and source assemblies are installed in the fuel assembly without restriction or binding in the dry condition. Also a straightness of 0.01 in/ft is required on the entire inserted length of each rod assembly.

The rod cluster control assemblies are functionally tested, following core loading but prior to criticality to demonstrate reliable operation of the assemblies. Each assembly is operated (and tripped) one time at no flow/cold conditions and one time at full flow/hot conditions. In addition, selected assemblies, amounting to about 15 to 20% of the total assemblies are operated at no flow/operating temperature conditions and full flow/ambient conditions. Also the slowest rod and the fastest rod are tripped 10 times at no flow/ambient conditions and at full flow/operating temperature conditions. Thus, each assembly is tested a minimum of 2 times or up to a maximum of 14 times to ensure the assemblies are properly functioning.

In order to demonstrate continuous free movement of the rod cluster control assemblies, and to ensure acceptable core power distributions during operations, partial movement checks are performed on the rod

cluster control assemblies as required by the Technical Specifications. In addition, periodic drop tests of the rod cluster control assemblies are performed at each refueling shutdown to demonstrate continued ability to meet trip time requirements, to ensure core subcriticality after reactor trip, and to limit potential reactivity insertions from a hypothetical rod cluster control assembly ejection.

If a rod cluster control assembly cannot be moved by its mechanism, adjustments in the boron concentration ensure that adequate shutdown margin would be achieved following a trip. Thus, inability to move one rod cluster control assembly can be tolerated. More than one inoperable rod cluster control assembly could be tolerated, but would impose additional demands on the plant operator. Therefore, the number of inoperable rod cluster control assemblies has been limited to one.

#### 4.2.4.4 Tests and Inspections by Others

If any tests and inspections are to be performed on behalf of Westinghouse, Westinghouse will review and approve the quality control procedures, inspection plans, etc. to be utilized to ensure that they are equivalent to the description provided above and are performed properly to meet all Westinghouse requirements.

#### 4.2.4.5 Onsite Inspection

(This section provided by the Applicant).

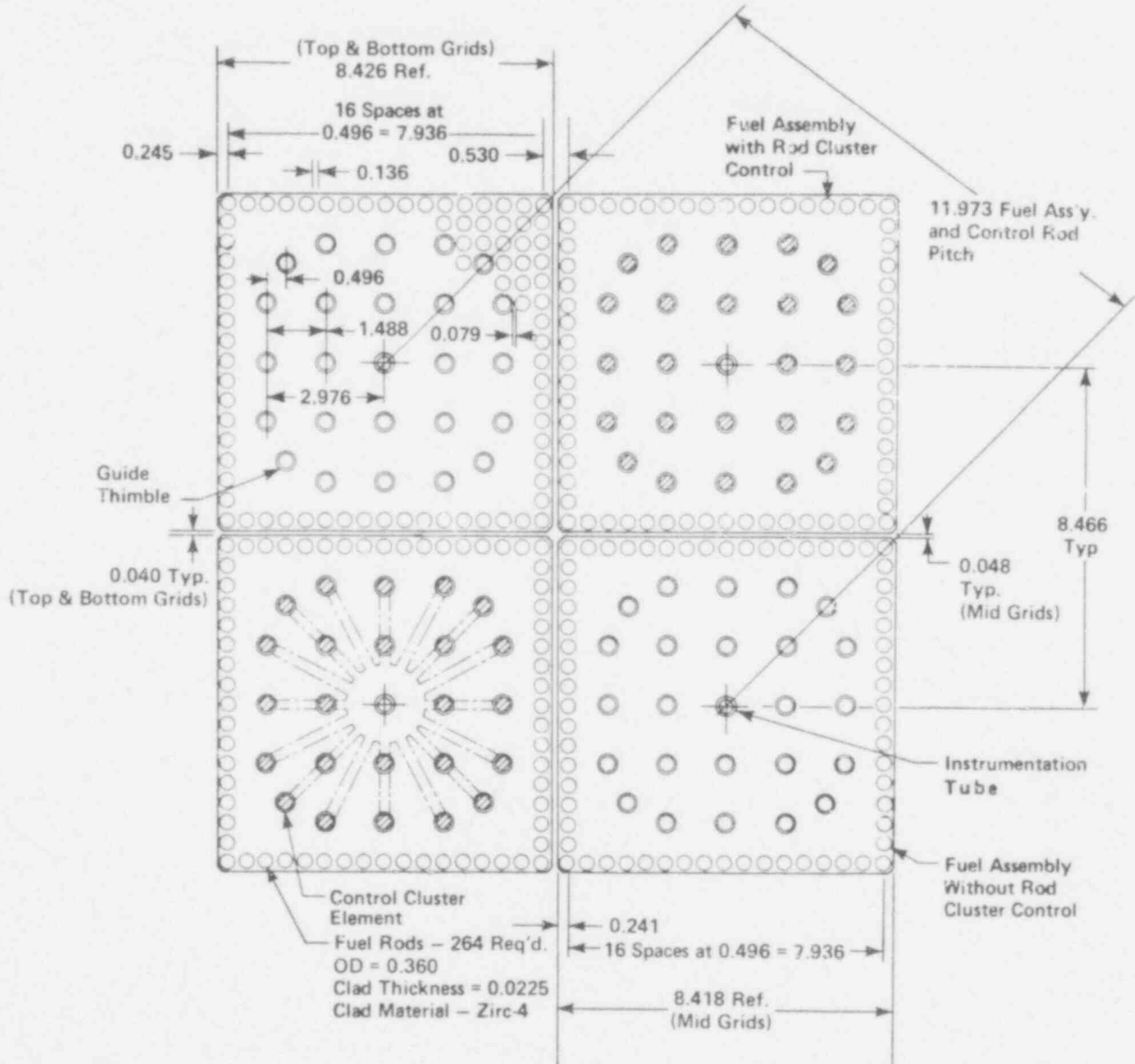
#### 4.2.5 REFERENCES

1. O'Hara, T. L., et. al., "Operational Experience with Westinghouse Cores," WCAP-8183, (Latest Revision).
2. Beaumont, M. D., et. al., (Ed.), Properties of Fuel and Core Component Materials," WCAP-9179, Revision 1 (Proprietary) and WCAP-9224, July, 1978.

3. Hellman, J. M., (Ed.), "Fuel Densification Experimental Results and Model for Reactor Operation," WCAP-8218-P-A, March 1975 (Proprietary) and WCAP-8219-A, March 1975.
4. Miller, J. V., (Ed.), "Improved Analytical Models Used in Westinghouse Fuel Rod Design Computations," WCAP-8785, October 1976.
5. George, R. A., et. al., "Revised Clad Flattening Model," WCAP-8377 (Proprietary) and WCAP-8381, July 1974.
6. Eggleston, F., "Safety Related Research and Development for Westinghouse Pressurized Water Reactors - Program Summaries, WCAP-8758, Revision 2, October 1978.
7. Beaumont, M. D., et. al., (Ed.), "Verification Testing and Analyses of the 17x17 Optimized Fuel Assembly," WCAP-9401 (Proprietary) and WCAP-9402, March 1979.
8. O'Donnell, W. J. and Langer, B. F., "Fatigue Design Basis for Zircaloy Components," Nuclear Science and Engineering, 20, 1-12, 1964.
9. Western New York Nuclear Research Center Correspondence with the AEC on February 11 and August 27, 1971, Docket 50-57.
10. Stephan, L. A., "The Effects of Cladding Material and Heat Treatment on the Response of Waterlogged UO<sub>2</sub> Fuel Rods to Power Bursts," IN-ITR-111, January 1970.
11. Dollard, W. J., "Nuclear Fuel Division Quality Assurance Program Plan," WCAP-7800, Revision 4-A, April 1975.
12. Risher, D. et. al., "Safety Analysis for the Revised Fuel Rod Internal Pressure Design Basis," WCAP-8963 (Proprietary), November 1976, WCAP-8964, August 1977.
13. Skaritka, J. (Ed.), "Hybrid B<sub>4</sub>C Absorber Control Rod Evaluation Report," WCAP-8846-A, October 1977.

14. Letter from T. M. Anderson (Westinghouse) to J. F. Stolz (NRC),  
Subject: Fuel Rod Bowing, NS-TMA-1760, April 19, 1978.
  
15. "Internal Safety Evaluation Report on Effects of Fuel Rod Bowing on  
Thermal Margin Calculations for Light Water Reactors," Revision 1,  
USNRC, February 16, 1977.

612 096

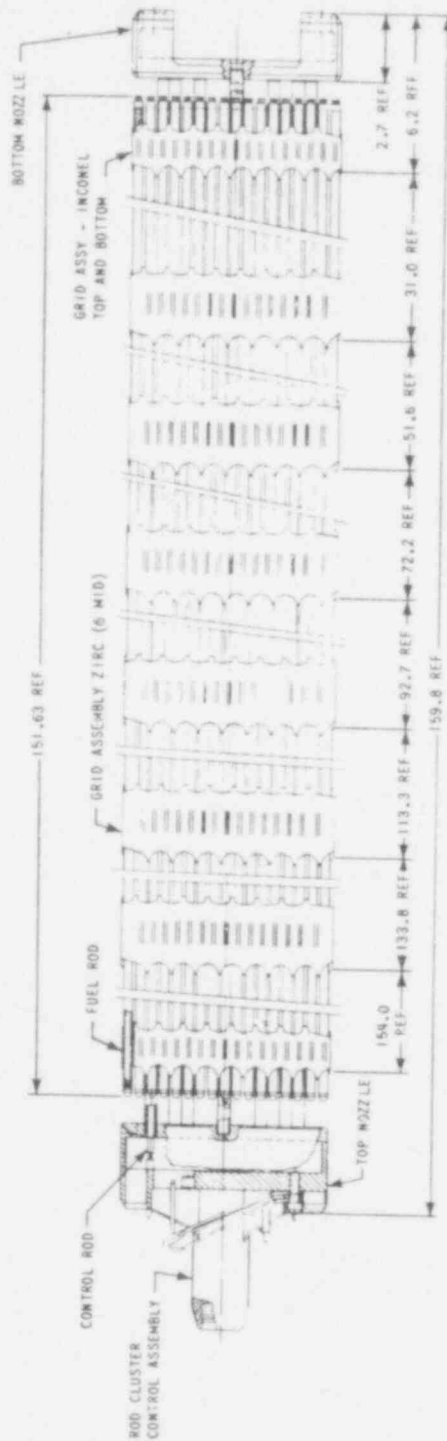
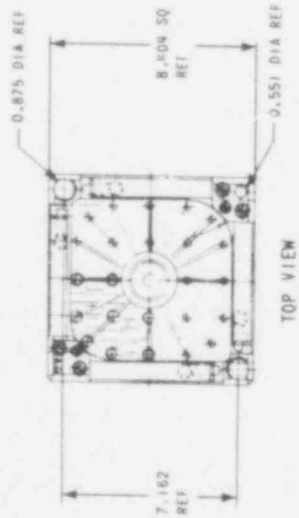
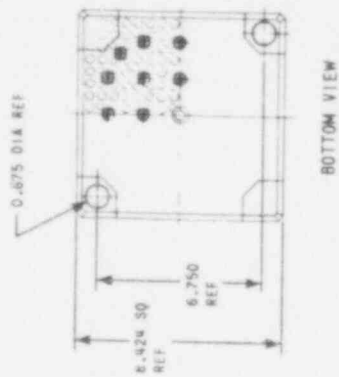


612 097

WCAP - 9500

Figure 4.2-1.

17 X 17 Optimized Fuel Assembly Cross Section



POOR ORIGINAL

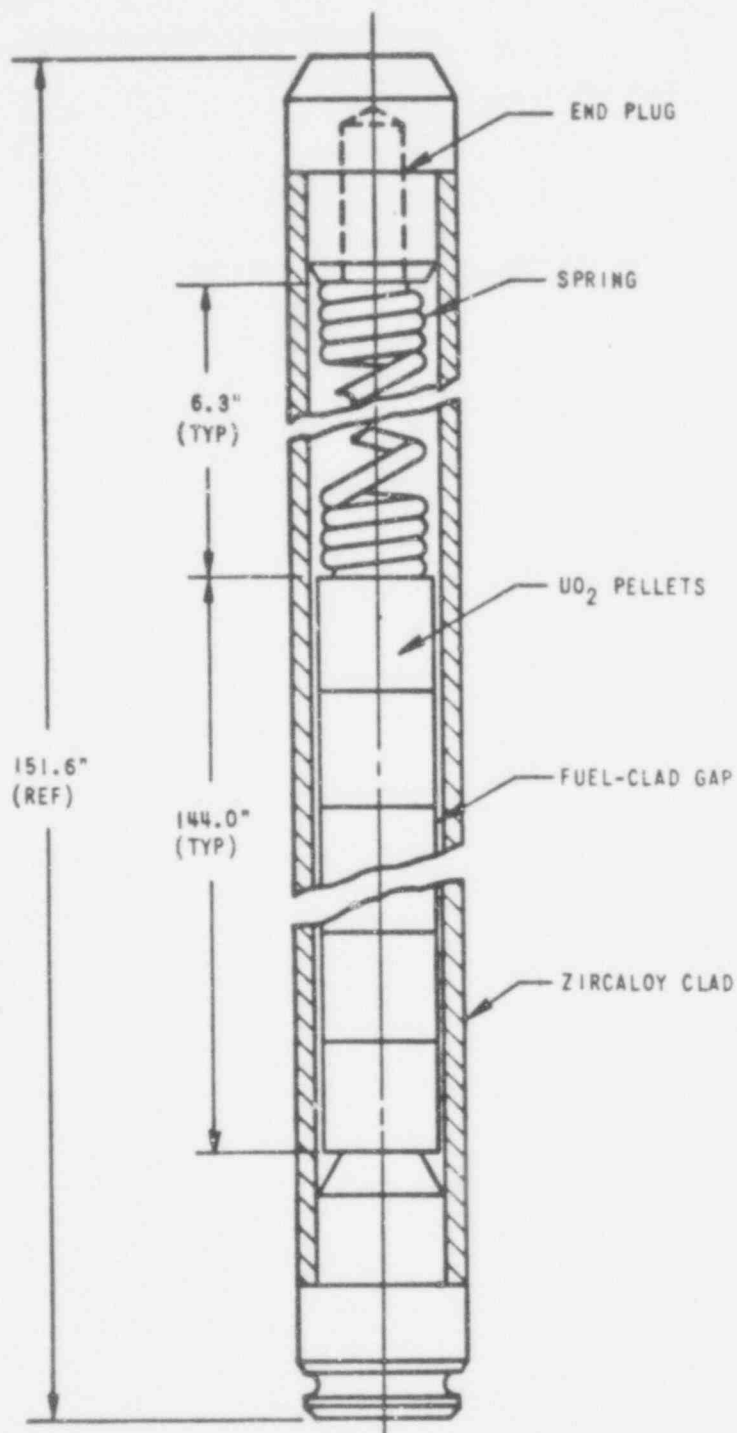
WCAP-9500

Figure 4.2-2.

17 X 17 Optimized Fuel Assembly Outline

612 098



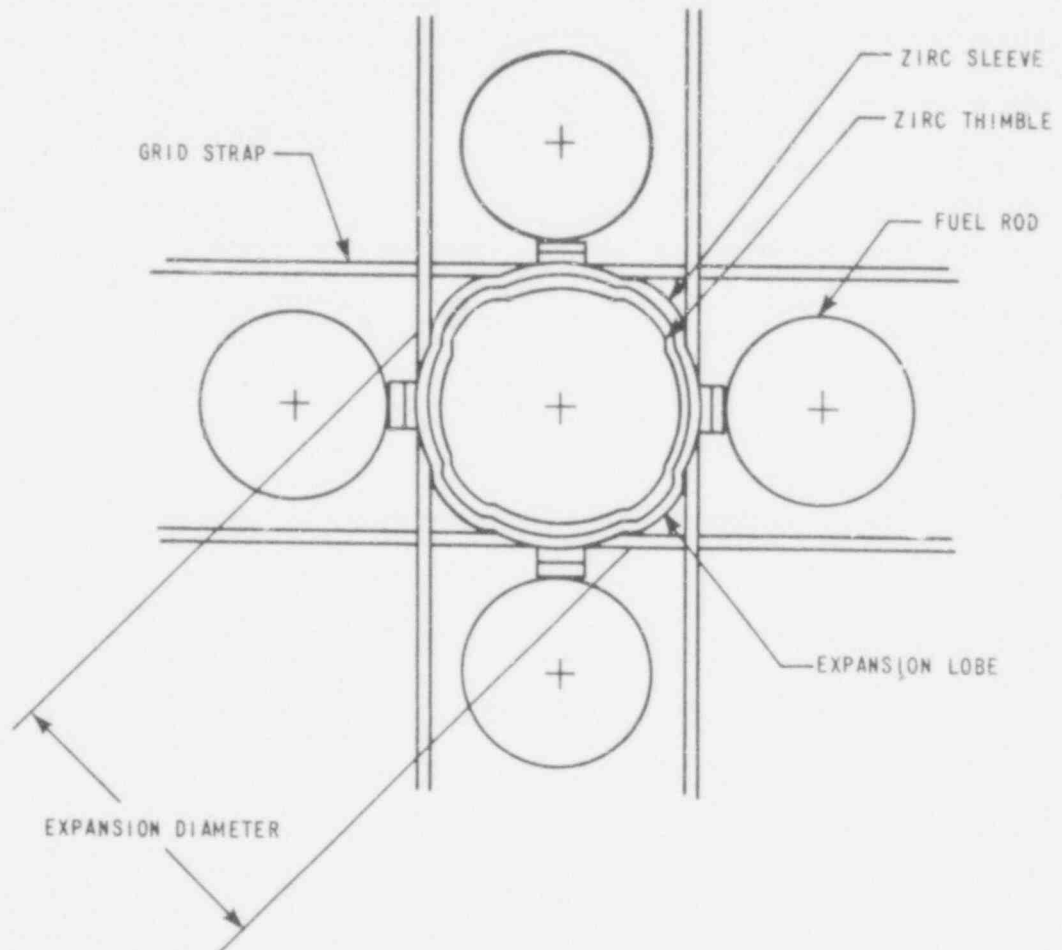


SPECIFIC DIMENSIONS DEPEND ON DESIGN VARIABLES SUCH AS  
 PRE-PRESSURIZATION, POWER HISTORY, AND DISCHARGE BURNUP

612 099

|                    |
|--------------------|
| WCAP - 9500        |
| Figure 4.2.3.      |
| Fuel Rod Schematic |

## MID GRID EXPANSION JOINT DESIGN

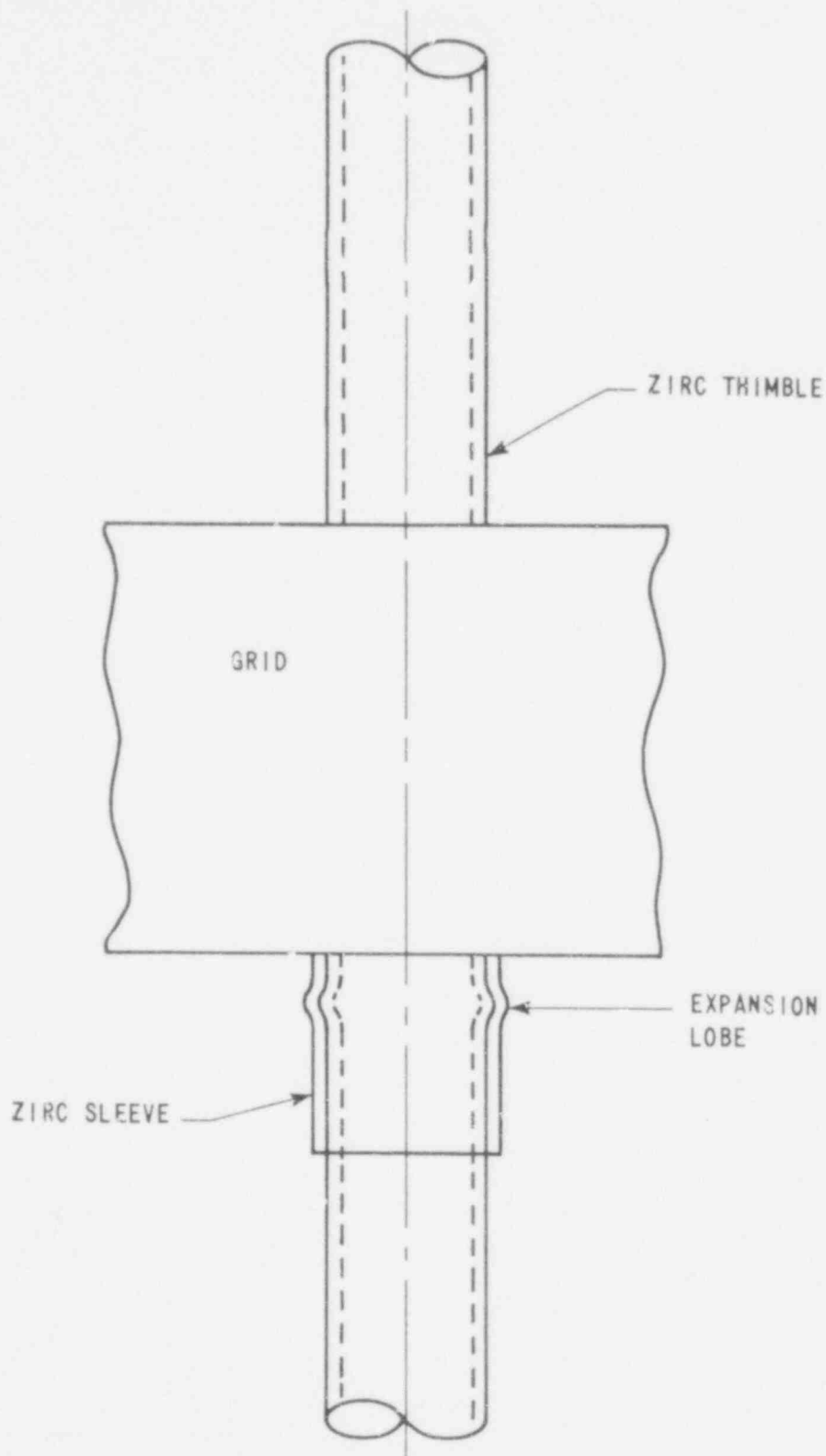


WCAP - 9500

Figure 4.2-4.

Plan View of Mid Grid to Guide Thimble Joint  
(Bottom View)

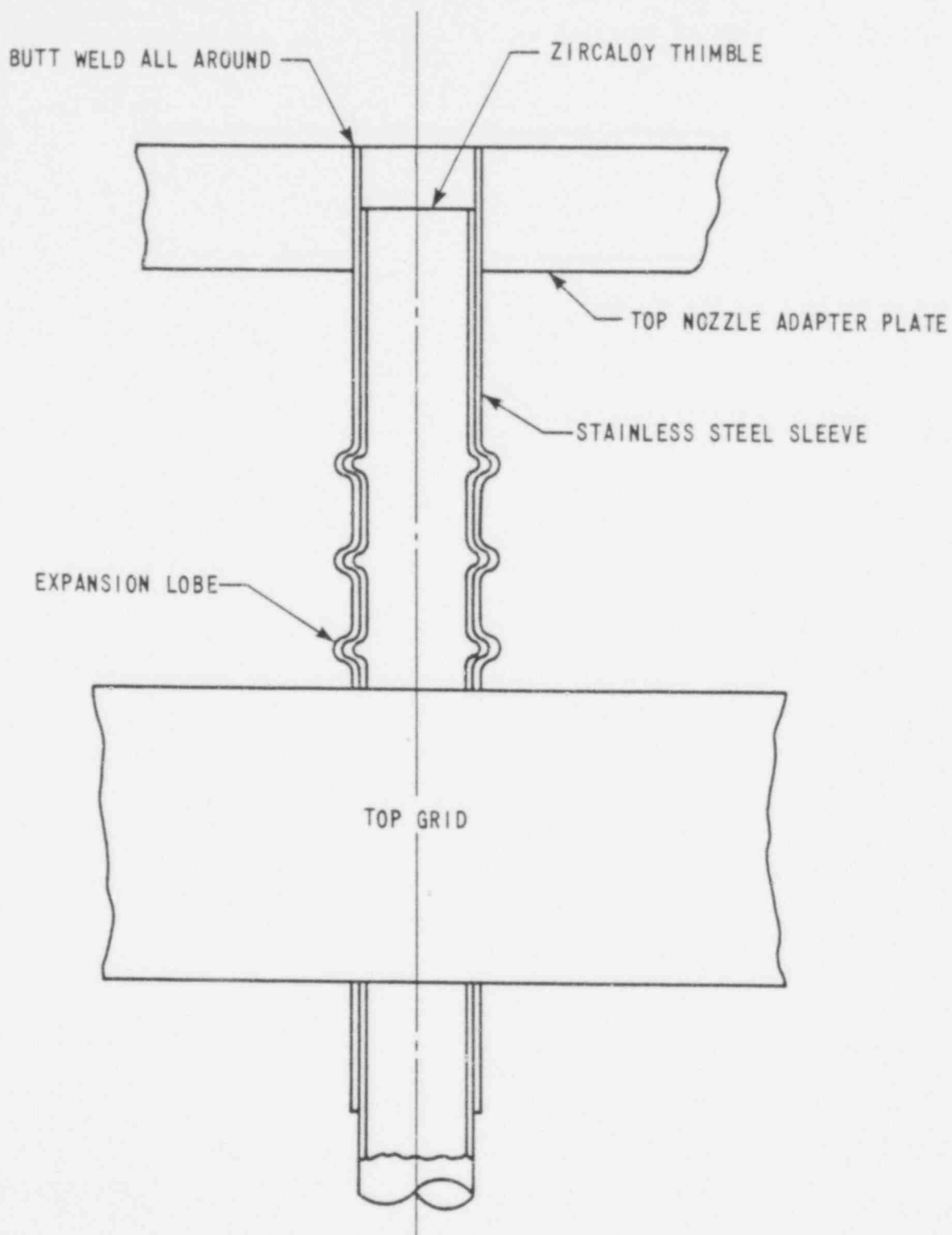
612 100



WCAP - 9500

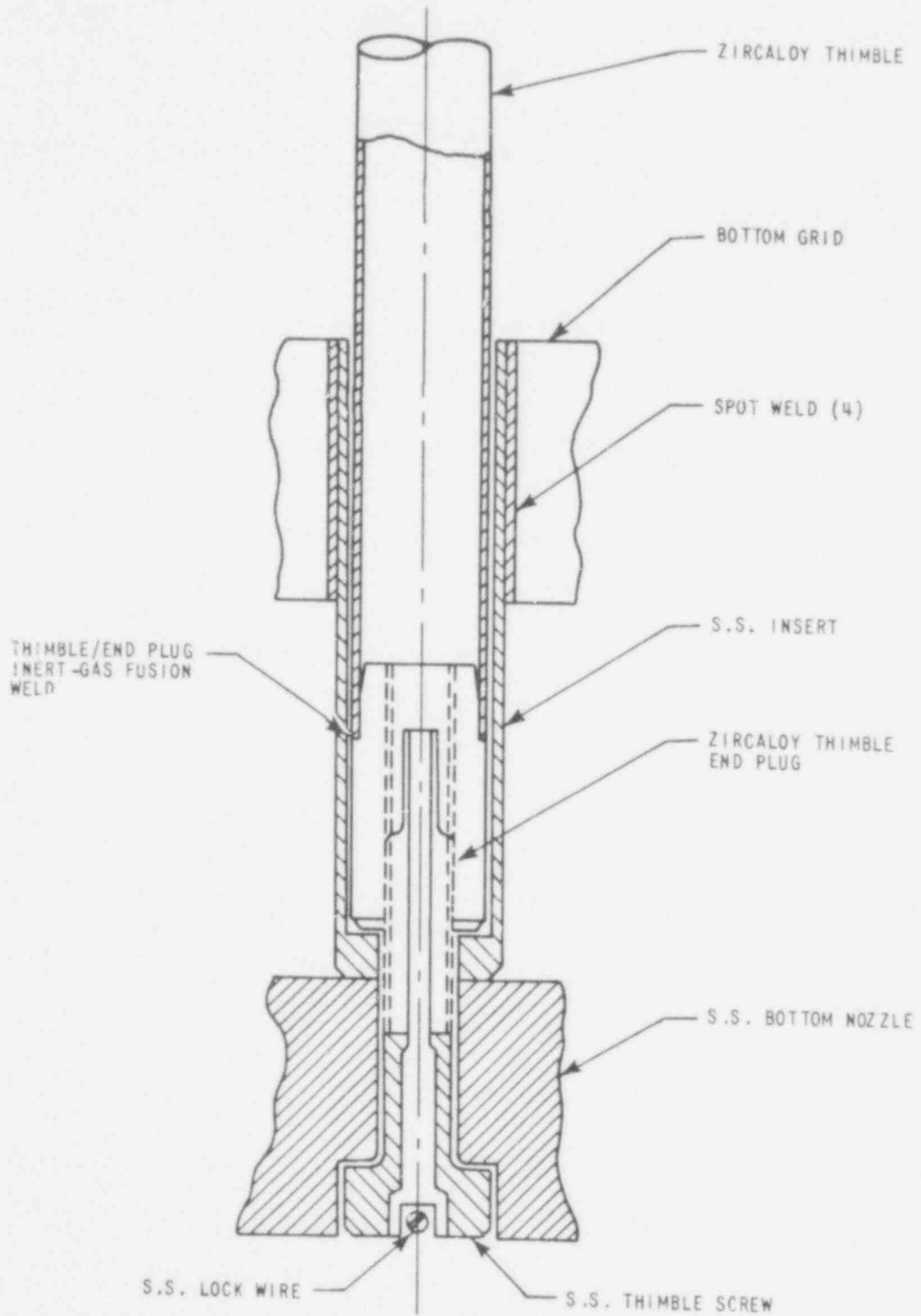
Figure 4.2-5.  
Elevation View of Mid-Grid  
to Guide Thimble Joint

612 101



612 102

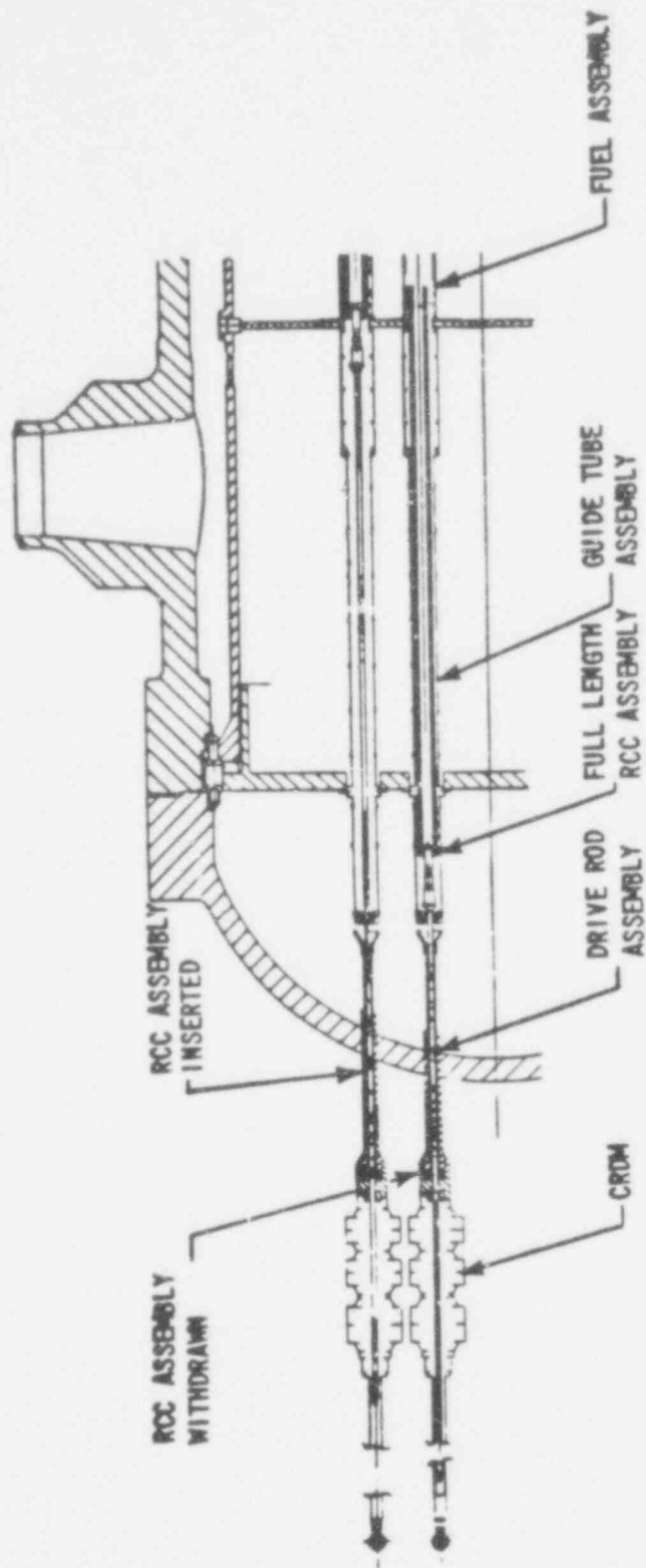
|   |
|---|
| WCAP - 9500   |
| Figure 4.2-6.<br>Top Grid to Guide Thimble<br>and Top Nozzle Attachment |



WCAP - 9500

Figure 4.2-7.  
Guide Thimble to Bottom Grid  
and Nozzle Joint

612 103

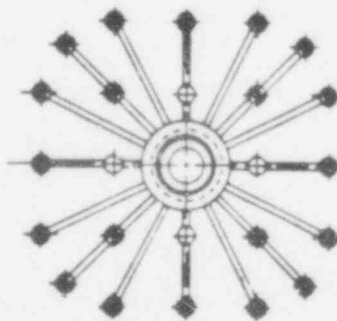
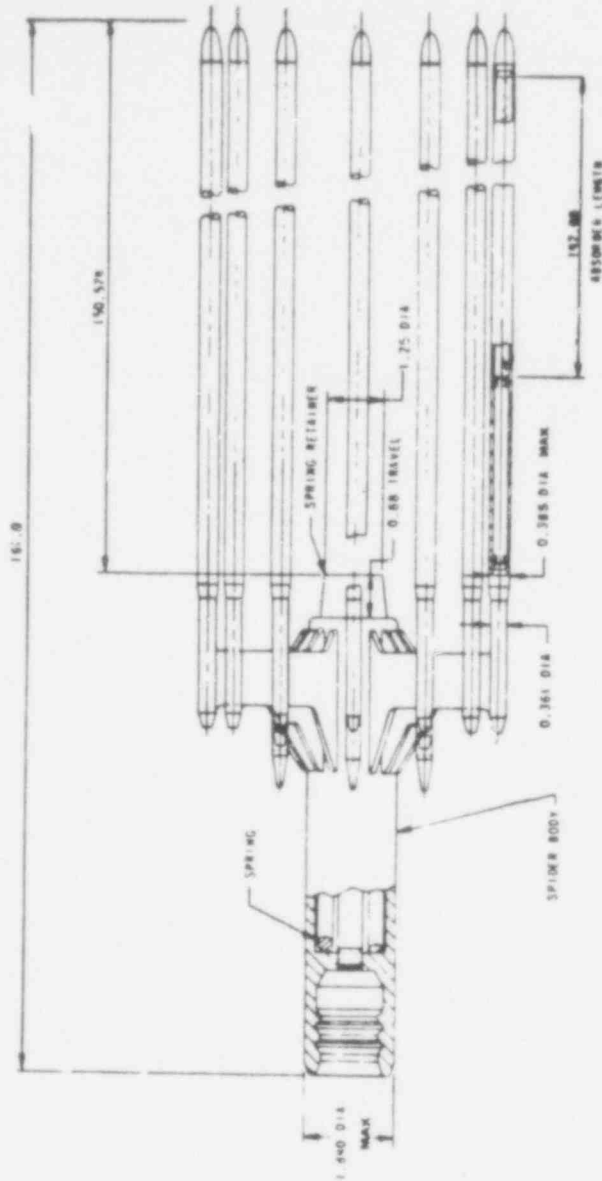


WCAP - 9500

Figure 4.2-8.

Rod Cluster Control and Drive Rod

612 104

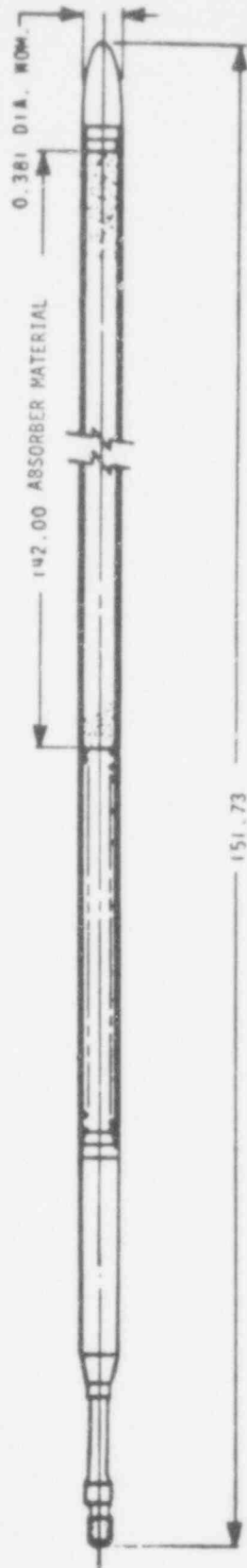


WCAP - 9500

Figure 4.2-9.

Rod Cluster Control Assembly Outline

612 105



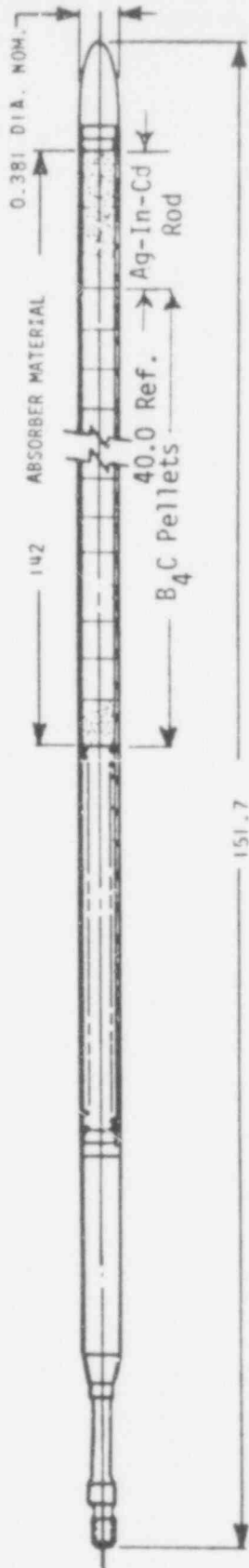
WCAP - 9500

Figure 4.2-10.

Absorber Rod, All Ag-In-Cd Design

612 106



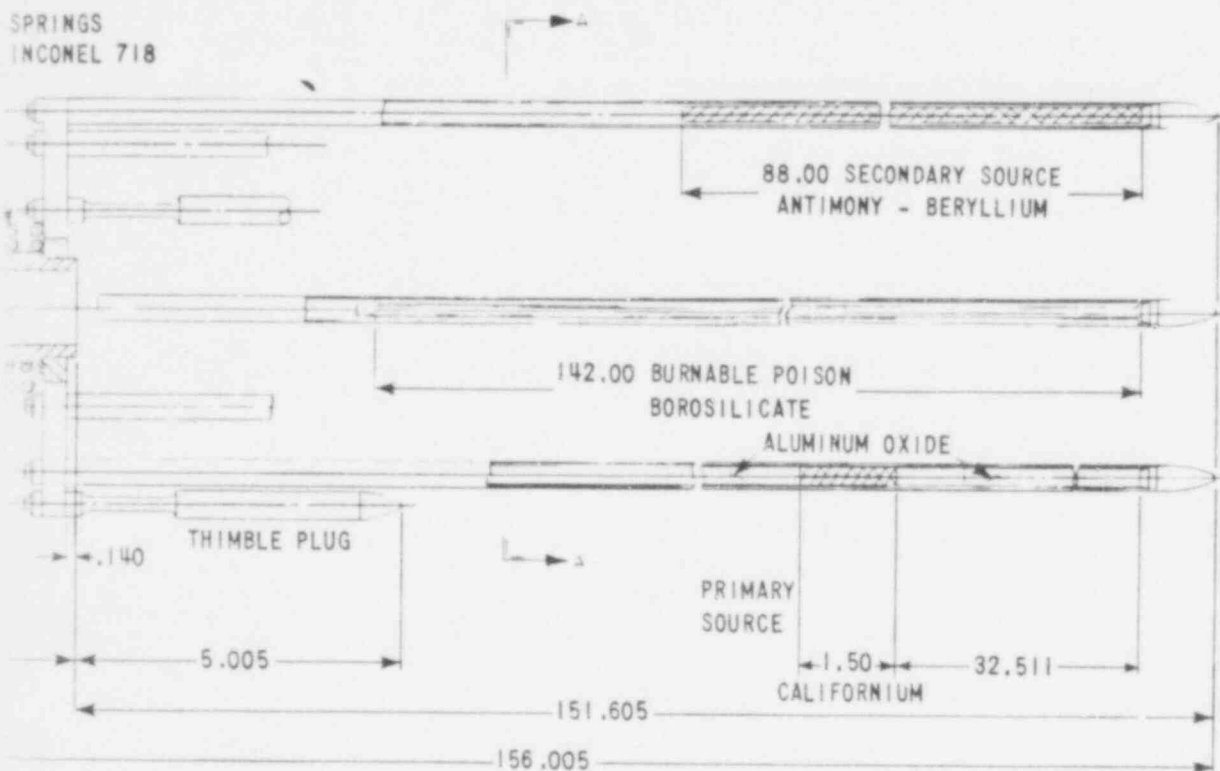


WCAP - 9500

Figure 4.2-11.

Hybrid B<sub>4</sub>C Absorber Rod

612 107

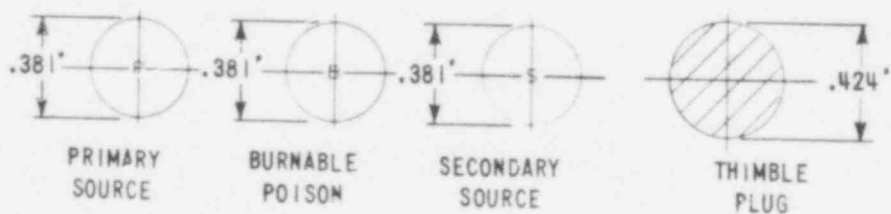
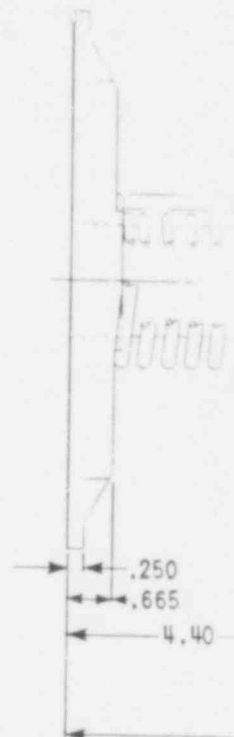
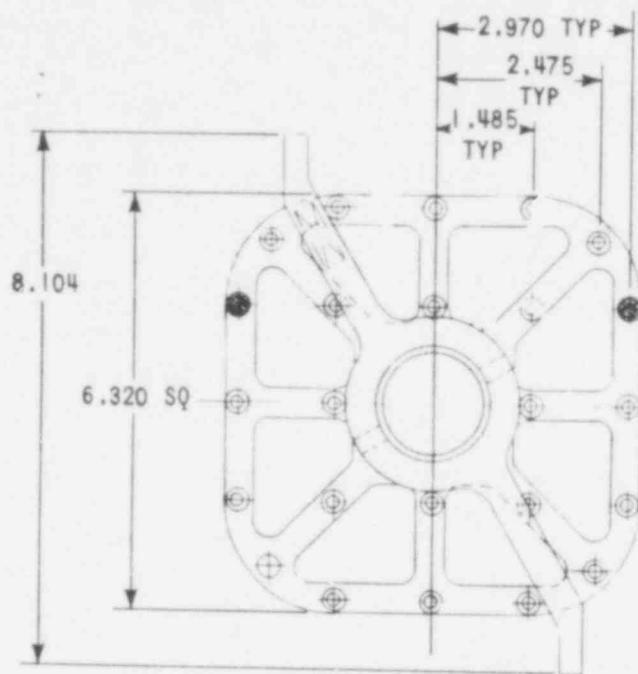


WCAP - 9500

Figure 4.2-12.

Composite Core Component Rods  
and Assembly Outline (UHI Plants)

612-103



612 109



## 4.3 NUCLEAR DESIGN

### 4.3.1 DESIGN BASES

This section describes the design bases and functional requirements used in the nuclear design of the fuel and reactivity control system and relates these design bases to the General Design Criteria (GDC) in 10CFR50, Appendix A. Where appropriate, supplemental criteria such as the Final Acceptance Criteria for Emergency Core Cooling Systems are addressed. Before discussing the nuclear design bases, it is appropriate to briefly review the four major categories ascribed to conditions of plant operation.

The full spectrum of plant conditions is divided into four categories, in accordance with the anticipated frequency of occurrence and risk to the public:

1. Condition I - Normal Operation
2. Condition II - Incidents of Moderate Frequency
3. Condition III - Infrequent Faults
4. Condition IV - Limiting Faults

In general, the Condition I occurrences are accommodated with margin between any plant parameter and the value of that parameter which would require either automatic or manual protective action. Condition II incidents are accommodated with, at most, a shutdown of the reactor with the plant capable of returning to operation after corrective action. Fuel damage (fuel damage as used here is defined as penetration of the fission product barrier, i.e., the fuel rod clad) is not expected during Condition I and Condition II events. It is not possible, however, to preclude a small number of rod failures. These are within the capability of the plant cleanup system and are consistent with the plant design basis.

612 111

Condition III incidents shall not cause more than a small fraction of the fuel elements in the reactor to be damaged, although sufficient fuel element damage might occur to preclude immediate resumption of operation. The release of radioactive material due to Condition III incidents should not be sufficient to interrupt or restrict public use of these areas beyond their exclusion radius. Furthermore, a Condition III incident shall not, by itself, generate a Condition IV fault or result in a consequential loss of function of the reactor coolant or reactor containment barriers.

Condition IV occurrences are faults that are not expected to occur but are defined as limiting faults which must be designed against. Condition IV faults shall not cause a release of radioactive material that results in an undue risk to public health and safety.

The core design power distribution limits related to fuel integrity are met for Condition I occurrences through conservative design and maintained by the action of the control system. The requirements for Condition II occurrences are met by the integrated protection system. The control and protection systems are described in Chapter 7, and the consequences of Condition II, III and IV occurrences are given in Chapter 15.

#### 4.3.1.1 Fuel Burnup

##### Basis

The fuel rod design basis is described in Section 4.2. The nuclear design basis is to install sufficient reactivity in the fuel to attain a region discharge burnup of 36,000 MWD/MTU. The above, along with the design basis in Section 4.3.1.3, Control of Power Distribution, satisfies GDC-10.

##### Discussion

Fuel burnup is a measure of fuel depletion which represents the integrated energy output of the fuel (MWD/MTU) and is a convenient means for quantifying fuel exposure criteria.

Condition III incidents shall not cause more than a small fraction of the fuel elements in the reactor to be damaged, although sufficient fuel element damage might occur to preclude immediate resumption of operation. The release of radioactive material due to Condition III incidents should not be sufficient to interrupt or restrict public use of these areas beyond their exclusion radius. Furthermore, a Condition III incident shall not, by itself, generate a Condition IV fault or result in a consequential loss of function of the reactor coolant or reactor containment barriers.

Condition IV occurrences are faults that are not expected to occur but are defined as limiting faults which must be designed against. Condition IV faults shall not cause a release of radioactive material that results in an undue risk to public health and safety.

The core design power distribution limits related to fuel integrity are met for Condition I occurrences through conservative design and maintained by the action of the control system. The requirements for Condition II occurrences are met by providing an adequate protection system which monitors reactor parameters. The control and protection systems are described in Chapter 7, and the consequences of Condition II, III and IV occurrences are given in Chapter 15.

#### 4.3.1.1 Fuel Burnup

##### Basis

The fuel rod design basis is described in Section 4.2. The nuclear design basis is to install sufficient reactivity in the fuel to attain a region discharge burnup of 36,000 MWD/MTU. The above, along with the design basis in Section 4.3.1.3, Control of Power Distribution, satisfies GDC-10.

##### Discussion

Fuel burnup is a measure of fuel depletion which represents the integrated energy output of the fuel (MWD/MTU) and is a convenient means for quantifying fuel exposure criteria.

The core design lifetime or design discharge burnup is achieved by installing sufficient initial excess reactivity in each fuel region and by following a fuel replacement program (such as that described in Section 4.3.2) that meets all safety related criteria in each cycle of operation.

Initial excess reactivity installed in the fuel, although not a design basis, must be sufficient to maintain core criticality at full power operating conditions throughout cycle life with equilibrium xenon, samarium, and other fission products present. The end of design cycle life is defined to occur when the chemical shim concentration is essentially zero with control rods present to the degree necessary for operational requirements (e.g., the controlling bank at the "bite" position). In terms of chemical shim boron concentration, this represents approximately 10 ppm with no control rod insertion.

A limitation on initial installed excess reactivity is not required other than as is quantified in terms of other design bases such as core negative reactivity feedback and shutdown margin discussed below.

#### 4.3.1.2 Negative Reactivity Feedbacks (Reactivity Coefficient)

##### Basis

The fuel temperature coefficient will be negative and the moderator temperature coefficient of reactivity will be non-positive for power operating conditions, thereby providing negative reactivity feedback characteristics. The design basis meets GDC-11.

##### Discussion

When compensation for a rapid increase in reactivity is considered, there are two major effects. These are the resonance absorption effects (Doppler) associated with changing fuel temperature and the spectrum effect resulting from changing moderator density. These basic physics

612 114



characteristics are often identified by reactivity coefficients. The use of slightly enriched uranium ensures that the Doppler coefficient of reactivity is negative. This coefficient provides the most rapid reactivity compensation. The core is also designed to have an overall negative moderator temperature coefficient of reactivity so that average coolant temperature or void content provides another slower compensatory effect. Nominal power operation is permitted only in a range of overall negative moderator temperature coefficient. The negative moderator temperature coefficient can be achieved through use of fixed burnable poison and/or control rods by limiting the reactivity held down by soluble boron.

Burnable poison content (quantity and distribution) is not stated as a design basis other than as it relates to accomplishment of a non-positive moderator temperature coefficient at power operating conditions discussed above.

#### 4.3.1.3 Control of Power Distribution

##### Basis

The nuclear design basis is that, with at least a 95 percent confidence level:

1. The fuel will not be operated at greater than 12.9 KW/ft under normal operating conditions including an allowance of 2 percent for calorimetric error and not including power spike factor due to densification.
2. Under abnormal conditions, including the maximum overpower condition, the fuel peak power will not cause melting as defined in Section 4.4.1.2.
3. The fuel will not operate with a power distribution that violates the departure from nucleate boiling (DNB) design basis (discussed in

Section 4.4.1) under Condition I and II events including the maximum overpower condition.

4. Fuel management will be such as to produce rod powers and burnups consistent with the assumptions in the fuel rod mechanical integrity analysis of Section 4.2.

The above basis meets GDC-10.

#### Discussion

Calculation of extreme power shapes which affect fuel design limits is performed with proven methods and verified frequently with measurements from operating reactors. The conditions under which limiting power shapes are assumed to occur are chosen conservatively with regard to any permissible operating state.

Even though there is good agreement between measured peak power calculations and measurements, a nuclear uncertainty margin (Section 4.3.2.2.1) is applied to calculated peak local power. Such a margin is provided both for the analysis for normal operating states and for anticipated transients.

#### 4.3.1.4 Maximum Controlled Reactivity Insertion Rate

##### Basis

The maximum reactivity insertion rate due to withdrawal of rod cluster control assemblies at power or by boron dilution is limited. During normal at power operation, the maximum controlled reactivity rate change is less than 45 pcm/sec.\* A maximum reactivity change rate of 75 pcm/sec for accidental withdrawal of control banks is set such that peak heat generation rate and DNBR do not exceed the maximum allowable at overpower conditions. This satisfies GDC-25.

---

\* 1 pcm =  $10E-5 \Delta\rho$  (see footnote Table 4.3-2).

The maximum reactivity worth of control rods and the maximum rates of reactivity insertion employing control rods are limited so as to preclude rupture of the coolant pressure boundary or disruption of the core internals to a degree which would impair core cooling capacity due to a rod withdrawal or ejection accident (see Chapter 15).

Following any Condition IV event (rod ejection, steamline break, etc.) the reactor can be brought to the shutdown condition and the core will maintain acceptable heat transfer geometry. This satisfies GDC-28.

#### Discussion

Reactivity addition associated with an accidental withdrawal of a control bank (or banks) is limited by the maximum rod speed (or travel rate) and by the worth of the bank(s). The maximum control rod speed is 45 inches per minute and the maximum rate of reactivity change considering two control banks moving is less than 75 pcm/sec. During normal operation at power and with normal control rod overlap, the maximum reactivity change rate is less than 45 pcm/sec.

The reactivity change rates are conservatively calculated assuming unfavorable axial power and xenon distributions. The peak xenon burnout rate is 25 pcm/min, significantly lower than the maximum reactivity addition rate of 45 pcm/sec for normal operation and 75 pcm/sec for accidental withdrawal of two banks.

#### 4.3.1.5 Shutdown Margins

##### Basis

Minimum shutdown margin as specified in the technical specifications is required at any power operating condition, in the hot standby shutdown condition and in the cold shutdown conditions.

In all analysis involving reactor trip, the single, highest worth rod cluster control assembly is postulated to remain untripped in its full-out position (stuck rod criterion). This satisfies GDC-26.

## Discussion

Two independent reactivity control systems are provided, namely control rods and soluble boron in the coolant. The control rod system can compensate for the reactivity effects of the fuel and water temperature changes accompanying power level changes over the range from full-load to no-load. In addition, the control rod system provides the minimum shutdown margin under Condition I events and is capable of making the core subcritical rapidly enough to prevent exceeding acceptable fuel damage limits assuming that the highest worth control rod is stuck out upon trip.

The boron system can compensate for all xenon burnout reactivity changes and will maintain the reactor in the cold shutdown. Thus, backup and emergency shutdown provisions are provided by a mechanical and a chemical shim control system which satisfies GDC-26.

## Basis

When fuel assemblies are in the pressure vessel and the vessel head is not in place,  $k_{\text{eff}}$  will be maintained at or below 0.95 with control rods and soluble boron. Further, the fuel will be maintained sufficiently subcritical that removal of all rod cluster control assemblies will not result in criticality.

## Discussion

ANSI Standard N210-1976 specifies a  $k_{\text{eff}}$  not to exceed 0.95 in spent fuel storage racks and transfer equipment flooded with pure water. No criterion is given for the refueling operation; however, a five percent margin, which is consistent with spent fuel storage and transfer is adequate for the controlled and continuously monitored operations involved.

612 118

The boron concentration required to meet the refueling shutdown criteria is specified in the Technical Specifications. Verification that this shutdown criteria is met, including uncertainties, is achieved using standard Westinghouse design methods such as the LEOPARD (Reference 19) TURTLE (Reference 10) a diffusion theory code, and PALADON (Reference 38) a nodal analysis code. The subcriticality of the core is continuously monitored as described in the Technical Specifications.

#### 4.3.1.6 Stability

##### Basis

The core will be inherently stable to power oscillations at the fundamental mode. This satisfies GDC-12. Spatial power oscillations within the core with a constant core power output, should they occur, can be reliably and readily detected and suppressed.

##### Discussion

Oscillations of the total power output of the core, from whatever cause, are readily detected by the N-16 power detectors, the loop temperature sensors and by the nuclear instrumentation. The core is protected by these systems and a reactor trip would occur if power increased unacceptably, preserving the design margins to fuel design limits. The stability of the turbine/steam generator/core systems and the reactor control system is such that total core power oscillations are not normally possible. The redundancy of the protection circuits ensures an extremely low probability of exceeding design power levels.

The core is designed so that diametral and azimuthal oscillations due to spatial xenon effects are self-damping and no operator action or control action is required to suppress them. The stability to diametral oscillations is so great that this excitation is highly improbable. Convergent azimuthal oscillations can be excited by prohibited motion of individual control rods. Such oscillations are readily observable and alarmed, using the multisection excore ion detectors. Indications are also continuously available from incore thermocouples and loop

temperature measurements. Moveable incore detectors can be activated to provide more detailed information. In all presently proposed cores, these horizontal plane oscillations are self-damping by virtue of reactivity feedback effects designed into the core.

However, axial xenon spatial power oscillations may occur late in core life. The control bank and excore detectors are provided for control and monitoring of axial power distributions. Assurance that fuel design limits are not exceeded is provided by reactor Overpower  $\Delta T$  and Over-temperature  $\Delta T$  trip functions which use the measured axial power imbalance as an input.

#### 4.3.1.7 Anticipated Transients Without Trip

The effects of anticipated transients with failure to trip are not considered in the design bases of the plant. Analysis has shown that the likelihood of such a hypothetical event is negligibly small. Furthermore, analysis of the consequences of a hypothetical failure to trip following anticipated transients has shown that no significant core damage would result, system peak pressures would be limited to acceptable values and no failure of the Reactor Coolant System would result (Reference 1).

### 4.3.2 DESCRIPTION

#### 4.3.2.1 Nuclear Design Description

The reactor core consists of a specified number of fuel rods which are held in bundles by spacer grids and top and bottom fittings. The fuel rods are constructed of Zircaloy cylindrical tubes containing  $UO_2$  fuel pellets. The bundles, known as fuel assemblies, are arranged in a pattern which approximates a right circular cylinder.

Each fuel assembly contains a 17 x 17 rod array composed of 264 fuel rods, 24 rod cluster control thimbles and an incore instrumentation

temperature measurements. Moveable incore detectors can be activated to provide more detailed information. In all presently proposed cores, these horizontal plane oscillations are self-damping by virtue of reactivity feedback effects designed into the core.

However, axial xenon spatial power oscillations may occur late in core life. The control bank and excore detectors are provided for control and monitoring of axial power distributions. Assurance that fuel design limits are not exceeded is provided by the reactor protection system which uses the measured detailed axial power shape as input.

#### 4.3.1.7 Anticipated Transients Without Trip

The effects of anticipated transients with failure to trip are not considered in the design bases of the plant. Analysis has shown that the likelihood of such a hypothetical event is negligibly small. Furthermore, analysis of the consequences of a hypothetical failure to trip following anticipated transients has shown that no significant core damage would result, system peak pressures would be limited to acceptable values and no failure of the Reactor Coolant System would result (Reference 1).

### 4.3.2 DESCRIPTION

#### 4.3.2.1 Nuclear Design Description

The reactor core consists of a specified number of fuel rods which are held in bundles by spacer grids and top and bottom fittings. The fuel rods are constructed of Zircaloy cylindrical tubes containing  $UO_2$  fuel pellets. The bundles, known as fuel assemblies, are arranged in a pattern which approximates a right circular cylinder.

Each fuel assembly contains a 17 x 17 rod array composed of 264 fuel rods, 24 rod cluster control thimbles and an incore instrumentation

612 121

thimble. Figure 4.2-1 shows a cross sectional view of a 17 x 17 fuel assembly and the related rod cluster control locations. Further details of the fuel assembly are given in Section 4.2.

The fuel rods within a given assembly have the same uranium enrichment in both the radial and axial planes. Fuel assemblies of three different enrichments are used in the initial core loading to establish a favorable radial power distribution. Figure 4.3-1 shows the fuel loading pattern to be used in the first core. Two regions consisting of the two lower enrichments are interspersed so as to form a checkerboard pattern in the central portion of the core. The third region is arranged around the periphery of the core and contains the highest enrichment. The enrichments for the first core are shown in Table 4.3-1.

The reference reloading pattern is typically similar to Figure 4.3-1 with depleted fuel interspersed checkerboard style in the center and new fuel on the periphery. The core will normally operate approximately one year between refueling, accumulating approximately 12,000 MWD/MTU per year. The exact reloading pattern, initial and final positions of assemblies, number of fresh assemblies and their placement are dependent on the energy requirement for the next cycle and burnup and power histories of the previous cycles.

The core average enrichment is determined by the amount of fissionable material required to provide the desired core lifetime and energy requirements, namely a region average discharge burnup of 36,000 MWD/MTU. The physics of the burnout process is such that operation of the reactor depletes the amount of fuel available due to the absorption of neutrons by the U-235 atoms and their subsequent fission. The rate of U-235 depletion is directly proportional to the power level at which the reactor is operated. In addition, the fission process results in the formation of fission products, some of which readily absorb neutrons. These effects, depletion and the buildup of fission products, are partially offset by the buildup of plutonium shown in Figure 4.3-2 for the 17 x 17 fuel assembly, which occurs due to the non-fission absorption of neutrons in U-238. Therefore, at the beginning of any



cycle, a reactivity reserve equal to the depletion of the fissionable fuel and the buildup of fission product poisons over the specified cycle life must be "built" into the reactor. This excess reactivity is controlled by removable neutron absorbing material in the form of boron dissolved in the primary coolant and burnable poison rods.

The concentration of boric acid in the primary coolant is varied to provide control and to compensate for long-term reactivity requirements. The concentration of the soluble neutron absorber is varied to compensate for reactivity changes due to fuel burnup, fission product poisoning including xenon and samarium, burnable poison depletion, and the cold-to-operating moderator temperature change. Using its normal makeup path, the Chemical and Volume Control System (CVCS) is capable of inserting negative reactivity at a rate of approximately 30 pcm/min when the reactor coolant boron concentration is 100 ppm. If the emergency boration path is used, the CVCS is capable of inserting negative reactivity at a rate of approximately 65 pcm/min when the reactor coolant concentration is 1000 ppm and approximately 75 pcm/min when the reactor coolant boron concentration is 100 ppm. The peak burnout rate for xenon is 25 pcm/min (Section 9.3.4.3.1 discusses the capability of the CVCS to counteract xenon decay). Rapid transient reactivity requirements and safety shutdown requirements are met with control rods.

As the boron concentration is increased, the moderator temperature coefficient becomes less negative. The use of a soluble poison alone would result in a positive moderator coefficient at beginning-of-life for the first cycle. Therefore, burnable poison rods are used in the first core to reduce the soluble boron concentration sufficiently to ensure that the moderator temperature coefficient is negative for power operating conditions. During operation the poison content in these rods is depleted, thus adding positive reactivity to offset some of the negative reactivity from fuel depletion and fission product buildup. The depletion rate of the burnable poison rods is not critical since chemical shim is always available and flexible enough to cover any possible deviations in the expected burnable poison depletion rate. Figure 4.3-3 is a graph of a typical core depletion with and without

burnable poison rods. Note that even at end-of-life conditions some residual poison remains in the burnable poison rods resulting in a net decrease in the first cycle lifetime. Upon completion of the first cycle all the burnable poison rods are normally removed because the moderator temperature coefficient in reload cores is sufficiently negative.

In addition to reactivity control, the burnable poison rods are strategically located to provide a favorable radial power distribution. Figure 4.3-4 shows the burnable poison distribution within a fuel assembly for the several burnable patterns used in a 17 x 17 array. A typical burnable poison loading pattern is shown in Figure 4.3-5.

Tables 4.3-1 through 4.3-3 contain a summary of the reactor core design parameters for the first fuel cycle, including reactivity coefficients, delayed neutron fraction and neutron lifetimes. Sufficient information is included to permit an independent calculation of the nuclear performance characteristics of the core.

#### 4.3.2.2 Power Distributions

The accuracy of power distribution calculations has been confirmed through approximately one thousand flux maps during some twenty years of operation under conditions very similar to those expected. Details of this confirmation are given in Reference [2] and in Section 4.3.2.2.6.

##### 4.3.2.2.1 Definitions

Power distributions are quantified in terms of hot channel factors. These factors are a measure of the peak pellet power within the reactor core and the total energy produced in a coolant channel and are expressed in terms of quantities related to the nuclear or thermal design namely:

Power density is the thermal power produced per unit volume of the core (KW/liter).

612 124

Linear power density is the thermal power produced per unit length of active fuel (KW/ft). Since fuel assembly geometry is standardized, this is the unit of power density most commonly used. For all practical purposes, it differs from KW/liter by a constant factor which includes geometry and the fraction of the total thermal power which is generated in the fuel rod.

Average linear power density is the total thermal power produced in the fuel rods divided by the total active fuel length of all rods in the core.

Local heat flux is the heat flux at the surface of the cladding (BTU-ft<sup>-2</sup>-hr<sup>-1</sup>). For nominal rod parameters, this differs from linear power density by a constant factor.

Rod power or rod integral power is the length integrated linear power density in one rod (KW).

Average rod power is the total thermal power produced in the fuel rods divided by the number of fuel rods (assuming all rods have equal length).

The hot channel factors used in the discussion of power distributions in this section are defined as follows:

$F_Q$ , Heat Flux Hot Channel Factor, is defined as the maximum local fuel rod linear power density divided by the average fuel rod linear power density, assuming nominal fuel pellet and rod parameters.

$F_Q^E$ , Engineering Heat Flux Hot Channel Factor, is the allowance on heat flux required for manufacturing tolerances. The engineering factor allows for local variations in enrichment, pellet density and diameter, surface area of the fuel rod and eccentricity of the gap between pellet and clad.

Combined statistically, the net effect is a factor of 1.03 to be applied to fuel rod surface heat flux.

612 125

$F_{\Delta H}^N$ , Nuclear Enthalpy Rise Hot Channel Factor, is defined as the ratio of the integral of linear power along the rod with the highest integrated power to the average rod power.

Manufacturing tolerances, hot channel power distribution and surrounding channel power distributions are treated explicitly in the calculation of the DNB ratio described in Section 4.4.

It is convenient for the purposes of discussion to define subfactors of  $F_Q$ , however, design limits are set in terms of the total peaking factor.

$$\begin{aligned} F_Q &= \text{Total peaking factor or heat flux hot-channel factor} \\ &= \frac{\text{Maximum KW/ft}}{\text{Average KW/ft}} \end{aligned}$$

without densification effects

$$\begin{aligned} F_Q &= F_Q^N \times F_Q^E \\ &= F_{XY}^N \times F_Z^N \times F_U^N \times F_Q^E \end{aligned}$$

where

$F_Q^N$  and  $F_Q^E$  are defined above.

$F_U^N$  = factor for conservatism, assumed to be 1.05.

$F_{XY}^N$  = ratio peak power density to average power density in the horizontal plane of peak local power.

$F_Z^N$  = ratio of the power per unit core height in the horizontal plane of peak local power to the average value of power per unit core height. If the plane of peak local power coincides with the plane of maximum power per unit core height than  $F_Z^N$  is the core average axial peaking factor.

To include the allowances made for densification effects, which are height dependent, the following quantities are defined.

$S(Z)$  = the allowance made for densification effects at height  $Z$  in the core. See Section 4.3.2.2.5.

$P(Z)$  = ratio of the power per unit core height in the horizontal plane at height  $Z$  to the average value of power per unit core height.

Then

$$F_Q = \text{Total peaking factor} \\ = \frac{\text{Maximum KW/ft}}{\text{Average KW/ft}}$$

Including densification allowance

$$F_Q = \max_{\text{on } Z} \left\{ F_{XY}^N(Z) \times P(Z) \times S(Z) \right\} \times F_U^N \times F_Q^E$$

#### 4.3.2.2.2 Radial Power Distributions

The power shape in horizontal sections of the core at full power is a function of the fuel and burnable poison loading patterns and the presence or absence of a single bank of full length control rods. Thus, at any time in the cycle, a horizontal section of the core can be characterized as unrodded or with group D control rods. These two situations combined with burnup effects determine the radial power shapes which can exist in the core at full power. Typical values of  $F_{XY}^N$  are given in Table 4.3-2. The effect on radial power shapes of power level, xenon, samarium and moderator density are considered also but these are small. The effect of non-uniform flow distribution is negligible. While radial power distributions in various planes of the core are often illustrated, the core radial enthalpy rise distribution as determined by the integral of power up each channel is of greater interest. Figures 4.3-6 through 4.3-11 show representative radial power distributions for

one eighth of the core for representative operating conditions. These conditions are 1) Hot Full Power (HFP) near Beginning-of-Life (BOL) - unrodded - no xenon, 2) HFP near BOL - unrodded - equilibrium xenon, 3) HFP near BOL - Bank D in - equilibrium xenon, 4) HFP near Middle-of-Life (MOL) - unrodded - equilibrium xenon, 5) HFP near End-of-Life (EOL) - unrodded - equilibrium xenon, and 6) HFP near End-of-Life (EOL) - Bank D in - equilibrium xenon.

Since the location of the hot channel varies from time to time, a single reference radial design power distribution is selected for DNB calculations. This reference power distribution is chosen conservatively to concentrate power in one area of the core, minimizing the benefits of flow redistribution. Assembly powers are normalized to core average power. The radial power distribution within a fuel rod and its variation with burnup is utilized in thermal calculations and fuel rod design is discussed in Section 4.2.

#### 4.3.2.2.3 Assembly Power Distributions

For the purpose of illustration, assembly power distributions from the BOL and EOL conditions corresponding to Figures 4.3-7 and 4.3-10 respectively, are given for the same assembly in Figures 4.3-12 and 4.3-13 respectively.

Since the detailed power distribution surrounding the hot channel varies from time to time, a conservatively flat assembly power distribution is assumed in the DNB analysis, described in Section 4.4, with the rod of maximum integrated power artificially raised to the design value of  $F_{\Delta H}^N$ . Care is taken in the nuclear design of all fuel cycles and all operating conditions to ensure that a flatter assembly power distribution does not occur with limiting values of  $F_{\Delta H}^N$ .

#### 4.3.2.2.4 Axial Power Distributions

The shape of the power profile in the axial or vertical direction is largely under the control of the operator through either the manual operation of the full length control rods or automatic motion of full

length rods responding to manual operation of the CVCS. Nuclear effects which cause variations in the axial power shape include moderator density, Doppler effect on resonance absorption, spatial xenon and burnup. Automatically controlled variations in total power output and full length rod motion are also important in determining the axial power shape at any time. Four-section power range ion detectors mounted outside the reactor vessel parallel to the axis of the core provide the required input to monitor the core average axial power shape. The core average axial power distribution is analytically constructed from the signals from each of the four axial segments of the multi-section excore ion detectors using a Fourier fitting technique which is discussed in Reference [40]. The resulting Fourier expansion-based core average axial power shape is then input to the kW/ft and DNBR calculators in the integrated protection system. The core axial power distribution as monitored by redundant multi-section excore detectors is continuously reconstructed to not only accurately reproduce the true core average axial power but also to accurately follow axial power shape changes. A direct reading of the reconstituted core average axial power shape is available to the operator. The axial flux difference,  $\Delta I$ , is also displayed in the control room for the operator. The axial flux difference is defined as the difference between the sum of the top pair and the sum of the bottom pair detector readings. The axial offset is defined as:

$$\text{axial offset} = \frac{\phi_t - \phi_b}{\phi_t + \phi_b}$$

and  $\phi_t$  and  $\phi_b$  are the sum of the top pair and the sum of the bottom pair of detector readings, respectively.

Representative axial power shapes for BOL, MOL, and EOL conditions are shown in Figures 4.3-14 through 4.3-16. These figures cover a wide range of axial offset including values not permitted at full power. Reference [3] also illustrates representative axial power shapes for other reactor conditions.

The radial power distributions shown in Figures 4.3-8 and 4.3-11 involving the partial insertion of control rods represent a synthesis of power shapes from the rodded and unrodded planes. The applicability of the

separability assumption upon which this procedure is based is assured through extensive three-dimensional calculations of possible rodded conditions. As an example, Figure 4.3-17 compares the axial power distribution for several assemblies at different distances from inserted control rods with the core average distribution.

The only significant difference from the average occurs in the low power peripheral assemblies, thus, confirming the validity of the separability assumption.

Significant variations on the axial power distributions in terms of both the magnitude and location of the peak power can result from control rod, xenon, and depletion effects. To ensure that the reactor is protected, the core average axial power distribution is continually monitored and allowances are automatically made in the protection system setpoints to offset the effects of any adverse axial power distribution as described in Section 7 and 15.

#### 4.3.2.2.5 Local Power Peaking

Fuel densification, which has been observed to occur under irradiation in several operating reactors, causes the fuel pellets to shrink both axially and radially. The pellet shrinkage combined with random hang-up of fuel pellets results in gaps in the fuel column when the pellets below the hung-up pellet settle in the fuel rod. The gaps vary in length and location in the fuel rod. Because of decreased neutron absorption in the vicinity of the gap, power peaking occurs in the adjacent fuel rods resulting in an increased power peaking factor. A quantitative measure of this local peaking is given by the power spike factor  $S(Z)$  where  $Z$  is the axial location in the core.

The method used to compute the power spike factor is described in Reference [4] and is summarized in Figure 4.3-18. The information flow outlined in Figure 4.3-18 is as follows:



length rods responding to manual operation of the CVCS. Nuclear effects which cause variations in the axial power shape include moderator density, Doppler effect on resonance absorption, spatial xenon and burnup. Automatically controlled variations in total power output and full length rod motion are also important in determining the axial power shape at any time. Signals are available to the operator from the excore ion chambers which are long ion chambers outside the reactor vessel running parallel to the axis of the core. Separate signals are taken from the top and bottom halves of the chambers. The difference between top and bottom signals from each of four pairs of detectors is displayed on the control panel and called the flux difference,  $\Delta I$ . Calculations of core average peaking factor for many plants and measurements from operating plants under many operating situations are associated with either  $\Delta I$  for axial offset in such a way that an upper bound can be placed on the peaking factor. For these correlations, axial offset is defined as:

$$\text{axial offset} = \frac{\phi_t - \phi_b}{\phi_t + \phi_b}$$

and  $\phi_t$  and  $\phi_b$  are the top and bottom detector readings.

Representative axial power shapes for BOL, MQL, and EOL conditions are shown in Figures 4.3-14 through 4.3-16. These figures cover a wide range of axial offset including values not permitted at full power. Reference [3] also illustrates representative axial power shapes for other reactor conditions.

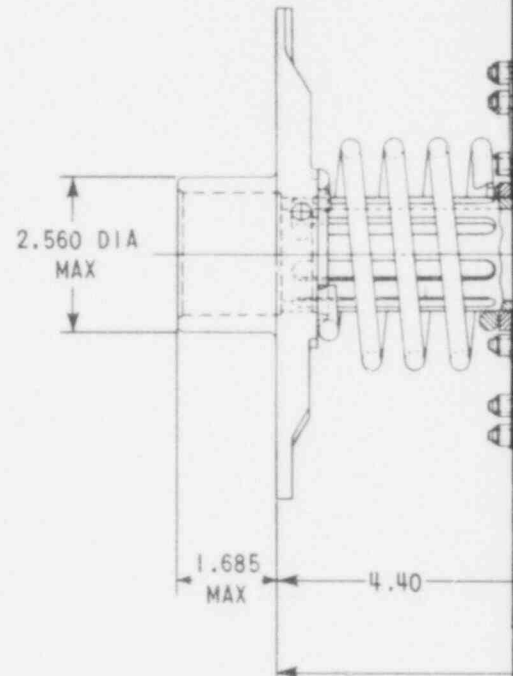
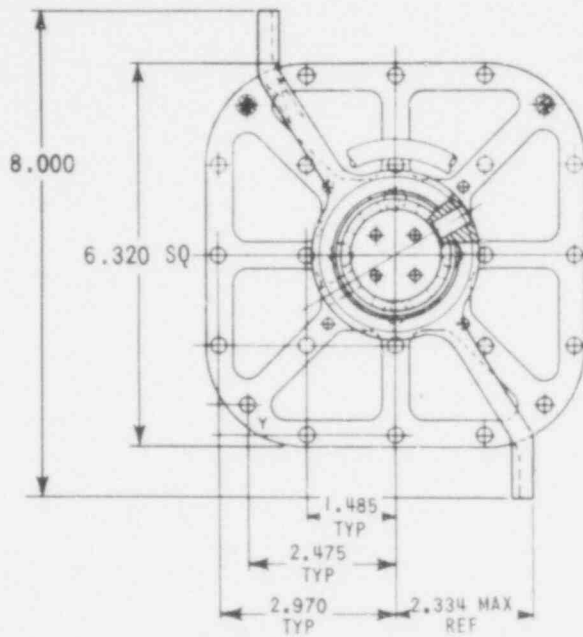
The radial power distributions shown in Figures 4.3-8 and 4.3-11 involving the partial insertion of control rods represent a synthesis of power shapes from the rodded and unrodded planes. The applicability of the separability assumption upon which this procedure is based is assured through extensive three-dimensional calculations of possible rodded conditions. As an example, Figure 4.3-17 compares the axial power distribution for several assemblies at different distances from inserted control rods with the core average distribution.

The only significant difference from the average occurs in the low power peripheral assemblies, thus, confirming the validity of the separability assumption.

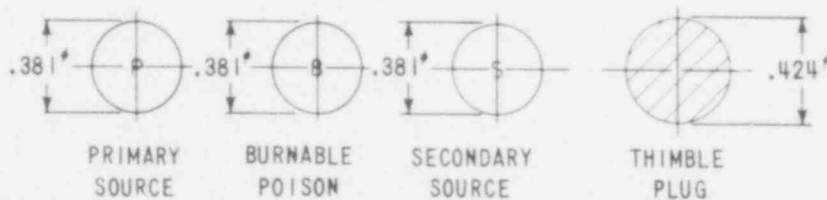
#### 4.3.2.2.5 Local Power Peaking

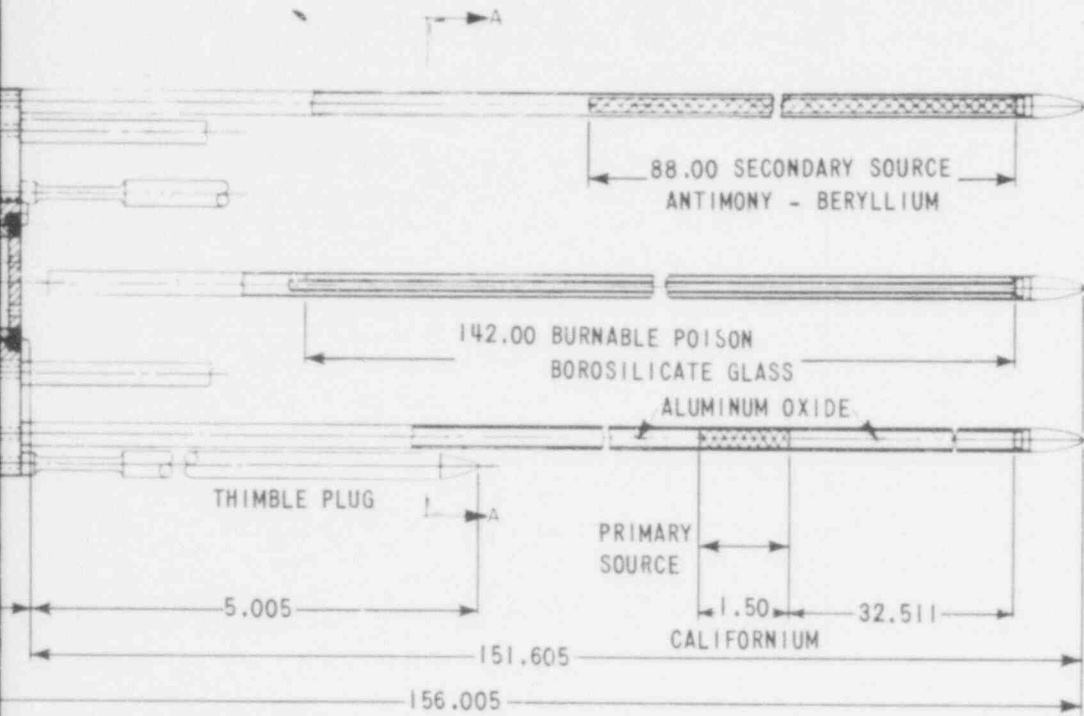
Fuel densification, which has been observed to occur under irradiation in several operating reactors, causes the fuel pellets to shrink both axially and radially. The pellet shrinkage combined with random hang-up of fuel pellets results in gaps in the fuel column when the pellets below the hung-up pellet settle in the fuel rod. The gaps vary in length and location in the fuel rod. Because of decreased neutron absorption in the vicinity of the gap, power peaking occurs in the adjacent fuel rods resulting in an increased power peaking factor. A quantitative measure of this local peaking is given by the power spike factor  $S(Z)$  where  $Z$  is the axial location in the core.

The method used to compute the power spike factor is described in Reference [4] and is summarized in Figure 4.3-18. The information flow outlined in Figure 4.3-18 is as follows:



F





WCAP - 9500

Figure 4.2-12.

Composite Core Component Rods  
and Assembly Outline (Non-UHI Plants)

612  
13A

1. The probability that an axial gap of a certain size will occur at a given location in the core is determined from fuel performance data.
2. The magnitude of the power spike caused by a single axial gap of a certain size is determined from nuclear calculations as shown in Figure 4.3-19.
3. For each axial interval to be analyzed, axial gap occurrence probabilities and the single event power spikes are entered into the DRAW computer code. The code produces a curve of power spike versus probability of exceeding power spike for each elevation in the core. The power census for a core is then statistically combined with the power spike probability curve to obtain a power spike penalty for the core such that less than one rod will exceed  $F_Q^N$  at a 95 percent confidence level.

The power spike factor due to densification is assumed to be a local perturbation applicable to overpower transients. Thus, densification affects  $F_Q$  but not  $F_{\Delta H}^N$ . The magnitude of the increase power peaking increases from no effect at the bottom of the core to a few percent at the top of the core as shown in Figure 4.3-20, which is applicable to the 94.5 percent (geometric) dense pellets.

For fuel produced by a process other than those for which Reference [4] is applicable, specifications will be followed to ensure that the effects of densification will be no greater than has been allowed in the design. The specifications for quantifying the extent of densification will be based on the NRC report on Fuel Densification (Reference 31).

Results reported in Reference [5] show that the power spike penalty should not be included in the LOCA envelope.

#### 4.3.2.2.6 Limiting Power Distributions

According to the ANSI classification of plant conditions (See Chapter 15).

Condition I occurrences are those which are expected frequently or regularly in the course of power operation, maintenance, or maneuvering of the plant. As such, Condition I occurrences are accommodated with margin between any plant parameter and the value of that parameter which would require either automatic or manual protective action. Inasmuch as Condition I occurrences occur frequently or regularly, they must be considered from the point of view of affecting the consequences of fault conditions (Conditions II, III and IV). In this regard, analysis of each fault condition described is generally based on a conservative set of initial conditions corresponding to the most adverse set of conditions which can occur during Condition I operation.

The list of steady state and shutdown conditions, permissible deviations (such as one coolant loop out of service) and operational transients is given in Section 15.0. Implicit in the definition of normal operation is proper and timely action by the reactor operator. That is, the operator follows recommended operating procedures for maintaining appropriate power distributions and takes any necessary remedial actions when alerted to do so by the plant instrumentation. Thus, as stated above, the worst or limiting power distribution which can occur during normal operation is to be considered as the starting point for analysis of ANSI Conditions II, III and IV events.

Improper procedural actions or errors by the operator are assumed in the design as occurrences of moderate frequency (ANSI Condition II). Some of the Consequences which might result are discussed in Section 15.0. Therefore, the limiting power shapes which result from such Condition II events, are those power shapes which deviate from the normal operating condition at the recommended axial offset bank, e.g., due to lack of proper action by the operator during a xenon transient following a change in power level brought about by control rod motion. Power shapes which fall in this category are used for determination of the reactor protection system setpoints so as to maintain margin to overpower or DNB limits.

1. The probability that an axial gap of a certain size will occur at a given location in the core is determined from fuel performance data.
2. The magnitude of the power spike caused by a single axial gap of a certain size is determined from nuclear calculations as shown in Figure 4.3-19.
3. For each axial interval to be analyzed, axial gap occurrence probabilities and the single event power spikes are entered into the DRAW computer code. The code produces a curve of power spike versus probability of exceeding power spike for each elevation in the core. The power census for a core is then statistically combined with the power spike probability curve to obtain a power spike penalty for the core such that less than one rod will exceed  $F_Q^N$  at a 95 percent confidence level.

The power spike factor due to densification is assumed to be a local perturbation applicable to overpower transients. Thus, densification affects  $F_Q$  but not  $F_{\Delta H}^N$ . The magnitude of the increase power peaking increases from no effect at the bottom of the core to a few percent at the top of the core as shown in Figure 4.3-20, which is applicable to the 94.5 percent (geometric) dense pellets.

For fuel produced by a process other than those for which Reference [4] is applicable, specifications will be followed to ensure that the effects of densification will be no greater than has been allowed in the design. The specifications for quantifying the extent of densification will be based on the NRC report on Fuel Densification (Reference 31).

Results reported in Reference [5] show that the power spike penalty should not be included in the LOCA envelope.

#### 4.3.2.2.6 Limiting Power Distributions

According to the ANSI classification of plant conditions (See Chapter 15).

Condition I occurrences are those which are expected frequently or regularly in the course of power operation, maintenance, or maneuvering of the plant. As such, Condition I occurrences are accommodated with margin between any plant parameter and the value of that parameter which would require either automatic or manual protective action. Inasmuch as Condition I occurrences occur frequently or regularly, they must be considered from the point of view of affecting the consequences of fault conditions (Conditions II, III and IV). In this regard, analysis of each fault condition described is generally based on a conservative set of initial conditions corresponding to the most adverse set of conditions which can occur during Condition I operation.

The list of steady state and shutdown conditions, permissible deviations (such as one coolant loop out of service) and operational transients is given in Section 15.0. Implicit in the definition of normal operation is proper and timely action by the reactor operator. That is, the operator follows recommended operating procedures for maintaining appropriate power distributions and takes any necessary remedial actions when alerted to do so by the plant instrumentation. Thus, as stated above, the worst or limiting power distribution which can occur during normal operation is to be considered as the starting point for analysis of ANSI Conditions II, III and IV events.

Improper procedural actions or errors by the operator are assumed in the design as occurrences of moderate frequency (ANSI Condition II). Some of the Consequences which might result are discussed in Section 15.0. Therefore, the limiting power shapes which result from such Condition II events, are those power shapes which deviate from the normal operating condition at the recommended axial offset bank, e.g., due to lack of proper action by the operator during a xenon transient following a change in power level brought about by control rod motion. Power shapes which fall in this category are used for determination of the reactor protection system setpoints so as to maintain margin to overpower or DNB limits.



The means for maintaining power distributions within the required hot channel factor limits are described in the Technical Specifications. A complete discussion of power distribution control in Westinghouse PWRs is included in Reference [6]. Detailed background information on the design constraints on local power density in a Westinghouse PWR, on the defined operating procedures and on the measures taken to preclude exceeding design limits is presented in the Westinghouse Topical Report on power distribution control and load following procedures (Reference 7). The following paragraphs summarize these reports and describe the calculations used to establish the upper bound on peaking factors.

The calculations used to establish the upper bound on peaking factors,  $F_Q$  and  $F_{\Delta H}^N$ , include all of the nuclear effects which influence the radial and/or axial power distributions throughout core life for various modes of operation including load follow, reduced power operation, and axial xenon transients.

Radial power distributions are calculated for the full power condition and fuel and moderator temperature feedback effects are included for the average enthalpy plane of the reactor. The steady state nuclear design calculations are done for normal flow with the same mass flow in each channel and flow redistribution is calculated explicitly where it is important in the DNB analysis of accidents. The effect of xenon on radial power distribution is small (compare Figures 4.3-6 and 4.3-7) but is included as part of the normal design process. Radial power distributions are relatively fixed and easily bounded with upper limits.

The core average axial profile, however, can experience significant changes which can occur rapidly as a result of rod motion and load changes and more slowly due to xenon distribution. For the study of points of closest approach to axial power distribution limits, several thousand cases are examined. Since the properties of the nuclear design dictate what axial shapes can occur, boundaries on the limits of interest can be set in terms of the parameters which are readily observed on the plant. Specifically, the nuclear design parameters which are significant to the axial power distribution analysis are:

612 139

1. Core power level
2. Core height
3. Coolant temperature and flow
4. Coolant temperature program as a function of reactor power
5. Fuel cycle lifetimes
6. Rod bank worths
7. Rod bank overlaps

Normal operation of the plant assumes compliance with the following conditions:

1. Control rods in a single bank move together with no individual rod insertion differing by more than 13 steps (indicated) from the bank demand position;
2. Control banks are sequenced with overlapping banks;
3. The control full length bank insertion limits are not violated;
4. The design peak linear power density versus core elevation envelope is not violated. (See Figure 4.3-21)

Allowing for fuel densification effects, the average linear power density at 3411 MWt core power is 5.44 KW/ft. The design limit of normalized local power density, including uncertainty allowances, is 2.32 as shown in Figure 4.3-21 which corresponds to a peak linear power density of 12.9 KW/ft at 102 percent power.

1. Core power level
2. Core height
3. Coolant temperature and flow
4. Coolant temperature program as a function of reactor power
5. Fuel cycle lifetimes
6. Rod bank worths
7. Rod bank overlaps

Normal operation of the plant assumes compliance with the following conditions:

1. Control rods in a single bank move together with no individual rod insertion differing by more than 13 steps (indicated) from the bank demand position;
2. Control banks are sequenced with overlapping banks;
3. The control full length bank insertion limits are not violated;
4. Axial power distribution procedures, which are given in terms of flux difference control and control bank position, are observed.

The axial power distribution procedures referred to above are part of the required operating procedures which are followed in normal operation. Briefly, they require control of the axial offset (flux difference divided by fractional power) at all power levels within a permissible operating band of a target value corresponding to the equilibrium full power value. In the first cycle, the target value changes from about -10 to 0 percent linearly through the life of the

The means for maintaining power distributions within the required hot channel factor limits is simply by direct surveillance of the limits and margin to the limits. A complete discussion of the history of power distribution control in Westinghouse designed PWR's is included in References [6], [7], and [9]. Detailed background information on design constraints on local power density, on base load and load follow operating procedures, and measures taken to preclude exceeding design limits are contained in these reports.

The major difference between this method for maintaining power distribution control compared to the methods described in Reference [7] is that direct peaking factor surveillance removes the previous requirement for constant axial offset control. Constant axial offset control imposed limitations on observed flux difference in order to bound the maximum local power density and to insure the continued applicability of limiting initial conditions assumed in the analysis of transients.

Even though the conservative axial offset operating limit restrictions described in Reference [7], are a sufficient means to meet design peaking factor limits, they are no longer necessary due to the direct peaking factor surveillance and protection functions of the integrated control and protection system. (See Section 7)

The following discussion describes in this order.

1. The anticipated method of operation.
2. The results of the nuclear aspects of the LOCA analysis by previous methods and with the current surveillance system, and
3. A brief description of the method by which overpower and DNBR protection was previously accomplished relative to the current method of protection.

612 142

Manual and automatic axial power distribution operating procedures are part of the recommended and automatic operating procedures to be followed during normal operation. These procedures are provided as a convenient means of ensuring operation below the normal operation linear power density limit shown in Figure 4.3-21 and referred to in item 4 above. Briefly they involve control of the axial offset (flux-difference divided by fractional power) at all power levels within a given operating band of a target value corresponding to the equilibrium full power value. However, it must be emphasized that contrary to the previous method<sup>(7)</sup> of restricting violations of axial offset limits, no such restrictions are required herein for assurance of meeting the design  $F_0(Z) \times \text{Power}$  envelope since the peak power density is being continuously monitored by the surveillance system and violations will be alarmed. In the first cycle, the target value of offset changes from about -10 to 0 percent linearly through the life of the cycle. Operating to this target offset minimizes xenon transient effects on the axial power distribution and aids in the control of the plant, since the procedure essentially keeps the xenon distribution in phase with the power distribution. When the maximum return to power capability from reduced power operation is desired, there is also a target position for the full length control banks which corresponds to a power dependent degree of insertion equal to the reactivity defect required to return to full power.

Calculations are performed for normal operation of the reactor including load following maneuvers. Beginning, middle and end of cycle conditions are included in the calculations. Different histories of operation are assumed prior to calculating the effect of load follow transients on the axial power distribution. These different histories assume base loaded operation and extensive load following. For a given plant and fuel cycle a finite number of maneuvers are studied to determine the general behavior of the local power density as a function of core elevation. These cases represent many possible reactor states in the life of one fuel cycle and they have been chosen as sufficiently definitive of the cycle by comparison with much more exhaustive studies performed on some 20 or 30 different, but typical, plant and fuel cycle combinations. The cases are described in detail in Reference [7].

612 143

cycle. This minimizes xenon transient effects on the axial power distribution, since the procedures essentially keep the xenon distribution in phase with the power distribution.

Calculations are performed for normal operation of the reactor including load following maneuvers. Beginning, middle and end of cycle conditions are included in the calculations. Different histories of operation are assumed prior to calculating the effect of load follow transients on the axial power distribution. These different histories assume base loaded operation and extensive load following. For a given plant and fuel cycle, a finite number of maneuvers are studied to determine the general behavior of the local power density as a function of core elevation.

These cases represent many possible reactor states in the life of one fuel cycle, and they have been chosen as sufficiently definitive of the cycle by comparison with much more exhaustive studies performed on some 20 or 30 different, but typical, plant and fuel cycle combinations. The cases are described in detail in Reference [7], and they are considered to be necessary and sufficient to generate a local power density limit which, when increased by 5 percent for conservatism, will not be exceeded with a 95 percent confidence level. Many of the points do not approach the limiting envelope; however, they are part of the time histories which lead to the hundreds of shapes which do define the envelope. They also serve as a check that the reactor studied is typical of those studied more exhaustively.

Thus it is not possible to single out any transient or steady state condition which defines the most limiting case. It is not even possible to separate out a small number which form an adequate analysis. The process of generating a myriad of shapes is essential to the philosophy that leads to the required level of confidence. A maneuver which provides a limiting case for one reactor fuel cycle (defined as approaching the line of Figure 4.3-21) is not necessarily a limiting case for another reactor or fuel cycle with different control bank worths, enrichments, burnup, coefficient, etc. Each shape depends on the

detailed history of operation up to that time and on the manner in which the operator conditioned xenon in the days immediately prior to the time at which the power distribution is calculated.

The calculated points are synthesized from axial calculations combined with radial factors appropriate for rodded and unrodded planes in the first cycle. In these calculations, the effects on the unrodded radial peak of xenon redistribution that occurs following the withdrawal of a control bank (or banks) from a rodded region is obtained from two-dimensional XY calculations. A 1.03 factor to be applied on the unrodded radial peak was obtained from calculations in which xenon distribution was preconditioned by the presence of control rods and then allowed to redistribute for several hours. A detailed discussion of this effect may be found in Reference [7]. The calculated values have been increased by a factor of 1.05 for conservatism and a factor of 1.03 for the engineering factor  $F_Q^E$ .

The envelope drawn over the calculated (  $\max F_Q \times \text{Power}$  ) points in Figure 4.3-21 represents an upper bound envelope on local power density versus elevation in the core. It should be emphasized that this envelope is a conservative representation of the bounding values of local power density. Expected values are considerably smaller and, in fact, less conservative bounding values may be justified with additional analysis or surveillance requirements. For example, Figure 4.3-21 bounds both BOL and EOL conditions but without consideration of radial power distribution flattening with burnup, i.e., both BOL and EOL points presume the same radial peaking factor. Inclusion of the burnup flattening effect would reduce the local power densities corresponding to EOL conditions which may be limiting at the higher core elevations. Additionally, Figure 4.3-21 is based on a radial power distribution invariant with core elevation.

Finally, as previously discussed, this upper bound envelope is based on procedures of load follow which require operation within an allowed deviation from a target equilibrium value of axial flux difference.

Using these procedures, the calculated points are synthesized from axial calculations combined with radial factors appropriate for rodged and unrodged planes in the first cycle. In these calculations the effects on the radial peak of xenon redistribution that occurs following the withdrawal of a control bank (or banks) from a rodged region is obtained from two-dimensional XY calculations. A 1.03 factor to be applied on the unrodged radial peak was obtained from calculations in which xenon distribution was preconditioned by the presence of control rods and then allowed to redistribute for several hours. A detailed discussion of this effect may be found in Reference [7]. The calculated values have been increased by a factor of 1.05 for conservatism and a factor of 1.03 for the engineering factor  $F_Q^E$ .

The results demonstrate that the design basis limits of  $F_Q(Z)$  times relative-power shown in Figure 4.3-21 provides a conservative upper bound for any cycle of operation. This method of analysis, however, is no longer necessary since compliance with the design envelope will be demonstrated by the peak linear power density surveillance system as described in Sections 7, 15 and 16.

Finally, as previously discussed, normal operation is based on manual or automatic operating procedures for base load and load follow operation. These procedures require computer based surveillance supplemented by the normal periodic full core map requirement and a computer-based alarm for violations of the design limit envelope.

The reactor KW/ft protection system setpoints are adjusted to prevent the peak linear power density from exceeding 18 KW/ft for Condition II events e.g., rod control equipment malfunction, operator errors of commission and operator errors of omission. The direct KW/ft and DNB protection eliminates the historical need for the detailed overpower analyses described in Reference [7] to demonstrate compliance with DNB and peak linear power density limits based on a correlation between hot channel factors and axial offset.

612 146



The key nuclear inputs to the protection system are the methods for generating  $F_{XY}(Z)$  and  $F_{\Delta H}$  as a function of power and rod position. The  $F_{XY}(Z)$  is employed in determining peak linear power density as a function of elevation which is used in the overpower protection system and the LOCA surveillance system (See Section 7). The  $F_{\Delta H}$  is employed in the DNBR protection system (See Section 4.4). The following discussion describes the method by which, first,  $F_{XY}(Z)$  is obtained and, secondly,  $F_{\Delta H}$  is obtained.

The maximum linear power density protection and surveillance systems continuously determine the peak KW/ft as a function of core elevation from the measured core power, axial power distribution, and elevation dependent radial peaking factor. The elevation dependent radial peaking factor is also dependent on the measured rod positions and core power level. Asymptotic  $F_{XY}(Z)$  for rodded and unrodded core configurations (ARO, D in, D+C in, D+C+B in) are determined along with the associated power dependence for each configuration during the core design and form part of the input to the KW/ft protection and surveillance systems. As described in more detail in Chapter 7, the composite core  $F_{XY}(Z)$  is formed from the asymptotic  $F_{XY}(Z)$  for the unrodded and various rodded configurations, the known power dependence for each configuration, and the measured core power and rod positions. The radial peaking factors at selected axial elevations are routinely verified by incore measurements using the moveable detector system as described in the technical specifications and may be updated at various times throughout the cycle to take advantage of improved margin to core limits due to burnup flattening.

Allowance for the total error in the protection system input parameters is included in the determination of the protection system setpoints as described in Chapter 7.

Increasing  $F_{\Delta H}^N$  with decreasing power and increasing control bank insertion is permitted by the DNB protection setpoints as described in Section 4.4. This includes the radial power shape changes with control rods inserted deeper than the insertion limits.

These procedures are detailed in the Technical Specifications and are followed by relying only upon excore surveillance supplemented by the normal monthly full core map requirement and by computer based alarms on deviation and time of deviation from the allowed flux difference band.

Allowing for fuel densification effects, the average linear power at 3411 Mwt is 5.44 KW/ft. From Figure 4.3-21, the conservative upper bound value of normalized local power density, including uncertainty allowances, is 2.32 corresponding to a peak linear power of 12.9 KW/ft at 102 percent power.

To determine reactor protection system setpoints, with respect to power distributions, three categories of events are considered, namely rod control equipment malfunctions, operator errors of commission and operator errors of omission. In evaluating these three categories of events, the core is assumed to be operating within four constraints described above.

The first category comprises uncontrolled rod withdrawal (with rods moving in the normal bank sequence) for full length banks. Also included are motions of the full length banks below their insertion limits, which could be caused, for example, by uncontrolled dilution or primary coolant cooldown. Power distributions were calculated throughout these occurrences assuming short term corrective action, that is, no transient xenon effects were considered to result from the malfunction. The event was assumed to occur from typical normal operating situations which include normal xenon transients. It was further assumed in determining the power distributions that total core power level would be limited by reactor trip to below 118 percent. Since the study is to determine protection limits with respect to power and axial offset, no credit was taken for trip setpoint reduction due to flux difference. Results are given in Figure 4.3-22 in units of KW/ft. The peak power density which can occur in such events, assuming reactor trip at or below 118 percent, is less than that required for centerline melt including uncertainties and densification effects.

The second category, also appearing in Figure 4.3-22, assumes that the operator mispositions the full length rod bank in violation of the insertion limits and creates short term conditions not included in normal operating conditions.

The third category assumes that the operator fails to take action to correct a flux difference violation. The results shown on Figure 4.3-23 are  $F_Q$  multiplied by 102 percent power including an allowance for calorimetric error. The figure shows that provided the assumed error in operation does not continue for a period which is long compared to the xenon time constant, the peak linear power does not exceed 18 KW/ft including the above factors.

Analyses of possible operating power shapes show that the appropriate hot channel factors  $F_Q$  and  $F_{\Delta H}^N$  for peak local power density and for DNB analysis at full power are the values given in Table 4.3-2 and addressed in the Technical Specifications.

$F_Q$  can be increased with decreasing power as shown in the Technical Specifications. Increasing  $F_{\Delta H}^N$  with decreasing power is permitted by the DNB protection setpoints and allows radial power shape changes with rod insertion to the insertion limits as described in Section 4.4.4.3. The allowance for increased  $F_{\Delta H}^N$  permitted is  $F_{\Delta H}^N = 1.55 (1 + 0.3 (1-P))$ . This becomes a design basis criterion which is used for establishing acceptable control rod patterns and control bank sequencing. Likewise fuel loading patterns for each cycle are selected with consideration of this design criterion. The worst values of  $F_{\Delta H}^N$  for possible rod configurations occurring in normal operation are used in verifying that this criterion is met. Typical radial factors and radial power distributions are shown in Figures 4.3-6 through 4.3-11. The worst values generally occur when the rods are assumed to be at their insertion limits. Maintenance of constant axial offset control establishes rod positions which are above the allowed rod insertion limits, thus providing increased margin to the  $F_{\Delta H}^N$  criterion. As discussed in Section 3.2 of Reference [9], it has been determined that provided the above conditions 1 through 4 are observed,

The allowance permitted for increased  $F_{\Delta H}^N$  due to decreased power is of the form:

$$F_{\Delta H}^N(\text{Relative Power, Rod Positions}) = F_{\Delta H}^{\text{HFP}}(\text{Rod Positions}) [1 + C[1 - P]]$$

where P is the relative core power and C, the power correction constant, is conservatively determined for each cycle. A value of C=0.10 is typical for most first cycles.

The allowance permitted for increased  $F_{\Delta H}^N$  due to increased rod insertion is shown in figure 4.3-46 for full power first cycle operation. The normal operation design basis full power  $F_{\Delta H}$  is 1.435 without uncertainty allowance, which is used for establishing acceptable control rod patterns and control bank sequencing. Similarly fuel loading patterns for each cycle are selected with consideration of this design criterion. The worst full power values of  $F_{\Delta H}^N$  for possible rod configurations occurring in normal operation are used in verifying that this criterion is met. Typical radial factors are given in Table 4.3-2 and the radial power distributions are shown in Figures 4.3-6 through 4.3-11. The worst normal operation values generally occur when the rods are assumed to be at their insertion limits. However, the worst abnormal  $F_{\Delta H}^N$  values for rod bank insertions below their insertion limits are also used in verifying the rod position dependence to ensure  $F_{\Delta H}^N$  conservatism during Condition II events. The effect of axial power shape variations on  $F_{\Delta H}^N$  although small, are also considered. These limits are taken as input to the thermal-hydraulic design basis as described in Section 4.4.

When a situation is possible in normal operation which could result in local power densities in excess of those assumed as the pre-condition for a subsequent hypothetical accident, but which would not itself cause fuel failure, administrative controls and alarms are provided for returning the core to a safe condition. These alarms are described in detail in Chapters 7 and 16.

The appropriate hot channel factors,  $F_Q^N$  and  $F_{\Delta H}^N$ , for peak local power density and for DNB analysis at full power are the values given in Table 4.3-2 and addressed in the technical specifications.

$F_Q$  can be increased with decreasing power as shown in the technical specifications.

#### 4.3.2.2.7 Experimental Verification of Power Distribution Analysis

This subject is discussed in depth in Reference [2]. A summary of this report is given below. It should be noted that power distribution related measurements are incorporated into the evaluation of calculated power distribution using the INCORE code described in Reference [8]. A detailed description of this code's input and output is included in this reference. The measured vs. calculational comparison is normally performed periodically throughout the cycle lifetime of the reactor as required by Technical Specifications.

In a measurement of the heat flux hot channel factor,  $F_Q$ , with the movable detector system described in Sections 7.7.1 and 4.4.6, the following uncertainties have to be considered:

1. Reproducibility of the measured signal
2. Errors in the calculated relationship between detector current and local flux
3. Errors in the calculated relationship between detector flux and peak rod power some distance from the measurement thimble.

The appropriate allowance for Category 1 above has been quantified by repetitive measurements made with several inter-calibrated detectors by using the common thimble features of the incore detector system. This system allows more than one detector to access any thimble. Errors in Category 2 above are quantified to the extent possible, by using the fluxes measured at one thimble location to predict fluxes at another location which is also measured. Local power distribution predictions are verified in critical experiments on arrays of rods with simulated guide thimbles, control rods, burnable poisons, etc. These critical experiments provide quantification of errors of types 2 and 3 above.

the Technical Specifications limits, are met. These limits are taken as input to the thermal-hydraulic design basis as described in Section 4.4.4.3.1.

When a situation is possible in normal operation which could result in local power densities in excess of those assumed as the pre-condition for a subsequent hypothetical accident, but which would not itself cause fuel failure, administrative controls and alarms are provided for returning the core to a safe condition. These alarms are described in Chapters 7 and 16.

#### 4.3.2.2.7 Experimental Verification of Power Distribution Analysis

This subject is discussed in depth in Reference [2]. A summary of this report is given below. It should be noted that power distribution related measurements are incorporated into the evaluation of calculated power distribution using the INCORE code described in Reference [8]. A detailed description of this code's input and output is included in this reference. The measured vs. calculational comparison is normally performed periodically throughout the cycle lifetime of the reactor as required by Technical Specifications.

In a measurement of the heat flux hot channel factor,  $F_Q$ , with the movable detector system described in Sections 7.7.1 and 4.4.6, the following uncertainties have to be considered:

1. Reproducibility of the measured signal
2. Errors in the calculated relationship between detector current and local flux
3. Errors in the calculated relationship between detector flux and peak rod power some distance from the measurement thimble.

The appropriate allowance for Category I above has been quantified by repetitive measurements made with several inter-calibrated detectors by using the common thimble features of the incore detector system. This

system allows more than one detector to access any thimble. Errors in Category 2 above are quantified to the extent possible, by using the fluxes measured at one thimble location to predict fluxes at another location which is also measured. Local power distribution predictions are verified in critical experiments on arrays of rods with simulated guide thimbles, control rods, burnable poisons, etc. These critical experiments provide quantification of errors of types 2 and 3 above.

Reference [2] describes critical experiments performed at the Westinghouse Reactor Evaluation Center and measurements taken on two Westinghouse plants with incore systems of the same type as used in this plant described herein. The report concludes that the uncertainty associated with  $F_Q$  (heat flux) is 4.58 percent at the 95 percent confidence level with only 5 percent of the measurements greater than the inferred value. This is the equivalent of a  $1.645\sigma$  limit on a normal distribution and is the uncertainty to be associated with a full core flux map with movable detectors reduced with a reasonable set of input data incorporating the influence of burnup on the radial power distribution. The uncertainty is usually rounded up to 5 percent.

In comparing measured power distributions (or detector currents) against the calculations for the same situation, it is not possible to subtract out the detector reproducibility. Thus a comparison between measured and predicted power distributions has to include some measurement error. Such a comparison is given in Figure 4.3-24 for one of the maps used in Reference [2]. Since the first publication of the report, hundreds of maps have been taken on these and other reactors. The results confirm the adequacy of the 5 percent uncertainty allowance on the calculated  $F_Q$ .

A similar analysis for the uncertainty in  $F_{\Delta H}^N$  (rod integral power) measurements results in an allowance of 3.65 percent at the equivalent of a  $1.645\sigma$  confidence level. For historical reasons, an 8 percent uncertainty factor is allowed in the nuclear design calculational basis; that is, the predicted rod integrals at full power must not exceed the design  $F_{\Delta H}^N$  less 8 percent. This 8 percent may be reduced in final design to 4 percent to allow a wider range of acceptable axial power distributions in the DNB analysis and still meet the design bases of Section 4.3.1.3.

A recent measurement in the second cycle of a 121 assembly, 12 foot, core is compared with a simplified one-dimensional core average axial calculation in Figure 4.3-25. This calculation does not give explicit representation to the fuel grids.

612 154



The accumulated data on power distributions in actual operation is basically of three types:

1. Much of the data is obtained in steady state operation at constant power in the normal operating configuration;
2. Data with unusual values of axial offset are obtained as part of the excore detector calibration exercise which is performed monthly;
3. Special tests have been performed in load follow and other transient xenon conditions which have yielded useful information on power distributions.

These data are presented in detail in References [9, 39]. Figure 4.3-26 contains a summary of measured values of  $F_Q$  as a function of axial offset for several plants from these reports.

#### 4.3.2.2.8 Testing

A very extensive series of physics tests is performed on the first core, even though this core is not a prototype design. These tests and the criteria for satisfactory results are described in Chapter 14. Since not all limiting situation can be created at beginning-of-life, the main purpose of the tests is to provide a check on the calculational methods used in the predictions for the conditions of the test. Tests performed at the beginning of each reload cycle are limited to verification of steady state power distributions, on the assumptions that the reload fuel is supplied by the first core designer.

#### 4.3.2.2.9 Monitoring Instrumentation

The adequacy of instrument numbers, spatial deployment, required correlations between readings and peaking factors, calibration and errors are described in References [2, 6, and 9]. The relevant conclusions are summarized here in Sections 4.3.2.2.7 and 4.4.6.

Provided the limitations given in Section 4.3.2.2.6 on control rods moving together in a single bank and control banks sequenced with design overlap, the multi-section excore detector based surveillance system provides adequate online monitoring of power distributions. Further details of specific limits on the observed rod positions and power distributions are given in the Technical Specifications. Descriptions of the systems provided are given in Section 7.7.

#### 4.3.2.3 Reactivity Coefficients

The kinetic characteristics of the reactor core determine the response of the core to changing plant conditions or to operator adjustments made during normal operation, as well as the core response during abnormal or accidental transients. The reactivity coefficients reflect the changes in the neutron multiplication due to varying plant conditions such as power, moderator or fuel temperatures, or less significantly due to a change in pressure or void conditions. Since reactivity coefficients change during the life of the core, ranges of coefficients are employed in transient analysis to determine the response of the plant throughout life. The results of such simulations and the reactivity coefficients used are presented in Chapter 15. The reactivity coefficients are calculated on a corewise basis by radial and axial diffusion theory methods and with nodal analysis methods. The effect of radial and axial power distribution on core average reactivity coefficients is implicit in those calculations and is not significant under normal operating conditions. For example, a skewed xenon distribution which results in changing axial offset by 5 percent changes the moderator and Doppler temperature coefficients by less than 0.01 pcm/<sup>o</sup>F and 0.03 pcm/<sup>o</sup>F respectively. An artificially skewed xenon distribution which results in changing the radial  $F_{\Delta H}$  by 3 percent changes the moderator and Doppler temperature coefficients by less than 0.03 pcm/<sup>o</sup>F and 0.001 pcm/<sup>o</sup>F respectively. The spatial effects are accentuated in some transient conditions; for example, in postulated rupture of the main steamline break and rupture of RCCA mechanism housing described in Sections 15.1.5 and 15.4.8, and are included in these analyses.

The analytical methods and calculational models used in calculating the reactivity coefficients are given in Section 4.3.3. These models have been confirmed through extensive testing of more than thirty cores similar to the plant described herein; results of these tests are discussed in Section 4.3.3.

Quantitative information for calculated reactivity coefficients, including fuel-Doppler coefficient, moderator coefficients (density, temperature, pressure, void) and power coefficient is given in the following sections.

#### 4.3.2.3.1 Fuel Temperature (Doppler) Coefficient

The fuel temperature (Doppler) coefficient is defined as the change in reactivity per degree change in effective fuel temperature and is primarily a measure of the Doppler broadening of U-238 and Pu-240 resonance absorption peaks. Doppler broadening of other isotopes such as U-236, Np-237 etc. are also considered but their contributions to the Doppler effect is small. An increase in fuel temperature increases the effective resonance absorption cross sections of the fuel and produces a corresponding reduction in reactivity.

The fuel temperature coefficient is calculated by performing two-group X-Y calculations using an updated version of the TURTLE (Reference 10) Code. Moderator temperature is held constant and the power level is varied. Spatial variation of fuel temperature is taken into account by calculating the effective fuel temperature as a function of power density as discussed in Section 4.3.3.1.

The Doppler temperature coefficient is shown in Figure 4.3-27 as a function of the effective fuel temperature (at beginning-of-life and end-of-life conditions). The effective fuel temperature is lower than the volume averaged fuel temperature since the neutron flux distribution is non-uniform through the pellet and gives preferential weight to the surface temperature. The Doppler-only contribution to the power coefficient, defined later, is shown in Figure 4.3-28 as a function of relative core power. The integral of the differential curve on Figure

Provided the limitations given in Section 4.3.2.2.6 on rod insertion and flux difference are observed, the excore detector system provides adequate online monitoring of power distributions. Further details of specific limits on the observed rod positions and flux difference are given in the Technical Specifications. Descriptions of the systems provided are given in Section 7.7.

#### 4.3.2.3 Reactivity Coefficients

The kinetic characteristics of the reactor core determine the response of the core to changing plant conditions or to operator adjustments made during normal operation, as well as the core response during abnormal or accidental transients. The reactivity coefficients reflect the changes in the neutron multiplication due to varying plant conditions such as power, moderator or fuel temperatures, or less significantly due to a change in pressure or void conditions. Since reactivity coefficients change during the life of the core, ranges of coefficients are employed in transient analysis to determine the response of the plant throughout life. The results of such simulations and the reactivity coefficients used are presented in Chapter 15. The reactivity coefficients are calculated on a corewise basis by radial and axial diffusion theory methods and with nodal analysis methods. The effect of radial and axial power distribution on core average reactivity coefficients is implicit in those calculations and is not significant under normal operating conditions. For example, a skewed xenon distribution which results in changing axial offset by 5 percent changes the moderator and Doppler temperature coefficients by less than 0.01 pcm/°F and 0.03 pcm/°F respectively. An artificially skewed xenon distribution which results in changing the radial  $F_{\Delta H}$  by 3 percent changes the moderator and Doppler temperature coefficients by less than 0.03 pcm/°F and 0.001 pcm/°F respectively. The spatial effects are accentuated in some transient conditions; for example, in postulated rupture of the main steamline break and rupture of RCCA mechanism housing described in Sections 15.1.5 and 15.4.8, and are included in these analyses.

4.3-28 is the Doppler contribution to the power defect and is shown in Figure 4.3-29 as a function of relative power. The Doppler coefficient becomes more negative as a function of life as the Pu-240 content increases, thus increasing the Pu-240 resonance absorption, but overall becomes less negative since the fuel temperature changes with burnup as described in Section 4.3.3.1. The upper and lower limits of Doppler coefficient used in accident analyses are given in Chapter 15.

#### 4.3.2.3.2 Moderator Coefficients

The moderator coefficient is a measure of the change in reactivity due to a change in specific coolant parameters such as density, temperature, pressure or void. The coefficients so obtained are moderator density, temperature, pressure and void coefficients.

##### Moderator Density and Temperature Coefficients

The moderator temperature (density) coefficient is defined as the change in reactivity per degree change in the moderator temperature. Generally, the effect of the changes in moderator density as well as the temperature are considered together. A decrease in moderator density means less moderation which results in a negative moderator coefficient. An increase in coolant temperature, keeping the density constant, leads to a hardened neutron spectrum and results in an increase in resonance absorption in U-238, Pu-240 and other isotopes. The hardened spectrum also causes a decrease in the fission to capture ratio in U-235 and Pu-239. Both of these effects make the moderator coefficient more negative. Since water density changes more rapidly with temperature as temperature increases, the moderator temperature (density) coefficient becomes more negative with increasing temperature.

The soluble boron used in the reactor as a means of reactivity control also has an effect on moderator density coefficient since the soluble boron poison density as well as the water density is decreased when the coolant temperature rises. A decrease in the soluble poison concentration introduces a positive component in the moderator coefficient.

612 157

Thus, if the concentration of soluble poison is large enough, the net value of the coefficient may be positive. With the burnable poison rods present; however, the initial hot boron concentration is sufficiently low that the moderator temperature coefficient is negative at operating temperatures. The effect of control rods is to make the moderator coefficient more negative by reducing the required soluble boron concentration and by increasing the "leakage" of the core.

With burnup, the moderator coefficient becomes more negative primarily as a result of boric acid dilution but also to a significant extent from the effects of the buildup of plutonium and fission products.

The moderator coefficient is calculated for the various plant conditions discussed above by performing two-group X-Y calculations, varying the moderator temperature (and density) by about  $\pm 5^{\circ}\text{F}$  about each of the mean temperatures. The moderator coefficient is shown as a function of core temperature and boron concentration for the unrodded and rodded core in Figures 4.3-30 through 4.3-32. The temperature range covered is from cold ( $68^{\circ}\text{F}$ ) to about  $600^{\circ}\text{F}$ . The contribution due to Doppler coefficient (because of change in moderator temperature) has been subtracted from these results. Figure 4.3-33 shows the hot, full power moderator temperature coefficient plotted as a function of first cycle lifetime for the just critical boron concentration condition based on the design boron letdown condition.

The moderator coefficients presented here are calculated on a corewide basis, since they are used to describe the core behavior in normal and accident situations when the moderator temperature changes can be considered to affect the entire core.

#### Moderator Pressure Coefficient

The moderator pressure coefficient relates the change in moderator density, resulting from a reactor coolant pressure change, to the corresponding effect on neutron production. This coefficient is of much less

significance in comparison with the moderator temperature coefficient. A change of 50 psi in pressure has approximately the same effect on reactivity as a half-degree change in moderator temperature. This coefficient can be determined from the moderator temperature coefficient by relating change in pressure to the corresponding change in density. The moderator pressure coefficient may be negative over a portion of the moderator temperature range at beginning-of-life (-0.004 pcm/psi, BOL) but is always positive at operating conditions and becomes more positive during life (+0.3 pcm/psi, EOL).

#### Moderator Void Coefficient

The moderator void coefficient relates the change in neutron multiplication to the presence of voids in the moderator. In a PWR this coefficient is not very significant because of the low void content in the coolant. The core void content is less than one-half of one percent and is due to local or statistical boiling. The void coefficient varies from 50 pcm/percent void at BOL and at low temperatures to -250 pcm/percent void at EOL and at operating temperatures. The negative void coefficient at operating temperature becomes more negative with fuel burnup.

#### 4.3.2.3.3 Power Coefficient

The combined effect of moderator temperature and fuel temperature change as the core power level changes is called the total power coefficient and is expressed in terms of reactivity change per percent power change. The power coefficient at BOL and EOL conditions is given in Figure 4.3-34.

It becomes more negative with burnup reflecting the combined effect of moderator and fuel temperature coefficients with burnup. The power defect (integral reactivity effect) at BOL and EOL is given in Figure 4.3-35.

612 161

#### 4.3.2.3.4 Comparison of Calculated and Experimental Reactivity Coefficients

Section 4.3.3 describes the comparison of calculated and experimental reactivity coefficients in detail. Based on the data presented there, the accuracy of the current analytical model is:

- +0.2 percent  $\Delta\rho$  for Doppler and power defect
- +2 pcm/ $^{\circ}$ F for the moderator coefficient.

Experimental evaluation of the calculated coefficients will be done during the physics startup tests described in Chapter 14.

#### 4.3.2.3.5 Reactivity Coefficients Used in Transient Analysis

Table 4.3-2 gives the limiting values as well as the best estimate values for the reactivity coefficients. The limiting values are used as design limits in the transient analysis. The exact values of the coefficient used in the analysis depend on whether the transient of interest is examined at the BOL or EOL, whether the most negative or the most positive (least negative) coefficients are appropriate, and whether spatial nonuniformity must be considered in the analysis. Conservative values of coefficients, considering various aspects of analysis are used in the transient analysis. This is described in Chapter 15.

The reactivity coefficients shown in Figures 4.3-27 through 4.3-35 are best estimate values calculated for this cycle and apply to the core described in Table 4.3-1. The limiting values shown in Table 4.3-2 are chosen to encompass the best estimate reactivity coefficients, including the uncertainties given in Section 4.3.3.3 over appropriate operating conditions calculated for this cycle and the expected values for the subsequent cycles. The most positive as well as the most negative values are selected to form the design basis range used in the transient analysis. A direct comparison of the best estimate and design limit values shown in Table 4.3-2 can be misleading since in many instances,



the most conservative combination of reactivity coefficients is used in the transient analysis even though the extreme coefficients assumed may not simultaneously occur at the conditions of lifetime, power level, temperature and boron concentration assumed in the analysis. The need for a reevaluation of any accident in a subsequent cycle is contingent upon whether or not the coefficients for that cycle fall within the identified range used in the analysis presented in Chapter 15 with due allowance for the calculational uncertainties given in Section 4.3.3.3. Control rod requirements are given in Table 4.3-3 for the core described and for a hypothetical equilibrium cycle since these are markedly different. These latter numbers are provided for information only and their validity in a particular cycle would be an unexpected coincidence.

#### 4.3.2.4 Control Requirements

To ensure the shutdown margin stated in the Technical Specifications under conditions where a cooldown to ambient temperature is required, concentrated soluble boron is added to the coolant. Boron concentrations for several core conditions are listed in Table 4.3-2. For all core conditions including refueling, the boron concentration is well below the solubility limit. The rod cluster control assemblies are employed to bring the reactor to the hot shutdown condition. The minimum required shutdown margin is given in the Technical Specifications.

The ability to accomplish the shutdown for hot conditions is demonstrated in Table 4.3-3 by comparing the difference between the rod cluster control assembly reactivity available with an allowance for the worst stuck rod with that required for control and protection purposes. The shutdown margin includes an allowance of 10 percent for analytic uncertainties (see Section 4.3.2.4.9). The largest reactivity control requirement appears at the EOL when the moderator temperature coefficient reaches its peak negative value as reflected in the larger power defect.

612 163

The control rods are required to provide sufficient reactivity to account for the power defect from full power to zero power and to provide the required shutdown margin. The reactivity addition resulting from power reduction consists of contributions from Doppler, variable average moderator temperature, flux redistribution, and reduction in void content as discussed below.

#### 4.3.2.4.1 Doppler

The Doppler effect arises from the broadening of U-238 and Pu-240 resonance peaks with an increase in effective pellet temperature. This effect is most noticeable over the range of zero power to full power due to the large pellet temperature increase with power generation.

#### 4.3.2.4.2 Variable Average Moderator Temperature

When the core is shutdown to the hot, zero power condition, the average moderator temperature changes from the equilibrium full load value determined by the steam generator and turbine characteristics (steam pressure, heat transfer, tube fouling, etc.) to the equilibrium no load value, which is based on the steam generator shell side design pressure. The design change in temperature is conservatively increased by 40°F to account for the control dead band and measurement errors.

Since the moderator coefficient is negative, there is a reactivity addition with power reduction. The moderator coefficient becomes more negative as the fuel depletes because the boron concentration is reduced. This effect is the major contributor to the increased requirement at end-of-life.

#### 4.3.2.4.3 Redistribution

During full power operation, the coolant density decreases with core height, and this, together with partial insertion of control rods, results in less fuel depletion near the top of the core. Under steady

state conditions, the relative power distribution will be slightly asymmetric towards the bottom of the core. On the other hand, at hot zero power conditions, the coolant density is uniform up the core, and there is no flattening due to Doppler. The result will be a flux distribution which at zero power can be skewed toward the top of the core. The reactivity insertion due to the skewed distribution is calculated with an allowance for effects of xenon distribution.

#### 4.3.2.4.4 Void Content

A small void content in the core is due to nucleate boiling at full power. The void collapse coincident with power reduction makes a small reactivity contribution.

#### 4.3.2.4.5 Rod Insertion Allowance

At full power, the control bank is operated within a prescribed band of travel to compensate for small periodic changes in boron concentration, changes in temperature and very small changes in the xenon concentration not compensated for by a change in boron concentration. When the control bank reaches either limit of this band, a change in boron concentration is required to compensate for additional reactivity changes. Since the insertion limit is set by a rod travel limit, a conservatively high calculation of the inserted worth is made which exceeds the normally inserted reactivity.

#### 4.3.2.4.6 Burnup

Excess reactivity of 10 percent  $\Delta\rho$  (hot) is installed at the beginning of each cycle to provide sufficient reactivity to compensate for fuel depletion and fission products throughout the cycle. This reactivity is controlled by the addition of soluble boron to the coolant and by burnable poison. The soluble boron concentration for several core configurations, the unit boron worth, and burnable poison worth are given in Tables 4.3-1 and 4.3-2. Since the excess reactivity for burnup is controlled by soluble boron and/or burnable poison, it is not included in control rod requirements.

#### 4.3.2.4.7 Xenon and Samarium Poisoning

Changes in xenon and samarium concentrations in the core occur at a sufficiently slow rate, even following rapid power level changes, that the resulting reactivity change is controlled by changing the soluble boron concentration.

#### 4.3.2.4.8 pH effects

Changes in reactivity due to a change in coolant pH, if any, are sufficiently small in magnitude and occur slowly enough to be controlled by the boron system. Further details are provided in Reference [11].

#### 4.3.2.4.9 Experimental Confirmation

Following a normal shutdown, the total core reactivity change during cooldown with a stuck rod has been measured on a 121 assembly, 10 foot high core and 121 assembly, 12 foot high core. In each case, the core was allowed to cooldown until it reached criticality simulating the steamline break accident. For the ten foot core, the total reactivity change associated with the cooldown is overpredicted by about 0.3 percent  $\Delta\rho$  with respect to the measured result. This represents an error of about 5 percent in the total reactivity change and is about half the uncertainty allowance for this quantity. For the 12 foot core, the difference between the measured and predicted reactivity change was an even smaller 0.2 percent  $\Delta\rho$ . These measurements and others demonstrate the ability of the methods described in Section 4.3.3

#### 4.3.2.4.10 Control

Core reactivity is controlled by means of a chemical poison dissolved in the coolant, rod cluster control assemblies, and burnable poison rods as described below.

#### 4.3.2.4.11 Chemical Poison

Boron in solution as boric acid is used to control relatively slow reactivity changes associated with:

1. The moderator temperature defect in going from cold shutdown at ambient temperature to the hot operating temperature at zero power,
2. The transient xenon and samarium poisoning, such as that following power changes or changes in rod cluster control position,
3. The excess reactivity required to compensate for the effects of fissile inventory depletion and buildup of long-life fission products.
4. The burnable poison depletion.

The boron concentrations for various core conditions are presented in Table 4.3-2.

#### 4.3.2.4.12 Rod Cluster Control Assemblies

Full length Rod Cluster Control Assemblies exclusively are employed in this reactor. The number of respective full length assemblies is shown in Table 4.3-1. The full length rod cluster control assemblies are used for shutdown and control purposes to offset fast reactivity changes associated with:

1. The required shutdown margin in the hot zero power, stuck rod condition,
2. The reactivity compensation as a result of an increase in power above hot zero power (power defect including Doppler, and moderator reactivity changes),

3. Unprogrammed fluctuations in boron concentration, coolant temperature, or xenon concentration (with rods not exceeding the allowable rod insertion limits),
4. Reactivity ramp rates resulting from load changes.

The allowed full length control bank reactivity insertion is limited at full power to maintain shutdown capability. As the power level is reduced, control rod reactivity requirements are also reduced and more rod insertion is allowed. The control bank position is monitored and the operator is notified by an alarm if the limit is approached. The determination of the insertion limit uses conservative xenon distributions and axial power shapes. In addition, the rod cluster control assembly withdrawal pattern determined from these analyses is used in determining power distribution factors and in determining the maximum worth of an inserted rod cluster control assembly ejection accident. For further discussion, refer to the Technical Specifications on rod insertion limits.

Power distribution, rod ejection and rod misalignment analyses are based on the arrangement of the shutdown and control groups of the rod cluster control assemblies shown in Figure 4.3-36. All shutdown rod cluster control assemblies are withdrawn before withdrawal of the control banks is initiated. In going from zero to 100 percent power, control banks A, B, C and D are withdrawn sequentially. The limits of rod positions and further discussion on the basis for rod insertion limits are provided in the Technical Specifications.

#### 4.3.2.4.13 Reactor Coolant Temperature

Reactor coolant (or moderator) temperature control has added flexibility in reactivity control of the Westinghouse PWR. This feature takes advantage of the negative moderator temperature coefficient inherent in a PWR to:

1. Maximize return to power capabilities.

612 168

2. Provide +5 percent power load regulation capabilities without requiring control rod compensation, and
3. Extend the time in cycle life to which daily load follow operations can be accomplished.

Reactor coolant temperature control supplements the dilution capability of the plant by lowering the reactor coolant temperature to supply positive reactivity through the negative moderator coefficient of the reactor. After the transient is over, the system automatically recovers the reactor coolant temperature to the programmed value.

Moderator temperature control of reactivity, like soluble boron control, has the advantage of not significantly affecting the core power distribution. However, unlike boron control, temperature control can be rapid enough to achieve reactor power change rates of 5 percent/minute.

#### 4.3.2.4.14 Burnable Poison Rods

The burnable poison rods provide partial control of the excess reactivity available during the first fuel cycle. In doing so, these rods prevent the moderator temperature coefficient from being positive at normal operating conditions. They perform this function by reducing the requirement for soluble poison in the moderator at the beginning of the first fuel cycle as described previously. For purposes of illustration a typical burnable poison rod pattern in the core together with the number of rods per assembly is shown in Figure 4.3-5, while the arrangements within an assembly are displayed in Figure 4.3-4. The reactivity worth of these rods is shown in Table 4.3-1. The boron in the rods is depleted with burnup but at a sufficiently slow rate so that the resulting critical concentration of soluble boron is such that the moderator temperature coefficient remains negative all times for power operating conditions.

612 169

#### 4.3.2.4.15 Peak Xenon Startup

Compensation for the peak xenon buildup is accomplished using the boron control system. Startup from the peak xenon condition is accomplished with a combination of rod motion and boron dilution. The boron dilution may be made at any time, including during the shutdown period, provided the shutdown margin is maintained.

#### 4.3.2.4.16 Load Follow Control and Xenon Control

During load follow maneuvers, power changes are accomplished using control rod motion and dilution or boration by the boron system as required. Control rod motion is limited by the control rod insertion limits on full length rods as provided in the technical specifications and discussed in Sections 4.3.2.4.12 and 4.3.2.4.13. The power distribution is maintained within acceptable limits through the location of the full length rod bank. Reactivity changes due to the changing xenon concentration can be controlled by rod motion and/or changes in the soluble boron concentration.

Late in cycle life, extended load follow capability is obtained by augmenting the limited boron dilution capability at low soluble boron concentrations by temporary moderator temperature reductions.

Rapid power increases (5%/min) from part power during load follow operation are accomplished with a combination of rod motion, moderator temperature reduction, and boron dilution. Compensation for the rapid power increase is accomplished initially by a combination of rod withdrawal and moderator temperature reduction. As the slower boron dilution takes effect after the initial rapid power increase, the moderator temperature returns to the programmed value.

#### 4.3.2.4.17 Burnup

Control of the excess reactivity for burnup is accomplished using soluble boron and/or burnable poison. The boron concentration must be limited during operating conditions to ensure the moderator temperature



coefficient is negative. Sufficient burnable poison is installed at the beginning of a cycle to give the desired cycle lifetime without exceeding the boron concentration limit. The practical minimum boron concentration is 10 ppm.

#### 4.3.2.5 Control Rod Patterns and Reactivity Worth

The full length rod cluster control assemblies are designated by function as the control groups and the shutdown groups. The terms "group" and "bank" are used synonymously throughout this report to describe a particular grouping of control assemblies. The rod cluster assembly pattern is displayed in Figure 4.3-36 which is not expected to change during the life of the plant. The control banks are labeled A, B, C, and D and the shutdown banks are labeled SA, SB, etc., as applicable. Each bank, although operated and controlled as a unit, is comprised of two subgroups. The axial position of the full length rod cluster control assemblies may be controlled manually or automatically. The rod cluster control assemblies are all dropped into the core following actuation of reactor trip signals.

Two criteria have been employed for selection of the control groups. First the total reactivity worth must be adequate to meet the requirements specified in Table 4.3-3. Second, in view of the fact that these rods may be partially inserted at power operation, the total power peaking factor should be low enough to ensure that the power capability requirements are met. Analyses indicate that the first requirement can be met either by a single group or by two or more banks whose total worth equals at least the required amount. The axial power shape would be more peaked following movement of a single group of rods worth three to four percent  $\Delta\rho$ ; therefore, four banks (described as A, B, C, and D in Figure 4.3-36) each worth approximately one percent  $\Delta\rho$  have been selected.

The position of control banks for criticality under any reactor condition is determined by the concentration of boron in the coolant. On an approach to criticality boron is adjusted to ensure that criticality

will be achieved with control rods above the insertion limit set by shutdown and other considerations (see the Technical Specifications). Early in the cycle there may also be a withdrawal limit at low power to maintain a negative moderator temperature coefficient. For the reference first core design described in this chapter, however, no such withdrawal limit is required.

Ejected rod worths are given in Section 15.4.8 for several different conditions.

Allowable deviations due to misaligned control rods are discussed in the Technical Specifications.

A representative calculation for two banks of control rods withdrawn simultaneously (rod withdrawal accident) is given in Figure 4.3-37.

Calculation of control rod reactivity worth versus time following reactor trip involves both control rod velocity and differential reactivity worth. The rod position versus time of travel after rod release normalized to "Distance to Top of Dashpot" and Drop Time to Top of Dashpot" is given in Figure 4.3-38 for hybrid RCC material. For nuclear design purposes, the reactivity worth versus rod position is calculated by a series of steady state calculations at various control rod positions assuming all rods out of the core as the initial position in order to minimize the initial reactivity insertion rate. Also to be conservative, the rod of highest worth is assumed stuck out of the core and the flux distribution (and thus reactivity importance) is assumed to be skewed to the bottom of the core. The result of these calculations is shown on Figure 4.3-39.

The shutdown groups provide additional negative reactivity to assure an adequate shutdown margin. Shutdown margin is defined as the amount by which the core would be subcritical at hot shutdown if all rod cluster control assemblies are tripped, but assuming that the highest worth assembly remains fully withdrawn and no changes in xenon or boron take

place. The loss of control rod worth due to the material irradiation is negligible since only bank D and bank C may be in the core under normal operating conditions.

The values given in Table 4.3-3 show that the available reactivity in withdrawn rod cluster control assemblies provides the design bases minimum shutdown margin allowing for the highest worth cluster to be at its fully withdrawn position. An allowance for the uncertainty in the calculated worth of N-1 rods is made before determination of the shutdown margin.

#### 4.3.2.6 Criticality of the Reactor During Refueling and Criticality of Fuel Assemblies

Criticality of fuel assemblies outside the reactor is precluded by adequate design of fuel transfer, shipping and storage facilities and by administrative control procedures. The two principal methods of preventing criticality are limiting the fuel assembly array size and limiting assembly interaction by fixing the minimum separation between assemblies and/or inserting neutron poisons between assemblies.

The design basis for preventing criticality outside the reactor is that, considering possible variations, there is a 95 percent probability at a 95 percent confidence level that the effective multiplication factor ( $K_{eff}$ ) of the fuel assembly array will be less than 0.95 as recommended in ANSI N210-1976. The following are the conditions that are assumed in meeting this design basis:

1. The fuel assembly contains the highest enrichment authorized without any control rods or any noncontained burnable poison and is at its most reactive point in life.
2. For flooded conditions, the moderator is pure water at the temperature within the design limits which yields the largest reactivity.

612 173

3. The array is either infinite in lateral extent or is surrounded by a conservatively chosen reflector, whichever is appropriate for the design.
4. Mechanical uncertainties are treated by either using "worst case" conditions or by performing sensitivity studies and obtaining appropriate uncertainties.
5. Credit is taken for the neutron absorption in structural materials and in solid materials added specifically for neutron absorption.
6. Where borated water is present, credit for the dissolved boron is not taken except under postulated accident conditions where the double contingency principle of ANSI N16.1-1975 is applied. This principle states that it shall require at least two unlikely, independent, and concurrent events to produce a criticality accident.

For fuel storage application, water is usually present. However, the design methodology also prevents accidental criticality when fuel assemblies are stored in the dry condition. For this case possible sources of moderation such as those that could arise during fire fighting operations are included in the analysis. The design basis  $K_{eff}$  is 0.98 as recommended in ANSI N210-1976.

The design method which insures the criticality safety of fuel assemblies outside the reactor uses the AMPX system of codes (References 32 and 33) for cross-section generation and KENO IV (Reference 34) for reactivity determination.

The 218 energy group cross-section library (Reference 32) that is the common starting point for all cross-sections has been generated from ENDF/B-IV data. The NITAWL program (Reference 33) includes in this library the self-shielded resonance cross-sections that are appropriate for a particular geometry. The Nordheim Integral Treatment is used. Energy and spatial weighting of cross-sections is performed by the

XSDRNPM program (Reference 33) which is a one dimensional  $S_N$  transport theory code. These multi-group cross-section sets are then used as input to KENO IV (Reference 34) which is a three-dimensional Monte Carlo theory program designed for reactivity calculations.

A set of 27 critical experiments has been analyzed using the above method to demonstrate its applicability to criticality analysis and to establish the method bias and variability. The experiments range from water moderated oxide fuel arrays separated by various materials that simulate LWR fuel shipping and storage conditions (References 35, 36) to dry, harder spectrum uranium metal cylinder arrays with various interspersed materials (Reference 37) that demonstrate the wide range of applicability of the method.

Some descriptive facts about each of the 27 benchmark critical experiments are given in Table 4.3-4. The average  $K_{eff}$  of the benchmarks is 0.9998 which demonstrates that there is virtually no bias associated with the method. The standard deviation of the  $K_{eff}$  values is 0.0057  $\Delta k$ . The 95/95 one sided tolerance limit factor for 27 values is 2.26. There is thus a 95% probability with a 95% confidence level that the uncertainty in reactivity due to the method is not greater than 0.013  $\Delta k$ .

The total uncertainty to be added to a criticality calculation is:

$$TU = \left( (ks)_{method}^2 + (ks)_{KENO}^2 + \sum_i (ks)_{mech_i}^2 \right)^{1/2}$$

where  $(ks)_{method}$  is 0.013 as discussed above,  $(ks)_{KENO}$  is the statistical uncertainty associated with the particular KENO calculation being used and the  $(ks)_{mech}$  terms are a series of statistical uncertainties associated with mechanical tolerances such as thicknesses and spacings. If "worst case" assumptions are used for tolerances, this term will be zero.

The criticality design criteria are met when the calculated effective multiplication factor plus the total uncertainty (TU) is less than 0.95 or, in the special case defined above, 0.98.

These methods conform with ANSI N18.2-1973, "Nuclear Safety Criteria for the Design of Stationary Pressurized Water Reactor Plants," Section 5.7, Fuel Handling System; ANSI N210-1976, "Design Objectives for LWR Spent Fuel Storage Facilities at Nuclear Power Stations," Section 5.1.12; ANSI N16.9-1975, "Validation of Calculational Methods for Nuclear Criticality Safety;" NRC Standard Review Plan, Section 9.1.2, "Spent Fuel Storage;" and the NRC guidance, "Review and Acceptance of Spent Fuel Storage and Handling Applications.

#### 4.3.2.7 Stability

##### 4.3.2.7.1 Introduction

The stability of the PWR cores against xenon-induced spatial oscillations and the control of such transients are discussed extensively in References [6, 14, 15 and 16]. A summary of these reports is given in the following discussion and the design bases are given in Section 4.3.1.6.

In a large reactor core, xenon-induced oscillations can take place with no corresponding change in the total power of the core. The oscillation may be caused by a power shift in the core which occurs rapidly by comparison with the xenon-iodine time constants. Such a power shift occurs in the axial direction when a plant load change is made by control rod motion and results in a change in the moderator density and fuel temperature distributions. Such a power shift could occur in the diametral plane of the core as a result of abnormal control action.

Due to the negative power coefficient of reactivity, PWR cores are inherently stable to oscillations in total power. Protection against total power instabilities is provided by the Control and Protection System as described in Section 7.7. Hence, the discussion on the core stability will be limited here to xenon-induced spatial oscillations.

#### 4.3.2.7.2 Stability Index

Power distributions, either in the axial direction or in the X-Y plane, can undergo oscillations due to perturbations introduced in the equilibrium distributions without changing the total core power. The overtones in the current PWRs, and the stability of the core against xenon-induced oscillations can be determined in terms of the eigenvalues of the first flux overtones. Writing, either in the axial direction or in the X-Y plane, the eigenvalue  $\xi$  of the first flux harmonic as:

$$\xi = b + ic, \quad (4.3-1)$$

then  $b$  is defined as the stability index and  $T = 2\pi/c$  as the oscillation period of the first harmonic. The time-dependence of the first harmonic  $\delta\phi$  in the power distribution can now be represented as:

$$\delta\phi(t) = A e^{\xi t} = a e^{bt} \cos ct, \quad (4.3-2)$$

where  $A$  and  $a$  are constants. The stability index can also be obtained approximately by:

$$b = \frac{1}{T} \ln \frac{A_{n+1}}{A_n} \quad (4.3-3)$$

where  $A_n, A_{n+1}$  are the successive peak amplitudes of the oscillation and  $T$  is the time period between the successive peaks.

#### 4.3.2.7.3 Prediction of the Core Stability

The stability of the core described herein (i.e., with 17 x 17 fuel assemblies) against xenon-induced spatial oscillations is expected to be equal to or better than that of earlier designs for cores of similar size. The prediction is based on a comparison of the parameters which are significant in determining the stability of the core against the xenon-induced oscillations, namely 1) the overall core size is unchanged

and spatial power distributions will be similar, 2) the moderator temperature coefficient is expected to be similar to or slightly more negative, and 3) the Doppler coefficient of reactivity is expected to be equal to or slightly more negative at full power.

Analysis of both the axial and X-Y xenon transient tests, discussed in Section 4.3.2.7.5, shows that the calculational model is adequate for the prediction of core stability.

#### 4.3.2.7.4 Stability Measurements

##### 1. Axial Measurements

Two axial xenon transient tests conducted in a PWR with a core height of 12 feet and 121 fuel assemblies are reported in Reference [17], and will be briefly discussed here. The tests were performed at approximately 10 percent and 50 percent of cycle life.

Both a free-running oscillation test and a controlled test were performed during the first test. The second test at mid-cycle consisted of a free-running oscillation test only. In each of the free-running oscillation tests, a perturbation was introduced to the equilibrium power distribution through an impulse motion of the control Bank D and the subsequent oscillation period. In the controlled test conducted early in the cycle, the part length rods were used to follow the oscillations to maintain an axial offset within the prescribed limits. The axial offset of power was obtained from the excore ion chamber readings (which had been calibrated against the incore flux maps) as a function of time for both free-running tests as shown in Figure 4.3-40.

The total core power was maintained constant during these spatial xenon tests, and the stability index and the oscillation period were obtained from a least-square fit of the axial offset data in the form of Equation (4.3-2). The axial offset of power is the



quantity that properly represents the axial stability in the sense that it essentially eliminates any contribution from even order harmonics including the fundamental mode. The conclusions of the tests are:

- a. The core was stable against induced axial xenon transients both at the core average burnups of 1550 MWD/MTU and 7700 MWD/MTU. The measured stability indices are  $-0.041 \text{ hr}^{-1}$  for the first test (Curve 1 of Figure 4.3-40) and  $-0.014 \text{ hr}^{-1}$  for the second test (Curve 2 of Figure 4.3-40). The corresponding oscillation periods are 32.4 hrs. and 27.2 hrs., respectively.
- b. The reactor core becomes less stable as fuel burnup progresses and the axial stability index was essentially zero at 12,000 MWD/MTU.

## 2. Measurements in the X-Y Plane

Two X-Y xenon oscillation tests were performed at a PWR plant with a core height of 12 feet and 157 fuel assemblies. The first test was conducted at a core average burnup of 1540 MWD/MTU and the second at a core average burnup of 12900 MWD/MTU. Both of the X-Y xenon tests show that the core was stable in the X-Y plane at both burnups. The second test shows that the core became more stable as the fuel burnup increased and all Westinghouse PWRs with 121 and 157 assemblies are expected to be stable throughout their burnup cycles.

In each of the two X-Y tests, a perturbation was introduced to the equilibrium power distribution through an impulse motion of one rod cluster control unit located along the diagonal axis. Following the perturbation, the uncontrolled oscillation was monitored using the moveable detector and thermocouple system and the excore power range detectors. The quadrant tilt difference (QTD) is the quantity that properly represents the diametral oscillation in the X-Y plane of the reactor core in that the differences of the quadrant average

powers over two symmetrically opposite quadrants essentially eliminates the contribution to the oscillation from the azimuthal mode. The QTD data were fitted in the form of Equation (4.3-2) through a least-square method. A stability index of  $-0.076 \text{ hr}^{-1}$  with a period of 29.6 hours was obtained from the thermocouple data shown in Figure 4.3-41.

It was observed in the second X-Y xenon test that the PWR core with 157 fuel assemblies had become more stable due to an increased fuel depletion and the stability index was not determined.

#### 4.3.2.7.5 Comparison of Calculations with Measurements

The analysis of the axial xenon transient tests was performed in an axial slab geometry using a flux synthesis technique. The direct simulation of the axial offset data was carried out using the PANDA Code (Reference 18). The analysis of the X-Y xenon transient tests was performed in an X-Y geometry using a modified TURTLE (Reference 10) Code. Both the PANDA and TURTLE codes solve the two-group time-dependent neutron diffusion equation with time-dependent xenon and iodine concentrations. The fuel temperature and moderator density feed back is limited to a steady-state model. All the X-Y calculations were performed in an average enthalpy plane.

The basic nuclear cross-sections used in this study were generated from a unit cell depletion program which has evolved from the codes LEOPARD (Reference 19) and CINDER (Reference 20). The detailed experimental data during the tests including the reactor power level, enthalpy rise and the impulse motion of the control rod assembly, as well as the plant follow burnup data were closely simulated in the study.

The results of the stability calculation for the axial tests are compared with the experimental data in Table 4.3-5. The calculations show conservative results for both of the axial tests with a margin of approximately  $-0.01 \text{ hr}^{-1}$  in the stability index.

An analytical simulation of the first X-Y xenon oscillation test shows a calculated stability index of  $-0.081 \text{ hr}^{-1}$ , in good agreement with the measured value of  $-0.076 \text{ hr}^{-1}$ . As indicated earlier, the second X-Y xenon test showed that the core had become more stable compared to the first test and no evaluation of the stability index was attempted. This increase in the core stability in the X-Y plane due to increased fuel burnup is due mainly to the increased magnitude of the negative moderator temperature coefficient.

Previous studies of the physics of xenon oscillations, including three-dimensional analysis, are reported in the series of topical reports, References [14, 15 and 16]. A more detailed description of the experimental results and analysis of the axial and X-Y xenon transient tests is presented in Reference [17] and Section 1 of Reference [21].

#### 4.3.2.7.6 Stability Control and Protection

The excore detector system is utilized to provide indications of xenon-induced spatial oscillations. The readings from the multi-section excore detectors are available to the operator in the form of axial offset, quadrant power tilt, and a detailed relative core average axial power shape which is required input to the automatic control and protection systems.

##### 1. Axial Power Distribution

For maintenance of proper axial power distributions in manual control, the operator is instructed to maintain an axial offset within a recommended operating band, based on the excore detector readings. Should the axial offset be permitted to move far enough outside this band, the kW/ft or DNB protection limit will be reached and the power will be automatically runback.

Twelve foot PWR cores become less stable to axial xenon oscillations as fuel burnup progresses. However, free xenon oscillations are not allowed to occur except for special tests. The full length control rod banks present in all modern Westinghouse PWRs are sufficient to dampen and control any axial xenon oscillations present.

Should the axial offset be inadvertently permitted to move far enough outside the control band due to an axial xenon oscillation, or any other reason, the protection limits will be reached and the power will be automatically runback.

## 2. Radial Power Distribution

The core described herein is calculated to be stable against X-Y xenon induced oscillations at all times in life.

The X-Y stability of large PWRs has been further verified as part of the startup physics test program for PWR cores with 193 fuel assemblies. The measured X-Y stability of the cores with 157 and 193 assemblies was in good agreement with the calculated stability as discussed in Sections 4.3.2.7.4 and 4.3.2.7.5. In the unlikely event that X-Y oscillations occur, back-up actions are possible and would be implemented, if necessary, to increase the natural stability of the core. This is based on the fact that several actions could be taken to make the moderator temperature coefficient more negative, which will increase the stability of the core in the X-Y plane.

Provisions for protection against non-symmetric perturbations in the X-Y power distribution that could result from equipment malfunctions are made in the protection system design. This includes control rod drop, rod misalignment and asymmetric loss of coolant flow.

A more detailed discussion of the power distribution control in PWR cores is presented in References [6 and 7].

### 4.3.2.8 Vessel Irradiation

A brief review of the methods and analyses used in the determination of neutron and gamma ray flux attenuation between the core and the pressure vessel is given below. A more complete discussion on the pressure vessel irradiation and surveillance program is given in Section 5.3.

An analytical simulation of the first X-Y xenon oscillation test shows a calculated stability index of  $-0.081 \text{ hr}^{-1}$ , in good agreement with the measured value of  $-0.076 \text{ hr}^{-1}$ . As indicated earlier, the second X-Y xenon test showed that the core had become more stable compared to the first test and no evaluation of the stability index was attempted. This increase in the core stability in the X-Y plane due to increased fuel burnup is due mainly to the increased magnitude of the negative moderator temperature coefficient.

Previous studies of the physics of xenon oscillations, including three-dimensional analysis, are reported in the series of topical reports, References [14, 15 and 16]. A more detailed description of the experimental results and analysis of the axial and X-Y xenon transient tests is presented in Reference [17] and Section 1 of Reference [21].

#### 4.3.2.7.6 Stability Control and Protection

The excore detector system is utilized to provide indications of xenon-induced spatial oscillations. The readings from the excore detectors are available to the operator and also form part of the protection system.

##### 1. Axial Power Distribution

For maintenance of proper axial power distributions, the operator is instructed to maintain an axial offset within a prescribed operating band, based on the excore detector readings. Should the axial offset be permitted to move far enough outside this band, the protection limit will be reached and the power will be automatically reduced.

Twelve foot PWR cores become less stable to axial xenon oscillations as fuel burnup progresses. However, free xenon oscillations are not allowed to occur except for special tests. The full length control rod banks present in all modern Westinghouse PWRs are sufficient to dampen and control any axial xenon oscillations present.

Should the axial offset be inadvertently permitted to move far enough outside the control band due to an axial xenon oscillation, or any other reason, the protection limit on axial offset will be reached and the power will be automatically reduced.

## 2. Radial Power Distribution

The core described herein is calculated to be stable against X-Y xenon induced oscillations at all times in life.

The X-Y stability of large PWRs has been further verified as part of the startup physics test program for PWR cores with 193 fuel assemblies. The measured X-Y stability of the cores with 157 and 193 assemblies was in good agreement with the calculated stability as discussed in Sections 4.3.2.7.4 and 4.3.2.7.5. In the unlikely event that X-Y oscillations occur, back-up actions are possible and would be implemented, if necessary, to increase the natural stability of the core. This is based on the fact that several actions could be taken to make the moderator temperature coefficient more negative, which will increase the stability of the core in the X-Y plane.

Provisions for protection against non-symmetric perturbations in the X-Y power distribution that could result from equipment malfunctions are made in the protection system design. This includes control rod drop, rod misalignment and asymmetric loss of coolant flow.

A more detailed discussion of the power distribution control in PWR cores is presented in References [6 and 7].

### 4.3.2.8 Vessel Irradiation

A brief review of the methods and analyses used in the determination of neutron and gamma ray flux attenuation between the core and the pressure vessel is given below. A more complete discussion on the pressure vessel irradiation and surveillance program is given in Section 5.3.

The materials that serve to attenuate neutrons originating in the core and gamma rays from both the core and structural components consist of the core baffle, core barrel, neutron pads and associated water annuli all of which are within the region between the core and the pressure vessel.

In general, few group neutron diffusion theory and nodal analysis codes are used to determine fission power density distributions within the active core and the accuracy of these analyses is verified by incore measurements on operating reactors. Region and rodwise power sharing information from the core calculations is then used as source information in two-dimensional  $S_n$  transport calculations which compute the flux distributions throughout the reactor.

The neutron flux distribution and spectrum in the various structural components varies significantly from the core to the pressure vessel. Representative values of the neutron flux distribution and spectrum are presented in Table 4.3-6. The values listed are based on time averaged equilibrium cycle reactor core parameters and power distributions; and, thus, are suitable for long term nvt projections and for correlation with radiation damage estimates.

As discussed in Section 5.3, the irradiation surveillance program utilizes actual test samples to verify the accuracy of the calculated fluxes at the vessel.

#### 4.3.3 ANALYTICAL METHODS

Calculations required in nuclear design consist of three distinct types, which are performed in sequence:

1. Determination of effective fuel temperatures
2. Generation of macroscopic few-group parameters
3. Space-dependent, few-group diffusion calculations

612 185

These calculations are carried out by computer codes which can be executed individually, however, at Westinghouse most of the codes required have been linked to form an automated design sequence which minimizes design time, avoids errors in transcription of data, and standardizes the design methods.

#### 4.3.3.1 Fuel Temperature (Doppler) Calculations

Temperatures vary radially within the fuel rod, depending on the heat generation rate in the pellet, the conductivity of the materials in the pellet, gap, and clad; and the temperature of the coolant.

The fuel temperatures for use in most nuclear design Doppler calculations are obtained from a simplified version of the Westinghouse fuel rod design model described in Section 4.2.1.3 which considers the effect of radial variation of pellet conductivity, expansion-coefficient and heat generation rate, elastic deflection of the clad, and a gap conductance which depends on the initial fill gap, the hot open gap dimension, and the fraction of the pellet over which the gap is closed. The fraction of the gap assumed closed represents an empirical adjustment used to produce good agreement with observed reactivity data at beginning-of-life. Further gap closure occurs with burnup and accounts for the decrease in Doppler defect with burnup which has been observed in operating plants. For detailed calculations of the Doppler coefficient, such as for use in xenon stability calculations, a more sophisticated temperature model is used which accounts for the effects of fuel swelling, fission gas release, and plastic clad deformation.

Radial power distributions in the pellet as a function of burnup are obtained from LASER (Reference 22) calculations.

The effective U-238 temperature for resonance absorption is obtained from the radial temperature distribution by applying a radially dependent weighting function. The weighting function was determined from REPAD (Reference 23) Monte Carlo calculations of resonance escape probabilities in several steady state and transient temperature distributions. In each case a flat pellet temperature was determined which



produced the same resonance escape probability as the actual distribution. The weighting function was empirically determined from these results.

The effective Pu-240 temperature for resonance absorption is determined by a convolution of the radial distribution of Pu-240 densities from LASER burnup calculations and the radial weighting function. The resulting temperature is burnup dependent, but the difference between U-238 and Pu-240 temperatures, in terms of reactivity effects, is small.

The effective pellet temperature for pellet dimensional change is that value which produces the same outer pellet radius in a virgin pellet as that obtained from the temperature model. The effective clad temperature for dimensional change is its average value.

The temperature calculational model has been validated by plant Doppler defect data as shown in Table 4.3-7 and Doppler coefficient data as shown in Figure 4.3-42. Stability index measurements also provide a sensitive measure of the Doppler coefficient near full power (See Section 4.3.2.7). It can be seen that Doppler defect data is typically within 0.2 percent  $\Delta\rho$  of prediction.

#### 4.3.3.2 Macroscopic Group Constants

Macroscopic few-group constants and analogous microscopic cross sections (needed for feedback and microscopic depletion calculations) are generated for fuel cells by a recent version of the LEOPARD (Reference 19) and CINDER (Reference 20) codes, which are linked internally and provide burnup dependent cross sections. Normally a simplified approximation of the main fuel chains is used; however, where needed, a complete solution for all the significant isotopes in the fuel chains from Th-232 to Cm-244 is available (Reference 24). Fast and thermal cross section library tapes contain microscopic cross sections taken for the most part from the ENDF/B (Reference 25) library, with a few exceptions where other data provided better agreement with critical experiments, isotopic

measurements, and plant critical boron values. The effect on the unit fuel cell of non-lattice components in the fuel assembly is obtained by supplying an appropriate volume fraction of these materials in an extra region which is homogenized with the unit cell in the fast (MUFT) and thermal (SOFOCATE) flux calculations. In the thermal calculation, the fuel rod, clad, and moderator are homogenized by energy-dependent disadvantage factors derived from an analytical fit to integral transport theory results.

Group constants for burnable poison cells, guide thimbles, instrument thimbles and interassembly gaps are generated in a manner analogous to the fuel cell calculation. Reflector group constants are taken from infinite medium LEOPARD calculations. Baffle group constants are calculated from an average of core and radial reflector microscopic group constants for stainless steel.

Group constants for control rods are calculated in a linked version of the HAMMER (Reference 26) and AIM (Reference 27) codes. The Doppler broadened cross sections of the control rod materials are represented as smooth cross sections in the 54 group LEOPARD fast group structure and in 30 thermal groups. The four group constants in the rod cell and appropriate extra region are generated in the coupled space-energy transport HAMMER calculation. A corresponding AIM calculation of the homogenized rod cell with extra region is used to adjust the absorption cross sections of the rod cell to match the reaction rates in HAMMER. These transport-equivalent group constants are reduced to two-group constants for use in space-dependent diffusion calculations. In discrete X-Y calculations only one mesh interval per cell is used, and the rod group constants are further adjusted for use in this standard mesh by reaction rate matching the standard mesh unit assembly to a fine-mesh unit assembly calculation.

Nodal group constants are obtained by a flux-volume homogenization of the fuel cells, burnable poison cells, guide thimbles, instrumentation thimbles, interassembly gap, and control rod cells from one mesh interval per cell X-Y unit fuel assembly diffusion calculations.

Validation of the cross section method is based on analysis of critical experiments as shown in Table 4.3-4, isotopic data as shown in Table 4.3-8, plant critical boron ( $C_B$ ) values at HZP, BOL, as shown in Table 4.3-9 and at HFP as a function of burnup as shown in Figures 4.3-43 through 4.3-45. Control rod worth measurements shown in Table 4.3-10. Confirmatory critical experiments on burnable poisons are described in Reference [28].

#### 4.3.3.3 Spatial Few-Group Diffusion Calculations

Spatial few-group calculations consist primarily of two-group diffusion X-Y calculations using an updated version of the TURTLE Code, and two-group X-Y nodal calculations using PALADON (Reference 38), and two-group axial calculations using an updated version of the PANDA Code.

Discrete X-Y calculations (1 mesh per cell) are carried out to determine critical boron concentrations and power distributions in the X-Y plane. An axial average in the X-Y plane is obtained by synthesis from unrodded and rodded planes. Axial effects in unrodded depletion calculations are accounted for by the axial buckling, which varies with burnup and is determined by radial depletion calculations which are matched in reactivity to the analogous R-Z depletion calculation. The moderator coefficient is evaluated by varying the inlet temperature in the same X-Y calculations used for power distribution and reactivity predictions.

Validation of TURTLE reactivity calculations is associated with the validation of the group constants themselves, as discussed in Section 4.3.3.2. Validation of the Doppler calculations is associated with the fuel temperature validation discussed in Section 4.3.3.1. Validation of the moderator coefficient calculations is obtained by comparison with plant measurements at hot zero power conditions as shown in Table 4.3-11.

PALADON is used in two-dimensional and three-dimensional calculations. PALADON can be used in safety analysis calculations, critical boron concentrations, control rod worths, reactivity coefficients, etc.

Axial calculations are used to determine differential control rod worth curves (reactivity versus rod insertion) and axial power shapes during steady state and transient xenon conditions (flyspeck curve). Group constants and the radial buckling used in the axial calculation are obtained from the PANDA radial calculation, in which group constants in annular rings representing the various material regions in the X-Y plane are homogenized by flux-volume weighting.

Validation of the spatial codes for calculating power distributions involves the use of incore and excore detectors and is discussed in Section 4.3.2.2.7.

Based on comparison with measured data it is estimated that the accuracy of current analytical methods is:

- $\pm 0.2$  percent  $\Delta\rho$  for Doppler defect
- $\pm 2 \times 10^{-5}$   $\Delta\rho/^\circ\text{F}$  for moderator coefficient
- $\pm 50$  ppm for critical boron concentration with depletion
- $\pm 3$  percent for power distributions
- $\pm 0.2$  percent  $\Delta\rho$  for rod bank worth
- $\pm 4$  pcm/step for differential rod worth
- $\pm 0.5$  pcm/ppm for boron worth
- $\pm 0.1$  percent  $\Delta\rho$  for moderator defect

#### 4.3.4 CHANGES

The design methods for the criticality of fuel assemblies outside the reactor now uses the AMPX/KENO ORNL system of codes as described in Section 4.3.2.6.

The design methods for the nuclear analysis of the core now use both TURTLE (Reference 10) and PALADON (Reference 38) for multi-dimensional analyses.

annular rings representing the various material regions in the X-Y plane are homogenized by flux-volume weighting.

Validation of the spatial codes for calculating power distributions involves the use of incore and excore detectors and is discussed in Section 4.3.2.2.7.

Based on comparison with measured data it is estimated that the accuracy of current analytical methods is:

- ± 0.2 percent  $\Delta\rho$  for Doppler defect
- ±  $2 \times 10^{-5} \Delta\rho / \Delta T$  for moderator coefficient
- ± 50 ppm for critical boron concentration with depletion
- ± 3 percent for power distributions
- ± 0.2 percent  $\Delta\rho$  for rod bank worth
- ± 4 pcm/step for differential rod worth
- ± 0.5 pcm/ppm for boron worth
- ± 0.1 percent  $\Delta\rho$  for moderator defect

#### 4.3.4 CHANGES

The design methods for the criticality of fuel assemblies outside the reactor now uses the AMPX/KENO ORNL system of codes as described in Section 4.3.2.6.

The design methods for the nuclear analysis of the core now use both TURTLE (Reference 10) and PALADON (Reference 38) for multi-dimensional analyses.

The fuel assembly is of an improved mechanical design which employs a slightly reduced fuel rod clad outer diameter and pellet diameter while retaining the same fuel rod pitch. Another feature is the incorporation of Zircaloy spacer grids for all both the top and bottom spacer grid locations which will continue to be fabricated from Inconel. The physics characteristics are provided throughout Section 4.3.

The fuel assembly is of an improved mechanical design which employs a slightly reduced fuel rod clad outer diameter and pallet diameter while retaining the same fuel rod pitch. Another feature is the incorporation of Zircaloy spacer grids for all but the top and bottom spacer grid locations which will continue to be fabricated from Inconel. The physics characteristics are provided throughout Section 4.3.

The Overpower  $\Delta T$  and Overtemperature  $\Delta T$  protection system is replaced by the new integrated protection system (IPS) which provides DNB and overpower  $\frac{KW}{ft}$  protection as well as core power distribution and peaking factor monitoring. The system is based on microprocessor evaluation of local and global hot channel factors and comparison against core limit trip and alarm setpoints. Refer to Section 7 for a detailed discussion of the integrated protection system.

#### 4.3.5 REFERENCES

1. "Westinghouse Anticipated Transients Without Reactor Trip Analysis," WCAP-8330, August, 1974.
2. Langford, F. L. and Nath, R. J., "Evaluation of Nuclear Hot Channel Factor Uncertainties," WCAP-7308-L (Proprietary) and WCAP-7810 December, 1971.
3. McFarlane, A. F., "Core Power Capability in Westinghouse PWRs," WCAP-7267-L (Proprietary), October, 1969 and WCAP-7809, December, 1971.
4. Hellman, J. M., (Ed), "Fuel Densification Experimental Results and Model for Reactor Application," WCAP-8218-P-A (Proprietary) and WCAP-8219-A, March, 1975.
5. Hellman, J. M. and Yang, J. W., "Effects of Fuel Densification Power Spikes on Clad Thermal Transients," WCAP-8359, July, 1974.

612 192

6. Moore, J. S., "Power Distribution Control of Westinghouse Pressurized Water Reactors," WCAP-7208 (Proprietary), September, 1968 and WCAP-7811, December, 1971.
7. Morita, T., et al., "Topical Report, Power Distribution Control and Load Following Procedures," WCAP-8385 (Proprietary) and WCAP-8403, September, 1974.
8. Meyer, C. E. and Stover, R. L., "Incore Power Distribution Determination in Westinghouse Pressurized Water Reactors," WCAP-498, July, 1975.
9. McFarlane, A. F., "Power Peaking Factors," WCAP-7912-P-A (Proprietary) and WCAP-7912-A, January, 1975.
10. Altomare, S. and Barry, R. F., "The TURTLE 24.0 Diffusion Depletion Code," WCAP-7213-P-A (Proprietary) and WCAP-7758-A, January, 1975.
11. Cermak, J. O., et al., "Pressurized Water Reactor pH - Reactivity Effect Final Report," WCAP-3696-8 (EURAE-2074), October, 1968.
12. Strawbridge, L. E. and Barry, R. F., "Criticality Calculation for Uniform Water-Moderated Lattices," Nucl. Sci. and Eng. 23, 58 (1965).
13. Dominick, I. E. and Orr, W. L., "Experimental Verification of Wet Fuel Storage Criticality Analyses," WCAP-8682 (Proprietary) and WCAP-8683, December, 1975.
14. Poncelet, C. G. and Christie, A. M., "Xenon-Induced Spatial Instabilities in Large PWRs," WCAP-3680-20, (EURAE-1974) March, 1968.
15. Skogen, F. B. and McFarlane, A. F., "Control Procedures for Xenon-Induced X-Y Instabilities in Large PWRs," WCAP-3680-21, (EURAE2111), February, 1969.

#### 4.3.5 REFERENCES

1. "Westinghouse Anticipated Transients Without Reactor Trip Analysis," WCAP-8330, August, 1974.
2. Langford, F. L. and Nath, R. J., "Evaluation of Nuclear Hot Channel Factor Uncertainties," WCAP-7308-L (Proprietary) and WCAP-7810 December, 1971.
3. McFarlane, A. F., "Core Power Capability in Westinghouse PWRs," WCAP-7267-L (Proprietary), October, 1969 and WCAP-7809, December, 1971.
4. Hellman, J. M., (Ed), "Fuel Densification Experimental Results and Model for Reactor Application," WCAP-8218-P-A (Proprietary) and WCAP-8219-A, March, 1975.
5. Hellman, J. M. and Yang, J. W., "Effects of Fuel Densification Power Spikes on Clad Thermal Transients," WCAP-8359, July, 1974.



16. Skogen, F. B. and McFarlane, A. F., "Xenon-Induced Spatial Instabilities in Three-Dimensions," WCAP-3680-22 (EURAE-2116), September, 1969.
17. Lee, J. C., et al., "Axial Xenon Transient Tests at the Rochester Gas and Electric Reactor," WCAP-7964, June, 1971.
18. Barry, R. F., et al., "The PANDA Code," WCAP-7048-P-A (Proprietary) and WCAP-7757-A, January, 1975.
19. Barry, R. F., "LEOPARD - A Spectrum Dependent Non-Spatial Depletion Code for the IBM-7094," WCAP-3269-26, September, 1963.
20. England, T. R., "CINDER - A One-Point Depletion and Fission Product Program," WAPD-TM-334, August, 1962.
21. Eggleston, F. T., "Safety-Related Research and Development for Westinghouse Pressurized Water Reactors, Program Summaries, Spring 1976," WCAP-8768, June, 1976.
22. Poncelet, C. G., "LASER - A Depletion Program for Lattice Calculations Based on MUFT and THERMOS," WCAP-6073, April, 1966.
23. Olhoeft, J. E., "The Doppler Effect for a Non-Uniform Temperature Distribution in Reactor Fuel Elements," WCAP-2048, July, 1962.
24. Nodvik, R. J., et al., "Supplementary Report on Evaluation of Mass Spectrometric and Radiochemical Analyses of Yankee Core I Spent Fuel, Including Isotopes of Elements Thorium Through Curium," WCAP-6086, August, 1969.
25. Drake, M. K. (Ed), "Data Formats and Procedure for the ENDF/B Neutron Cross Section Library," BNL-50274, ENDF-102, Vol. 1, 1970.

612 195

26. Suich, J. E. and Honeck, H. C., "The HAMMER System, Heterogeneous Analysis by Multigroup Methods of Exponentials and Reactors," DP-1064, January, 1967.
27. Flatt, H. P. and Buller, D. C., "AIM-5, A Multigroup, One Dimensional Diffusion Equation Code," NAA-SR-4694, March, 1960.
28. Moore, J. S., "Nuclear Design of Westinghouse Pressurized Water Reactors with Burnable Poison Rods," WCAP-9000-L, Revision 1 (Proprietary), July, 1969 and WCAP-7806, December, 1971.
29. Nodvik, R. J., "Saxton Core II Fuel Performance Evaluation," WCAP-3385-56, Part II, "Evaluation of Mass Spectrometric and Radiochemical Analyses of Irradiated Saxton Plutonium Fuel," July, 1970.
30. Leamer, R. D., et al., "PUO<sub>2</sub>-UO<sub>2</sub> Fueled Critical Experiments," WCAP-3726-1, July, 1967.
31. Meyer, R. O., "The Analysis of Fuel Densification," Division of Systems Safety, USNRC, NUREG-0085, July, 1976.
32. W. E. Ford III, et al., "A 218-Group Neutron Cross-Section Library in the AMPX Master Interface Format for Criticality Safety Studies," ORNL/CSD/TM-4 (July, 1976).
33. N. M. Greene et al., "AMPX: A Modular Code System for Generating Coupled Multigroup Neutron-Gamma Libraries from ENDF/B," ORNL/TM-3706 (March 1976).
34. L. M. Petrie and N. F. Cross, "KENO IV--An Improved Monte Carlo Criticality Program," ORNL-4938 (Nov. 1975).
35. S. R. Bierman et al., "Critical Separation Between Subcritical Clusters of 2.35 wt % <sup>235</sup>U Enriched UO<sub>2</sub> Rods in Water with Fixed Neutron Posions," Battelle Pacific Northwest Laboratories PNL-2438 (Oct. 1977).

36. S. R. Bierman et al., "Critical Separation Between Subcritical Clusters of 4.29 wt %  $^{235}\text{U}$  Enriched  $\text{UO}_2$  Rods in Water with Fixed Neutron Poisons," Battelle Pacific Northwest Laboratories PNL-2615 (March 1978).
37. J. T. Thomas, "Critical Three-Dimensional Arrays of U (93.2) -- Metal Cylinders," Nuclear Science and Engineering, Vol. 52, pp 350-359 (1973).
38. T. M. Camden et. al., "PALADON - Westinghouse Nodal Computer Code," WCAP-9485 (Proprietary) and WCAP-9486 (December 1978).
39. "Augmented Startup and Cycle 1 Physics Program Supplement 1," WCAP-8575 Supplement 1, June 1976 (Westinghouse Proprietary and WCAP-8576, June 1976 (Non-proprietary)
40. J. R. Easter, "Axial Power Distribution Monitoring Using Four-Section Ex-core Detectors", WCAP-9105, July, 1977 (Proprietary).

612 197

36. S. R. Bierman et al., "Critical Separation Between Subcritical Clusters of 4.29 wt %  $^{235}\text{U}$  Enriched  $\text{UO}_2$  Rods in Water with Fixed Neutron Poisons," Battelle Pacific Northwest Laboratories PNL-2615 (March 1978).
37. J. T. Thomas, "Critical Three-Dimensional Arrays of U (93.2) -- Metal Cylinders," Nuclear Science and Engineering, Vol. 52, pp 350-359 (1973).
38. T. M. Camden et. al., "PALADON - Westinghouse Nodal Computer Code," WCAP-9485 (Proprietary) and WCAP-9486 (December 1978).
39. "Augmented Startup and Cycle 1 Physics Program Supplement 1," WCAP-8575 Supplement 1, June 1976 (Westinghouse Proprietary) and WCAP-8576, June 1976 (Non-proprietary)

TABLE 4.3-1

REACTOR CORE DESCRIPTION

(First Cycle)

Active Core

|   |       |
|---|-------|
| Equivalent Diameter, in.  | 132.7 |
| Core Average Active Fuel Height,<br>First Core, in. (cold dimensions) | 144   |
| Height-to-Diameter Ratio  | 1.09  |
| Total Cross-Section Area, ft <sup>2</sup>                             | 96.06 |
| H <sub>2</sub> O/U Molecular Ratio, Lattice (Cold)                    | 2.73  |

Reflector Thickness and Composition

|                                |     |
|--------------------------------|-----|
| Top - Water plus Steel, in.    | ~10 |
| Bottom - Water plus Steel, in. | ~10 |
| Side - Water plus Steel, in.   | ~15 |

Fuel Assemblies

|   |  |
|---|--|
| Number  | 193  |
| Rod Array                                       | 17 x 17  |
| Rods per Assembly                               | 264  |
| Rod Pitch, in.                                  | 0.496  |
| Overall Transverse Dimensions, in.              | 8.426 x 8.426                                  |
| Fuel Weight (as UO <sub>2</sub> ), lbs.         | 204,200  |
| Zircaloy Weight, lbs. (active core)             | 45,352   |
| Number of Grids per Assembly                    | two - R type<br>six - Z type                   |
| Composition of grids                            | two INC718 End Grids<br>six ZIRC4 Spacer Grids |
| Weight of Grids (Effective in Core) lbs         | INC - 332<br>Zirc - 2985                       |
| Number of Guide Thimbles per Assembly           | 24   |
| Composition of Guide Thimbles                   | Zircaloy 4                                     |
| Diameter of Guide Thimbles (upper<br>part), in. | 0.442 I.D. x 0.474 O.D.                        |

612 199

TABLE 4.3-1 (Continued)

REACTOR CORE DESCRIPTION

(First Cycle)

Fuel Assemblies (Cont'd)

|  |                         |
|--|-------------------------|
| Diameter of Guide Thimbles (lower part), in. | 0.397 I.D. x 0.429 O.D. |
| Diameter of Instrument Guide Thimbles, in.   | 0.442 I.D. x 0.474 O.D. |

Fuel Rods

|                       |            |
|-----------------------|------------|
| Number                | 50,952     |
| Outside Diameter, in. | 0.360      |
| Diametral Gap, in.    | 0.0062     |
| Clad Thickness, in.   | 0.0225     |
| Clad Material         | Zircaloy-4 |

Fuel Pellets

|   |                          |
|---|--------------------------|
| Material  | UO <sub>2</sub> Sintered |
| Density (percent of Theoretical)                    | 95                       |
| Fuel Enrichments w/o                                |                          |
| Region 1  | 2.10                     |
| Region 2  | 2.60                     |
| Region 3  | 3.10                     |
| Diameter, in.                                       | 0.3088                   |
| Length, in.   | 0.510                    |
| Mass of UO <sub>2</sub> per Foot of Fuel Rod, lb/ft | 0.334                    |

Hybrid Rod Cluster Control Assemblies

|                              |                  |
|------------------------------|------------------|
| Neutron Absorber             | B <sub>4</sub> C |
| Diameter, in.                | 0.294            |
| Density, lbs/in <sup>3</sup> | 0.064            |
| Tip Material                 | Ag-In-Cd         |
| Composition                  | 80%, 15%, 5%     |
| Diameter, in.                | 0.301            |
| Length, in.                  | 40               |
| Density, lbs/in <sup>3</sup> | 0.367            |

TABLE 4.3-1 (Continued)

REACTOR CORE DESCRIPTION

(First Cycle)

|  |  |
|--|--|
| Cladding Material                      | Type 304, Cold Worked<br>Stainless Steel |
| Clad Thickness                         | 0.0385                                   |
| Number of Clusters                     |  |
| Full Length                            | 53                                       |
| Number of Absorber Rods per Cluster    | 24                                       |
| Full Length Assembly Weight (dry), lb. | 90                                       |

Burnable Poison Rods (First Core)

|  |                         |
|--|-------------------------|
| Number   | 1934                    |
| Material   | Borosilicate Glass      |
| Outside Diameter, in.  | 0.381                   |
| Inner Tube, O.D., in.  | .1815                   |
| Clad Material  | Stainless Steel         |
| Inner Tube Material  | Stainless Steel         |
| Boron Loading (w/o B <sub>2</sub> O <sub>3</sub> in glass rod) | 12.5                    |
| Weight of Boron - 10 per foot of rod, lb/ft                    | .10419                  |
| Initial Reactivity Worth, %Δρ                                  | ~9.8 (hot), ~7.1 (cold) |

Excess Reactivity

|  |      |
|--|------|
| Maximum Fuel Assembly k <sub>∞</sub> (Cold, Clean,<br>Unborated Water) | 1.39 |
| Maximum Core Reactivity (Cold, Zero Power,<br>Beginning of Cycle)      | 1.22 |

612 201

TABLE 4.3-2

NUCLEAR DESIGN PARAMETERS  
(First Cycle)

|   |                         |                         |
|---|-------------------------|-------------------------|
| <u>Core Average Linear Power, kW/ft, including densification effects</u>                        | 5.44                    |                         |
| <u>Total Heat Flux Hot Channel Factor, <math>F_Q</math></u>                                     | 2.32                    |                         |
| <u>Nuclear Enthalpy Rise Hot Channel Factor, <math>F_{\Delta H}^N</math></u>                    | 1.55                    |                         |
| <u>Reactivity Coefficients<sup>+</sup></u>  | <u>Design Limits</u>    | <u>Best Estimate</u>    |
| Doppler-only Power, Coefficients, pcm/% Power (upper limit)<br>(See Figure 15.1-5), Lower Limit | -19.4 to -12.6          | -12.2 to -8.1           |
| Doppler Temperature Coefficient, pcm/ <sup>o</sup> F  | -9.5 to -6.0            | -11.8 to -7.9           |
| Moderator Temperature Coefficient, pcm/ <sup>o</sup> F  | -2.9 to -0.9            | -2.2 to -1.2            |
| Boron Coefficient, pcm/ppm  | $\leq 0$                | -1 to -30               |
| Rodded Moderator Density, pcm/gm/cc   | -16 to -7               | -13 to -9               |
|   | $\leq 0.43 \times 10^5$ | $\leq 0.24 \times 10^5$ |

+Uncertainties are given in Section 4.3.3.3



TABLE 4.3-2 (Continued)

NUCLEAR DESIGN PARAMETERS  
(First Cycle)

Delayed Neutron Fraction and Lifetime

|                                  |                  |
|----------------------------------|------------------|
| $\beta_{\text{eff}}$ BOL, (EOL)  | 0.0075, (0.0044) |
| $\lambda$ , BOL, (EOL) $\mu$ sec | 20.7 (21.3)      |

Control Rods

|                                       |                 |
|---------------------------------------|-----------------|
| Rod Requirements                      | See Table 4.3-3 |
| Maximum Bank Worth, pcm <sup>++</sup> | < 2000          |
| Maximum Ejected Rod Worth             | See Chapter 15  |

Radial Factor (BOL to EOL)

|           |              |
|-----------|--------------|
| Unrodded  | 1.37 to 1.25 |
| D bank    | 1.58 to 1.42 |
| D + C     | 1.63 to 1.42 |
| D + C + B | 1.80 to 1.55 |

Boron Concentrations

|  |      |
|--|------|
| Zero Power, $k_{\text{eff}} = 1.00$ , Cold Rod Cluster       |      |
| Control Assemblies Out, 1% $\Delta\rho$ uncertainty included | 1165 |
| Zero Power, $k_{\text{eff}} = 1.00$ , Hot Rod Cluster        |      |
| Control Assemblies Out, 1% $\Delta\rho$ uncertainty included | 1140 |
| Design Basis Refueling Boron Concentration                   | 2000 |

++Note: 1 pcm = (percent mille rho) =  $10^{-5} \Delta\rho$  where  $\Delta\rho$  is calculated from two statepoint values of  $k_{\text{eff}}$  by  $\ln(k_2/k_1)$

TABLE 4.3-2 (Continued)

NUCLEAR DESIGN PARAMETERS  
(First Cycle)

Boron Concentrations (Cont'd)

|   |                  |
|---|------------------|
| Zero Power, $k_{eff} \leq 0.95$ , Cold Rod Cluster<br>Control Assemblies In, 1% $\Delta\rho$ uncertainty included | 950              |
| Zero Power, $k_{eff} = 1.00$ , Hot Rod Cluster<br>Control Assemblies Out  | 1037             |
| Full Power, No Xenon, $k_{eff} = 1.0$ , Hot Rod<br>Cluster Control Assemblies Out                                 | 945              |
| Full Power, Equilibrium Xenon, $k_{eff} = 1.0$ ,<br>Hot Rod Cluster Control Assemblies Out                        | 683              |
| Reduction with Fuel Burnup  |                  |
| First Cycle, ppm/GWD/MTU**  | See Figure 4.3-3 |
| Reload Cycle, ppm/GWD/MTU   | ~ 100            |

\*\* Gigawatt Day (GWD) = 1000 Megawatt Day (1000 MWD). During the first cycle, fixed burnable poison rod are present which significantly reduce the boron depletion rate compared to reload cycles.

4.3-73

612 204

TABLE 4.3-3

REACTIVITY REQUIREMENTS FOR ROD CLUSTER CONTROL ASSEMBLIES

| <u>Reactivity Effects,</u><br><u>percent</u>  | <u>Beginning of Life</u><br><u>(First Cycle)</u> | <u>End of Life</u><br><u>(First Cycle)</u> | <u>End of Life</u><br><u>(Equilibrium Cycle)</u><br><u>(Preliminary)</u> |
|---|--|--|--|
| 1. Control requirements   |  |  |  |
| Fuel temperature (Doppler), % $\Delta\rho$  | 1.08   | 1.06                                       | 1.10   |
| Moderator temperature, % $\Delta\rho$   | .10  | 1.06                                       | 1.10   |
| Void, % $\Delta\rho$  | .01  | .05  | .05  |
| Redistribution, % $\Delta\rho$  | .50  | .85  | .95  |
| Rod Insertion Allowance, % $\Delta\rho$   | .50  | .50  | .50  |
| 2. Total Control, % $\Delta\rho$  | 2.19   | 3.52                                       | 3.70   |
| 3. Estimated Hybrid Rod Cluster Control<br>Assembly Worth (53 Rods)   |  |  |  |
| a. All full length assemblies<br>inserted, % $\Delta\rho$   | 8.85   | 8.13                                       | 7.65   |
| b. All but one (highest worth)<br>assemblies inserted, % $\Delta\rho$   | 7.51   | 6.68                                       | 6.49   |
| 4. Estimated Rod Cluster Control Assembly<br>credit with 10 percent adjustment to<br>accommodate uncertainties (3b - 10<br>percent), % $\Delta\rho$ | 6.76   | 6.01                                       | 5.84   |
| 5. Shutdown margin available (4-2),<br>% $\Delta\rho$   | 4.57   | 2.49                                       | 2.14 <sup>a</sup>  |

<sup>a</sup> The design basis minimum shutdown is 1.3%  $\Delta\rho$

TABLE 4.3-4

BENCHMARK CRITICAL EXPERIMENTS<sup>(35,36,37)</sup>

|     | General<br>Description      | Enrichment<br>w/o U235 | Reflector | Separating<br>Material | Characterizing<br>Separation (cm) |
|-----|-----------------------------|------------------------|-----------|------------------------|-----------------------------------|
| 1.  | UO <sub>2</sub> rod lattice | 2.35                   | water     | water                  | 11.92                             |
| 2.  | "                           | "                      | "         | "                      | 8.39                              |
| 3.  | "                           | "                      | "         | "                      | 6.39                              |
| 4.  | "                           | "                      | "         | "                      | 4.46                              |
| 5.  | "                           | "                      | "         | stainless steel        | 10.44                             |
| 6.  | "                           | "                      | "         | "                      | 11.47                             |
| 7.  | "                           | "                      | "         | "                      | 7.76                              |
| 8.  | "                           | "                      | "         | "                      | 7.42                              |
| 9.  | "                           | "                      | "         | boral                  | 6.34                              |
| 10. | "                           | "                      | "         | "                      | 9.03                              |
| 11. | "                           | "                      | "         | "                      | 5.05                              |
| 12. | "                           | 4.29                   | "         | water                  | 10.64                             |
| 13. | "                           | "                      | "         | stainless steel        | 9.76                              |
| 14. | "                           | "                      | "         | "                      | 8.08                              |
| 15. | "                           | "                      | "         | boral                  | 6.72                              |
| 16. | U metal cylinders           | 93.2                   | bare      | air                    | 15.43                             |
| 17. | "                           | "                      | paraffin  | air                    | 23.84                             |
| 18. | "                           | "                      | bare      | air                    | 19.97                             |
| 19. | "                           | "                      | paraffin  | air                    | 36.47                             |
| 20. | "                           | "                      | bare      | air                    | 13.74                             |
| 21. | "                           | "                      | paraffin  | air                    | 23.48                             |
| 22. | "                           | "                      | bare      | plexiglas              | 15.74                             |
| 23. | "                           | "                      | paraffin  | plexiglas              | 24.43                             |
| 24. | "                           | "                      | bare      | plexiglas              | 21.74                             |
| 25. | "                           | "                      | paraffin  | plexiglas              | 27.94                             |
| 26. | "                           | "                      | bare      | steel                  | 14.74                             |
| 27. | "                           | "                      | bare      | plexiglas, steel       | 16.67                             |

4.3-75

612

206

TABLE 4.3-5

AXIAL STABILITY INDEX PRESSURIZED WATER REACTOR  
CORE WITH A 12 FOOT HEIGHT

| Burnup<br>(MWD/MTU) | $F_Z$ | $C_B$<br>(ppm) | Stability Index ( $hr^{-1}$ ) |        |
|---------------------|-------|----------------|-------------------------------|--------|
|                     |       |                | Exp                           | Calc   |
| 1550                | 1.34  | 1065           | -0.041                        | -0.032 |
| 7700                | 1.27  | 700            | -0.014                        | -0.006 |
|                     |       | Difference:    | +0.027                        | +0.026 |

612 207

TABLE 4.3-6

TYPICAL NEUTRON FLUX LEVELS ( $n/cm^2$ -sec) AT FULL POWER

|   | $E > 1.0 \text{ Mev}$ | $5.53 \text{ Kev} < E \leq 1.0 \text{ Mev}$ | $.625 \text{ ev} \leq E < 5.53 \text{ Kev}$ | $E < .625 \text{ ev}$<br>$(nv)_0$ |
|---|-----------------------|---|---|-----------------------------------|
| CORE CENTER   | $6.51 \times 10^{13}$ | $1.12 \times 10^{14}$                       | $8.50 \times 10^{13}$                       | $3.00 \times 10^{13}$             |
| CORE OUTER RADIUS<br>AT MIDHEIGHT                                   | $3.23 \times 10^{13}$ | $5.74 \times 10^{13}$                       | $4.63 \times 10^{13}$                       | $8.60 \times 10^{12}$             |
| CORE TOP,<br>ON AXIS  | $1.53 \times 10^{13}$ | $2.42 \times 10^{13}$                       | $2.10 \times 10^{13}$                       | $1.63 \times 10^{13}$             |
| CORE BOTTOM<br>ON AXIS  | $2.36 \times 10^{13}$ | $3.94 \times 10^{13}$                       | $3.50 \times 10^{13}$                       | $1.46 \times 10^{13}$             |
| PRESSURE VESSEL<br>INNER WALL,<br>AZIMUTHAL PEAK,<br>CORE MIDHEIGHT | $2.77 \times 10^{10}$ | $5.75 \times 10^{10}$                       | $6.03 \times 10^{10}$                       | $8.38 \times 10^{10}$             |

4.3-77

612 208

TABLE 4.3-7

COMPARISON OF MEASURED AND CALCULATED DOPPLER DEFECTS

| <u>Plant</u> | <u>Fuel Type</u>         | <u>Core Burnup<br/>(MWD/MTU)</u> | <u>Measured (pcm)</u> | <u>Calculated<br/>(pcm)</u> |
|--------------|--------------------------|----------------------------------|-----------------------|-----------------------------|
| 1            | Air-filled               | 1800                             | 1700                  | 1710                        |
| 2            | Air-filled               | 7700                             | 1300                  | 1440                        |
| 3            | Air and<br>helium-filled | 8460                             | 1200                  | 1210                        |

612 207

TABLE 4.3-8

SAXTON CORE II ISOTOPICS  
ROD MY, AXIAL ZONE 6

| <u>Atom Ratio</u> | <u>Measured*</u>       | <u>2<math>\sigma</math> Precision (%)</u> | <u>LEOPARD<br/>Calculation</u> |
|-------------------|------------------------|---|--------------------------------|
| U-234/U           | $4.65 \times 10^{-5}$  | <u>+29</u>                                | $4.60 \times 10^{-5}$          |
| U-235/U           | $5.74 \times 10^{-3}$  | <u>+0.9</u>                               | $5.73 \times 10^{-3}$          |
| U-236/U           | $3.55 \times 10^{-4}$  | <u>+5.6</u>                               | $3.74 \times 10^{-4}$          |
| U-238/U           | 0.99386                | <u>+0.01</u>                              | 0.99385                        |
| Pu-238/Pu         | $1.32 \times 10^{-3}$  | <u>+2.3</u>                               | $1.222 \times 10^{-3}$         |
| Pu-239/Pu         | 0.73971                | <u>+0.03</u>                              | 0.74497                        |
| Pu-240/Pu         | 0.19302                | <u>+0.2</u>                               | 0.19102                        |
| Pu-241/Pu         | $6.014 \times 10^{-2}$ | <u>+0.3</u>                               | $5.74 \times 10^{-2}$          |
| Pu-242/Pu         | $5.81 \times 10^{-3}$  | <u>+0.9</u>                               | $5.38 \times 10^{-3}$          |
| Pu/U**            | $5.938 \times 10^{-2}$ | <u>+0.7</u>                               | $5.970 \times 10^{-2}$         |
| Np-237/U-238      | $1.14 \times 10^{-4}$  | <u>+15</u>                                | $0.86 \times 10^{-4}$          |
| Am-241/Pu-239     | $1.23 \times 10^{-2}$  | <u>+15</u>                                | $1.08 \times 10^{-2}$          |
| Cm-242/Pu-239     | $1.05 \times 10^{-4}$  | <u>+10</u>                                | $1.11 \times 10^{-4}$          |
| Cm-244/Pu-239     | $1.09 \times 10^{-4}$  | <u>+20</u>                                | $0.98 \times 10^{-4}$          |

\* Reported in Reference 29

\*\* Weight ratio

612 210



TABLE 4.3-9

CRITICAL BORON CONCENTRATIONS, HZP, BOL

| <u>Plant Type</u>                      | <u>Measured</u> | <u>Calculated</u> |
|--|-----------------|-------------------|
| 2-Loop, 121 Assemblies<br>10 foot core | 1583            | 1589              |
| 2-Loop, 121 Assemblies<br>12 foot core | 1625            | 1624              |
| 2-Loop, 121 Assemblies<br>12 foot core | 1517            | 1517              |
| 3-Loop, 157 Assemblies<br>12 foot core | 1169            | 1161              |
| 3-Loop, 157 Assemblies<br>12 foot core | 1344            | 1319              |
| 4-Loop, 193 Assemblies<br>12 foot core | 1370            | 1355              |
| 4 Loop, 193 Assemblies<br>12 foot core | 1321            | 1306              |

612 211

TABLE 4.3-10

BENCHMARK CRITICAL EXPERIMENTS  
B<sub>4</sub>C CONTROL ROD WORTH

| <u>WREC<br/>Critical<br/>Experiment</u> | <u>No. of<br/>Fuel<br/>Rods</u> | <u>No. of<br/>Control<br/>Rods</u> | <u>Measured(a)<br/>Worth,<br/>%Δρ</u> | <u>Calculated<br/>Worth,<br/>%Δρ</u> |
|---|---------------------------------|------------------------------------|---------------------------------------|--------------------------------------|
| 2A                                      | 888                             | 12 .395" O.D. B <sub>4</sub> C     | 8.20                                  | 8.37                                 |
| 3B                                      | 888                             | 12 .232" O.D. B <sub>4</sub> C     | 4.81                                  | 4.82                                 |
| 4B                                      | 884                             | 16 .232" O.D. B <sub>4</sub> C     | 6.57                                  | 6.35                                 |
| 5B                                      | 945                             | 16 .232" O.D. B <sub>4</sub> C     | 5.98                                  | 5.83                                 |

(a)

The measured worth was derived from the calculated value of  $\lambda_n$   $k_1/k_2$ , where  $k_1$  and  $k_2$  were calculated with the measured buckling before and after insertion of the control rods, which replace full rods in arrays at the center of the experiment. The standard deviation in the measured worth is about 0.3% Δρ based on the uncertainties in the measured axial bucklings.

AG-IN-CD COMPARISON OF MEASURED AND CALCULATED ROD WORTH

| <u>4-Loop Plant, 193 Assemblies,<br/>12-foot core</u>  | <u>Measured (pcm)</u> | <u>Calculated (pcm)</u> |
|--|-----------------------|-------------------------|
| Bank D   | 1403                  | 1366                    |
| Bank C   | 1196                  | 1154                    |
| All Rods In Less One   | 6437                  | 6460                    |
| <u>ESADA Critical*, 0.69 Inch<br/>Pitch, 2 w/o PuO<sub>2</sub>, 8% Pu<sup>240</sup><br/>9 Control Rods</u> |                       |                         |
| 6.21 inch rod separation   | 2250                  | 2250                    |
| 2.07 inch rod separation   | 4220                  | 4160                    |
| 1.38 inch rod separation   | 4100                  | 4019                    |

\* Reported in Reference 30.

TABLE 4.3-11

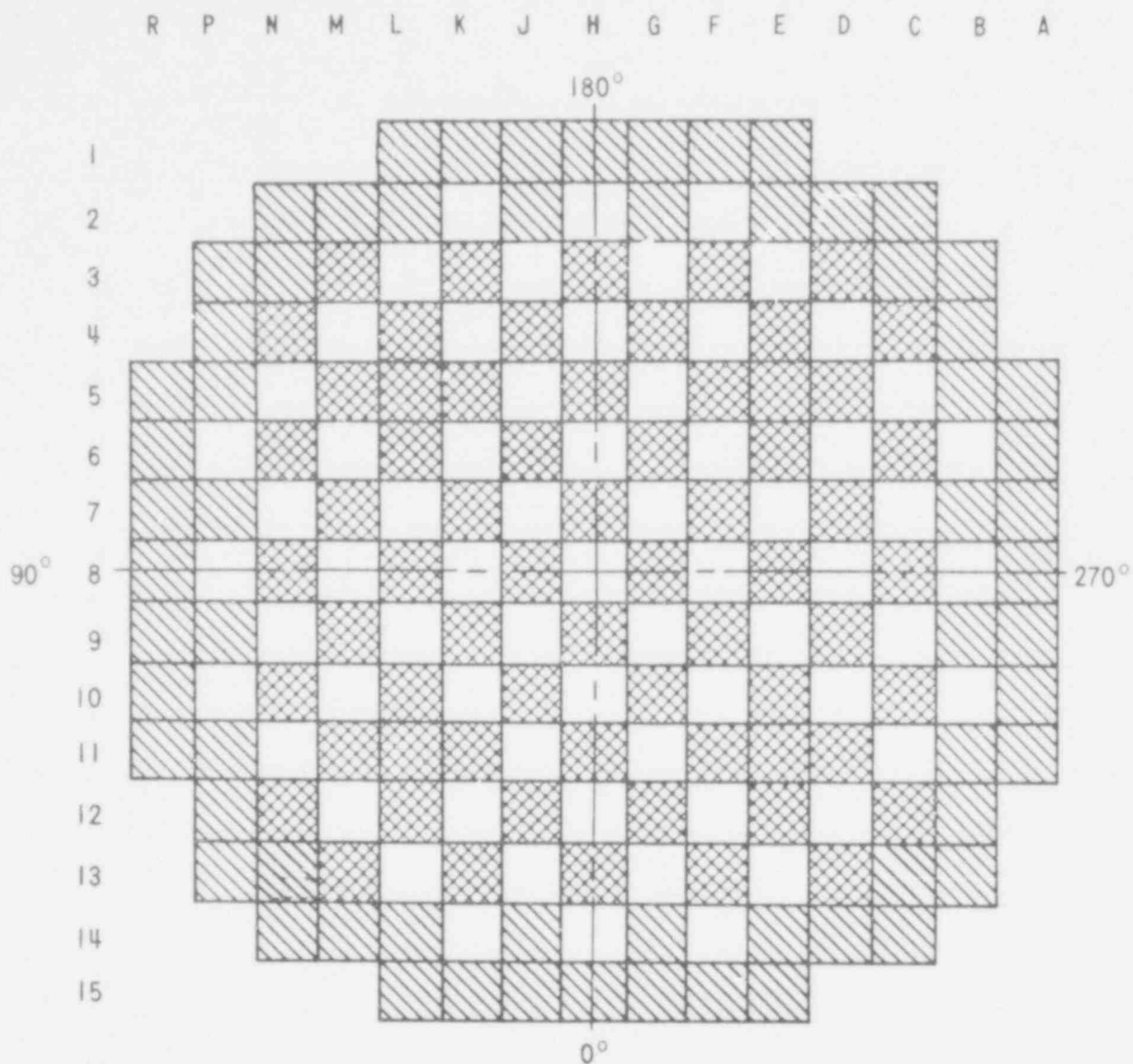
COMPARISON OF MEASURED AND CALCULATED MODERATOR  
COEFFICIENTS AT HZP, BOL





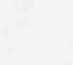
| <u>Plant Type/<br/>Control Bank Configuration</u> | <u>Measured <math>\alpha_{iso}^*</math><br/>(pcm/°F)</u> | <u>Calculated <math>\alpha_{iso}</math><br/>(pcm/°F)</u> |
|---|--|--|
| 2-Loop, 121 Assemblies,<br>12 foot core           |  |  |
| D at 180 steps                                    | +0.85  | +1.02  |
| D in, C at 180 steps                              | -2.40  | -1.90  |
| C and D in, B at 165 steps                        | -4.40  | -5.58  |
| B, C, and D in A at 174 steps                     | -8.70  | -8.12  |
| 3-Loop, 157 Assemblies,<br>12 foot core           |  |  |
| D at 160 steps                                    | -0.50  | -0.50  |
| D in, C at 190 steps                              | -3.01  | -2.75  |
| D in, C at 28 steps                               | -7.67  | -7.02  |
| B, C and D in                                     | -5.16  | -4.45  |
| 4-loop, 193 assemblies,<br>12 foot core           |  |  |
| ARO   | -0.52  | -1.2   |
| D in  | -4.35  | -5.7   |
| D + C in  | -8.59  | -10.0  |
| D + C + B in                                      | -10.14   | -10.55   |
| D + C + B + A in                                  | -14.63   | -14.45   |

\*Isothermal coefficients, which include the Doppler effect in the fuel.

$$\alpha_{iso} = 10^5 \ln \frac{k_2}{k_1} / \Delta T^{°F}$$

612 213

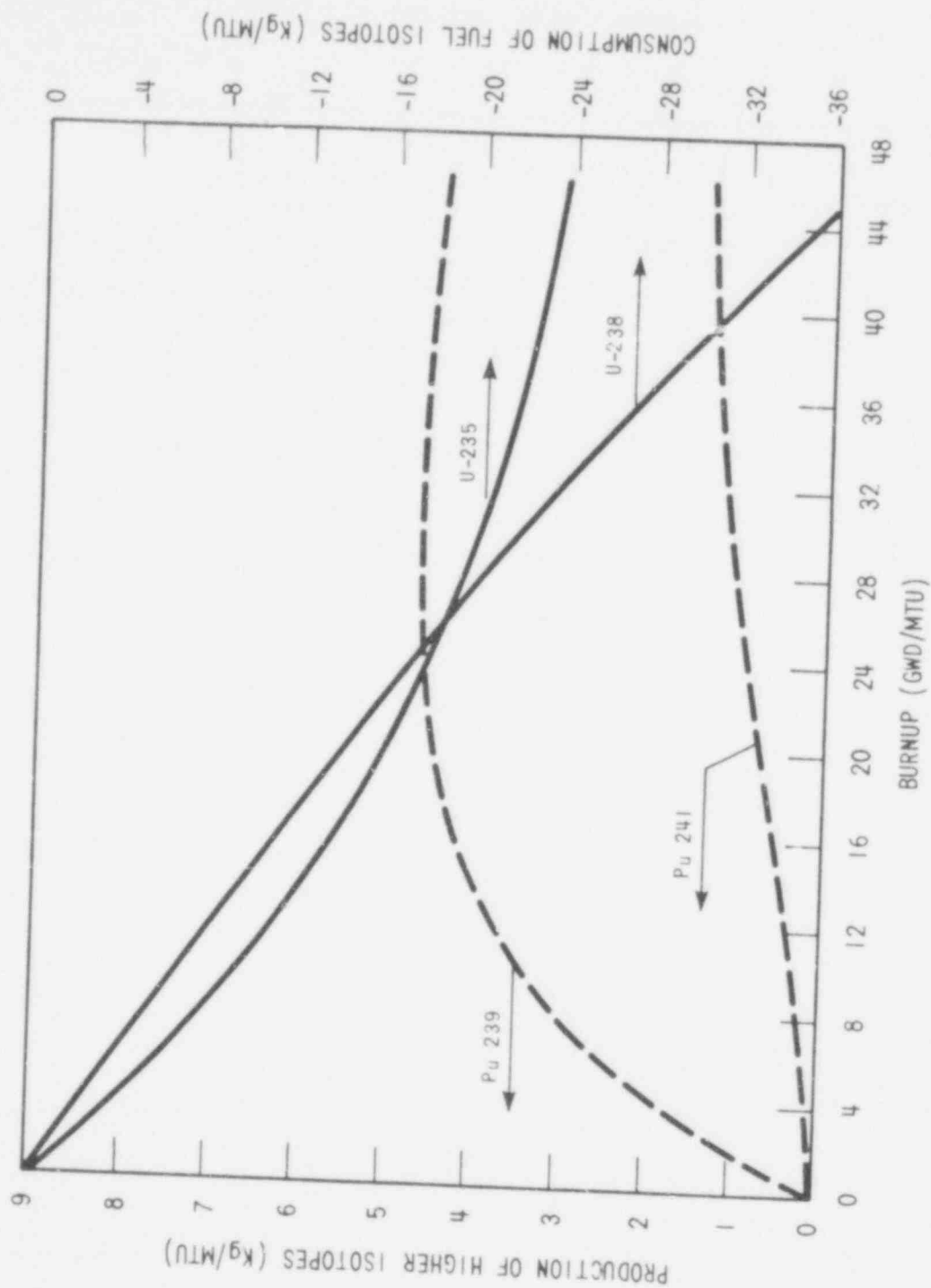


| FIRST CORE  |          | 3 REGION RELOAD CORE  |                           |
|---|----------|---|---------------------------|
|  | REGION 1 |  | ONCE OR TWICE BURNED FUEL |
|  | REGION 2 |  | ONCE OR TWICE BURNED FUEL |
|   | REGION 3 |  | FRESH FUEL                |

612 214

WCAP - 9500

Figure 4.3-1.  
Fuel Loading Arrangement

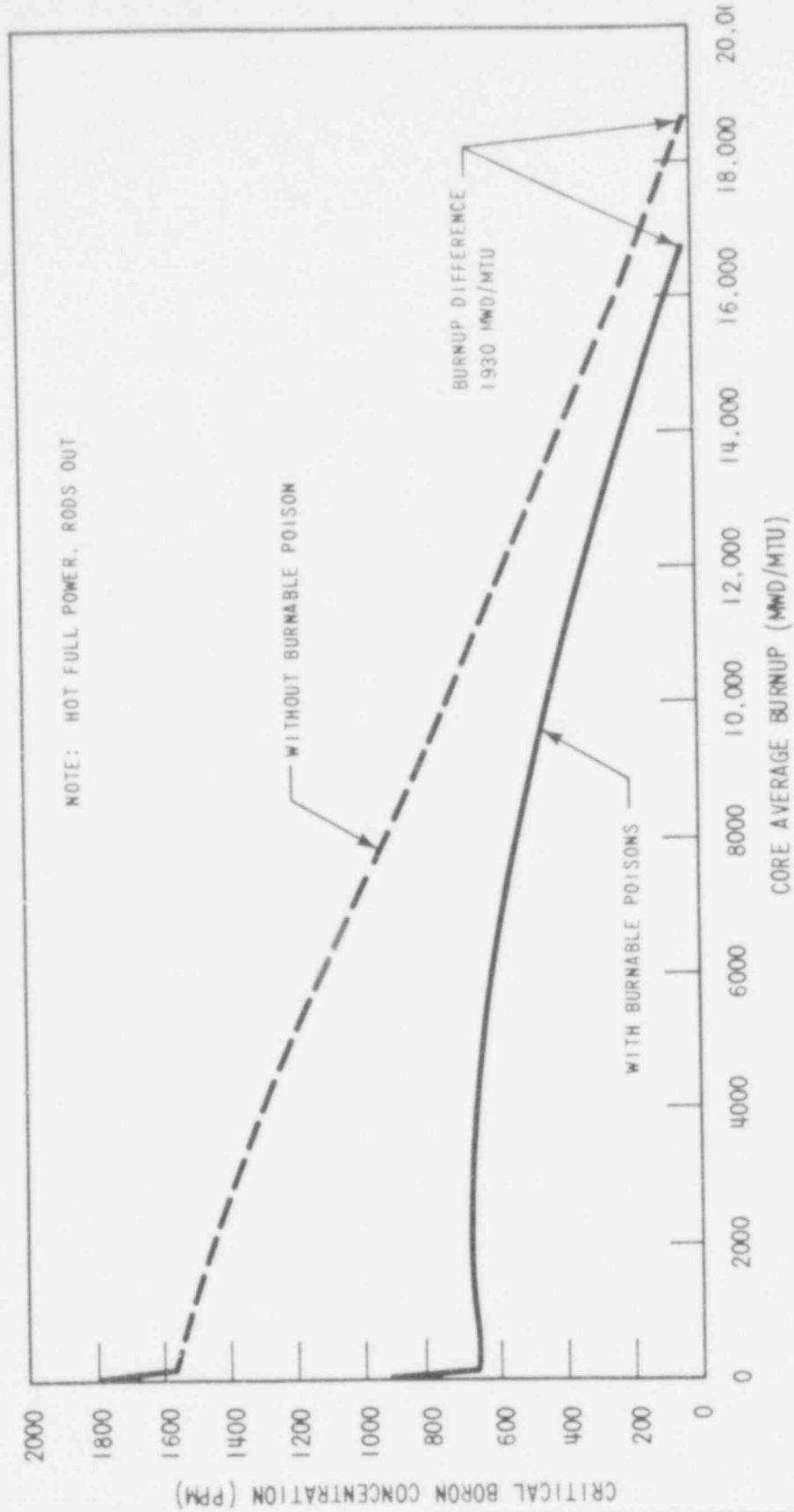


WCAP - 9500

Figure 4.3-2.

Production and Consumption of Higher Isotopes

612 215

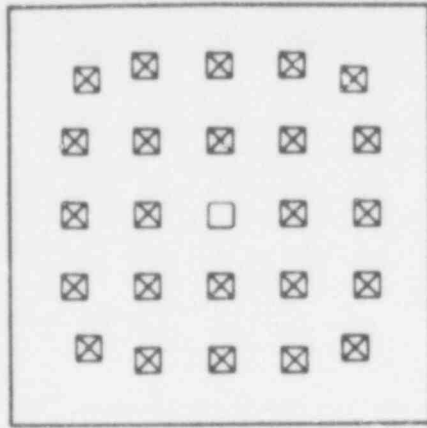


WCAP-9500

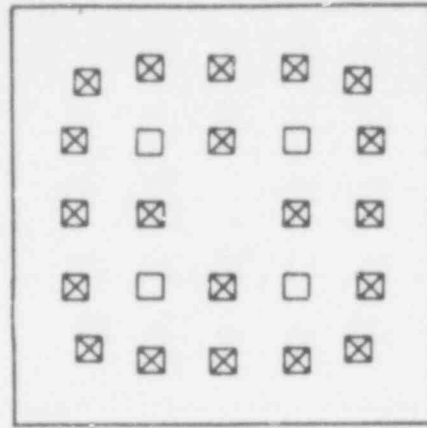
Figure 4.3-3.

Boron Concentration versus First Cycle Burnup With and Without Burnable Poison Rods

612 216

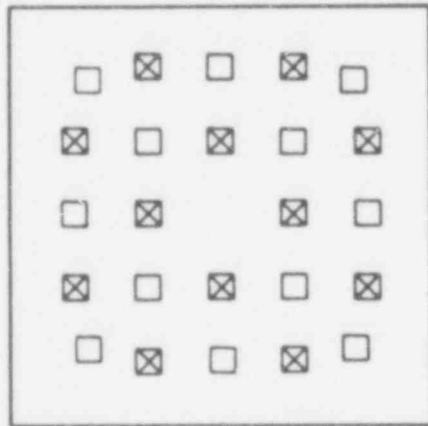


24 BPs

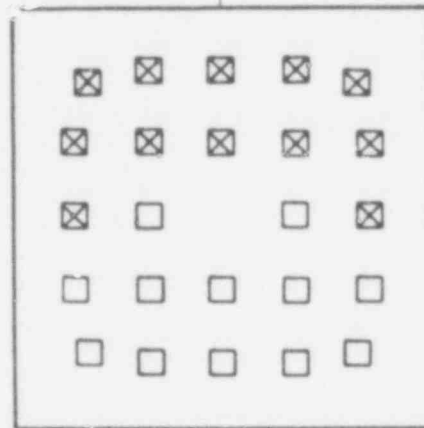


20 BPs

CORE CENTER



12 BPs

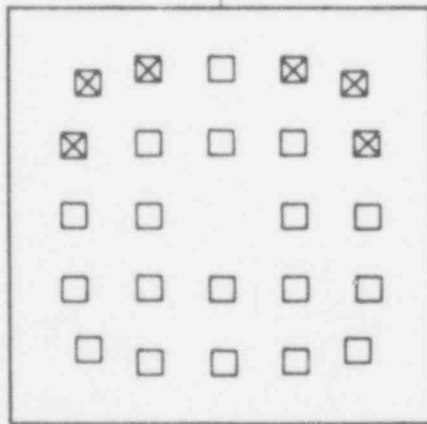


12A BPs (ASYMMETRIC)

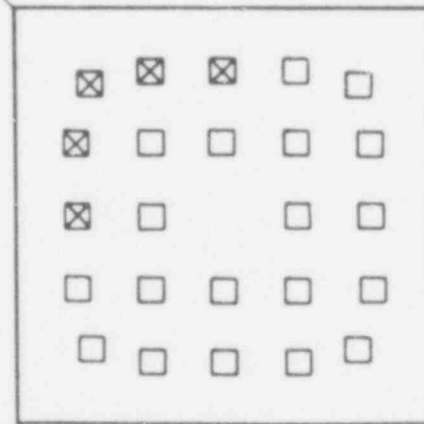
CORE CENTER



CORE CENTER



6 BPs



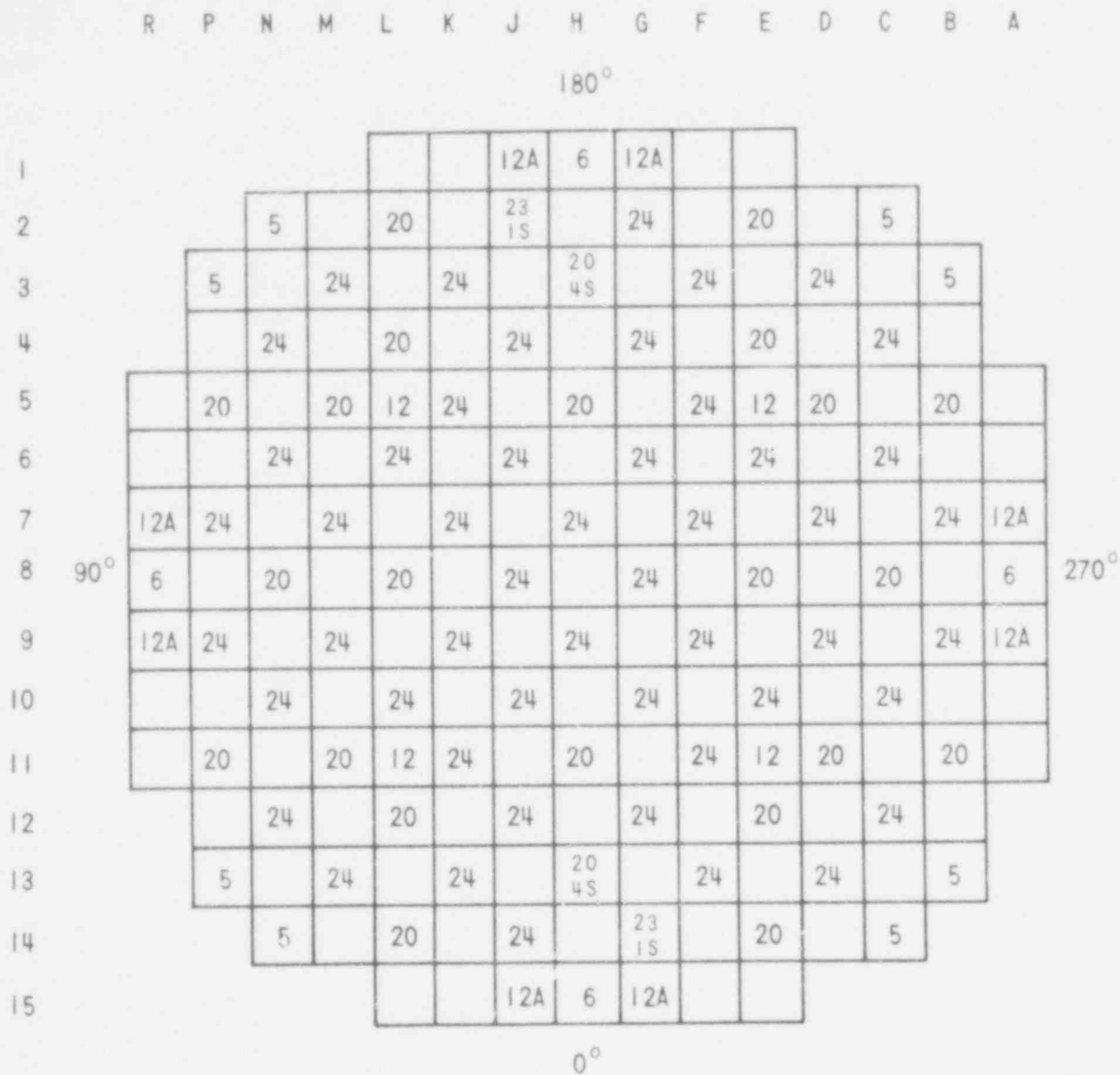
5 BPs

WCAP - 9500

Figure 4.3-4.

Burnable Poison Rod Arrangement  
Within an Assembly

612 217



NUMBER INDICATES NUMBER OF  
BURNABLE POISON RODS.  
S INDICATES SOURCE ROD

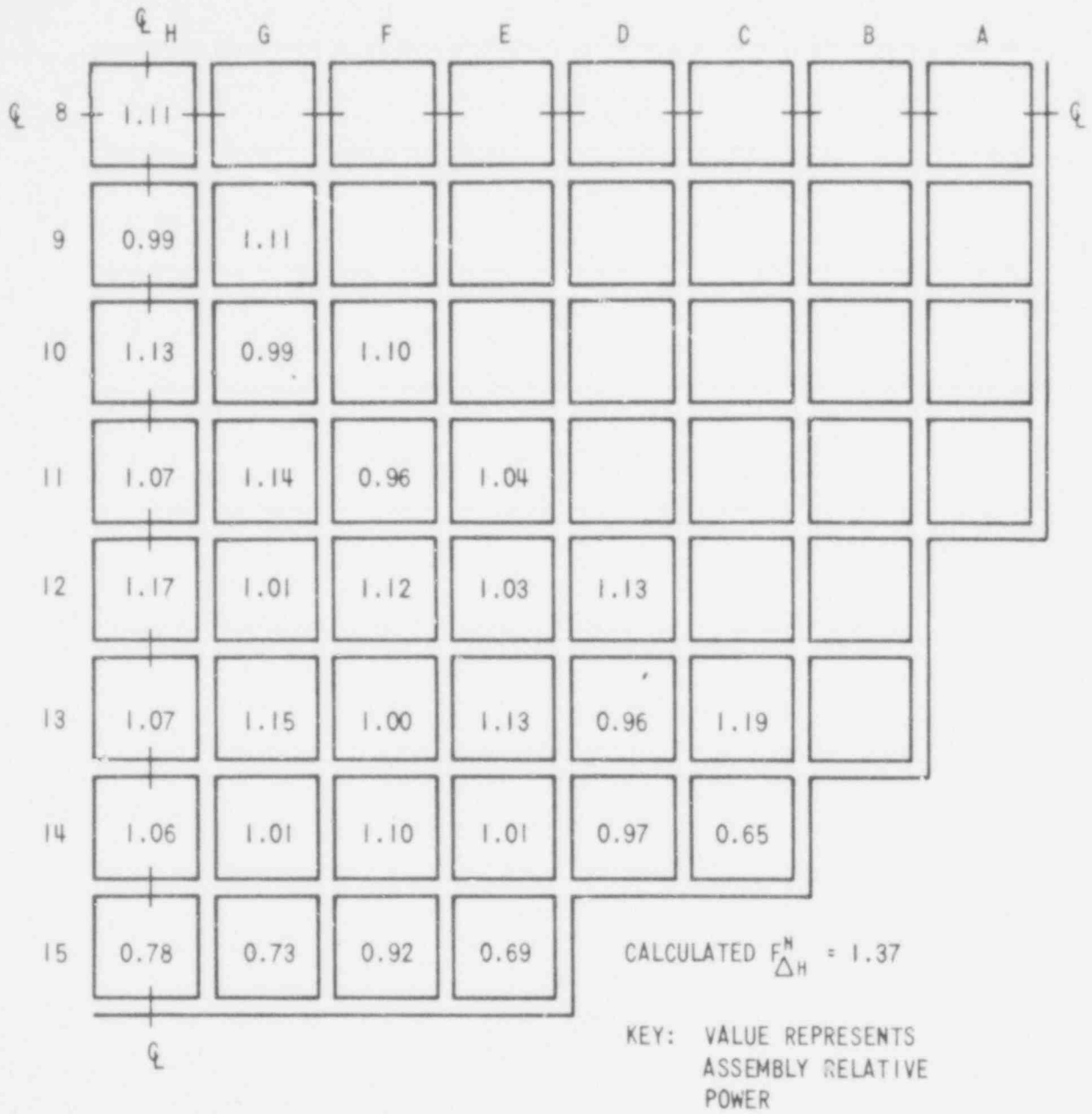
1934 BP RODS  
12.5 W/O B<sub>2</sub>O<sub>3</sub>

WCAP - 9500

Figure 4.3-5.  
Burnable Poison Loading Pattern  
(Typical)

612 218



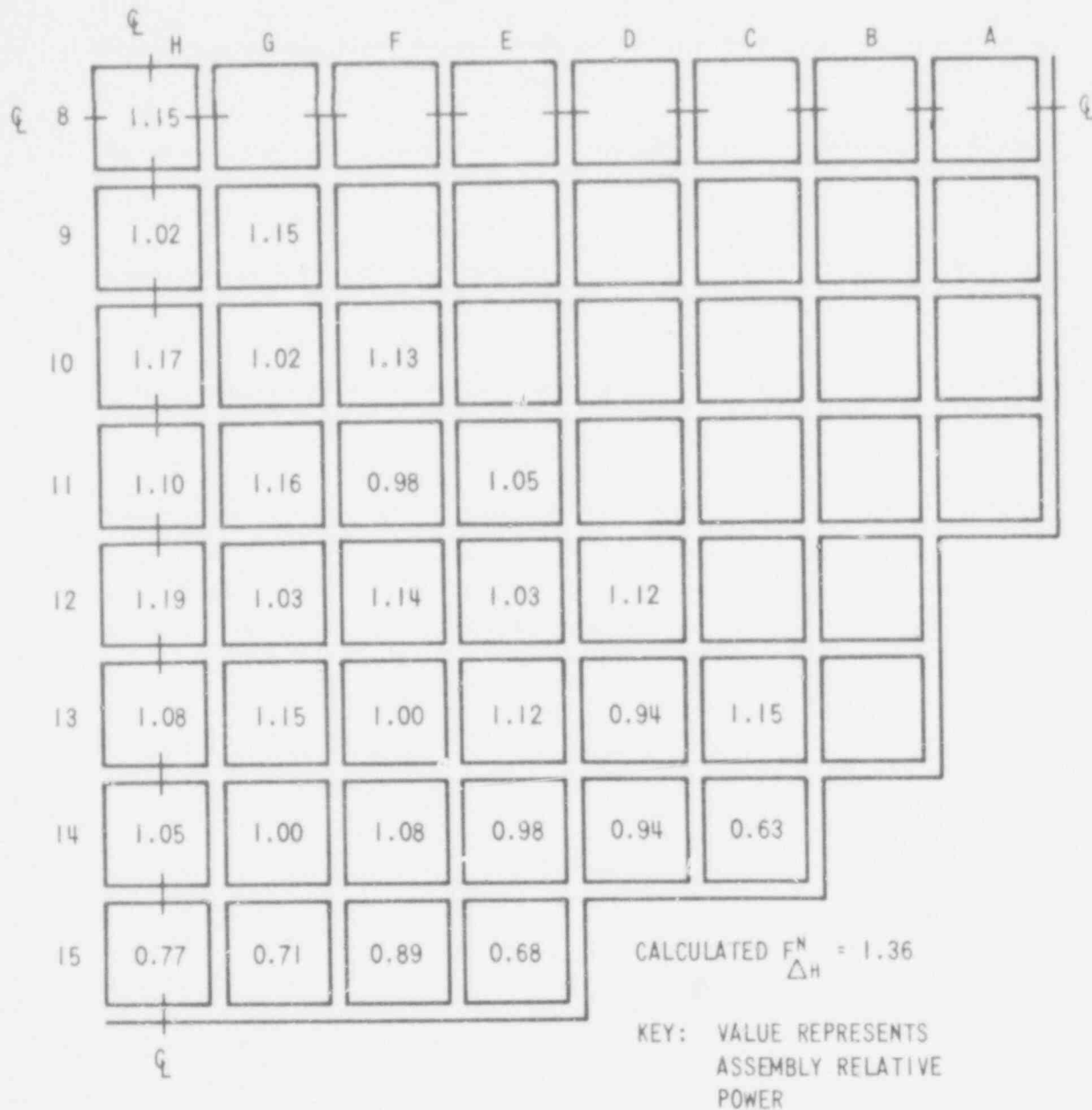


WCAP - 9500

Figure 4.3-6.

Normalized Power Density Distribution  
Near Beginning of Life, Unrodded Core,  
Hot Full Power, No Xenon

612 219

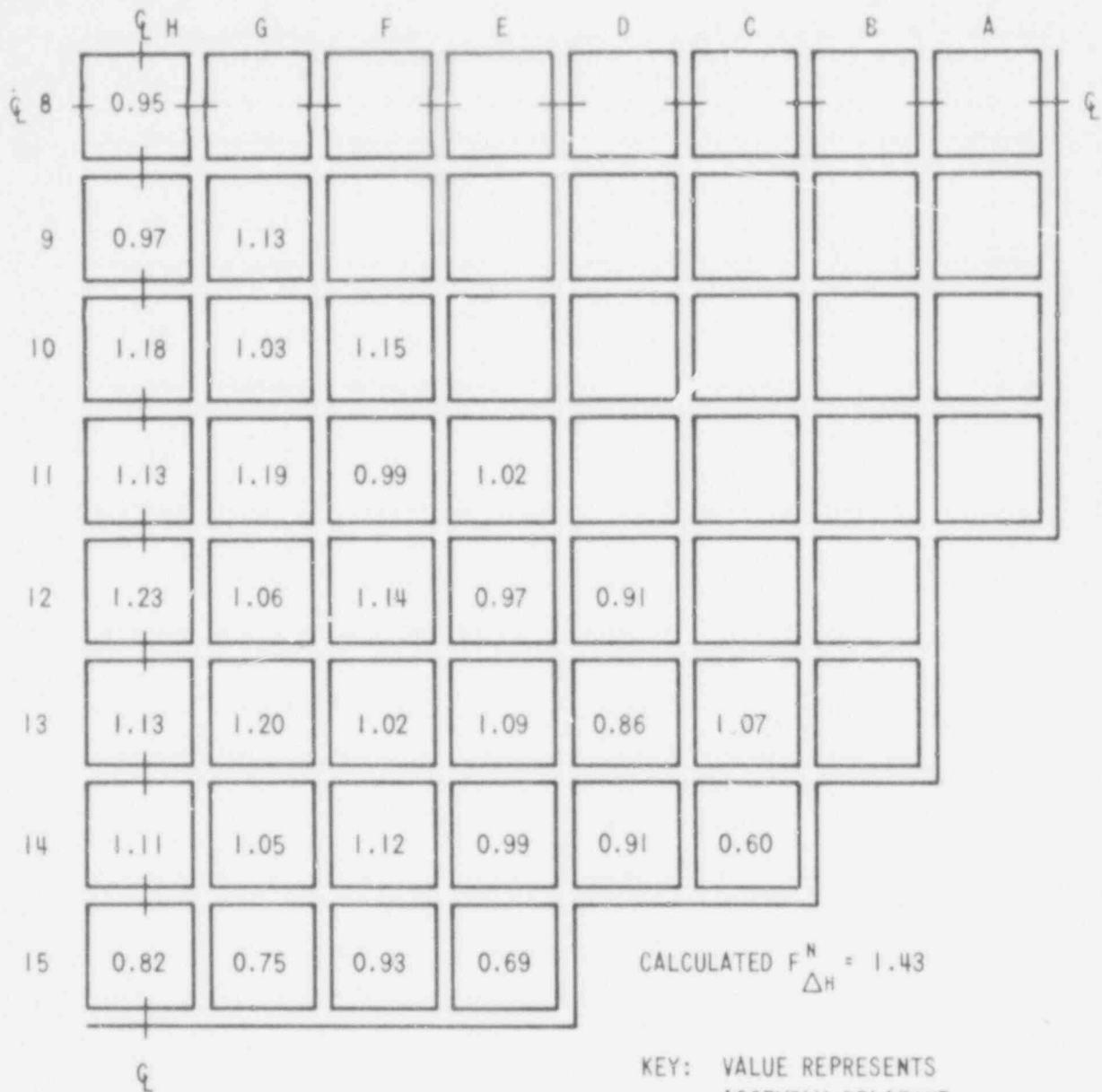


WCAP - 9500

Figure 4.3-7.

Normalized Power Density Distribution  
Near Beginning of Life, Unrodded Core,  
Hot Full Power, Equilibrium Xenon

612 220

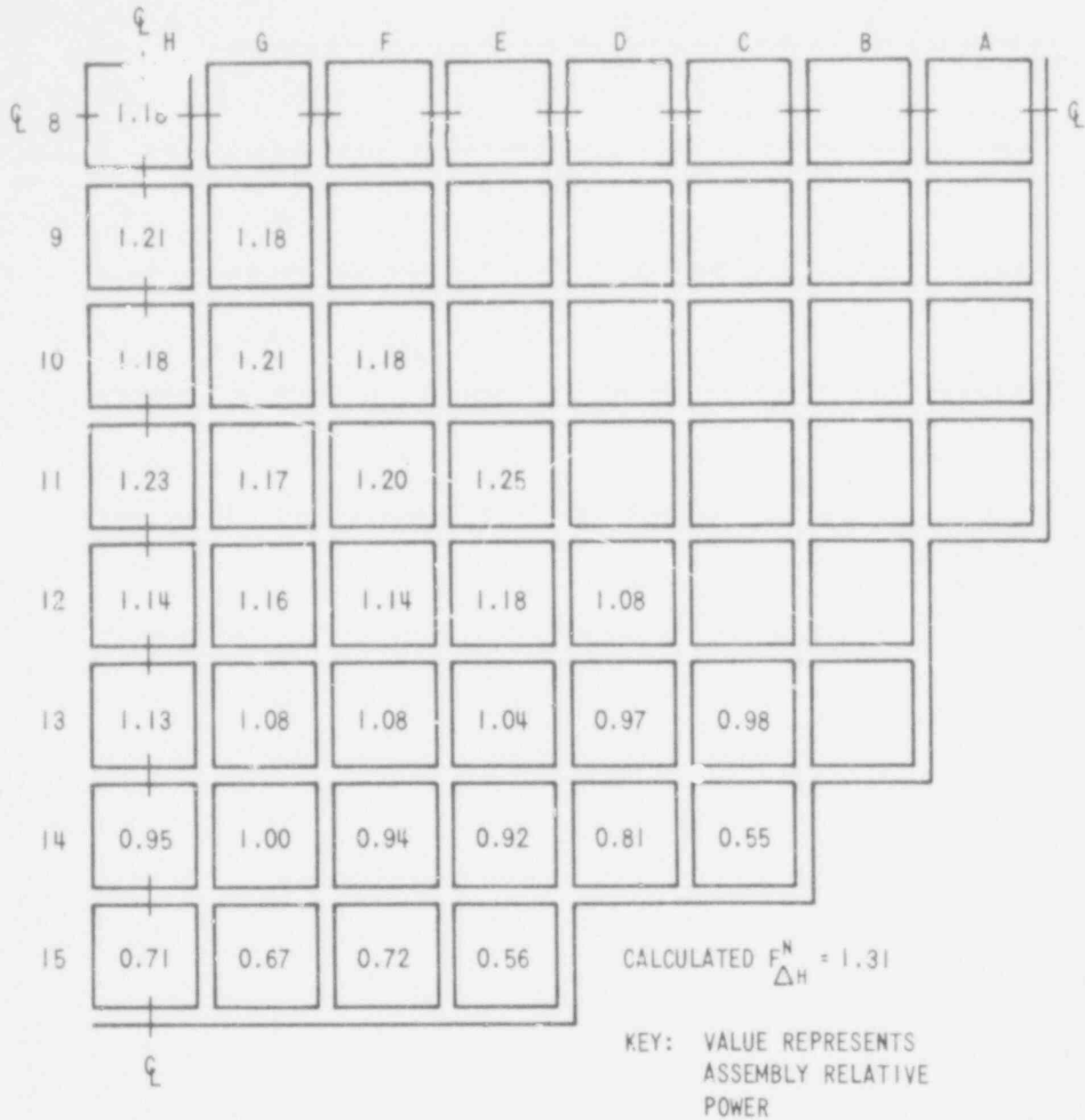


WCAP - 9500

Figure 4.3-8.

Normalized Power Density Distribution  
Near Beginning of Life, Group D at 28% Inserted  
Hot Full Power, Equilibrium Xenon

612 221

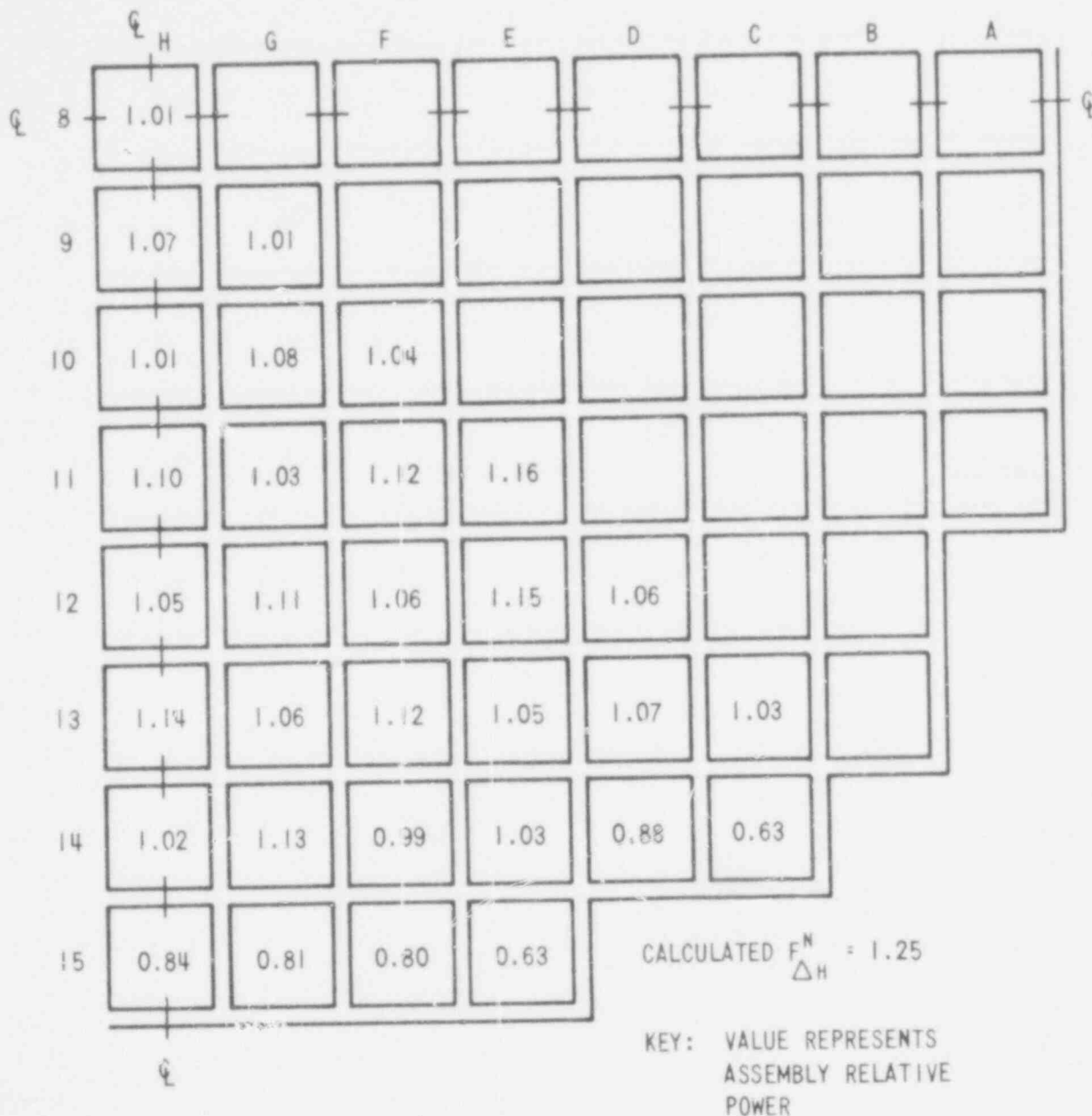


WCAP - 9500

Figure 4.3-9.

Normalized Power Density Distribution  
Near Middle of Life, Unrodded Core,  
Hot Full Power, Equilibrium Xenon

612 222

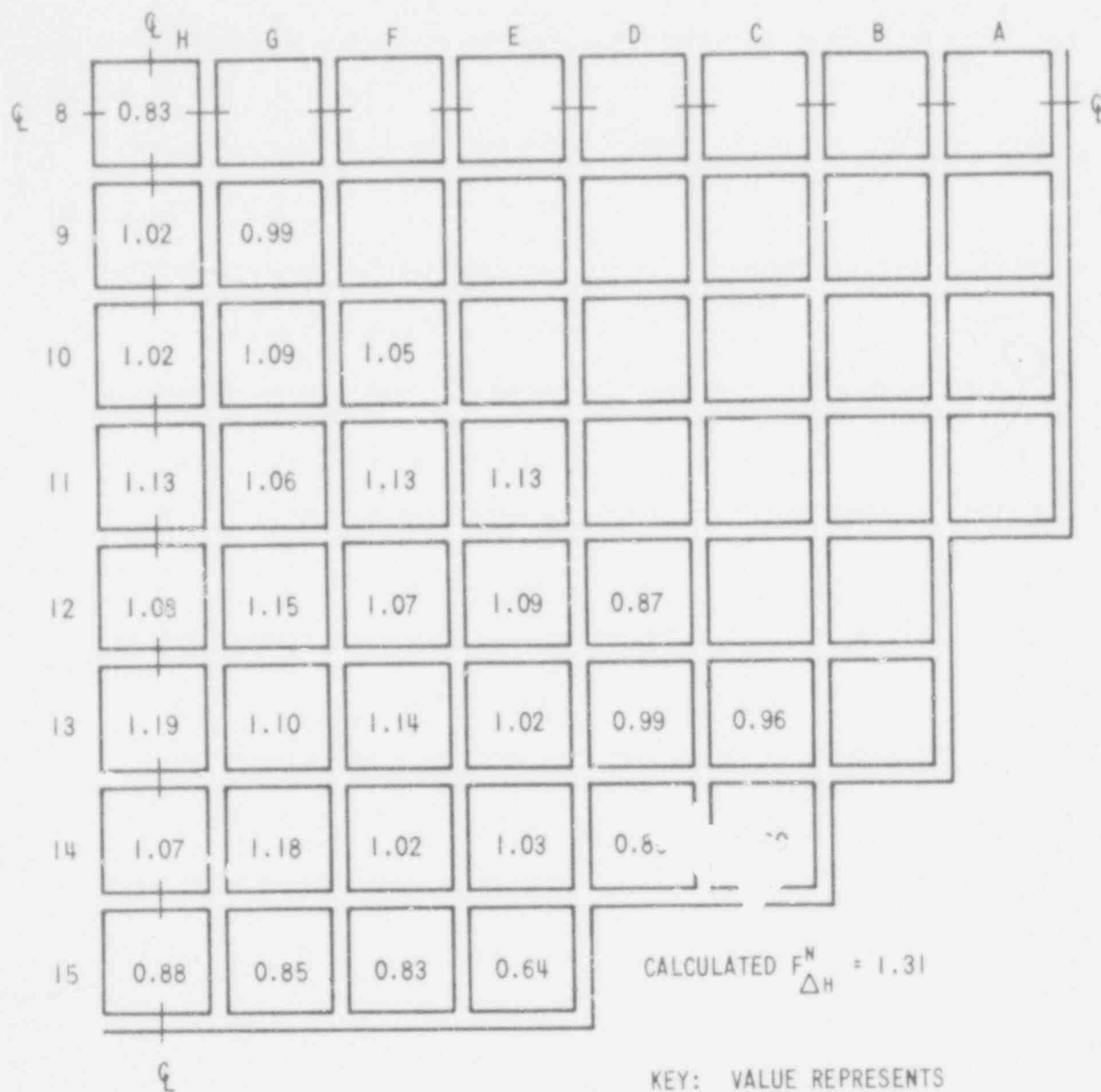


WCAP - 9500

Figure 4.3-10.

Normalized Power Density Distribution  
Near End of Life, Unrodded Cors,  
Hot Full Power, Equilibrium Xenon

612 223



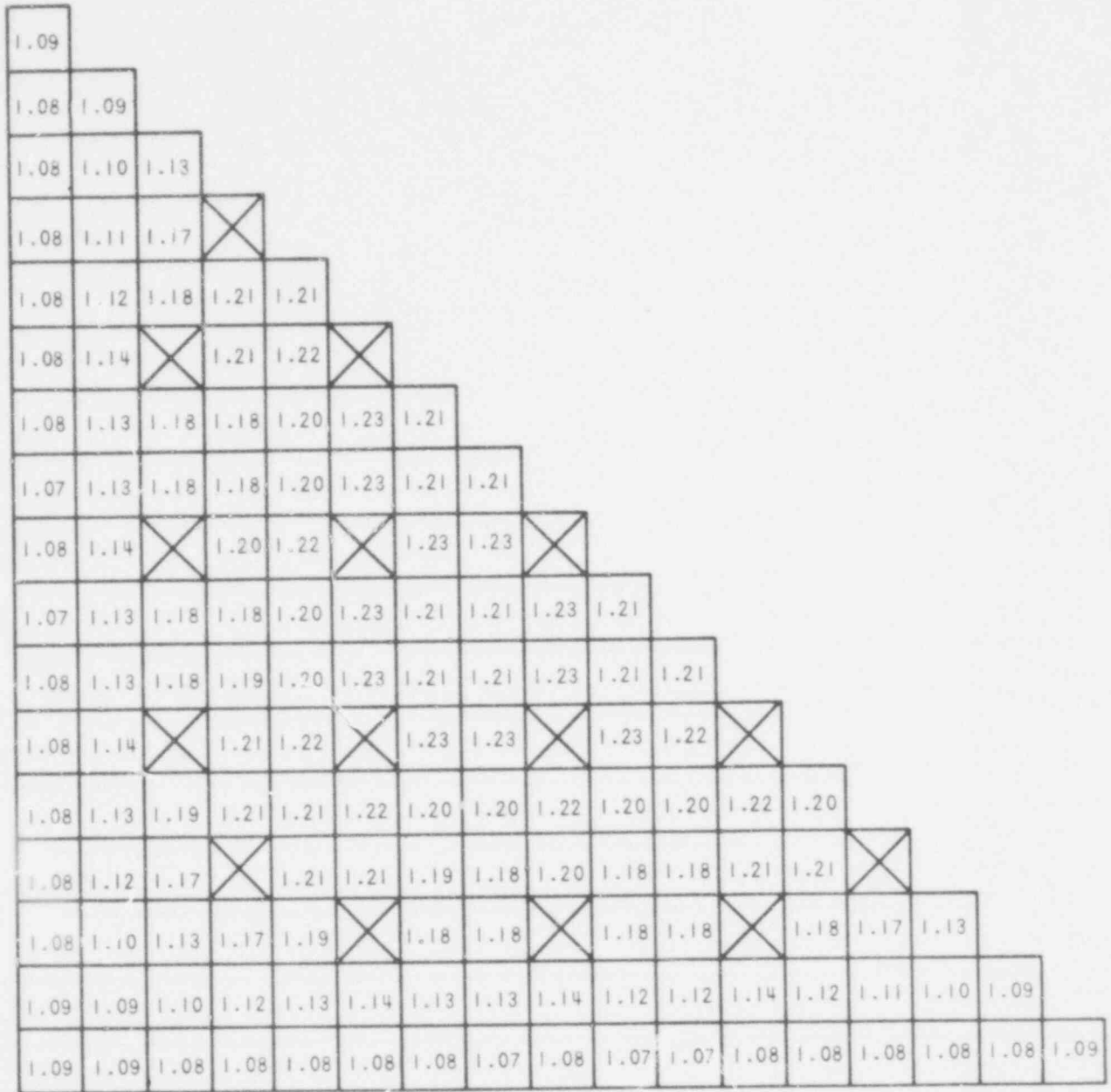
KEY: VALUE REPRESENTS  
ASSEMBLY RELATIVE  
POWER

WCAP - 9500

Figure 4.3 11.

Normalized Power Density Distribution  
Near End of Life, Group D at 28% Inserted  
Hot Full Power, Equilibrium Xenon

612 224



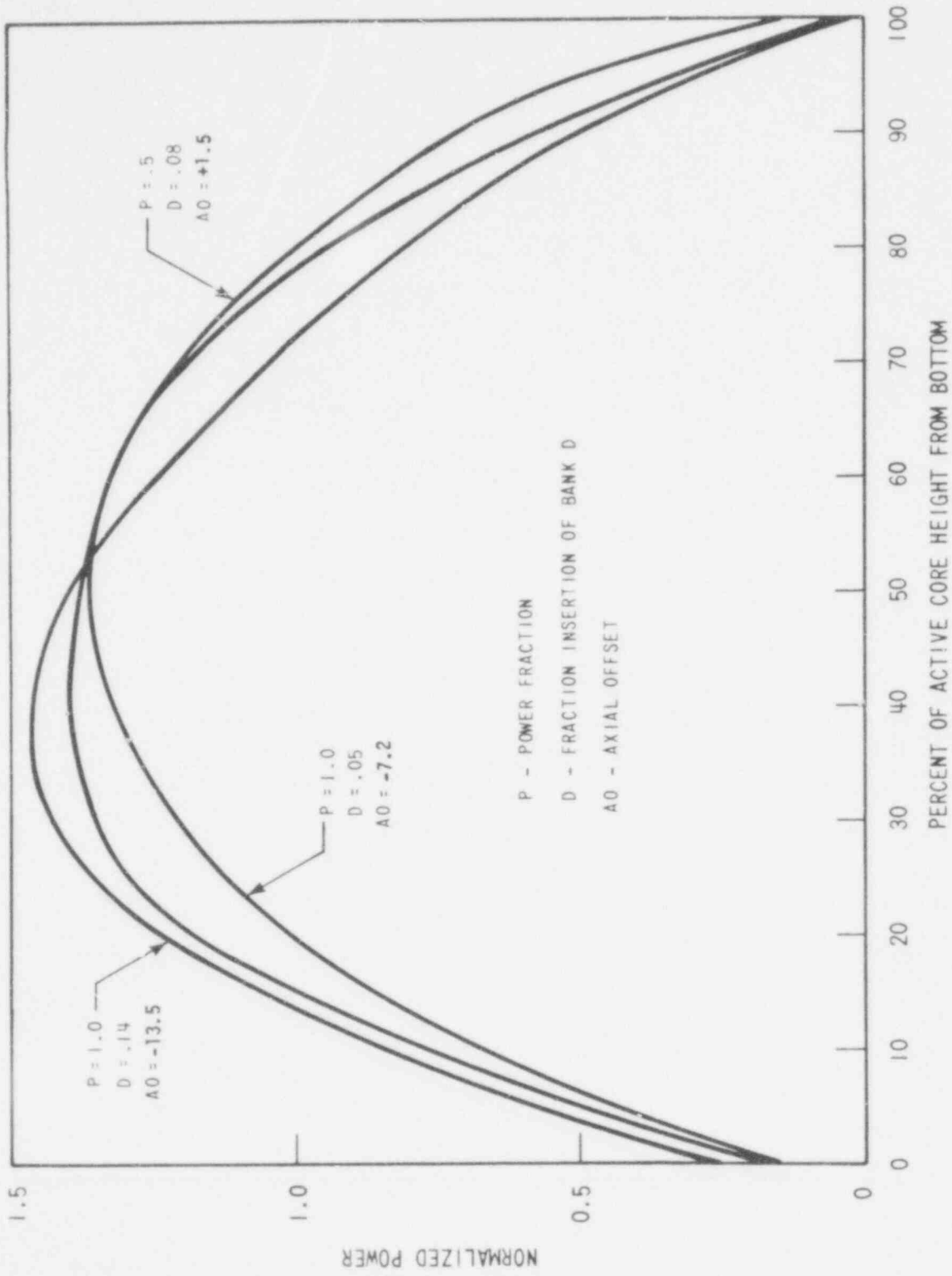
WCAP - 9500

Figure 4.3-12.

Rodwise Power Distribution in a Typical Assembly  
(Assembly G-9) Near Beginning of Life, Hot Full  
Power, Equilibrium Xenon, Unrodded Core





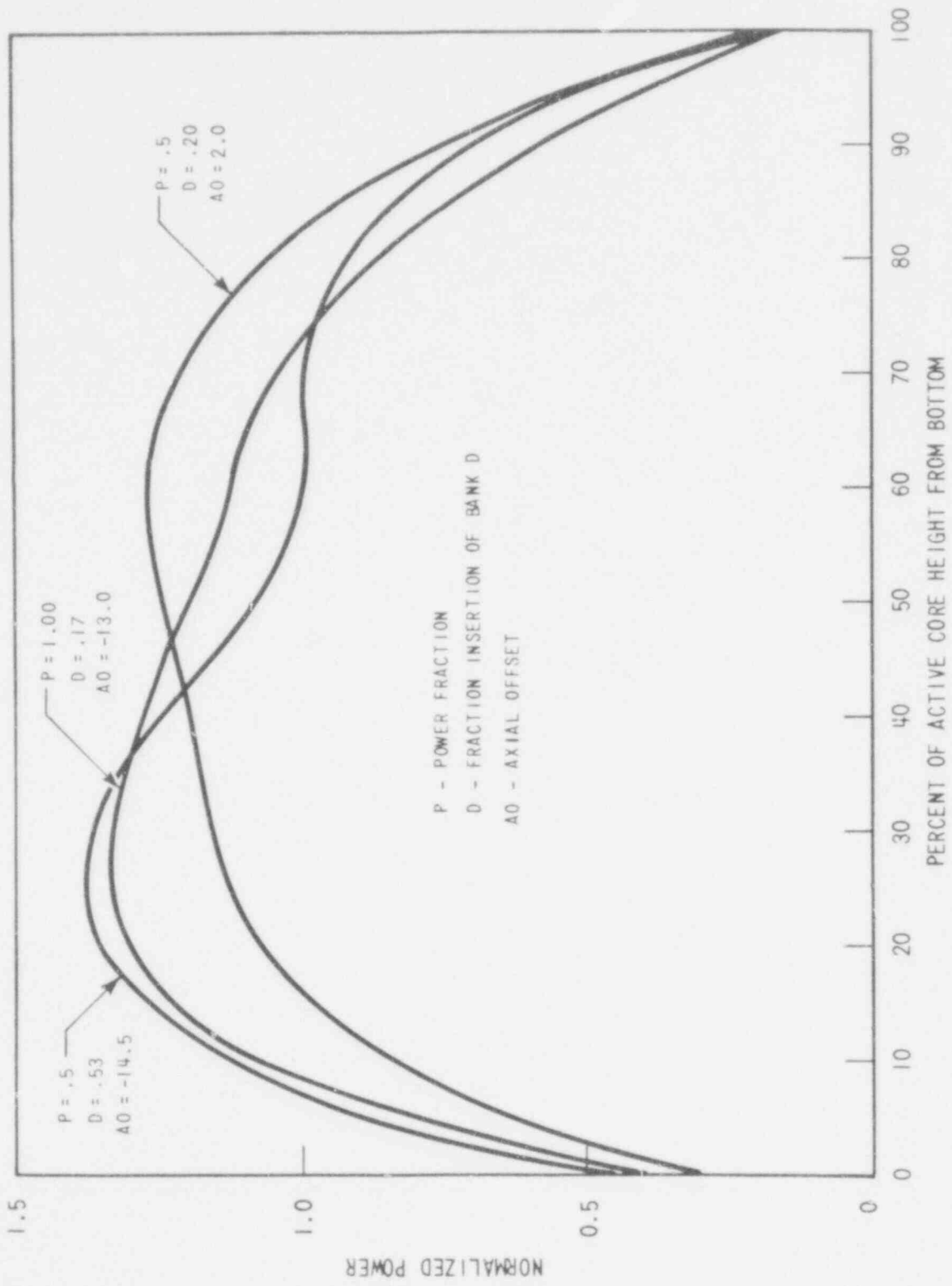


WCAP - 9500

Figure 4.3-14.

Typical Axial Power Shapes Occurring at Beginning of Life

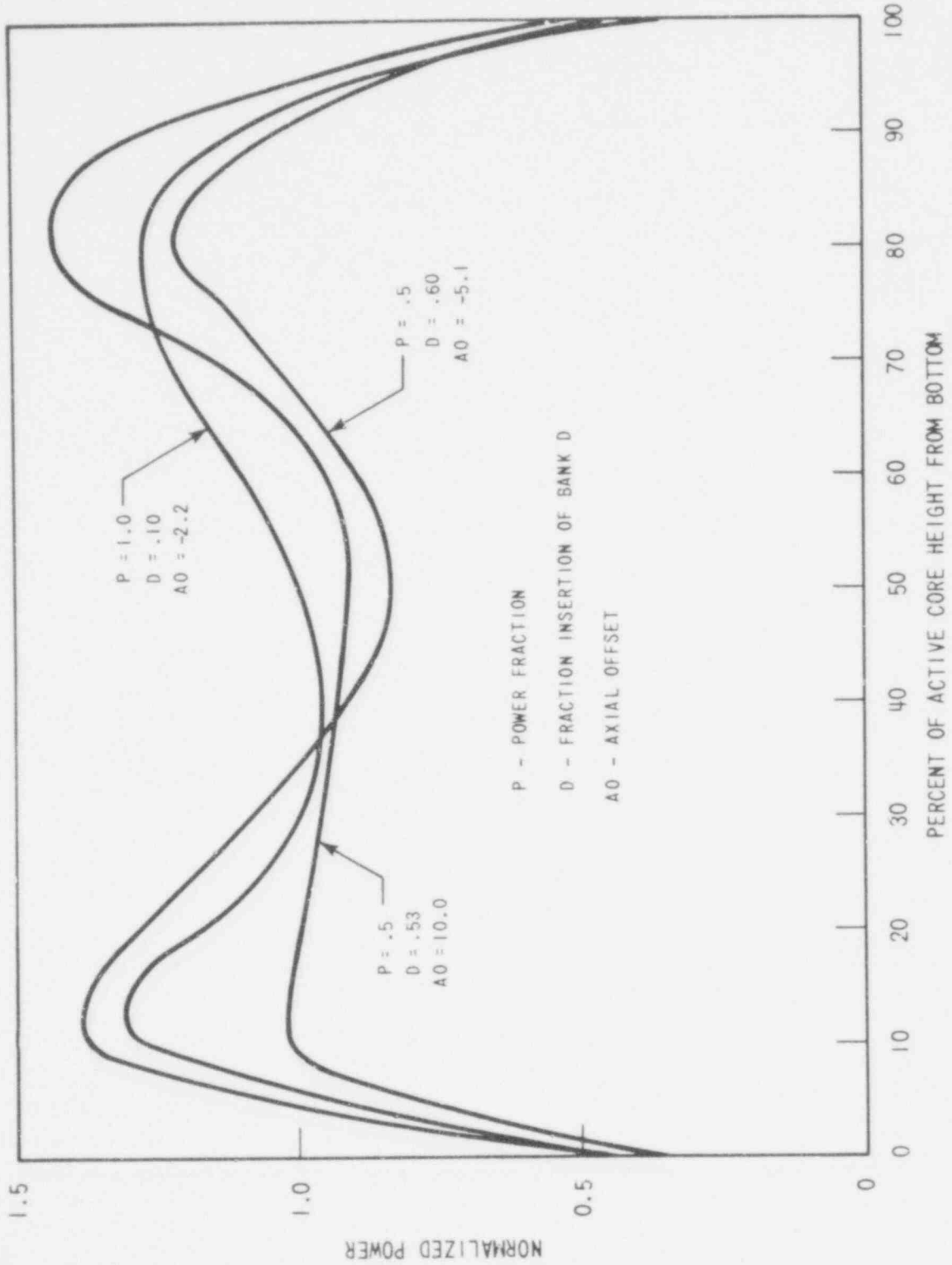
612 227



612 223

WCAP - 9500

Figure 4.3-15.  
Typical Axial Power Shapes Occurring  
at Middle of Life



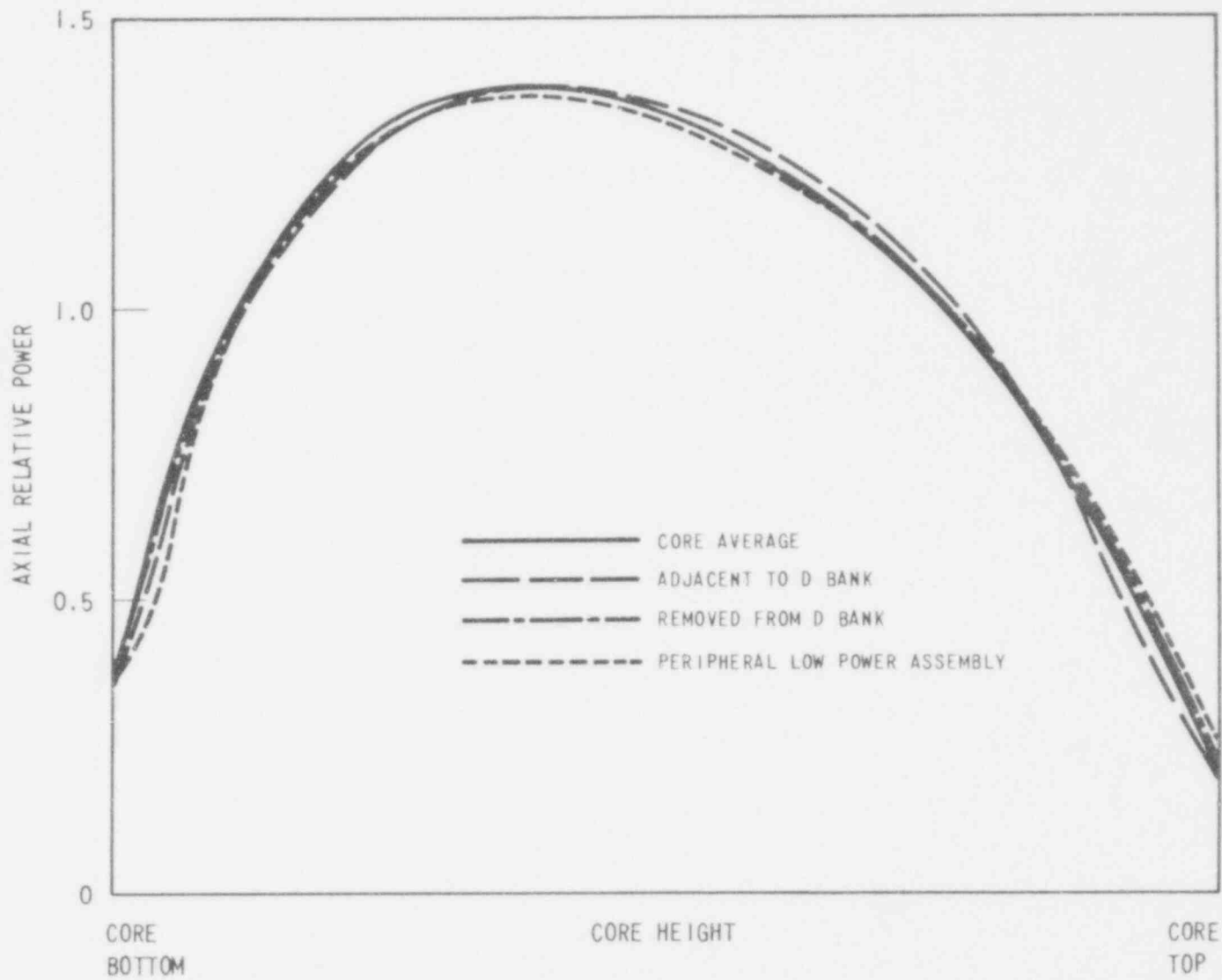
WCAP - 9500

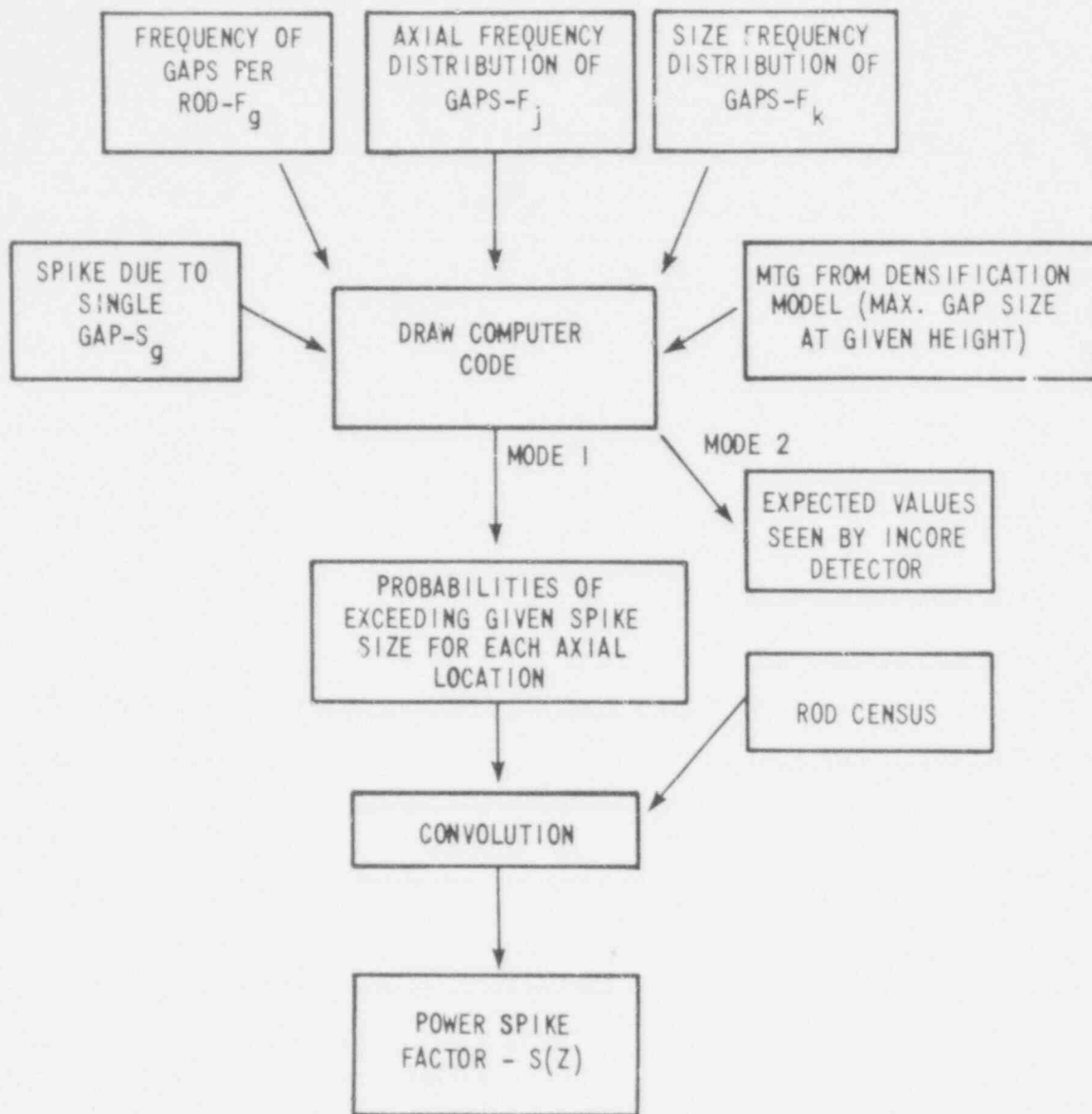
Figure 4.3-16.  
 Typical Axial Power Shapes Occurring  
 at End of Life

612 227

612  
230

WCAP - 9500  
Figure 4.3-17.  
Comparison of Assembly Axial Power  
Distribution with Core Average Axial  
Distribution Bank Slightly Inserted

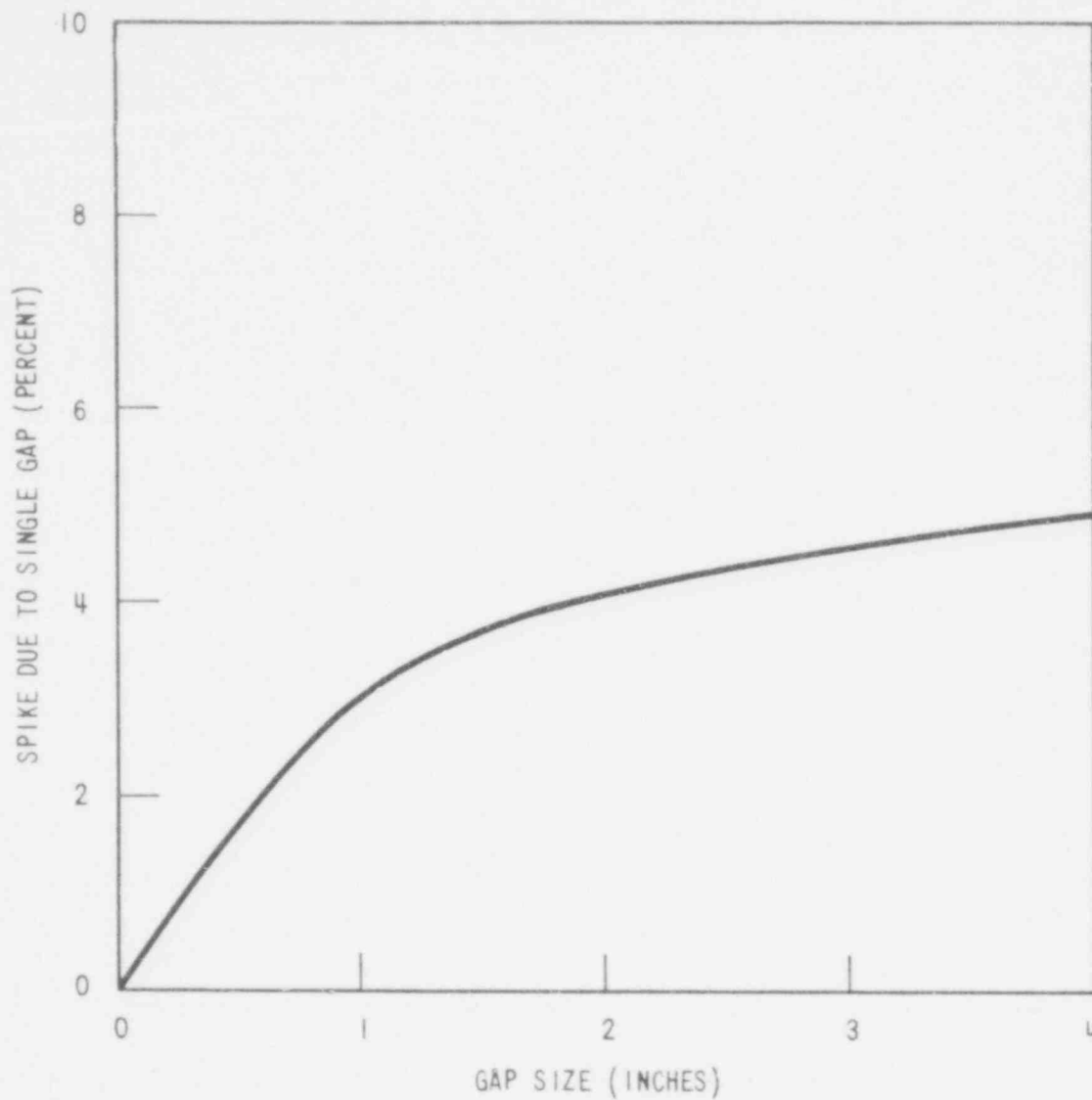




WCAP - 9500

Figure 4.3-18.

Flow Chart for Determining Spike Model

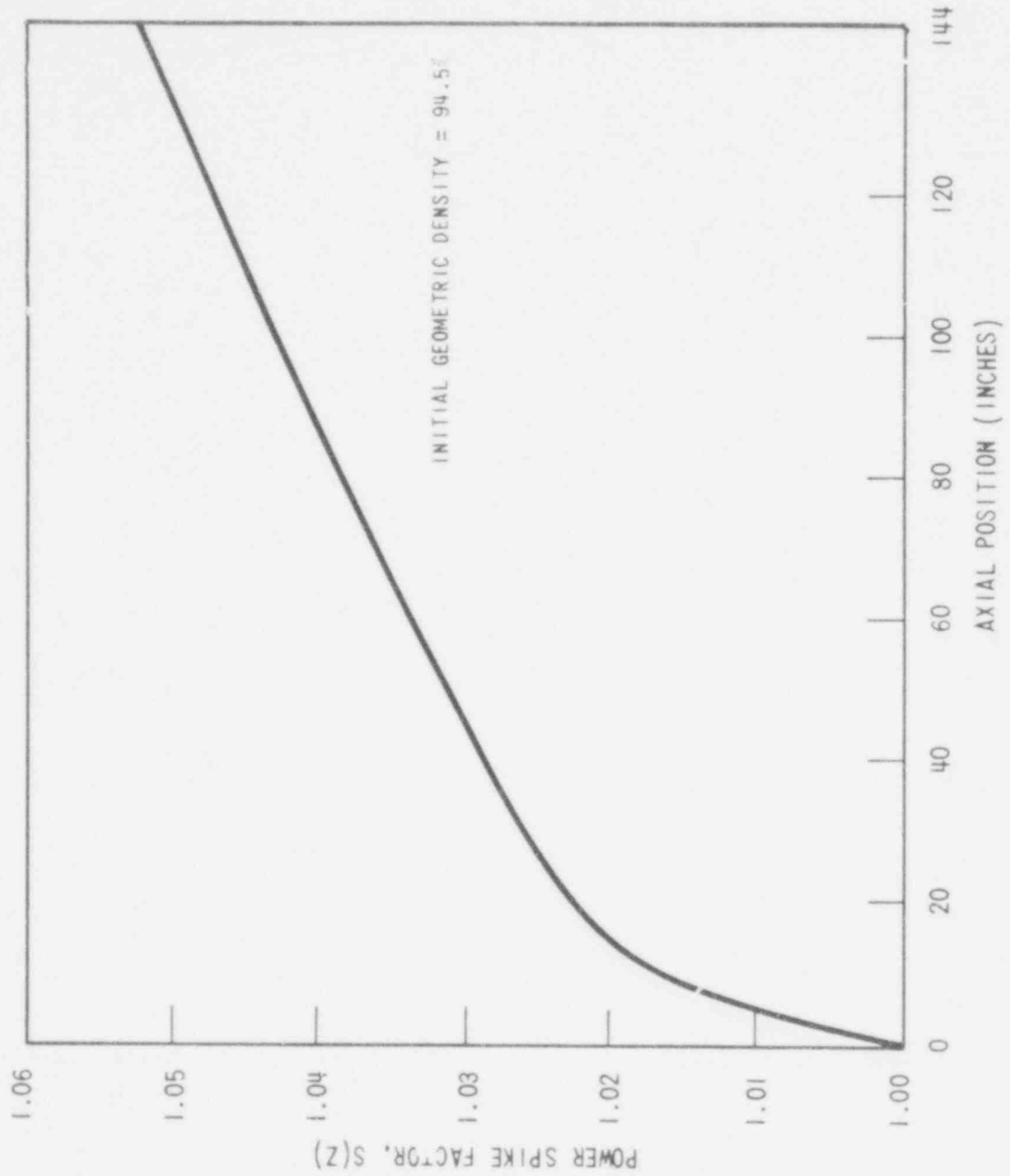


WCAP - 9500

Figure 4.3-19.

Predicted Power Spike Due to Single  
Non-Flattened Gap in the Adjacent Fuel

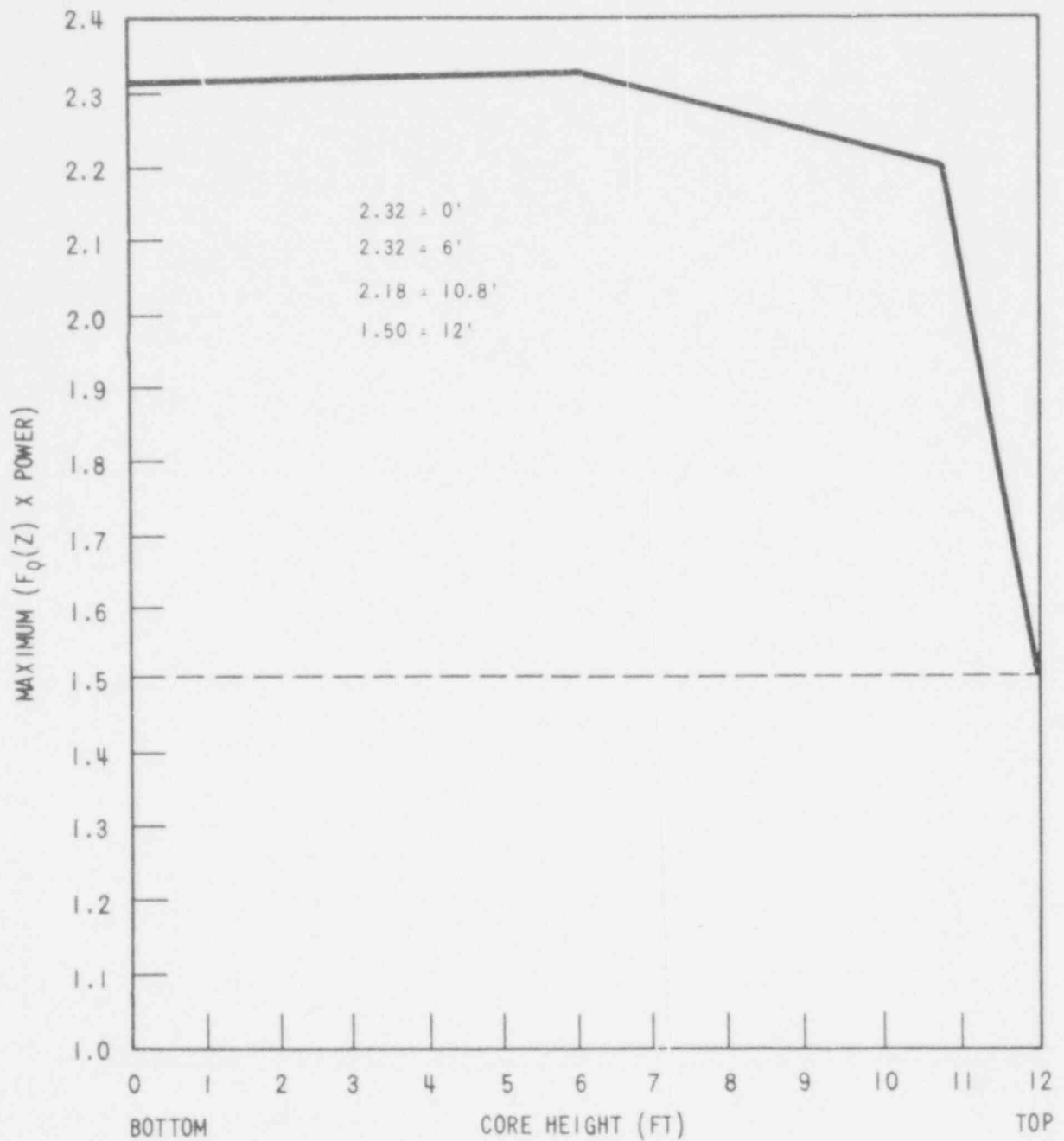
612 232



WCAP - 9500

Figure 4.3-20.  
Power Spike Factor as a Function of  
Axial Position

612 233



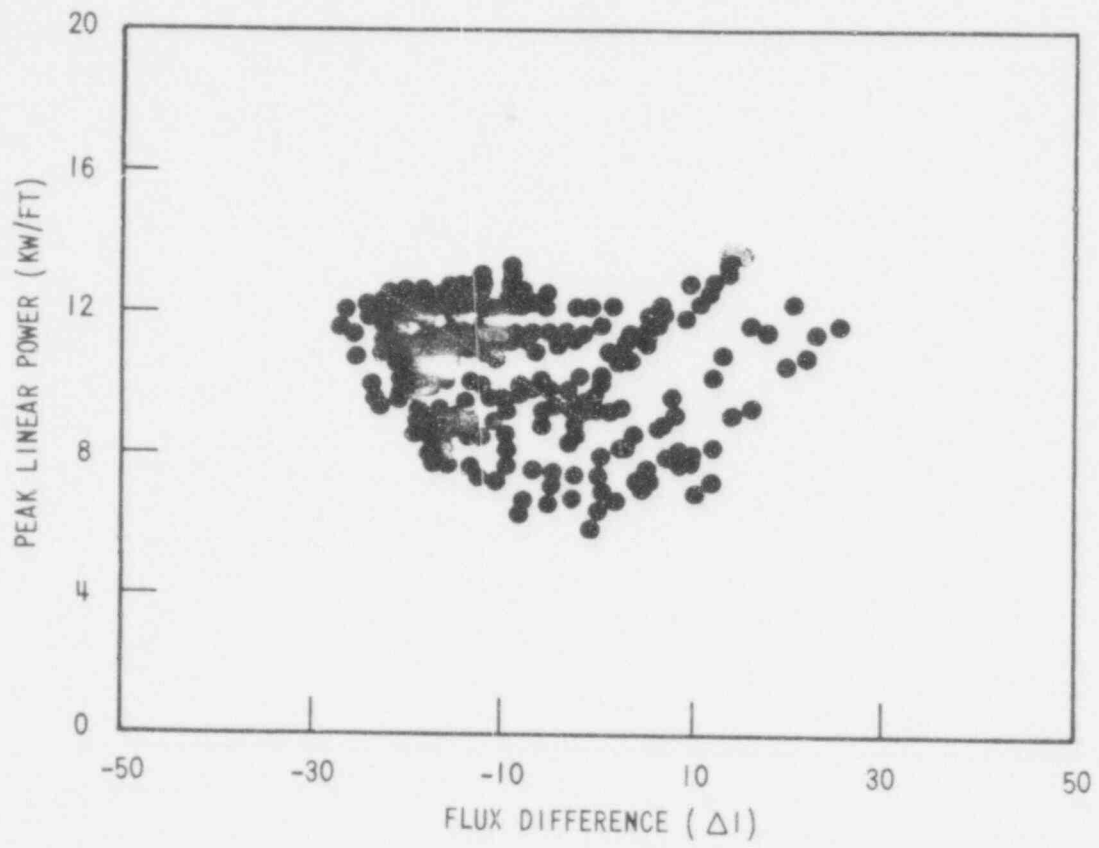
WCAP - 9500

Figure 4.3-21.

Maximum  $F_Q$  x Power versus Axial Height  
During Normal Operation

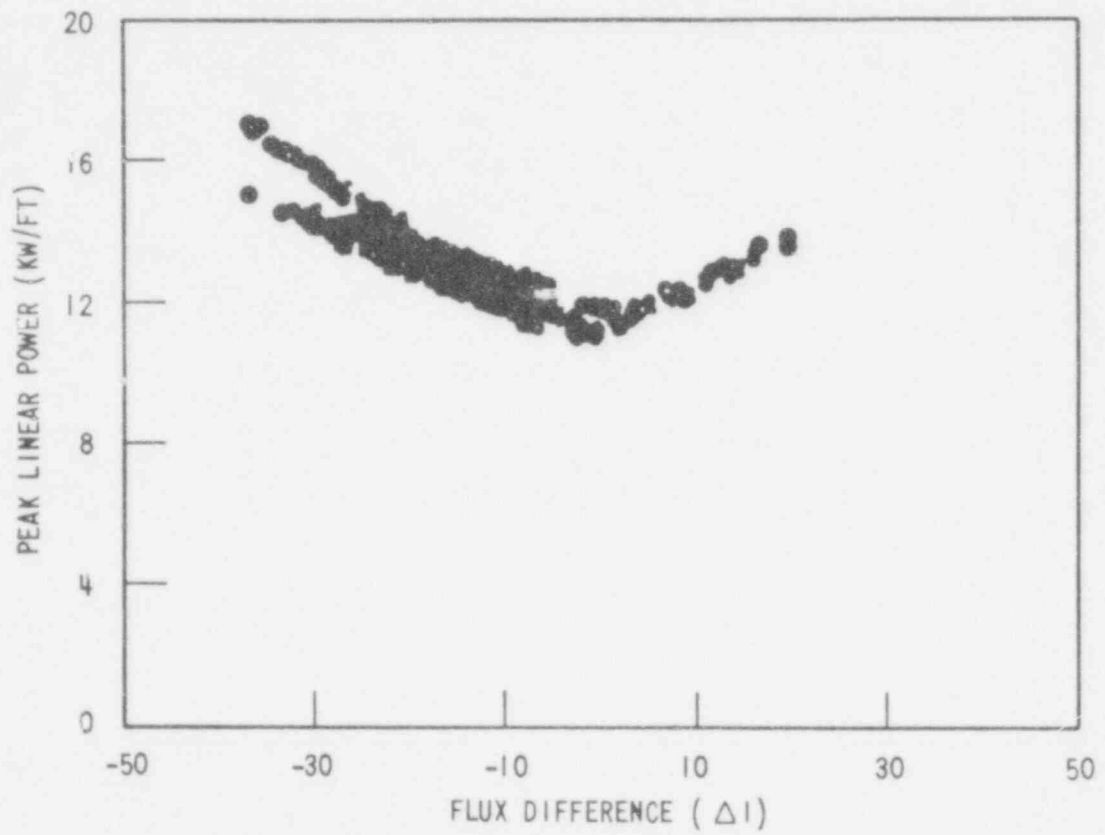
612 234





612 235

|  |
|--|
| WCAP - 9500  |
| Figure 4.3-22.<br>Peak Linear Power During Control<br>Rod Malfunction Overpower Transients |

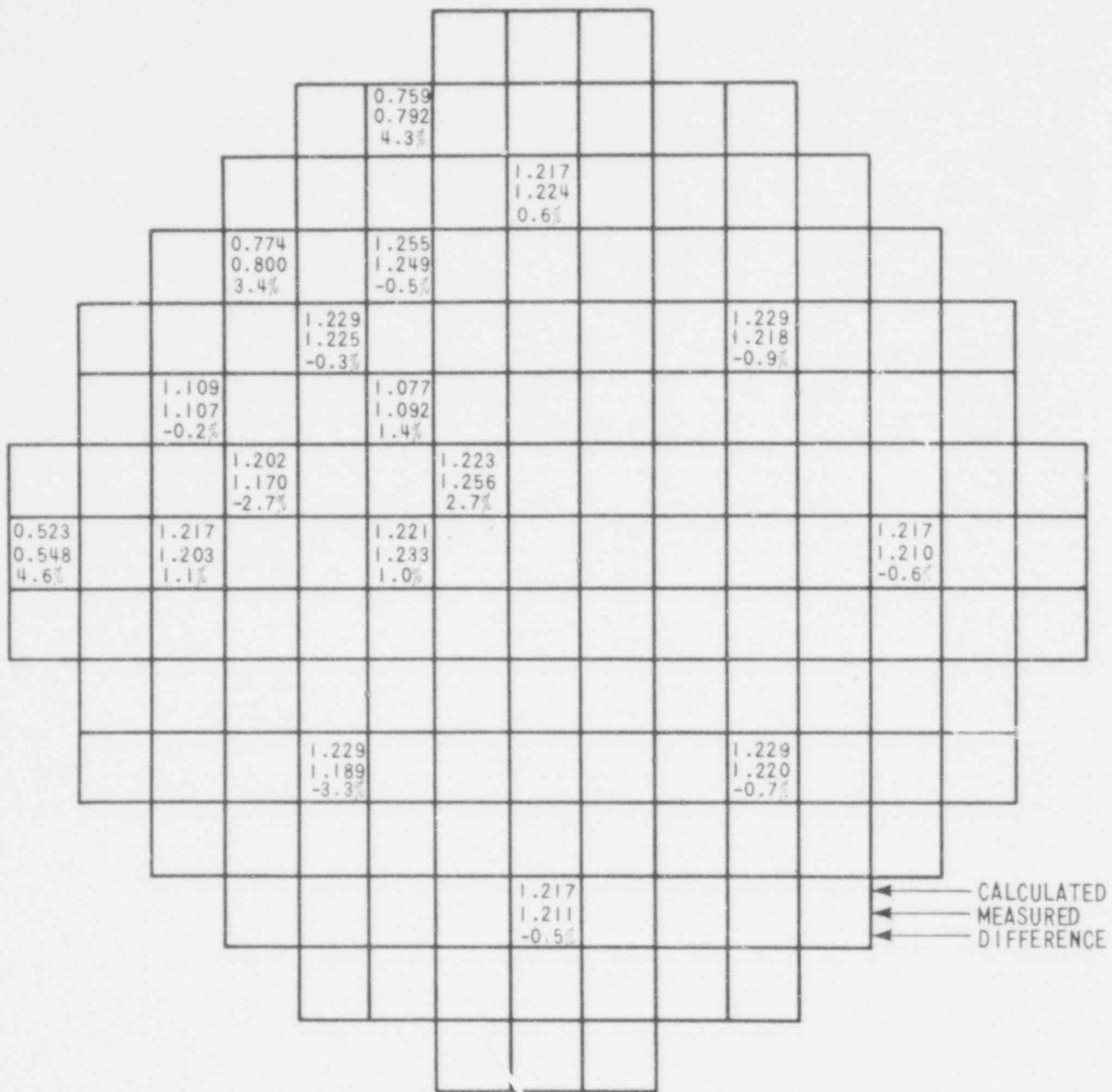


WCAP - 9500

Figure 4.3-23.

Peak Linear Power During  
Boration/Deboration Overpower Transients

612 235



PEAKING FACTORS

$\bar{F}_Z = 1.5$

$F_{\Delta H}^N = 1.357$

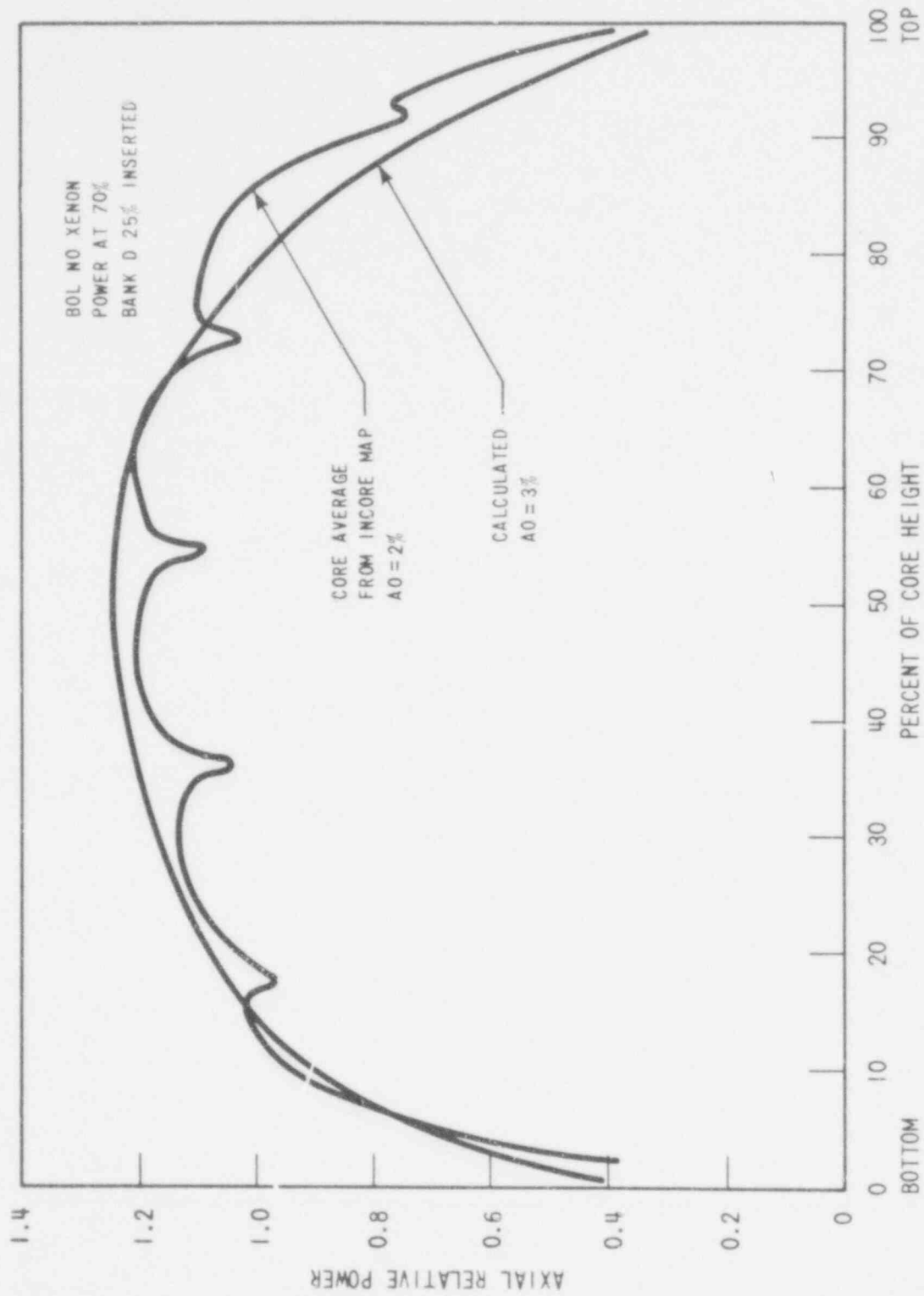
$F_Q^N = 2.07$

WCAP - 9500

Figure 4.3-24.

Typical Comparison Between Calculated and Measured Relative Fuel Assembly Power Distribution

612 237

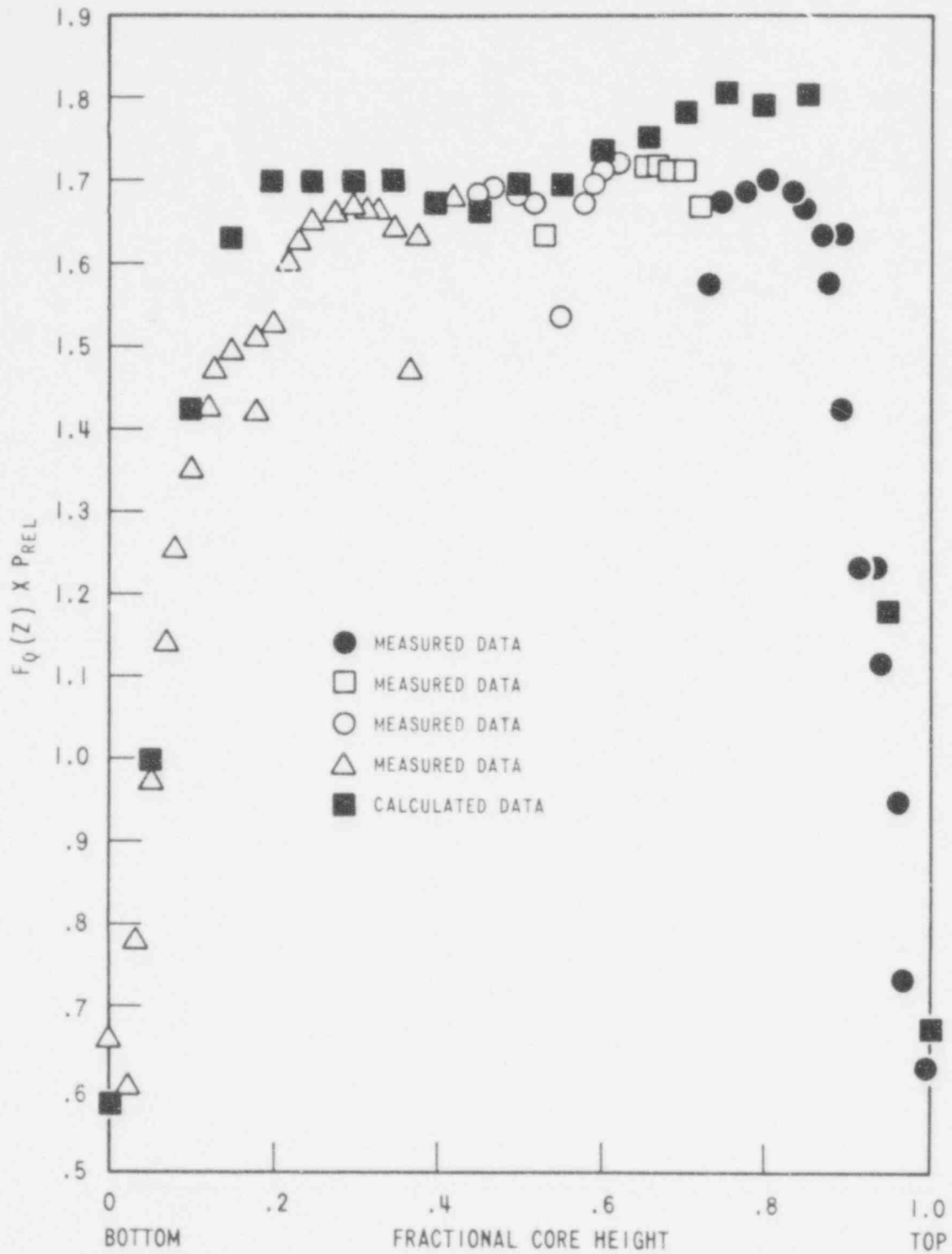


WCAP - 9500

Figure 4.3-25.

Comparison of Calculated and Measured Axial Shape

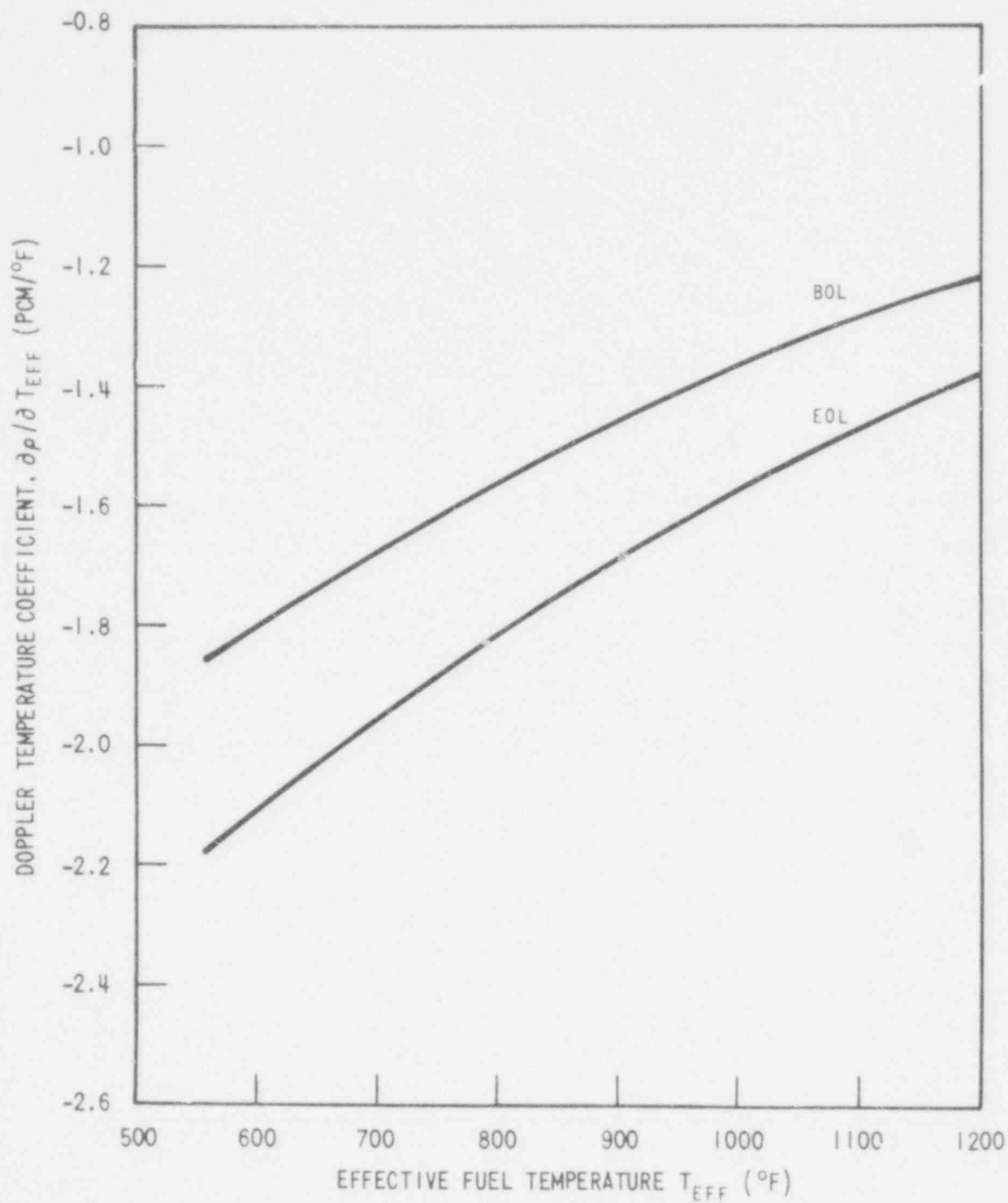
612-238



WCAP - 9500

Figure 4.3-26.

Comparison of Calculated and Measured Peaking Factors,  $[F_Q \times P_{REL}]_{MAX}$  Envelope as a Function of Core Height.

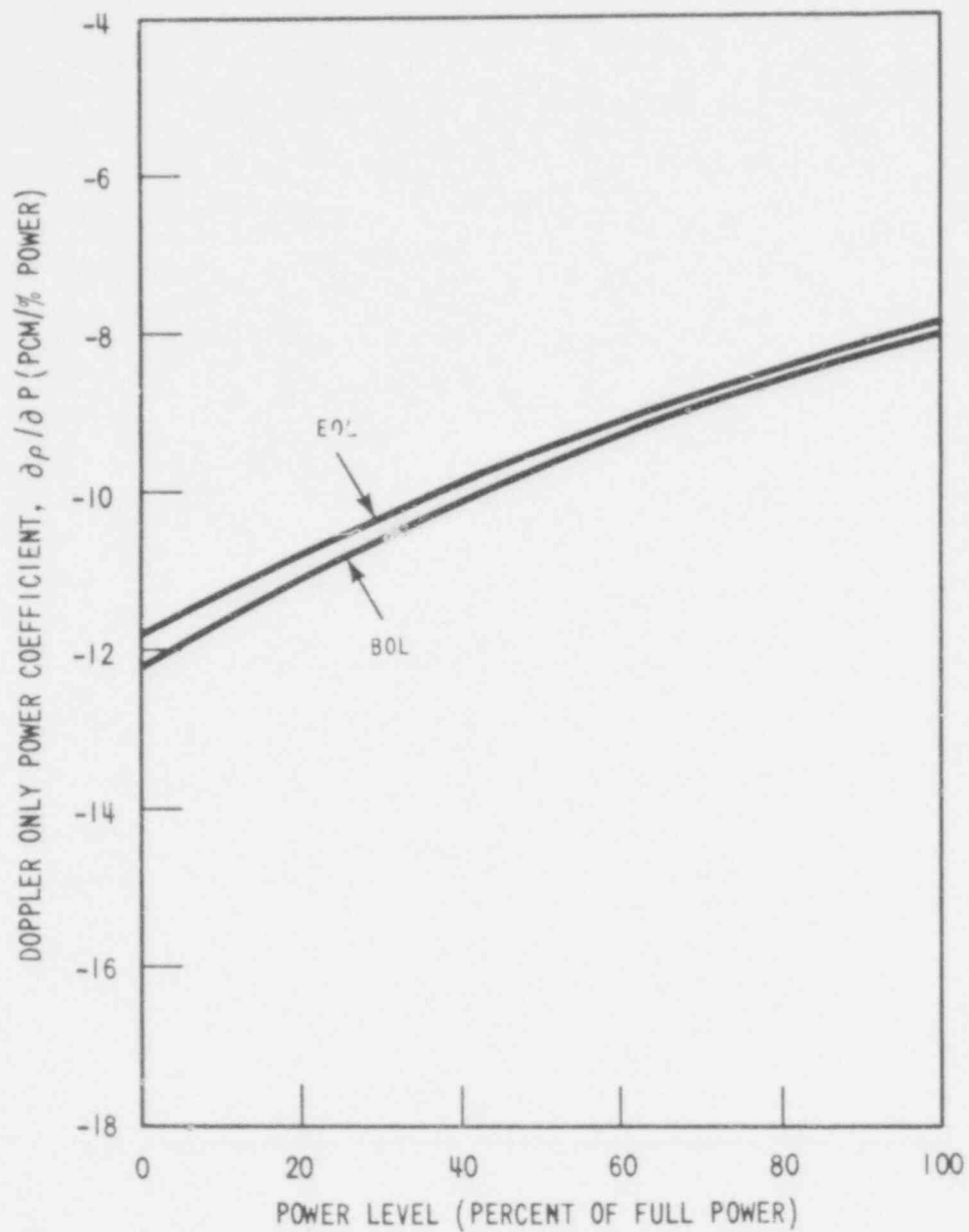


WCAP - 9500

Figure 4.3-27.

Doppler Temperature Coefficient at  
BOL and EOL, Cycle 1

612 240

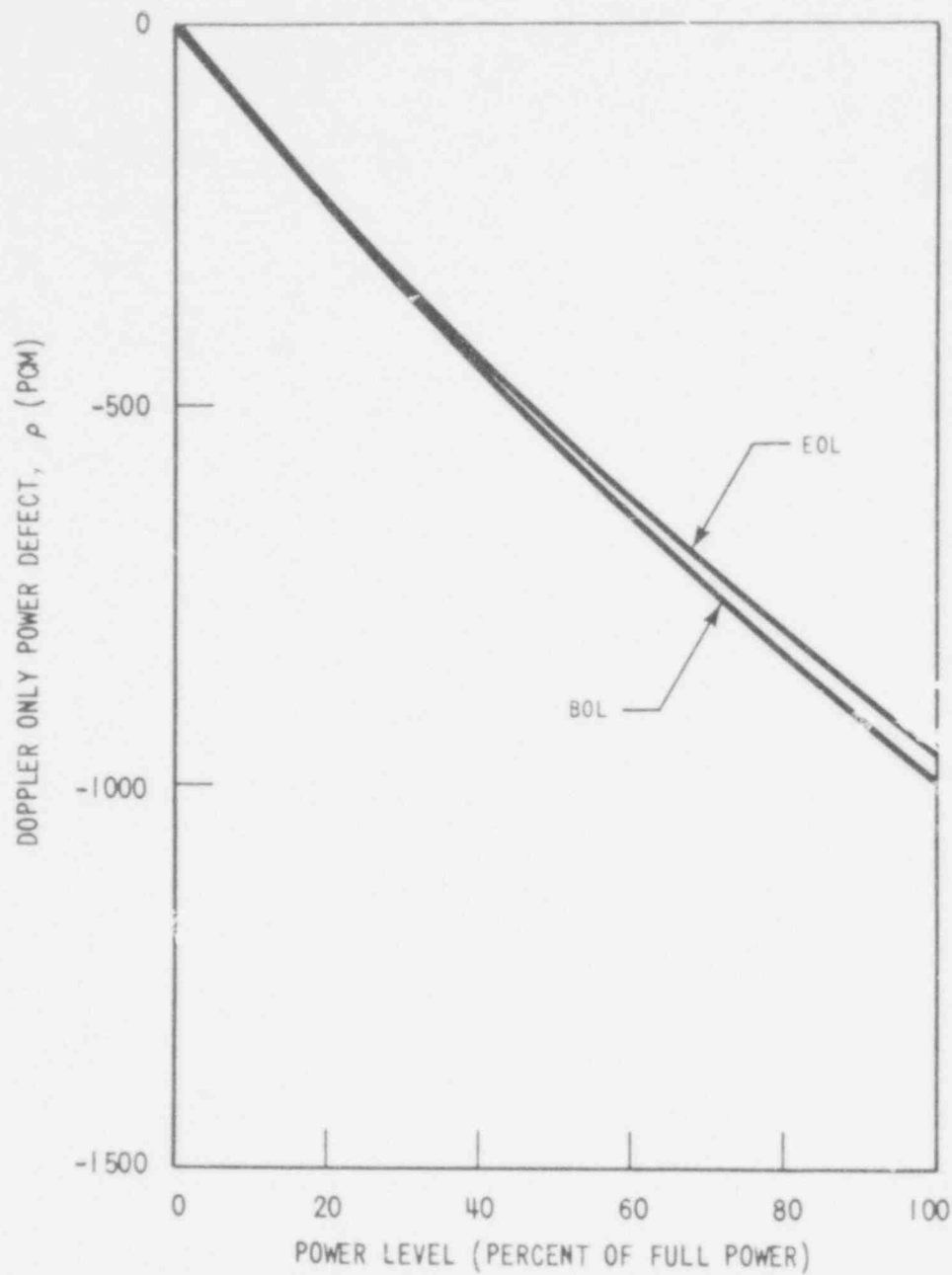


612 241

WCAP - 9500

Figure 4.3-28.

Doppler Only Power Coefficient  
BOL, EOL, Cycle 1



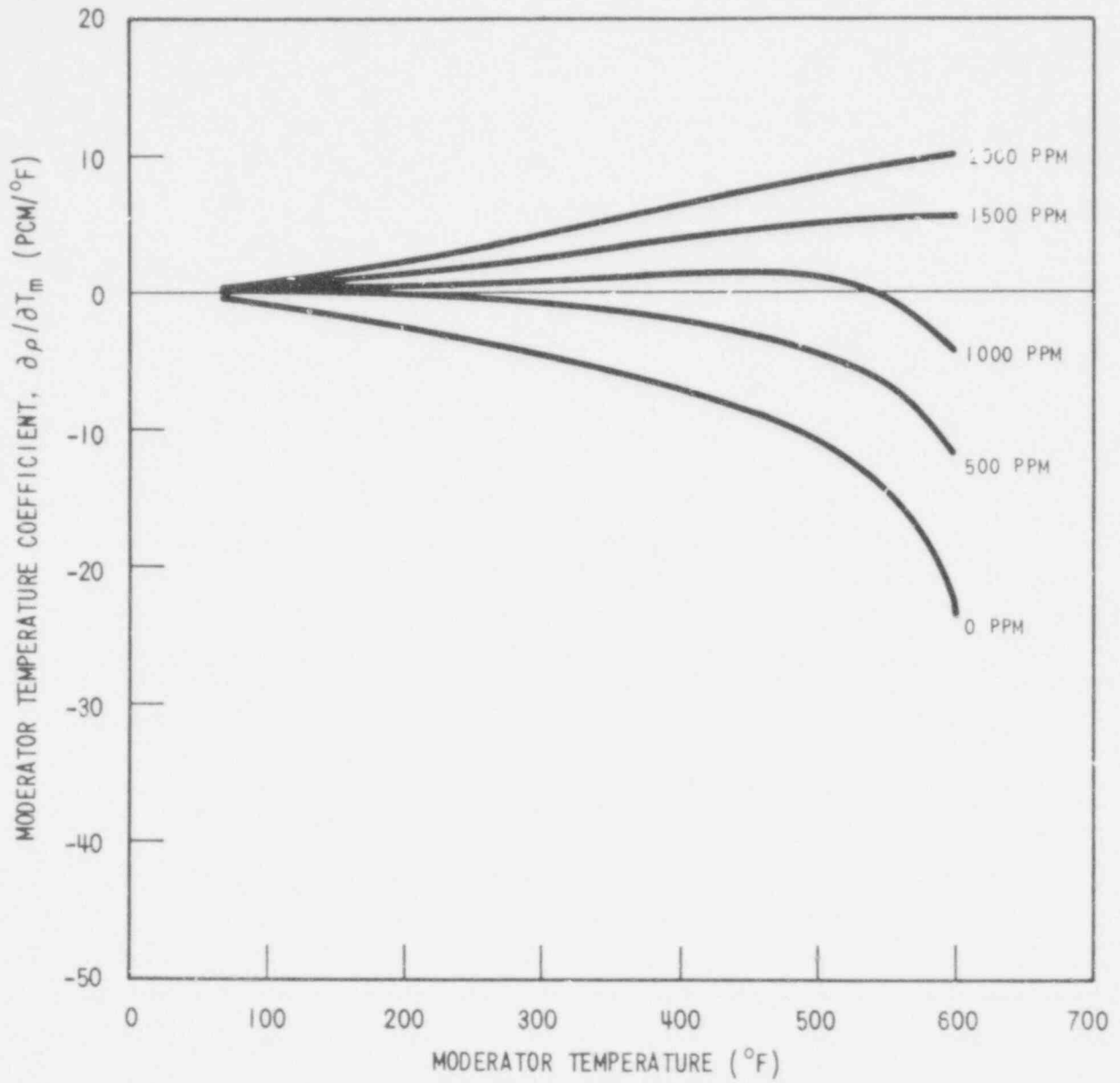
WCAP - 9500

Figure 4.3-29.

Doppler Only Power Defect  
BOL, EOL, Cycle 1

612 242



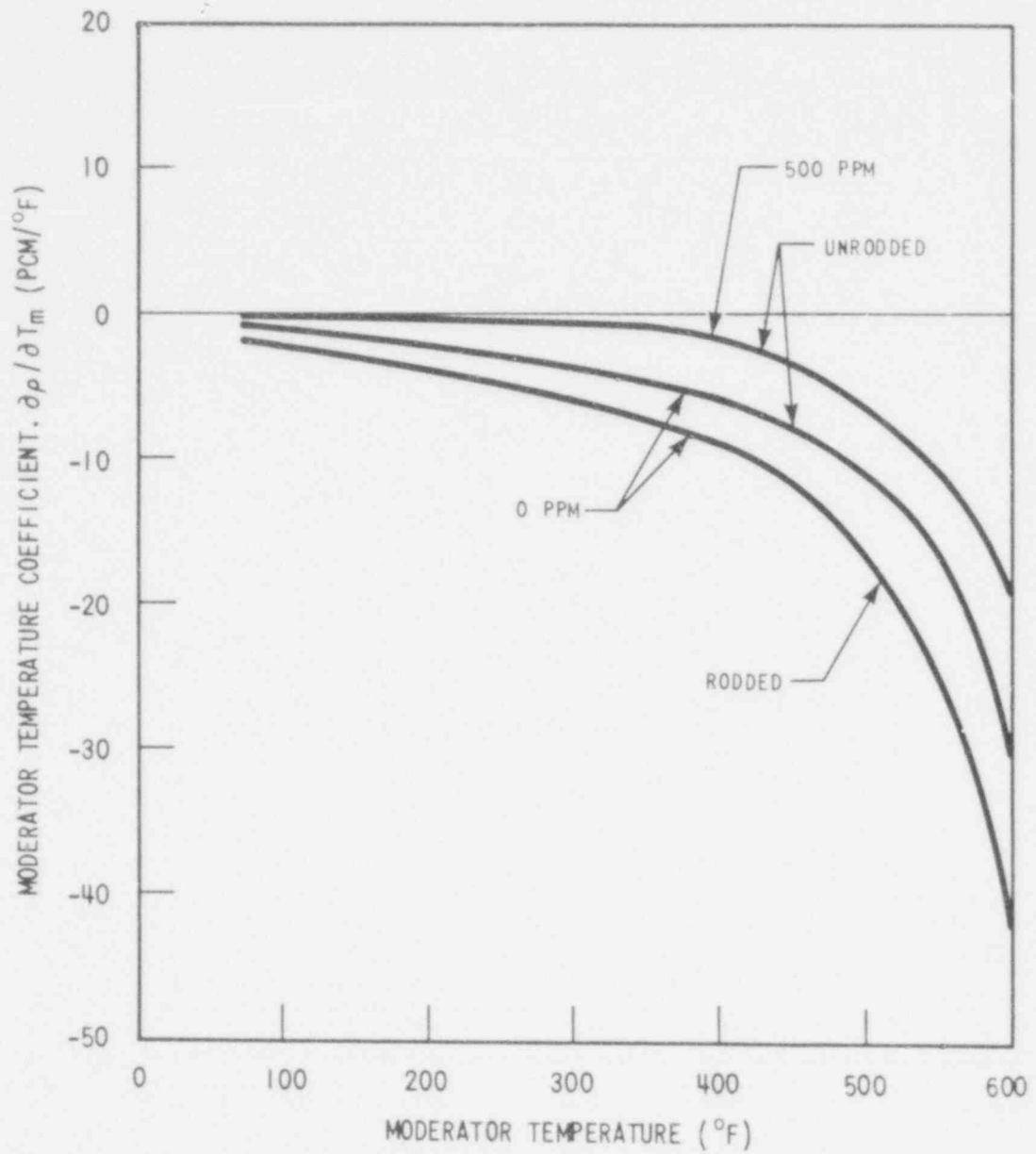


WCAP - 9500

Figure 4.3-30.

Moderator Temperature Coefficient  
BOL, Cycle 1, No Rods

612 243

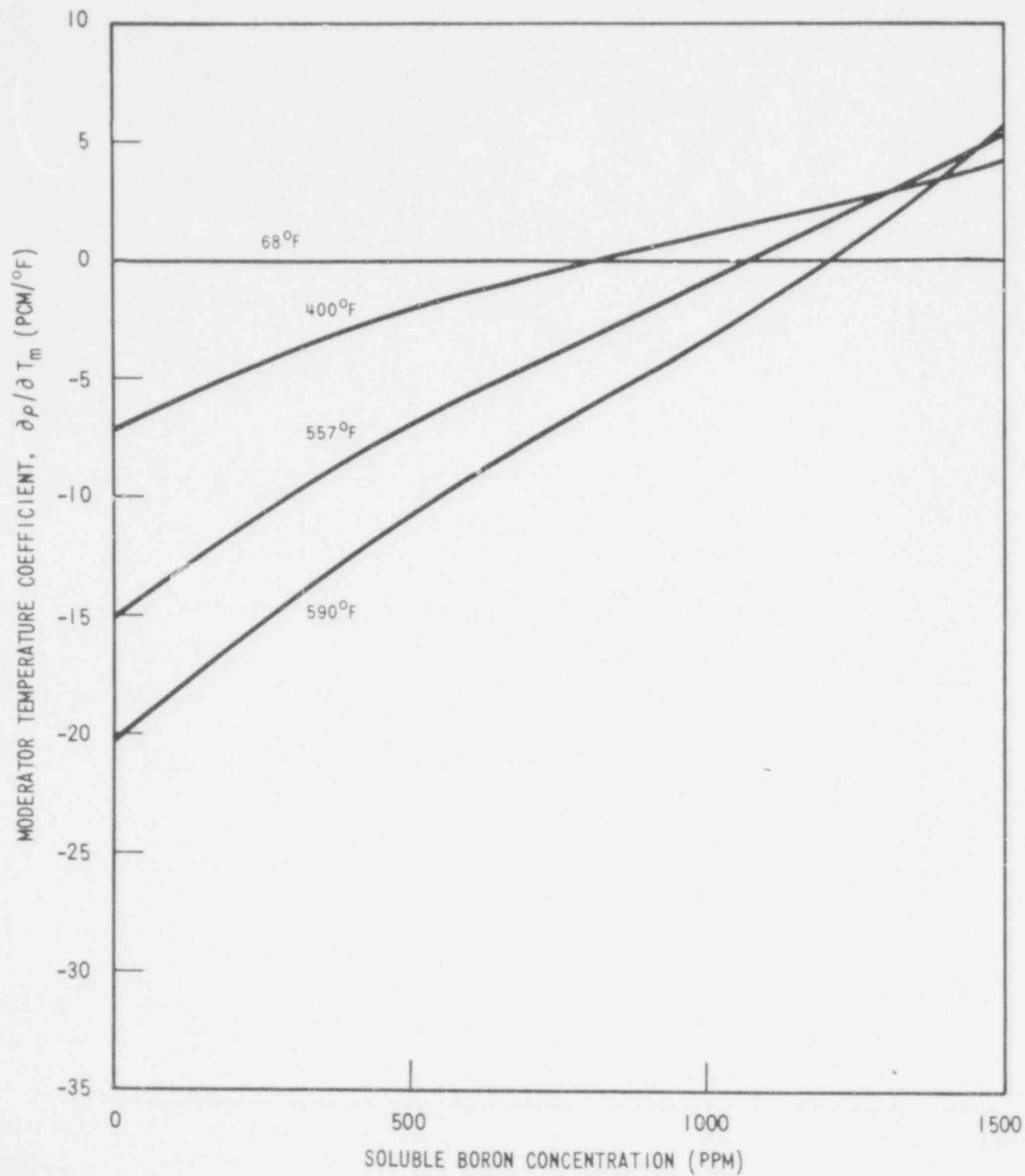


WCAP - 9500

Figure 4.3-31.

Moderator Temperature Coefficient  
EOL, Cycle 1

612 244

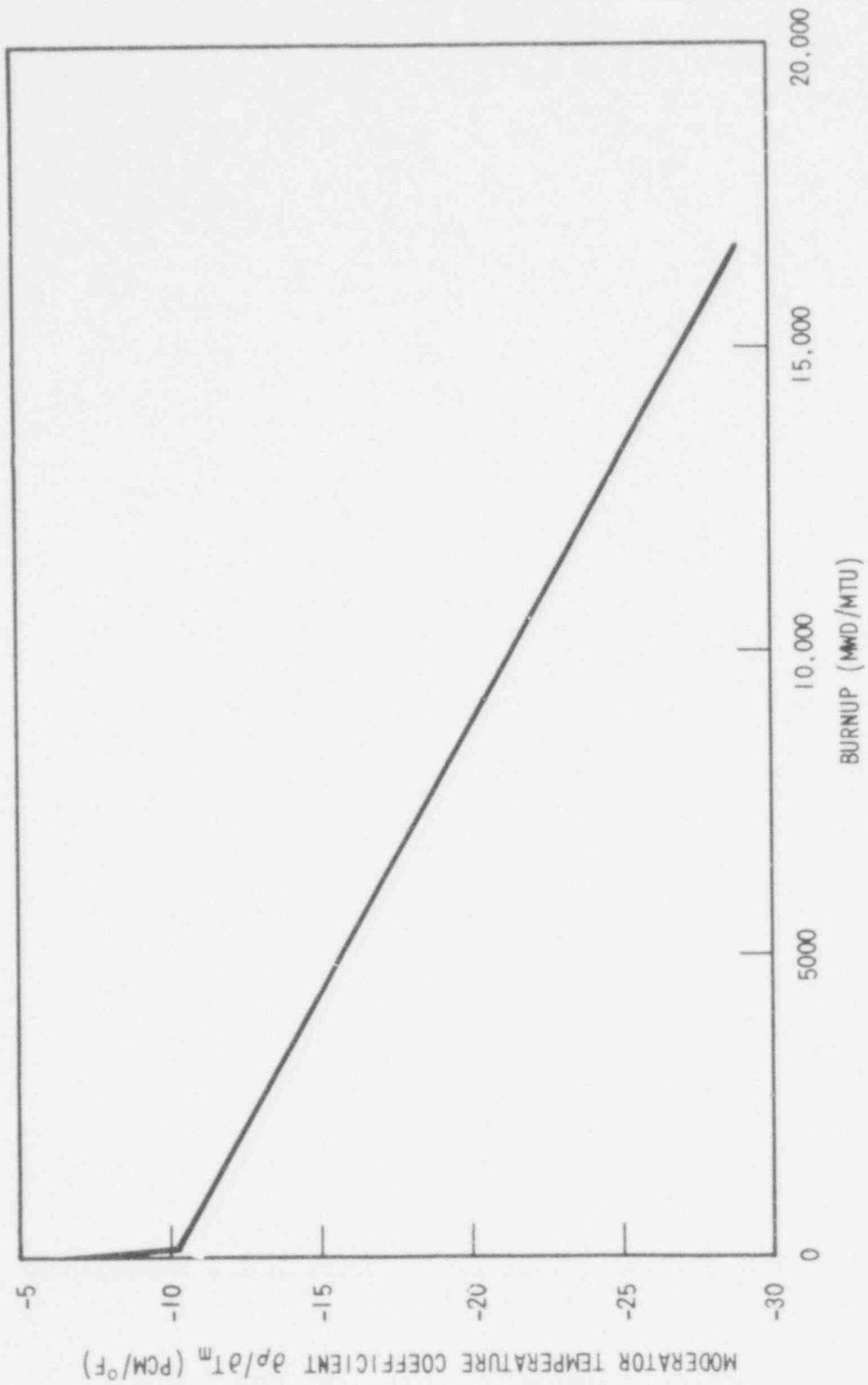


WCAP - 9500

Figure 4.3-32.

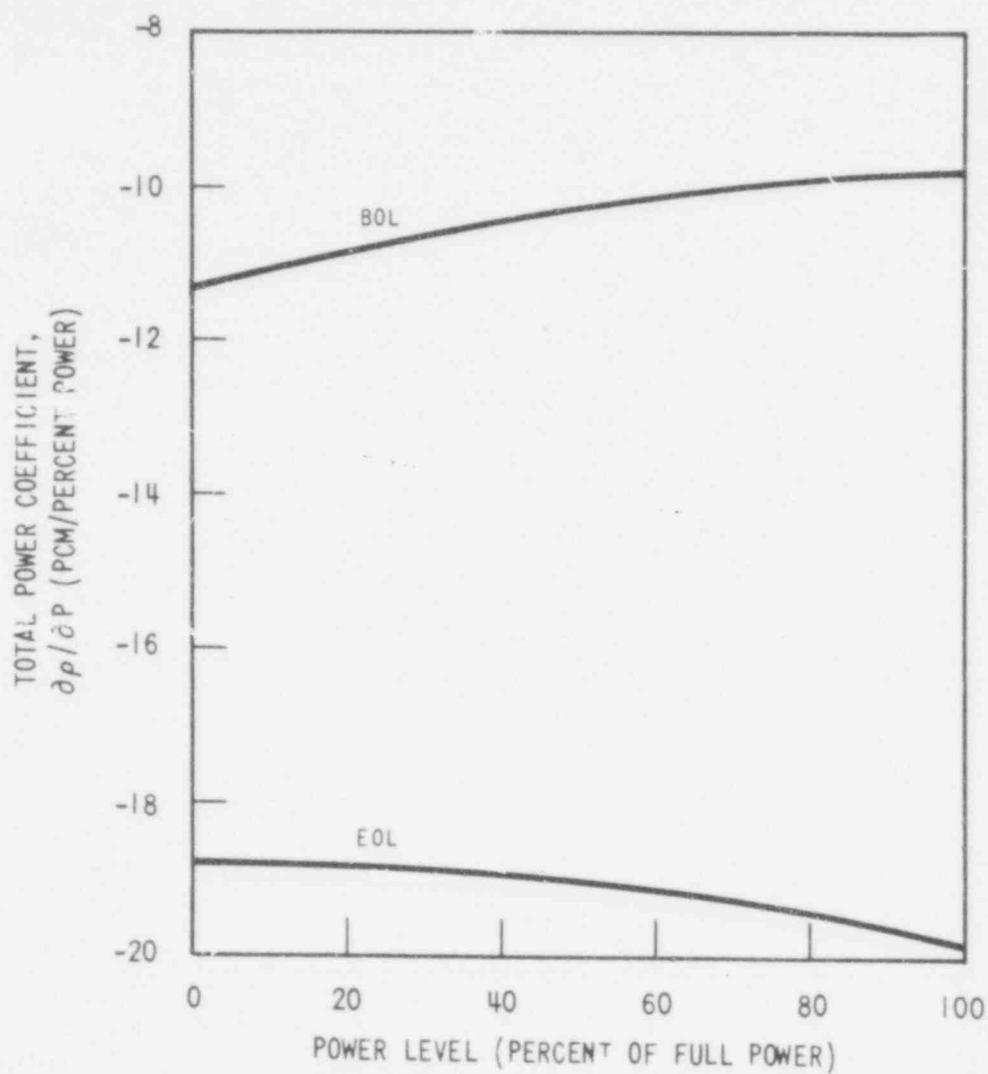
Moderator Temperature Coefficient as a  
Function of Boron Concentration BOL,  
Cycle 1, No Rods

612 245



612 246

|  |
|--|
| WCAP-9500  |
| Figure 4.3-33.   |
| Hot Full Power Temperature Coefficient<br>During Cycle 1 for the Critical<br>Boron Concentration |

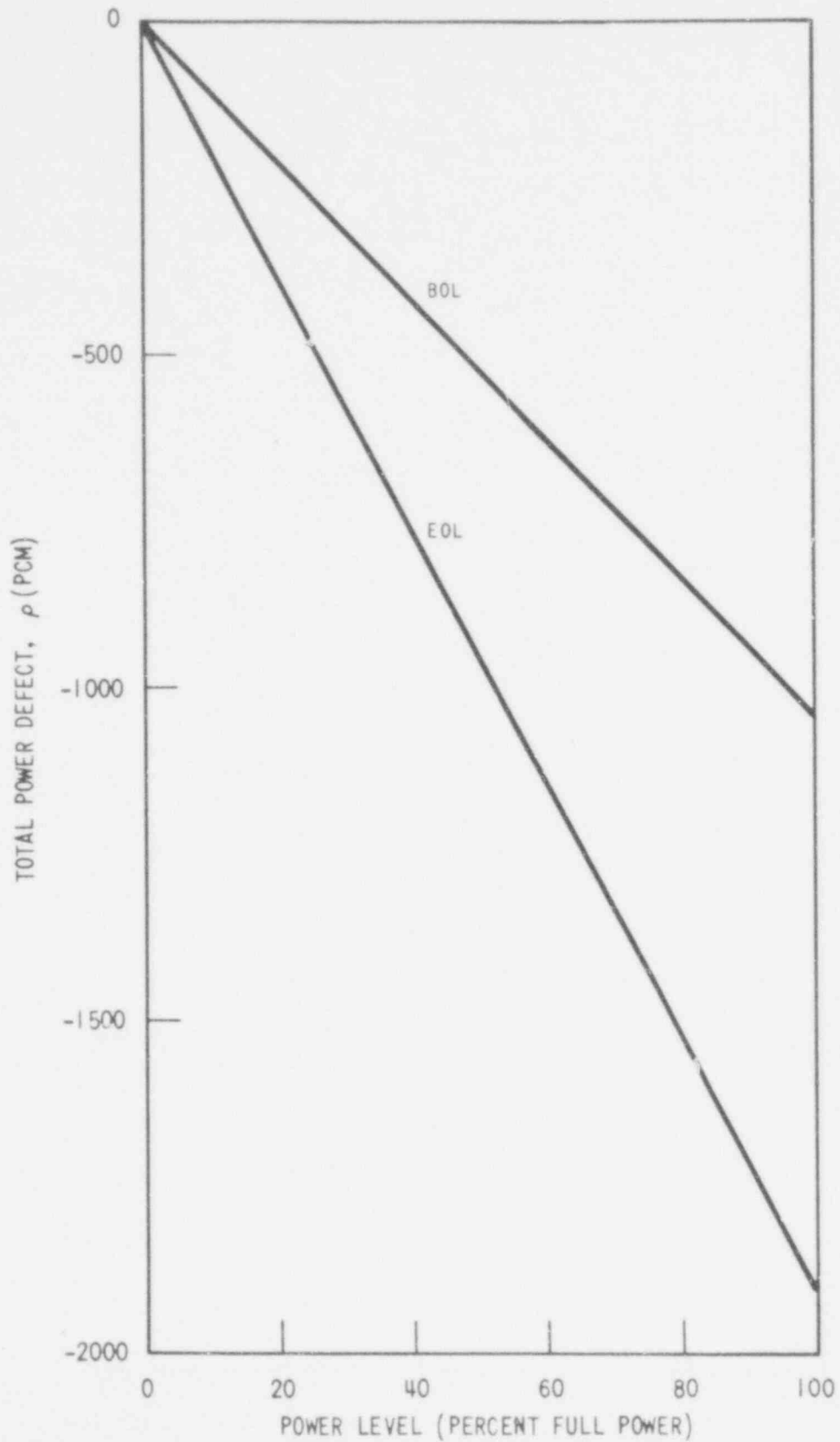


WCAP - 9500

Figure 4.3-34.

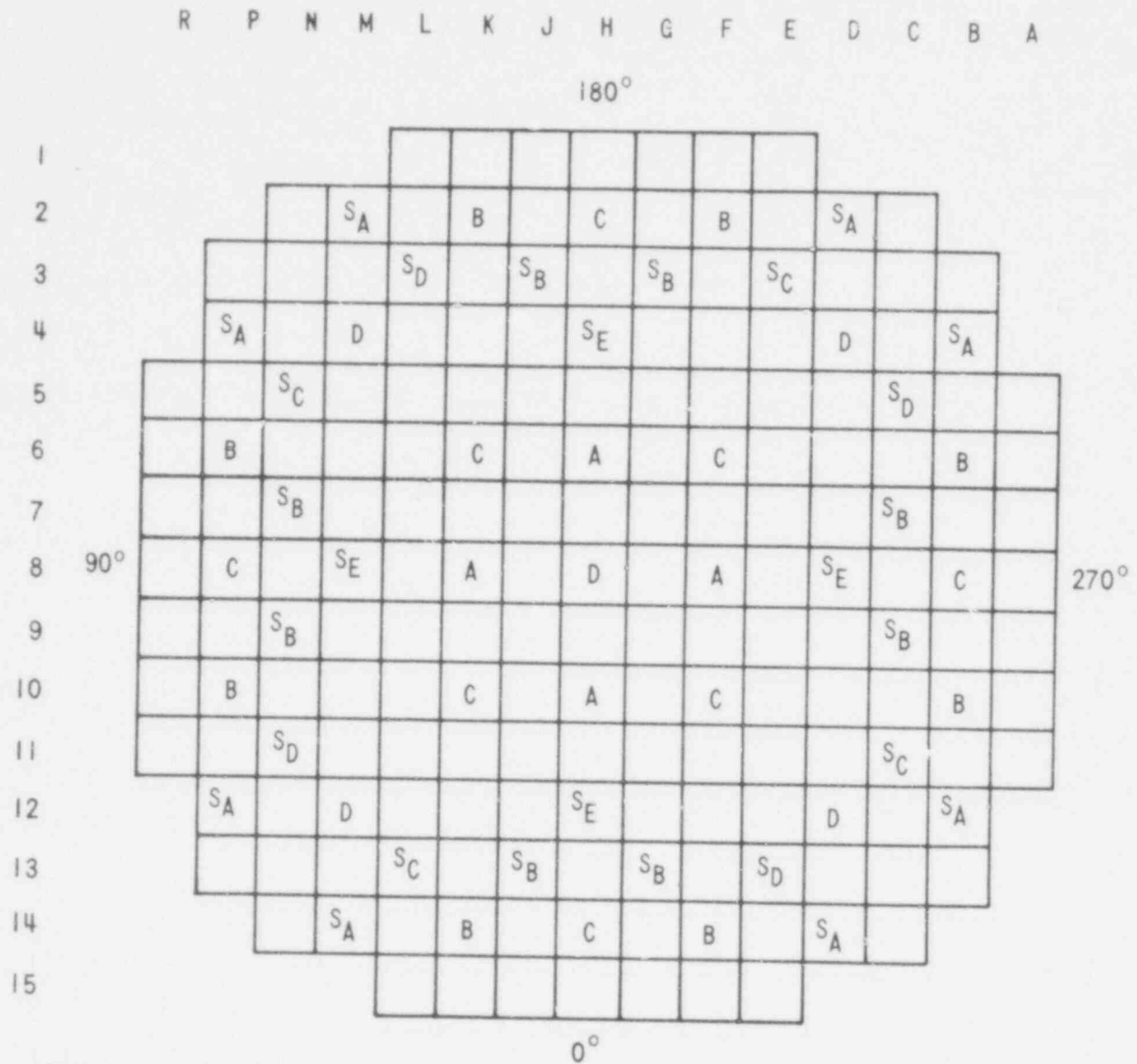
Total Power Coefficient  
BOL, EOL, Cycle 1

612 247



612 243

|                                      |
|--------------------------------------|
| WCAP - 9500                          |
| Figure 4.3-35.                       |
| Total Power Defect BOL, EOL, Cycle 1 |



| CONTROL BANK | NUMBER OF RODS |
|--------------|----------------|
| A            | 4              |
| B            | 8              |
| C            | 8              |
| D            | 5              |
| <b>TOTAL</b> | <b>25</b>      |

| SHUTDOWN BANK | NUMBER OF RODS |
|---------------|----------------|
| SA            | 8              |
| SB            | 8              |
| SC            | 4              |
| SD            | 4              |
| SE            | 4              |
| <b>TOTAL</b>  | <b>28</b>      |

612 249

WCAP - 9500

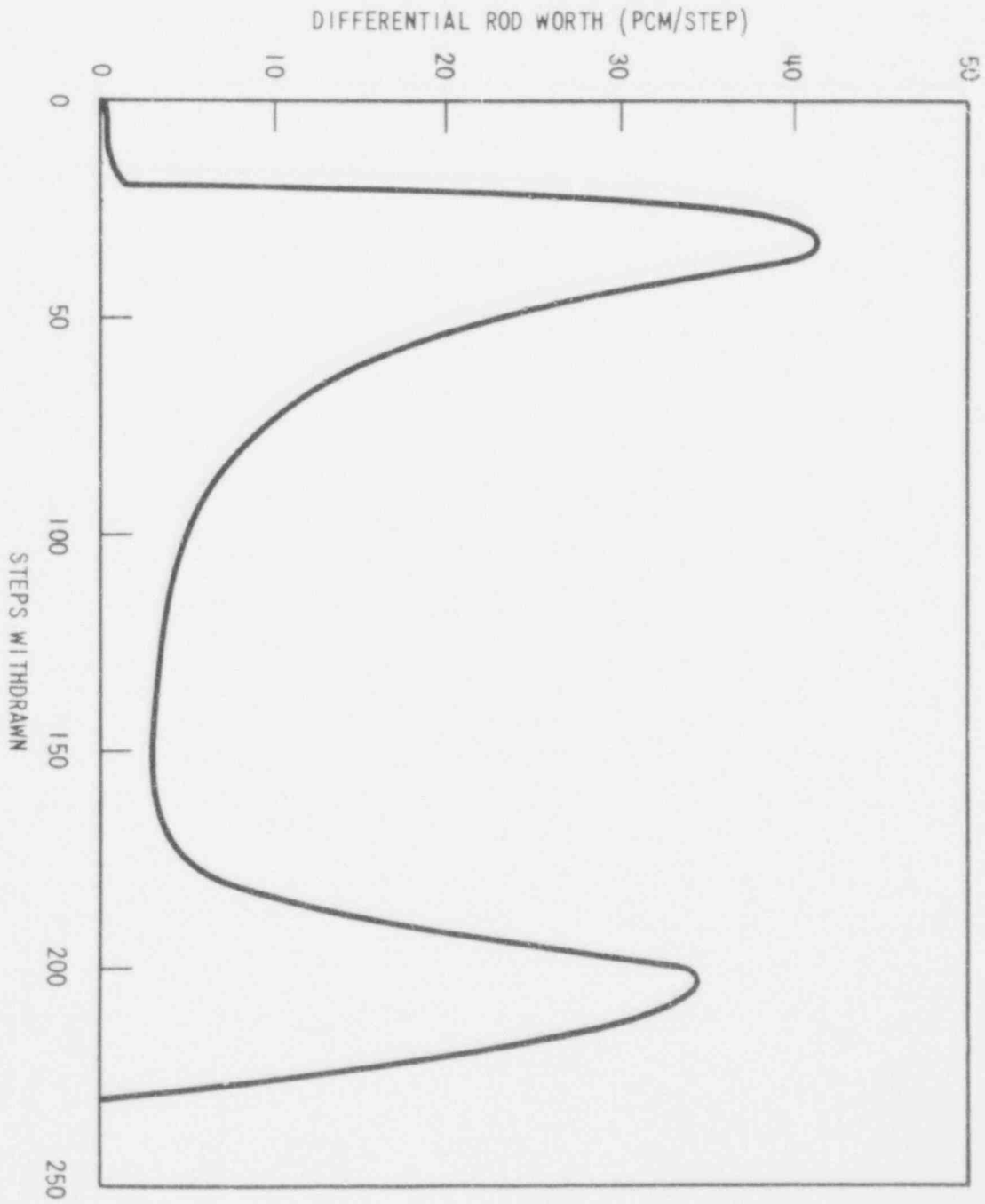
Figure 4.3-36.  
Rod Cluster Control Assembly Pattern

612 250

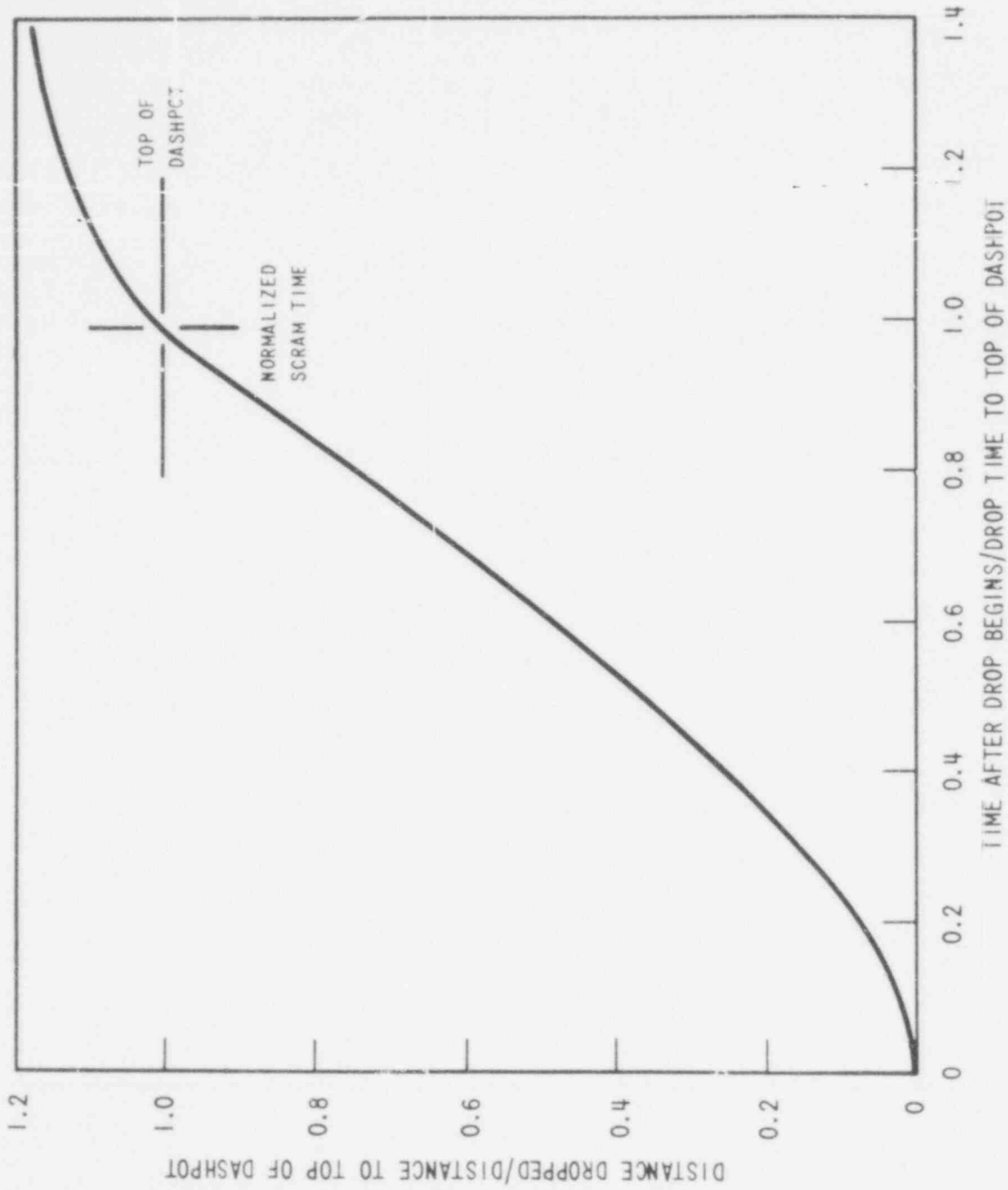
Accidental Simultaneous Withdrawal of  
Two Control Banks EOL, HZP, Banks C  
and B Moving in Same Plane

Figure 4.3-37.

WCAP - 9500

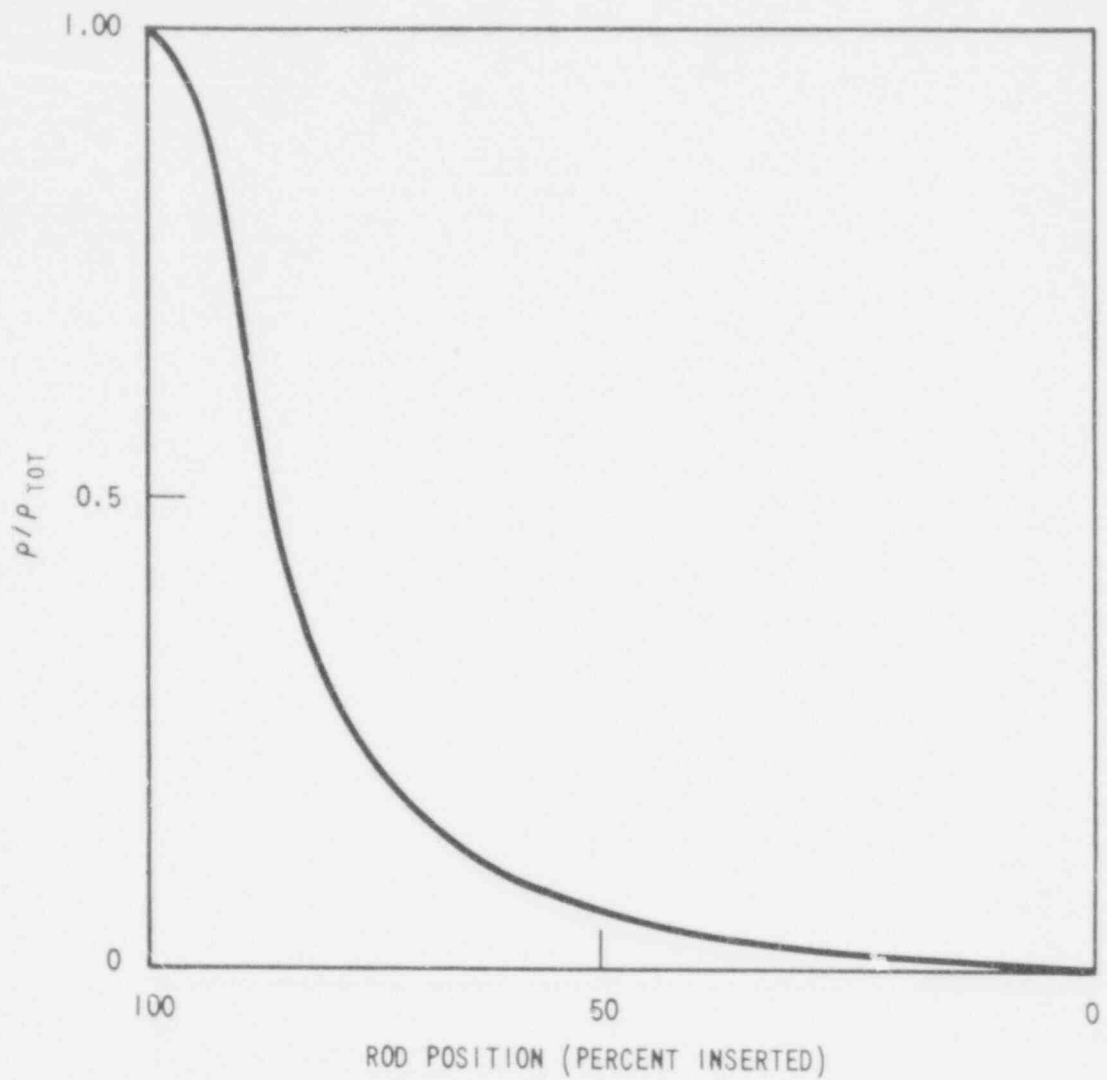






612 251

|                                       |
|---------------------------------------|
| WCAP - 9500                           |
| Figure 4.3-38.<br>Design - Trip Curve |



WCAP - 9500

Figure 4.3-39.

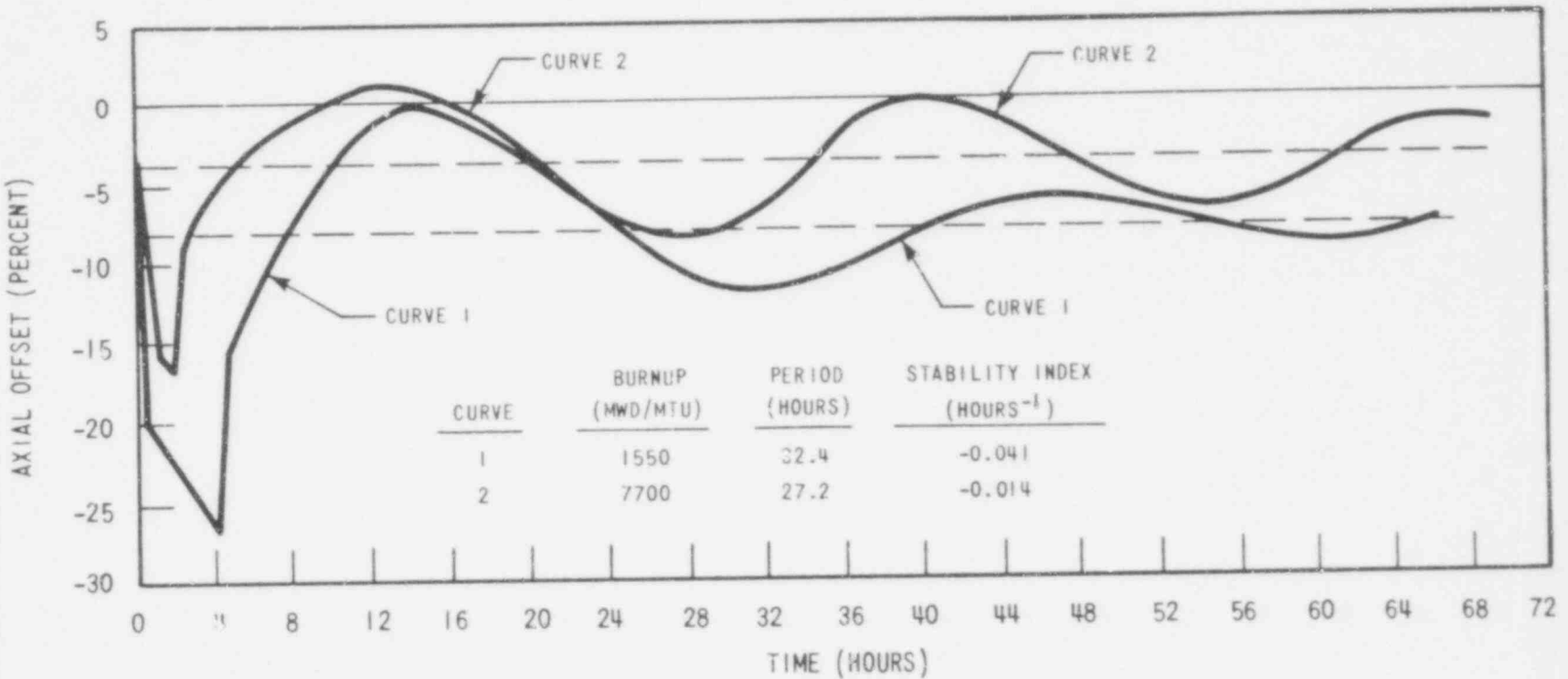
Normalized Rod Worth versus Percent  
Insertion All Rods but One

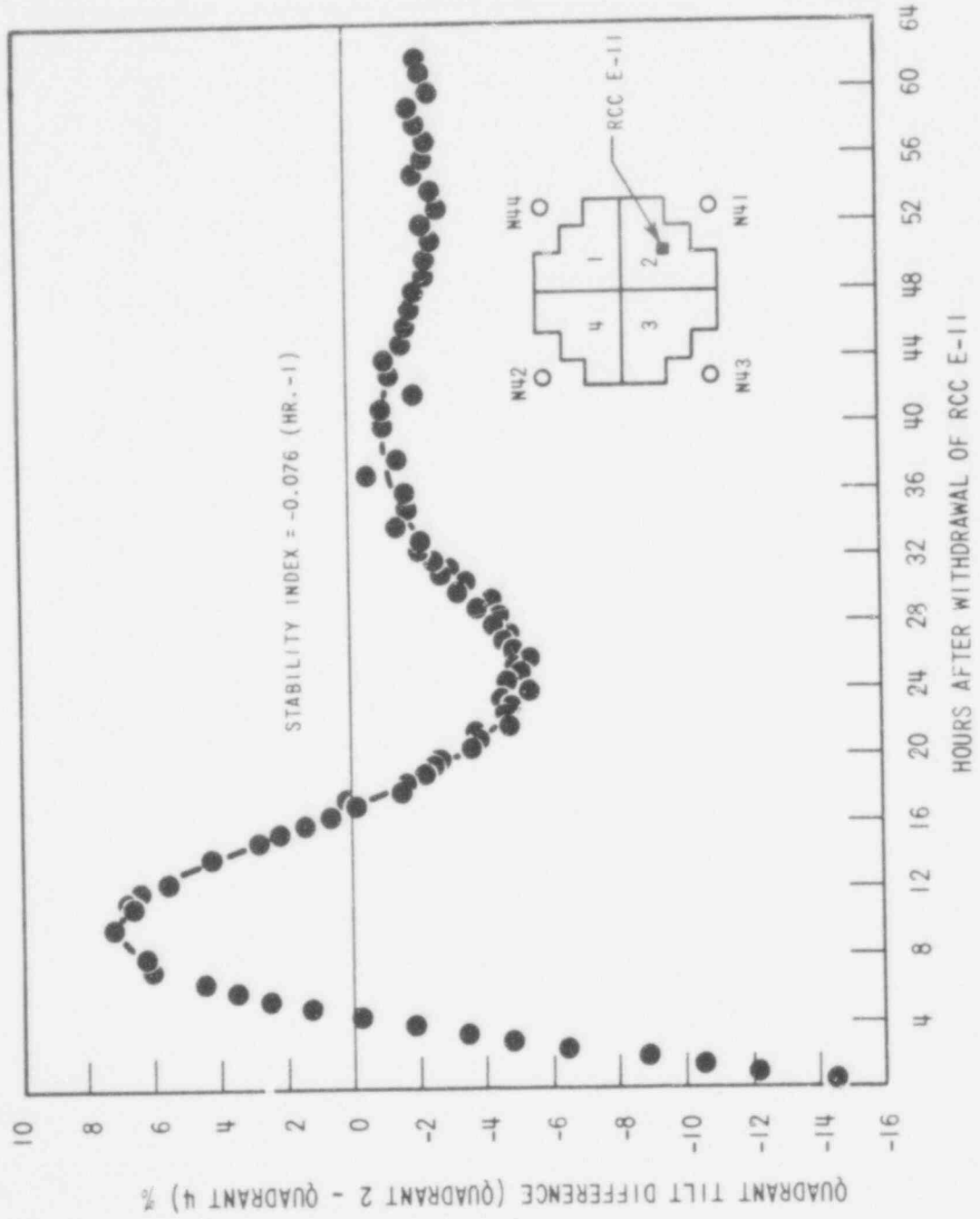
612 252

612  
253

WCAP - 9500

Figure 4.3-40.  
Axial Offset versus Time PWR Core With a  
12 FT Height and 121 Assemblies



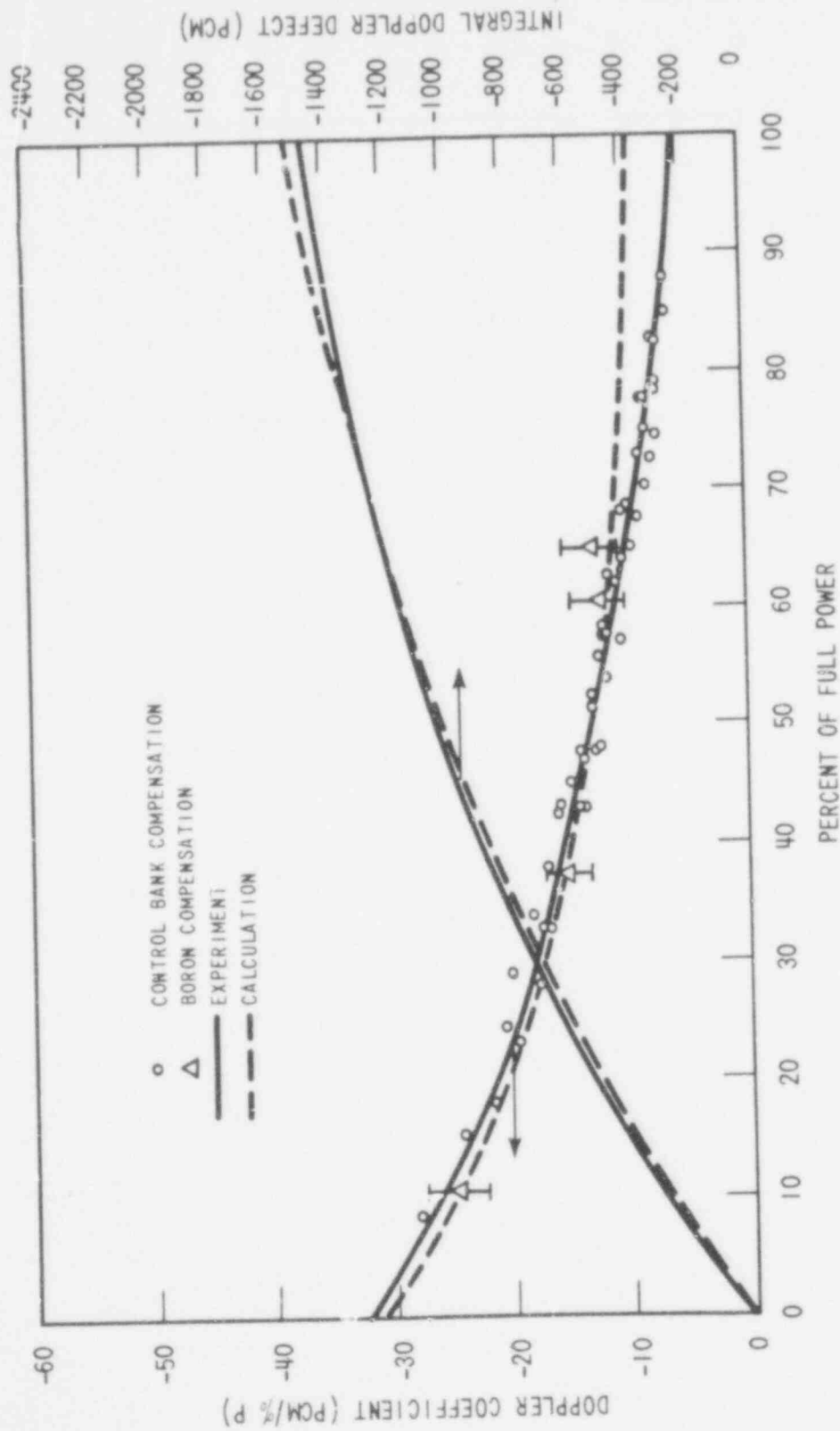


612 254

WCAP - 9500

Figure 4.3-41.

XY Xenon Test Thermocouple Response  
 Quadrant Tilt Difference versus Time

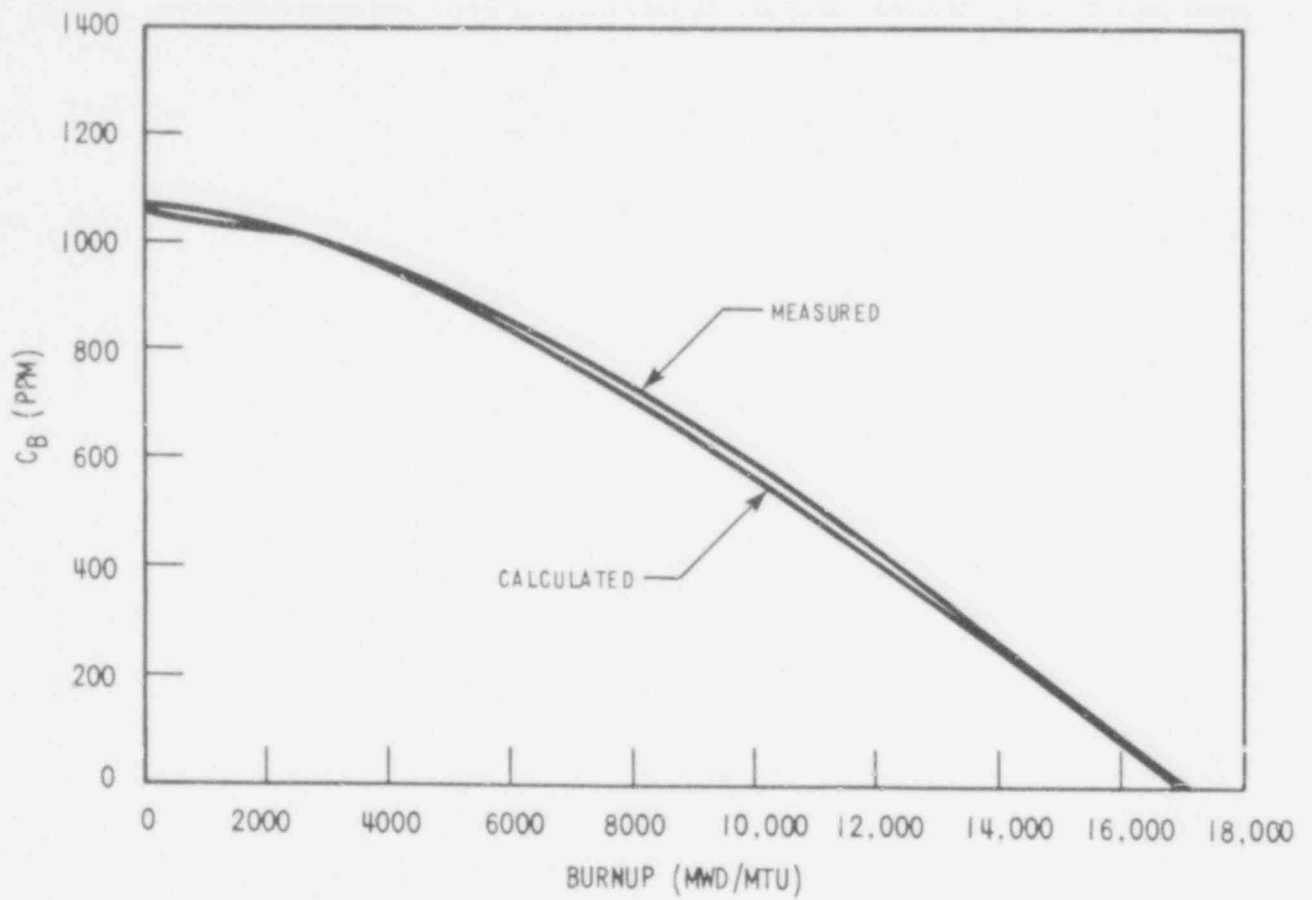


WCAP-9500

Figure 4.3-42.

Calculated and Measured Doppler Defect and Coefficients at BOL, 2-Loop Plant, 121 Assemblies, 12 FT Core

612 255

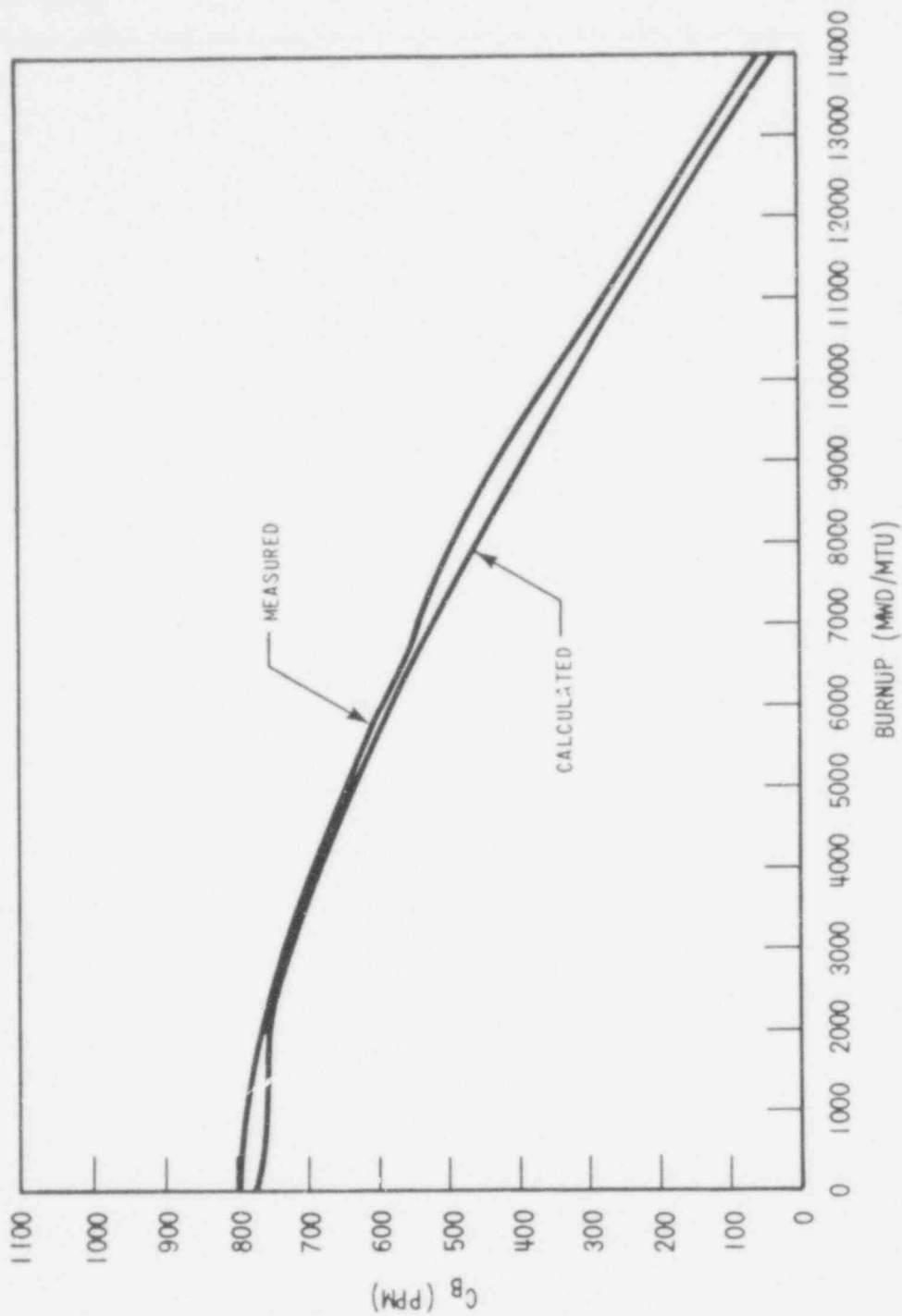


WCAP - 9500

Figure 4.3-43.

Comparison of Calculated and Measured  
Boron Concentration for 2-Loop Plant,  
121 Assemblies, 12 FT Core

612 256

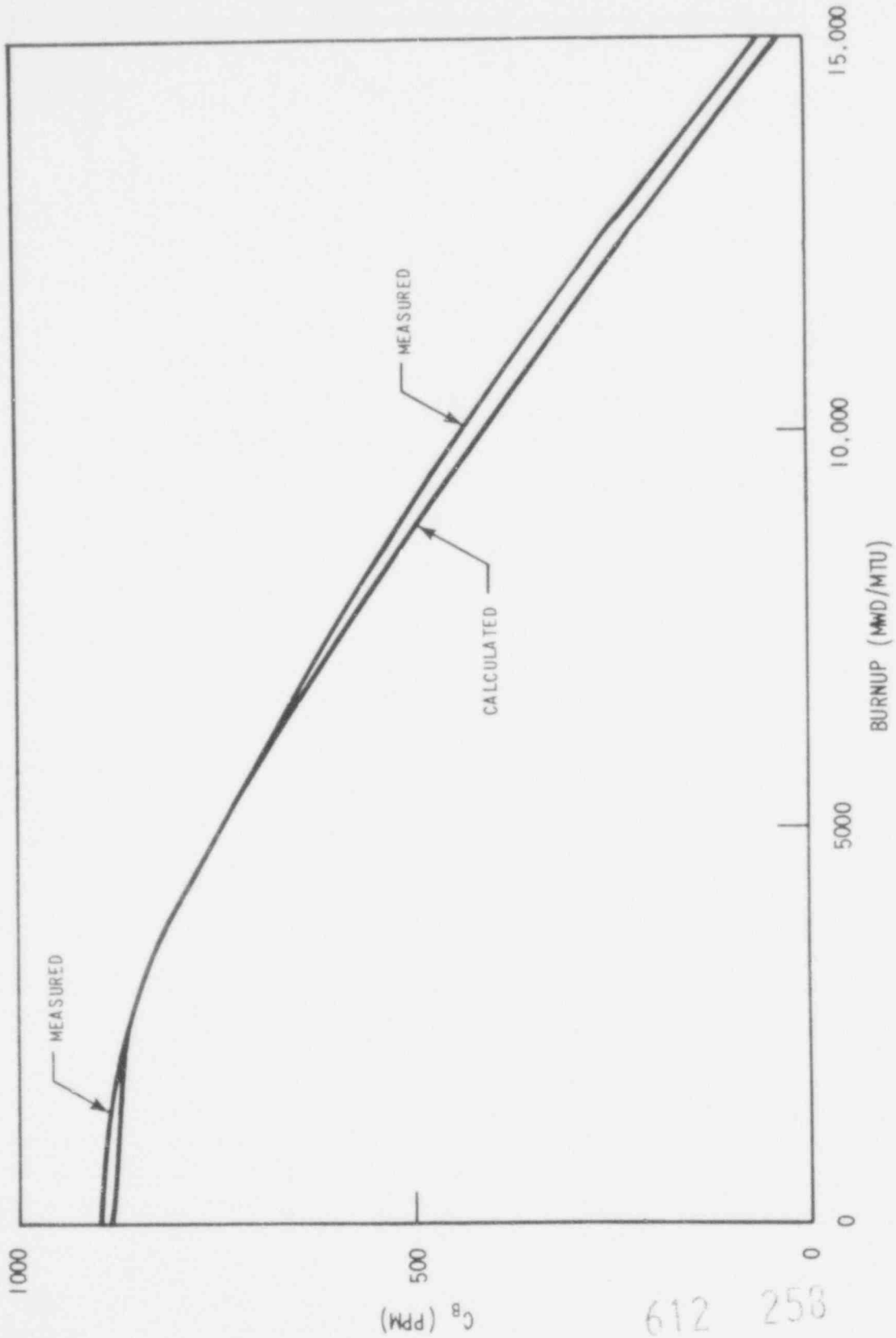


612 257

WCAP - 9500

Figure 4.3-44.

Comparison of Calculated and Measured  $C_B$  3-Loop Plant, 157 Assemblies, 12 FT Core

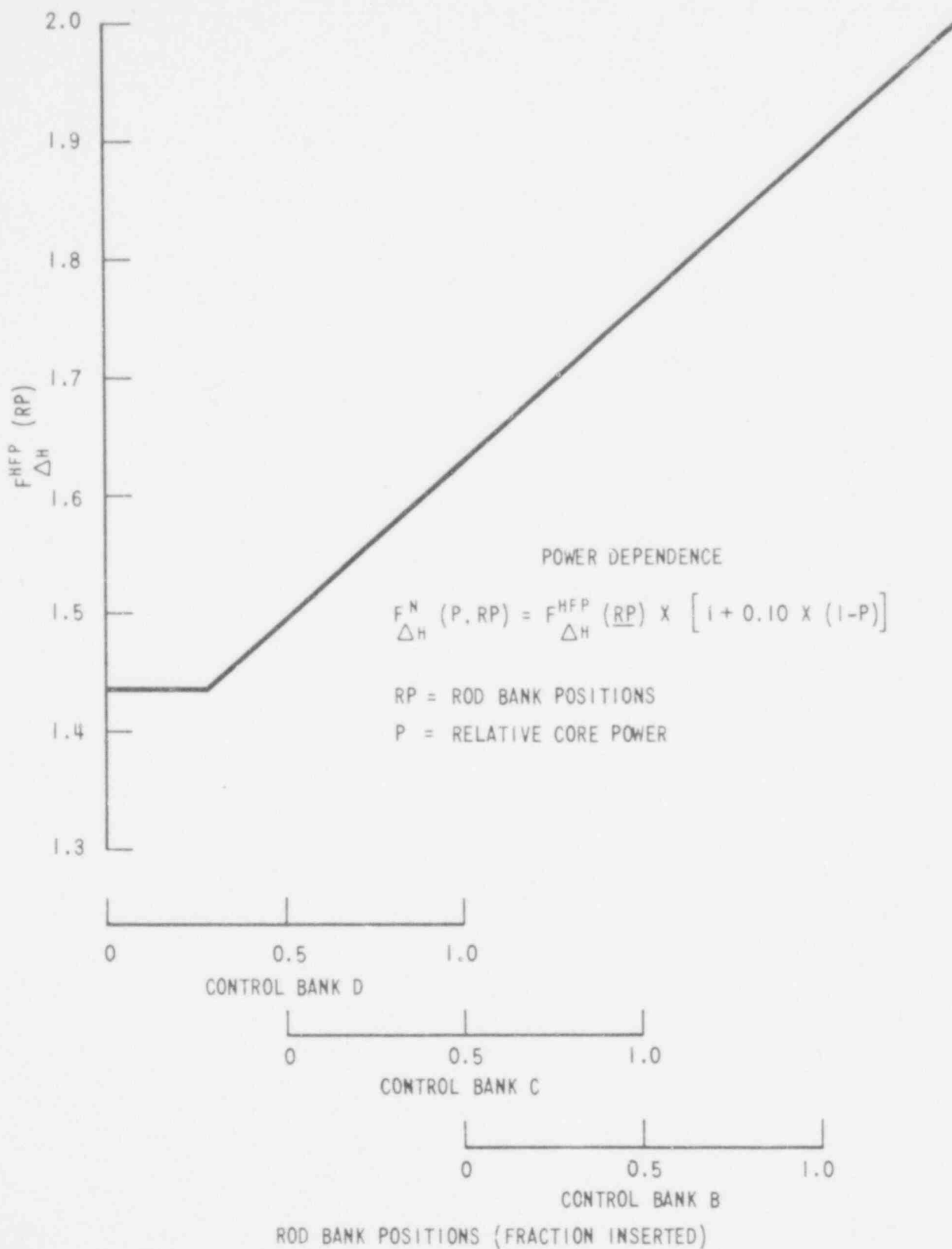


612 258

nCAP - 9500

Figure 4.3-45.  
Comparison of Calculated and Measured  
 $C_B$  4-Loop Plant, 193 Assemblies,  
12 FT Core





612 259

WCAP - 9500

Figure 4.3-46.  
Typical Nuclear Enthalpy Rise Limits for the  
First Cycle, Without Nuclear  
Uncertainty Allowance

612 260

#### 4.4 THERMAL AND HYDRAULIC DESIGN

##### 4.4.1 DESIGN BASIS

The overall objective of the thermal and hydraulic design of the reactor core is to provide adequate heat transfer which is compatible with the heat generation distribution in the core such that heat removal by the Reactor Coolant System or the Emergency Core Cooling System (when applicable) assures that the following performances and safety criteria requirements are met:

1. Fuel damage (defined as penetration of the fission product barrier, i.e., the fuel rod cladding) is not expected during normal operation and operational transients (Condition I) or any transient conditions arising from faults of moderate frequency (Condition II). It is not possible, however, to preclude a very small number of rod failures. These will be within the capability of the plant cleanup system and are consistent with the plant design bases.
2. The reactor can be brought to a safe state following a Condition III event with only a small fraction of fuel rods damaged (see above definition) although sufficient fuel damage might occur to preclude immediate resumption of operation.
3. The reactor can be brought to a safe state and the core can be kept subcritical with acceptable heat transfer geometry following transients arising from Condition IV events.

In order to satisfy the above requirements, the following design bases have been established for the thermal and hydraulic design of the reactor core.

##### 4.4.1.1 Departure from Nucleate Boiling Design Basis

###### Basis

These will be at least a 95 percent probability that departure from nucleate boiling (DNB) will not occur on the limiting fuel rods during

normal operation and operational transients and any transient conditions arising from faults of moderate frequency (Condition I and II events) at 95 percent confidence level. Historically this criterion has been conservatively met by adhering to the following thermal design basis: there must be at least a 95 percent probability that the minimum departure from nucleate boiling ratio (DNBR) of the limiting power rod during Condition I and II events is greater than or equal to the DNBR limit of the DNB correlation being used. The DNBR limit for the correlation is established based on the variance of the correlation such that there is a 95 percent probability with 95 percent confidence that DNB will not occur when the calculated DNBR is at the DNBR limit.

### Discussion

Historically this DNBR limit has been 1.30 for Westinghouse applications. In this application the WRB-1 correlation<sup>(1)</sup> is employed. With the significant improvement in the accuracy of the critical heat flux prediction with the WRB-1 correlation over previous DNB correlations a DNBR limit of 1.17 is applicable in this application based on the NRC evaluation and approval of this correlation<sup>(2)</sup>.

The design method employed to meet the DNB design basis is the "Improved Thermal Design Procedure"<sup>(3)</sup>. Uncertainties in plant operating parameters, nuclear and thermal parameters, and fuel fabrication parameters are considered statistically such that there is at least a 95 percent probability that the minimum DNBR will be greater than or equal to 1.17 for the limiting power rod. Plant parameter uncertainties are used to determine the plant DNBR uncertainty. This DNBR uncertainty, combined with the DNBR limit, establishes a design DNBR value which must be met in plant safety analyses. Since the parameter uncertainties are considered in determining the design DNBR value, the plant safety analyses are performed using values of input parameters without uncertainties. This design procedure is illustrated in Figure 4.4-1. For this application the design DNBR values are 1.31 for thimble coldwall cells (three fuel rods and a thimble tube) and 1.33 for typical cells (four fuel rods).

In addition to the above considerations, a specific plant allowance has been considered in the present analysis. In particular, the DNBR values of 1.82 and 1.85, for thimble and typical cells respectively, were employed in safety analyses. The plant allowance available between the DNBRs used in the safety analyses and the design DNBR values (1.31 for thimble cells and 1.33 for typical cells) is not required to meet the design basis discussed earlier. This allowance will be used for the flexibility in the design, operation, and analyses for this class of plants on a plant-by-plant basis. For instance, individual plant designs may use the allowance for improved fuel management or increased plant availability.

The design DNBRs of 1.31 and 1.33 are used as the bases for the Technical Specifications, as given in Chapter 16, and for consideration of the applicability of unreviewed safety questions as defined in 10 CFR 50.59

By preventing departure from nucleate boiling (DNB), adequate heat transfer is assured between the fuel cladding and the reactor coolant, thereby preventing cladding damage as a result of inadequate cooling. Maximum fuel rod surface temperature is not a design basis as it will be within a few degrees of coolant temperature during operation in the nucleate boiling region. Limits provided by the nuclear control and protection systems are such that this design basis will be met for transients associated with Condition II events including overpower transients. There is an additional large DNBR margin at rated power operation and during normal operating transients.

#### 4.4.1.2 Fuel Temperature Design Basis

##### Basis

During modes of operation associated with Condition I and Condition II events, there is at least a 95 percent probability that the peak kW/ft fuel rods will not exceed the  $UO_2$  melting temperature. The melting temperature of  $UO_2$  is taken as  $5080^{\circ}F^{(4)}$ , unirradiated and decreasing  $58^{\circ}F$  per 10,000 MWD/MTU. By precluding  $UO_2$  melting, the

fuel geometry is preserved and possible adverse effects of molten  $UO_2$  on the cladding are eliminated. To preclude center melting and as a basis for overpower protection system setpoints, a calculated centerline fuel temperature of  $4700^{\circ}F$  has been selected as the overpower limit. This provides sufficient margin for uncertainties in the thermal evaluations as described in Subsection 4.4.2.9.1.

#### Discussion

Fuel rod thermal evaluations are performed at rated power, maximum overpower and during transients at various burnups. These analyses assure that this design basis as well as the fuel integrity design bases given in Section 4.2 are met. They also provide input for the evaluation of Condition III and IV events given in Chapter 15.0.

#### 4.4.1.3 Core Flow Design Basis

##### Basis

A minimum of 94.2% of the thermal flow rate will pass through the fuel rod region of the core and be effective for fuel rod cooling. Coolant flow through the thimble tubes as well as the leakage from the core barrel-baffle region into the core are not considered effective for heat removal.

##### Discussion

Core cooling evaluations are based on the thermal flow rate (minimum flow) entering the reactor vessel. A maximum 7.5% of this value is allotted as bypass flow. This includes rod cluster control guide thimble cooling flow, head cooling flow, baffle leakage, and leakage to the vessel outlet nozzle.

6/2 26t

In addition to the above considerations, a specific plant allowance has been considered in the present analysis. In particular, the DNBR values of 1.47 and 1.49, for thimble and typical cells respectively, were employed in safety analyses. The plant allowance available between the DNBRs used in the safety analyses and the design DNBR values (1.31 for thimble cells and 1.33 for typical cells) is not required to meet the design basis discussed earlier. This allowance will be used for the flexibility in the design, operation, and analyses for this class of plants on a plant-by-plant basis. For instance, individual plant designs may use the allowance for improved fuel management or increased plant availability.

The design DNBRs of 1.31 and 1.33 are used as the bases for the Technical Specifications, as given in Chapter 16, and for consideration of the applicability of unreviewed safety questions as defined in 10 CFR 50.59

By preventing departure from nucleate boiling (DNB), adequate heat transfer is assured between the fuel cladding and the reactor coolant, thereby preventing cladding damage as a result of inadequate cooling. Maximum fuel rod surface temperature is not a design basis as it will be within a few degrees of coolant temperature during operation in the nucleate boiling region. Limits provided by the nuclear control and protection systems are such that this design basis will be met for transients associated with Condition II events including overpower transients. There is an additional large DNBR margin at rated power operation and during normal operating transients.

#### 4.4.1.2 Fuel Temperature Design Basis

##### Basis

During modes of operation associated with Condition I and Condition II events, there is at least a 95 percent probability that the peak kW/ft fuel rods will not exceed the  $UO_2$  melting temperature. The melting temperature of  $UO_2$  is taken as  $5080^{\circ}F^{(4)}$ , unirradiated and decreasing  $58^{\circ}F$  per 10,000 MWD/MTU. By precluding  $UO_2$  melting, the





fuel geometry is preserved and possible adverse effects of molten  $UO_2$  on the cladding are eliminated. To preclude center melting and as a basis for overpower protection system setpoints, a calculated centerline fuel temperature of  $4700^{\circ}F$  has been selected as the overpower limit. This provides sufficient margin for uncertainties in the thermal evaluations as described in Subsection 4.4.2.9.1.

#### Discussion

Fuel rod thermal evaluations are performed at rated power, maximum overpower and during transients at various burnups. These analyses assure that this design basis as well as the fuel integrity design bases given in Section 4.2 are met. They also provide input for the evaluation of Condition III and IV events given in Chapter 15.0.

#### 4.4.1.3 Core Flow Design Basis

##### Basis

A minimum of 92.5% of the thermal flow rate will pass through the fuel rod region of the core and be effective for fuel rod cooling. Coolant flow through the thimble tubes as well as the leakage from the core barrel-baffle region into the core are not considered effective for heat removal.

##### Discussion

Core cooling evaluations are based on the thermal flow rate (minimum flow) entering the reactor vessel. A maximum 5.8% of this value is allotted as bypass flow. This includes rod cluster control guide thimble cooling flow, head cooling flow, baffle leakage, and leakage to the vessel outlet nozzle.

#### 4.4.1.4 Hydrodynamic Stability Design Basis

##### Basis

Modes of operation associated with Condition I and II events shall not lead to hydrodynamic instability.

#### 4.4.1.5 Other Considerations

The above design bases together with the fuel cladding and fuel assembly design bases given in Subsection 4.2.1 are sufficiently comprehensive so additional limits are not required.

Fuel rod diametral gap characteristics, moderator-coolant flow velocity and distribution, and moderator void are not inherently limiting. Each of these parameters is incorporated into the thermal and hydraulic models used to ensure the above mentioned design criteria are met. For instance, the fuel rod diametral gap characteristics change with time (see Subsection 4.2.3.3) and the fuel rod integrity is evaluated on that basis. The effect of the moderator flow velocity and distribution (see Subsection 4.4.2.2) and moderator void distribution (see Subsection 4.4.2.4) are included in the core thermal (THINC) evaluation and thus affect the design bases.

Meeting the fuel cladding integrity criteria covers possible effects of cladding temperature limitations. As noted in Subsection 4.2.3.3, the fuel rod conditions change with time. A single cladding temperature limit for Condition I or Condition II events is not appropriate since of necessity it would be overly conservative. A cladding temperature limit is applied to the loss-of-coolant accident (Subsection 15.6.5), control rod ejection accident, and locked rotor accident.

#### 4.4.2 DESCRIPTION

##### 4.4.2.1 Summary Comparison

Table 4.4-1 provides a comparison of the design parameters for the core described herein with those given in the Byron-Braidwood FSAR (Dockets

#50-454 through 50-457) for the standard 12 foot 17x17 design. Thermal-hydraulic design parameters for one of four coolant loops out of service are provided in Table 4.4-2.

Examination of the tables demonstrates that in progressing from the standard 12 foot core to the current model a relatively small perturbation has been made in the core hardware while significant advances have been made in the methods of analysis of core performance.

The fundamental difference in core geometry between this application and previous 17x17 submittals is a decrease of 14 mils in the fuel rod outside diameter from .374" to .360". In addition, the grid design has changed from the standard Inconel R-grid design to a Zircaloy design. More detail on the new grid design is given in Section 4.2.

Both the average and peak linear heat generation rates (kW/ft) remain the same for the cores described herein as that of a standard design with a power rating of 3411 MW<sup>th</sup> (see Table 4.4-1). However, the reduction in fuel rod diameter results in a slightly higher average and peak heat flux. The overall fuel assembly pressure drop for the optimized fuel assembly design is essentially the same as that for the standard Inconel assembly design<sup>(5)</sup>.

The inability of Table 4.4-1 to permit a direct comparison of all plant operating parameters results from the significant advances and improvements made in the method of analysis of core performance for this application. The Byron-Braidwood cores have been analyzed on a worst case basis for all parameters involved in determining limiting setpoints. The core described herein is demonstrated to meet all design bases by considering the values of plant parameters and the uncertainties in these parameters in a more realistic fashion through the use of the improved thermal design procedure<sup>(3)</sup>. Additionally, the plant described herein contains the Integrated Protection System, which includes instruments not found in the Byron-Braidwood plants. This added measurement capability makes possible the use of current values of plant parameters to determine protection setpoints, rather than relying on analytically calculated or postulated worst case values.

#### 4.4.1.4 Hydrodynamic Stability Design Basis

##### Basis

Modes of operation associated with Condition I and II events shall not lead to hydrodynamic instability.

#### 4.4.1.5 Other Considerations

The above design bases together with the fuel cladding and fuel assembly design bases given in Subsection 4.2.1 are sufficiently comprehensive so additional limits are not required.

Fuel rod diametral gap characteristics, moderator-coolant flow velocity and distribution, and moderator void are not inherently limiting. Each of these parameters is incorporated into the thermal and hydraulic models used to ensure the above mentioned design criteria are met. For instance, the fuel rod diametral gap characteristics change with time (see Subsection 4.2.3.3) and the fuel rod integrity is evaluated on that basis. The effect of the moderator flow velocity and distribution (see Subsection 4.4.2.2) and moderator void distribution (see Subsection 4.4.2.4) are included in the core thermal (THINC) evaluation and thus affect the design bases.

Meeting the fuel cladding integrity criteria covers possible effects of cladding temperature limitations. As noted in Subsection 4.2.3.3, the fuel rod conditions change with time. A single cladding temperature limit for Condition I or Condition II events is not appropriate since of necessity it would be overly conservative. A cladding temperature limit is applied to the loss-of-coolant accident (Subsection 15.6.5), control rod ejection accident, and locked rotor accident.

#### 4.4.2 DESCRIPTION

##### 4.4.2.1 Summary Comparison

Table 4.4-1 provides a comparison of the design parameters for the core described herein with those given in the McGuire FSAR (Dockets #50-369, 370)

for the standard 12 foot 17x17 design. Thermal-hydraulic design parameters for one of four coolant loops out of service are provided in Table 4.4-2.

Examination of the tables demonstrates that in progressing from the standard 12 foot core to the current model a relatively small perturbation has been made in the core hardware while significant advances have been made in the methods of analysis of core performance.

The fundamental difference in core geometry between this application and previous 17x17 submittals is a decrease of 14 mils in the fuel rod outside diameter from .374" to .360". In addition, the grid design has changed from the standard Inconel R-grid design to a Zircaloy design. More detail on the new grid design is given in Section 4.2.

Both the average and peak linear heat generation rates (kW/ft) remain the same for the cores described herein as that of a standard design with a power rating of 3411 MWth (see Table 4.4-1). However, the reduction in fuel rod diameter results in a slightly higher average and peak heat flux. The overall fuel assembly pressure drop for the optimized fuel assembly design is essentially the same as that for the standard Inconel assembly design<sup>(5)</sup>.

The inability of Table 4.4-1 to permit a direct comparison of all plant operating parameters results from the significant advances and improvements made in the method of analysis of core performance for this application. The McGuire core has been analyzed on a worst case basis for all parameters involved in determining limiting setpoints. The core described herein is demonstrated to meet all design bases by considering the values of plant parameters and the uncertainties in these parameters in a more realistic fashion through the use of the improved thermal design procedure<sup>(3)</sup>.

#### 4.4.2.2 Critical Heat Flux Ratio or Departure from Nucleate Boiling Ratio and Mixing Technology

The minimum DNBR's for the rated power, design overpower, and anticipated transient conditions are given in Table 4.4-1. The minimum DNBR in the limiting flow channel will be downstream of the peak heat flux location (hot spot) due to the increased downstream enthalpy rise.

DNBR's are calculated by using the correlation and definitions described in the following Subsections 4.4.2.2.1 and 4.4.2.2.2. The THINC-IV computer code (discussed in Subsection 4.4.4.5.1) is used to determine the flow distribution in the core and the local conditions in the hot channel for use in the DNB correlation. The use of hot channel factors is discussed in Subsection 4.4.4.3.1 (nuclear hot channel factors) and in Subsection 4.4.2.2.4 (engineering hot channel factors).

##### 4.4.2.2.1 Departure from Nucleate Boiling Technology

The W-3 correlation, and several modifications of it, have been used in Westinghouse CHF calculations. The W-3 was originally developed from single tube data,<sup>(6)</sup> but was subsequently modified to apply to the 0.422 inch O.D. rod "R"-grid,<sup>(7)</sup> and "L" grid,<sup>(8)</sup> as well as the 0.374 inch O.D.,<sup>(9,10)</sup> rod bundle data. These modifications to the W-3 correlation have been demonstrated to be adequate for reactor rod bundle design.

The WRB-1<sup>(1)</sup> correlation was developed based exclusively on the large bank of mixing vane grid rod bundle CHF data (over 1100 points) that Westinghouse has collected. The WRB-1 correlation, based on local fluid conditions, represents the rod bundle data with better accuracy over a wide range of variables than previous correlation used in design. This correlation accounts directly for both typical and thimble cold wall cell effects, uniform and nonuniform heat flux profiles, and variations in rod heated length and in grid spacing.

The applicable range of variables is:

Pressure :  $1440 \leq P \leq 2490$  psia  
Local Mass Velocity :  $0.9 \leq G_{loc}/10^6 \leq 3.7$  lb/ft<sup>2</sup>-hr

|                                      |   |                                  |
|--------------------------------------|---|----------------------------------|
| Local Quality                        | : | $-0.2 \leq X_{loc} \leq 0.3$     |
| Heated Length, Inlet to CHF Location | : | $L_h \leq 14$ feet               |
| Grid Spacing                         | : | $13 \leq g_{sp} \leq 32$ inches  |
| Equivalent Hydraulic Diameter        | : | $0.37 \leq d_e \leq 0.60$ inches |
| Equivalent Heated Hydraulic Diameter | : | $0.46 \leq d_h \leq 0.58$ inches |

Figure 4.4-2 shows measured critical heat flux plotted against predicted critical heat flux using the WRB-1 correlation.

Critical heat flux tests which model the 17x17 optimized fuel assembly have been performed with the results described in detail in Reference 15. It was concluded that the CHF characteristics of the 17x17 optimized fuel assembly design are not significantly different from those of the current 17x17 standard design, and can be adequately described by the "R" grid form of the WRB-1 CHF correlation. Furthermore, the new data can be incorporated into the "R" grid data base without changing the DNBR design criterion of 1.17.

#### 4.4.2.2.2 Definition of Departure from Nucleate Boiling Ratio

The DNBR as applied to this design for both typical and thimble cold wall cells is:

$$DNBR = \frac{q_{DNB, N}''}{q_{loc}''} \quad (4.4-1)$$

Where:

$$q_{DNB, N}'' = \frac{q_{DNB, EU}''}{F} \quad (4.4-2)$$

and  $q_{DNB, EU}''$  is the uniform critical heat flux as predicted by the WRB-1 Correlation<sup>(1)</sup>.

F is the flux shape factor to account for nonuniform axial heat flux distributions<sup>(11)</sup> with the "C" term modified as in Reference [6].

#### 4.4.2.2.3 Mixing Technology

The rate of heat exchange by mixing between flow channels is proportional to the difference in the local mean fluid enthalpy of the respective channels, the local fluid density and flow velocity. The proportionality is expressed by the dimensionless thermal diffusion coefficient (TDC) which is defined as:

$$TDC = \frac{w'}{\rho Va} \quad (4.4-3)$$

where:

- w' = flow exchange rate per unit length, lb<sub>m</sub>/ft-sec
- ρ = fluid density, lb<sub>m</sub>/ft<sup>3</sup>
- V = fluid velocity, ft/sec
- a = lateral flow area between channels per unit length, ft<sup>2</sup>/ft

The application of the TDC in the THINC analysis for determining the overall mixing effect or heat exchange rate is presented in Reference 12.

Various mixing tests have been performed at Columbia University<sup>(13)</sup>. These series of tests, using the "R" mixing vane grid design on 13, 26, and 32 inch grid spacing, were conducted in pressurized water loops at Reynolds numbers similar to that of a PWR core under the following single and two phase (subcooled boiling) flow conditions:

|                     |  |
|---------------------|--|
| Pressure            | 1500 to 2400 psia  |
| Inlet temperature   | 332 to 642 <sup>0</sup> F  |
| Mass velocity       | 1.0 to 3.5 x 10 <sup>6</sup> lb <sub>m</sub> /hr-ft <sup>3</sup> |
| Reynolds number     | 1.34 to 7.45 x 10 <sup>5</sup>                                   |
| Bulk outlet quality | -52.1 to 13.5%   |



TDC is determined by comparing the THINC Code predictions with the measured subchannel exit temperatures. Data for 26-inch axial grid spacing are presented in Figure 4.4-3 where the thermal diffusion coefficient is plotted versus the Reynolds number. TDC is found to be independent of Reynolds number, mass velocity, pressure and quality over the ranges tested. The two-phase data (local, subcooled boiling) fell within the scatter of the single phase data. The effect of two-phase flow on the value of TDC has been demonstrated by Cadek<sup>(13)</sup>, Rowe and Angle<sup>(14,15)</sup>, and Gonzalez - Santalo and Griffith<sup>(16)</sup>. In the subcooled boiling region the values of TDC were indistinguishable from the single phase values. In the quality region, Rowe and Angle show that in the case with rod spacing similar to that in PWR reactor core geometry, the value of TDC increased with quality to a point and then decreased, but never below the single phase value. Gonzalez - Santalo and Griffith showed that the mixing coefficient increased as the void fraction increased.

The data from these tests on the "R" grid showed that a design TDC value of 0.038 (for 26-inch grid spacing) can be used in determining the effect of coolant mixing in the THINC analysis.

A mixing test program similar to the one described above was conducted at Columbia University for the current 17x17 geometry and mixing vane grids on 26-inch spacing<sup>(17)</sup>. The mean value of TDC obtained from these tests was 0.059 and all data was well above the current design value of 0.038.

The Zircaloy grid employed in the 17x17 optimized fuel assembly design was designed to have the same mixing characteristics as the current 17x17 R-grid design. This is verified by the fact that the DNB performance of the new grid design is similar to that of the current R-grid design, as discussed in Section 4.4.2.2. Thus, the current conservative design value of TDC is applicable to the 17x17 optimized fuel assembly design.

In addition, since the actual reactor grid spacing is approximately 20 inches, additional margin is available for this design, since the value of TDC increases as grid spacing decreases<sup>(13)</sup>.

#### 4.4.2.2.4 Hot Channel Factors

The total hot channel factors for heat flux and enthalpy rise are defined as the maximum-to-core average ratios of these quantities. The heat flux hot channel factor considers the local maximum linear heat generation rate at a point (the hot spot), and the enthalpy rise hot channel factor involves the maximum integrated value along a channel (the hot channel).

Each of the total hot channel factors considers a nuclear hot channel factor (see Subsection 4.4.4.3) describing the neutron power distribution and an engineering hot channel factor, which allows for variations in flow conditions and fabrication tolerances. The engineering hot channel factors are made up of subfactors which account for the influence of the variations of fuel pellet diameter, density, enrichment and eccentricity; inlet flow distribution; flow redistribution; and flow mixing.

kW/ft Engineering Hot Channel Factor,  $F_Q^E$

The kW/ft engineering hot channel factor is used to evaluate the maximum linear heat generation rate in the core. This subfactor is determined by statistically combining the fabrication variations for fuel pellet diameter, density, and enrichment, and has a value of 1.03 at the 95 percent probability level with 95 percent confidence. As shown in Reference (18), no DNB penalty need be taken for the short relatively low intensity heat flux spikes caused by variations in the above parameters, as well as fuel pellet eccentricity and fuel rod diameter variation.

Enthalpy Rise Engineering Hot Channel Factor,  $F_{\Delta H}^E$

The effect of variations in flow conditions and fabrication tolerances on the hot channel enthalpy rise is directly considered in the THINC

core thermal subchannel analysis (see Subsection 4.4.4.5.1) under any reactor operating condition. The items considered contributing to the enthalpy rise engineering hot channel factor are discussed below.

1. Pellet diameter, density and enrichment and fuel rod diameter:

Variations in pellet diameter, density and enrichment and fuel rod diameter, are considered statistically in establishing the limit DNBRs (see Section 4.4.1.1) for the improved thermal design procedure<sup>(3)</sup> employed in this application. Uncertainties in these variables are determined from sampling of manufacturing data.

2. Inlet Flow Maldistribution:

The consideration of inlet flow maldistribution in core thermal performances is discussed in Subsection 4.4.4.2.2. A design basis of 5% reduction in coolant flow to the hot assembly is used in the THINC-IV analysis.

3. Flow Redistribution:

The flow redistribution accounts for the reduction in flow in the hot channel resulting from the high flow resistance in the channel due to the local or bulk boiling. The effect of the nonuniform power distribution is inherently considered in the THINC analysis for every operating condition which is evaluated.

4. Flow Mixing:

The subchannel mixing model incorporated in the THINC Code and used in reactor design is based on experimental data<sup>(19)</sup> discussed in Subsection 4.4.4.5. The mixing vanes incorporated in the spacer grid design induce additional flow mixing among the various flow channels in a fuel assembly as well as between adjacent assemblies. This mixing reduces the enthalpy rise in the hot channel resulting from local power peaking or unfavorable mechanical tolerances.

#### 4.4.2.3 Linear Heat Generation Rate

The core average and maximum LHGRs are given in Table 4.4-1. The method of determining the maximum LHGR is given in Subsection 4.3.2.2.

#### 4.4.2.4 Void Fraction Distribution

The calculated core average and the hot subchannel maximum and average void fractions are presented in Table 4.4-3 for operation at full power with design hot channel factors. The void fraction distribution in the core at various radial and axial locations is presented in Reference [20]. The void models used in the THINC-IV computer code are described in Subsection 4.4.2.7.3. Normalized core flow and enthalpy rise distributions are shown in Figures 4.4-4 through 4.4-6.

#### 4.4.2.5 Core Coolant Flow Distribution

Assembly average coolant mass velocity and enthalpy at various radial and axial core locations are given below. Coolant enthalpy rise and flow distributions are shown for the 4-foot elevation (1/3 of core height) in Figure 4.4-4, and 8-foot elevation (2/3 of core height) in Figure 4.4-5 and at the core exit in Figure 4.4-6. These distributions are for the full power conditions as given in Table 4.4-1 and for the radial power density distribution shown in Figure 4.3-7. The THINC code analysis for this case utilized a uniform core inlet enthalpy and inlet flow distribution. No orificing is employed in the reactor design.

#### 4.4.2.6 Core Pressure Drops and Hydraulic Loads

##### 4.4.2.6.1 Core Pressure Drops

The analytical model and experimental data used to calculate the pressure drops shown in Table 4.4-1 are described in Section 4.4.2.7. The core pressure drop includes the fuel assembly, lower core plate, and upper core plate pressure drops. The full power operation pressure drop values shown in Table 4.4-1 are the unrecoverable pressure drops across

the vessel, including the inlet and outlet nozzles, and across the core. These pressure drops are based on the best estimate flow for actual plant operating conditions as described in Subsection 5.1.1. Subsection 5.1.1 also defines and describes the thermal design flow (minimum flow) which is the basis for reactor core thermal performance and the mechanical design flow (maximum flow) which is used in the mechanical design of the reactor vessel internals and fuel assemblies. Since the best estimate flow is that flow which is most likely to exist in an operating plant, the calculated pressure drops in Table 4.4-1 are based on this best estimate flow.

Uncertainties associated with the core pressure drop values are discussed in Subsection 4.4.2.9.2.

The pressure drops quoted in Table 4.4-1 are based on eight grids and the data obtained from the verification testing of the 17x17 optimized fuel assembly<sup>(5)</sup>.

#### 4.4.2.6.2 Hydraulic Loads

The fuel assembly hold down springs, Figure 4.2-2, are designed to keep the fuel assemblies in contact with the lower core plate under all Condition I and II events with the exception of the turbine overspeed transient associated with a loss of external load. The hold down springs are designed to tolerate the possibility of an over deflection associated with fuel assembly liftoff for this case and provide contact between the fuel assembly and the lower core plate following this transient. More adverse flow conditions occur during a loss-of-coolant accident. These conditions are presented in Subsection 15.6.5.

Hydraulic loads at normal operating conditions are calculated considering the mechanical design flow which is described in Section 5.1 and accounting for the minimum core bypass flow based on manufacturing tolerances. Core hydraulic loads at cold plant startup conditions are based on the cold mechanical design flow, but are adjusted to account for the coolant density difference. Conservative core hydraulic loads

for a pump overspeed transient, which could possibly create flow rates 20% greater than the mechanical design flow, are evaluated to be approximately twice the fuel assembly weight.

Core hydraulic loads were measured during the prototype assembly tests of the optimized fuel assembly. Reference [5] contains a detailed discussion of the results.

#### 4.4.2.7 Correlation and Physical Data

##### 4.4.2.7.1 Surface Heat Transfer Coefficients

Forced convection heat transfer coefficients are obtained from the familiar Dittus-Boelter correlation<sup>(21)</sup>, with the properties evaluated at bulk fluid conditions:

$$\frac{hD_e}{K} = 0.023 \left( \frac{D_e G}{\mu} \right)^{0.8} \left( \frac{C_p \mu}{K} \right)^{0.4} \quad (4.4-4)$$

where:

- h = heat transfer coefficient, Btu/hr-ft<sup>2</sup>-°F
- D<sub>e</sub> = equivalent diameter, ft
- K = thermal conductivity, Btu/hr-ft<sup>0</sup>F
- G = mass velocity, lb<sub>m</sub>/hr-ft<sup>2</sup>
- μ = dynamic viscosity, lb<sub>m</sub>/ft-hr
- C<sub>p</sub> = heat capacity, Btu/lb<sub>m</sub>-°F

This correlation has been shown to be conservative<sup>(22)</sup> for rod bundle geometries with pitch to diameter ratios in the range used by PWR's.

The onset of nucleate boiling occurs when the cladding wall temperature reaches the amount of superheat predicted by Thom's<sup>(23)</sup> correlation. After this occurrence the outer cladding wall temperature is determined by:

$$\Delta T_{\text{sat}} = \left[ 0.072 \exp(-P/1260) \right] (q'')^{0.5} \quad (4.4-5)$$

where:

$$\begin{aligned} \Delta T_{\text{sat}} &= \text{wall superheat, } T_W - T_{\text{sat}}, \text{ } ^\circ\text{F} \\ q'' &= \text{wall heat flux, Btu/hr-ft}^2 \\ P &= \text{pressure, psia} \\ T_W &= \text{outer cladding wall temperature, } ^\circ\text{F} \\ T_{\text{sat}} &= \text{saturation temperature of coolant at } P, \text{ } ^\circ\text{F} \end{aligned}$$

#### 4.4.2.7.2 Total Core and Vessel Pressure Drop

Unrecoverable pressure losses occur as a result of viscous drag (friction) and/or geometry changes (form) in the fluid flow path. The flow field is assumed to be incompressible, turbulent, single-phase water. These assumptions apply to the core and vessel pressure drop calculations for the purpose of establishing the primary loop flow rate. Two-phase considerations are neglected in the vessel pressure drop evaluation because the core average void is negligible (see Table 4.4-3). Two-phase flow considerations in the core thermal subchannel analyses are considered and the models are discussed in Subsection 4.4.4.2.3.

Core and vessel pressure losses are calculated by equations of the form:

$$\Delta P_L = \left( K + F \frac{L}{D_e} \right) \frac{\rho V^2}{2 g_c (144)} \quad (4.4-6)$$

where:

$$\begin{aligned} \Delta P_L &= \text{unrecoverable pressure drop, lb}_f\text{/in}^2 \\ \rho &= \text{fluid density, lb}_m\text{/ft}^3 \\ L &= \text{length, ft} \\ D_e &= \text{equivalent diameter, ft} \end{aligned}$$

- V = fluid velocity, ft/sec  
 $g_c = 32.174 \frac{\text{lb}_m\text{-ft}}{\text{lb}_f\text{-sec}^2}$   
 K = form loss coefficient, dimensionless  
 F = friction loss coefficient, dimensionless

Fluid density is assumed to be constant at the appropriate value for each component in the core and vessel. Because of the complex core and vessel flow geometry, precise analytical values for the form and friction loss coefficients are not available. Therefore, experimental values for these coefficients are obtained from geometrically similar models.

Values are quoted in Table 4.4-1 for unrecoverable pressure loss across the reactor vessel, including the inlet and outlet nozzles, and across the core. The results of full scale tests of core components and fuel assemblies were utilized in developing the core pressure loss characteristic. The pressure drop for the vessel was obtained by combining the core loss with correlation of 1/7th scale model hydraulic test data on a number of vessels<sup>(24, 25)</sup> and form loss relationships<sup>(26)</sup>. Moody<sup>(27)</sup> curves were used to obtain the single phase friction factors.

Core pressure drops were confirmed by the verification testing described in Reference [5]. These hydraulic verification tests include hydraulic head losses and effects of velocity changes as well as unrecoverable pressure losses. The effects of velocity changes are small since the static pressure taps are located at elevations of approximately equal flow areas (and therefore approximately equal velocities). When wall static pressure taps are used near ambient fluid conditions, it can be shown analytically that the elevation head losses do not contribute to the measured core pressure drops. Therefore, data from the hydraulic verifications tests can be directly applied to confirm the pressure drop values quoted in Table 4.4-1 which are based on unrecoverable pressure losses only.



Tests of the primary coolant loop flow rates will be made (see Subsection 4.4.5.1) prior to initial criticality to verify that the flow rates used in the design, which were determined in part from the pressure losses calculated by the method described here, are conservative.

#### 4.4.2.7.3 Void Fraction Correlation

There are three separate void regions considered in flow boiling in a PWR as illustrated in Figure 4.4-7. They are the wall void region (no bubble detachment), the subcooled boiling region (bubble detachment), and the bulk boiling region.

In the wall void region, the point where local boiling begins is determined when the cladding temperature reaches the amount of superheat predicted by Thom's<sup>(23)</sup> correlation (discussed in Subsection 4.4.2.7.1). The void fraction in this region is calculated using Maurer's<sup>(28)</sup> relationship. The bubble detachment point, where the superheated bubbles break away from the wall, is determined by using Griffith's<sup>(29)</sup> relationship.

The void fraction in the subcooled boiling region (that is, after the detachment point) is calculated from the Bowring<sup>(30)</sup> correlation. This correlation predicts the void fraction from the detachment point to the bulk boiling region.

The void fraction in the bulk boiling region is predicted by using homogeneous flow theory and assuming no slip. The void fraction in this region is therefore a function only of the thermodynamic quality.

#### 4.4.2.8 Thermal Effects of Operational Transients

DNB core safety limits are generated as a function of coolant temperature, pressure, core power, and the axial and radial power distributions. Operation within these DNB safety limits insures that the DNB design basis is met for both steady-state operation and for anticipated operational transients that are slow with respect to fluid transport.

delays in the primary system. In addition, for fast transients, e.g., uncontrolled rod bank withdrawal at power incident, specific protection functions are provided as described in Chapter 7 and the use of these protection functions are described in Chapter 15. The thermal response of the fuel is discussed in Section 4.2.3.3.

#### 4.4.2.9 Uncertainties in Estimates

##### 4.4.2.9.1 Uncertainties in Fuel and Cladding Temperatures

As discussed in subsection 4.4.2.11, the fuel temperature is a function of crud, oxide, cladding, gap, and pellet conductances. Uncertainties in the fuel temperature calculation are essentially of two types: fabrication uncertainties such as variations in the pellet and cladding dimensions and the pellet density; and model uncertainties such as variations in the pellet conductivity and the gap conductance. These uncertainties have been quantified by comparison of the thermal model to the in-pile thermocouple measurements<sup>(31 through 37)</sup> by out-of-pile measurements of the fuel and cladding properties<sup>(38 through 49)</sup>, and by measurements of the fuel and cladding dimensions during fabrication. The resulting uncertainties are then used in all evaluations involving the fuel temperature. The effect of densification on fuel temperature uncertainties is presented in Reference [50].

In addition to the temperature uncertainty described above, the measurement uncertainty in determining the local power, and the effect of density and enrichment variations on the local power are considered in establishing the heat flux hot channel factor. These uncertainties are described in Subsection 4.3.2.2.1.

Reactor trip setpoints, as specified in the Technical Specification, include allowance for instrument and measurement uncertainties such as calorimetric error, instrument drift and channel reproducibility, temperature measurement uncertainties, noise, and heat capacity variations.

Uncertainty in determining the cladding temperatures results from uncertainties in the crud and oxide thicknesses. Because of the excellent heat transfer between the surface of the rod and the coolant, the film temperature drop does not appreciably contribute to the uncertainty.

#### 4.4.2.9.2 Uncertainties in Pressure Drops

Core and vessel pressure drops based on the best estimate flow, as described in Section 5.1, are quoted in Table 4.4-1. The uncertainties quoted are based on the uncertainties in both the test results and the analytical extension of these values to the reactor application.

A major use of the core and vessel pressure drops is to determine the primary system coolant flow rates as discussed in Section 5.1. In addition, as discussed in Subsection 4.4.5.1, tests on the primary system prior to initial criticality will be made to verify that a conservative primary system coolant flow rate has been used in the design and analyses of the plant.

#### 4.4.2.9.3 Uncertainties Due to Inlet Flow Maldistribution

The effects of uncertainties in the inlet flow maldistribution criteria used in the core thermal analyses are discussed in Subsection 4.4.4.2.2.

#### 4.4.2.9.4 Uncertainty in DNB Correlation

The uncertainty in the DNB correlation (Subsection 4.4.2.2) can be written as a statement on the probability of not being in DNB based on the statistics of the DNB data. This is discussed in Subsection 4.4.2.2 and Reference [5].

#### 4.4.2.9.5 Uncertainties in DNBR Calculations

The uncertainties in the DNBRs calculated by THINC analysis (see Section 4.4.4.5.1) due to nuclear peaking factors are accounted for by applying

conservatively high values of the nuclear peaking factors and including measurement error allowances in the statistical evaluation of the limit DNBR (See Section 4.4.1.1) using the improved thermal design procedure<sup>(3)</sup>. In addition, engineering hot channel factors are employed as discussed in Section 4.4.2.4.

The results of a sensitivity study<sup>(20)</sup> with THINC-IV show that the minimum DNBR in the hot channel is relatively insensitive to variations in the corewide radial power distribution (for the same value of  $F_{\Delta H}^N$ ).

The ability of the THINC-IV computer code to accurately predict flow and enthalpy distributions in rod bundles is discussed in Subsection 4.4.4.5.1 and in Reference [51]. Studies have been performed<sup>(20)</sup> to determine the sensitivity of the minimum DNBR in the hot channel to the void fraction correlation (see also Subsection 4.4.2.7.3); the inlet velocity and exit pressure distributions assumed as boundary conditions for the analysis; and the grid pressure loss coefficients. The results of these studies show that the minimum DNBR in the hot channel is relatively insensitive to variations in these parameters. The range of variations considered in these studies covered the range of possible variations in these parameters.

As required in Reference [2], an uncertainty of 4% in DNBR is included in the design procedure to account for any THINC-IV Code uncertainty.

#### 4.4.2.9.6 Uncertainties in Flow Rates

The uncertainties associated with loop flow rates are discussed in Section 5.1. A thermal design flow is defined for use in core thermal performance evaluations which accounts for both prediction and measurement uncertainties. In the present case, the thermal design flow is 2.5% less than the Best Estimate Loop Flow.

The 2.5% uncertainty results from the use of an N-16 Transit Time Flowmeter (TTFM) which has a small measurement uncertainty associated with it. The N-16 system and measurement uncertainties are described in detail in Reference [81].

In addition, a maximum of 5.8% of the Thermal Design Flow is assumed to be ineffective for core heat removal capability because it bypasses through the various available vessel flow paths described in Section 4.4.4.2.1.

#### 4.4.2.9.7 Uncertainties in Hydraulic Loads

As discussed in Subsection 4.4.2.6.2, hydraulic loads on the fuel assembly are evaluated for a pump overspeed transient which create flow rates 20% greater than the mechanical design flow. The mechanical design flow as stated in Section 5.1 is greater than the best estimate or most likely flow rate value for the actual plant operating condition.

#### 4.4.2.9.8 Uncertainty in Mixing Coefficient

The value of the mixing coefficient, TDC, used in THINC analyses for this application is 0.038. The mean value of TDC obtained in the "R" grid mixing tests described in Subsection 4.4.2.2.3 was 0.042 (for 26-inch grid spacing). The value 0.038 is one standard deviation below the mean value; and approximately 90% of the data gives values of TDC greater than 0.038<sup>(13)</sup>.

The results of the mixing tests done on the current 17x17 geometry, as discussed in Subsection 4.4.2.2.3, had a mean value of TDC of 0.059 and standard deviation of  $\sigma = 0.007$ . Hence, the current design value of TDC is almost 3 standard deviations below the mean for 26-inch grid spacing.

As discussed in Subsection 4.4.2.2.3, the zircaloy grid employed in the 17x17 optimized fuel design has the same mixing characteristics as the current 17x17 R-grid design. Hence, the same value of TDC is used in this analysis (.038) which includes all the conservatism discussed above.

In addition, since the actual reactor grid spacing is approximately 20 inches, additional margin is available for this design, since the value of TDC increases as grid spacing decreases<sup>(13)</sup>.

conservatively high values of the nuclear peaking factors and including measurement error allowances in the statistical evaluation of the limit DNBR (See Section 4.4.1.1) using the improved thermal design procedure<sup>(3)</sup>. In addition, engineering hot channel factors are employed as discussed in Section 4.4.2.4.

The results of a sensitivity study<sup>(20)</sup> with THINC-IV show that the minimum DNBR in the hot channel is relatively insensitive to variations in the corewide radial power distribution (for the same value of  $\frac{F_N}{\Delta H}$ ).

The ability of the THINC-IV computer code to accurately predict flow and enthalpy distributions in rod bundles is discussed in Subsection 4.4.4.5.1 and in Reference [51]. Studies have been performed<sup>(20)</sup> to determine the sensitivity of the minimum DNBR in the hot channel to the void fraction correlation (see also Subsection 4.4.2.7.3); the inlet velocity and exit pressure distributions assumed as boundary conditions for the analysis; and the grid pressure loss coefficients. The results of these studies show that the minimum DNBR in the hot channel is relatively insensitive to variations in these parameters. The range of variations considered in these studies covered the range of possible variations in these parameters.

As required in Reference [2], an uncertainty of 4% in DNBR is included in the design procedure to account for any THINC-IV Code uncertainty.

#### 4.4.2.9.6 Uncertainties in Flow Rates

The uncertainties associated with loop flow rates are discussed in Section 5.1. A thermal design flow is defined for use in core thermal performance evaluations which accounts for both prediction and measurement uncertainties. In the present case, the thermal design flow is 4% less than the Best Estimate Loop Flow.

In addition, a maximum of 7.5% of the Thermal Design Flow is assumed to be ineffective for core heat removal capability because it bypasses through the various available vessel flow paths described in Section 4.4.4.2.1.

#### 4.4.2.9.7 Uncertainties in Hydraulic Loads

As discussed in Subsection 4.4.2.6.2, hydraulic loads on the fuel assembly are evaluated for a pump overspeed transient which create flow rates 20% greater than the mechanical design flow. The mechanical design flow as stated in Section 5.1 is greater than the best estimate or most likely flow rate value for the actual plant operating condition.

#### 4.4.2.9.8 Uncertainty in Mixing Coefficient

The value of the mixing coefficient, TDC, used in THINC analyses for this application is 0.038. The mean value of TDC obtained in the "R" grid mixing tests described in Subsection 4.4.2.2.3 was 0.042 (for 26-inch grid spacing). The value 0.038 is one standard deviation below the mean value; and approximately 90% of the data gives values of TDC greater than 0.038<sup>(13)</sup>.

The results of the mixing tests done on the current 17x17 geometry, as discussed in Subsection 4.4.2.2.3, had a mean value of TDC of 0.059 and standard deviation of  $\sigma = 0.007$ . Hence, the current design value of TDC is almost 3 standard deviations below the mean for 26-inch grid spacing.

As discussed in Subsection 4.4.2.2.3, the zircaloy grid employed in the 17x17 optimized fuel design has the same mixing characteristics as the current 17x17 R-grid design. Hence, the same value of TDC is used in this analysis (.038) which includes all the conservatism discussed above.

In addition, since the actual reactor grid spacing is approximately 20 inches, additional margin is available for this design, since the value of TDC increases as grid spacing decreases<sup>(13)</sup>.

#### 4.4.2.10 Flux Tilt Consideration

Significant quadrant power tilts are not anticipated during normal operation since this phenomenon is caused by some perturbation. For example, a dropped or misaligned RCCA could cause changes in the hot channel factors; however, these events are analyzed separately in Chapter 15. Other possible causes for quadrant power tilts include X-Y xenon transients, inlet temperature mismatches, enrichment variations within tolerances and so forth.

In addition to unanticipated quadrant power tilts as described above, other readily explainable asymmetries may be observed during calibration of the excore detector quadrant power tilt alarm. During operation, incore maps are taken at least one per month and, periodically, additional maps are obtained for calibration purposes. Each of these maps is reviewed for deviations from the expected power distributions. Asymmetry in the core, from quadrant to quadrant, is frequently a consequence of the design when assembly and/or component shuffling and rotation requirements do not allow exact symmetry preservation. In each case, the acceptability of an observed asymmetry, planned or otherwise depends solely on meeting the required accident analyses assumptions.

In practice, once acceptability has been established by review of the incore maps, the quadrant power tilt alarms and related instrumentation are adjusted to indicate zero Quadrant Power Tilt Ratio as the final step in the calibration process. This action ensures that the instrumentation is correctly calibrated to alarm in the event an unexplained or unanticipated change occurs in the quadrant to quadrant relationships between calibration intervals. Proper functioning of the quadrant power tilt alarm is significant because no allowances are made in the design for increased hot channel factors due to unexpected developing flux tilts since all likely causes are prevented by design or procedures or specifically analyzed. Finally in the event that unexplained flux tilts do occur, the technical specifications (Section 3/4.2.4) provide appropriate corrective actions to ensure continued safe operation of the reactor.



#### 4.4.2.11 Fuel and Cladding Temperatures

Consistent with the thermal-hydraulic design bases described in Subsection 4.4.1, the following discussion pertains mainly to fuel pellet temperature evaluation. A discussion of fuel clad integrity is presented in Subsection 4.2.3.1.

The thermal-hydraulic design assures that the maximum fuel temperature is below the melting point of  $UO_2$  (melting point of  $5080^{\circ}F^{(4)}$  unirradiated and decreasing by  $58^{\circ}F$  per 10,000 MWD/MTU). To preclude center melting and as a basis for overpower protection system setpoints, a calculated centerline fuel temperature of  $4700^{\circ}F$  has been selected as the overpower limit. This provides sufficient margin for uncertainties in the thermal evaluations as described in Subsection 4.4.2.9.1. The temperature distribution within the fuel pellet is predominantly a function of the local power density and the  $UO_2$  thermal conductivity. However, the computation of radial fuel temperature distributions combines crud, oxide, cladding gap and pellet conductances. The factors which influence these conductances, such as gap size (or contact pressure), internal gas pressure, gas composition, pellet density, and radial power distribution within the pellet, etc., have been combined into a semi-empirical thermal model (see Subsection 4.2.3.3) with the model modifications for time dependent fuel densification given in Reference [50]. This thermal model enables the determination of these factors and their net effects on temperature profiles. The temperature predictions have been compared to inpile fuel temperature measurements<sup>(31 through 37)</sup>, melt radius data<sup>(52, 53)</sup>, with good results.

As described in Reference [50], fuel rod thermal evaluations (fuel centerline, average and surface temperatures) are determined throughout the fuel rod lifetime with consideration of time dependent densification. To determine the maximum fuel temperatures, various burnup rods, including the highest burnup rod, are analyzed over the rod linear power range of interest.

The principal factors which are employed in the determination of the fuel temperature are discussed below.

#### 4.4.2.11.1 UO<sub>2</sub> Thermal Conductivity

The thermal conductivity of uranium dioxide was evaluated from data reported by Howard, et al.<sup>(38)</sup>; Lucks, et al.<sup>(39)</sup>; Canial, et al.<sup>(40)</sup>; Feith<sup>(41)</sup>; Vogt, et al.<sup>(42)</sup>; Nishijima, et al.<sup>(43)</sup>; Wheeler, et al.<sup>(44)</sup>; Godfrey, et al.<sup>(45)</sup>; Stora, et al.<sup>(46)</sup>; Bush<sup>(47)</sup>; Asamoto, et al.<sup>(48)</sup>; Kruger<sup>(49)</sup>; and Gyllander<sup>(54)</sup>.

At the higher temperatures, thermal conductivity is best obtained by utilizing the integral conductivity to melt which can be determined with more certainty.

From an examination of the data, it has been concluded that the best estimate for the value of  $\int_0^{2800^{\circ}\text{C}} K dt$  is 93 watts/cm. This conclusion is based on the integral values reported by Gyllander<sup>(54)</sup>, Lyons, et al.<sup>(55)</sup>, Coplin, et al.<sup>(56)</sup>, Duncan<sup>(52)</sup>, Bain<sup>(57)</sup>, and Stora<sup>(58)</sup>.

The design curve for the thermal conductivity is shown in Figure 4.4-8. The section of the curve at temperatures between 0°C and 1300°C is in excellent agreement with the recommendation of the IAEA panel<sup>(59)</sup>. The section of the curve above 1300°C is derived for an integral value of 93 watts/cm<sup>(52, 54, 58)</sup>.

Thermal conductivity for UO<sub>2</sub> at 95% theoretical density can be represented best by the following equation:

$$K = \frac{1}{11.8 + 0.0238T} + 8.775 \times 10^{-13} T^3 \quad (4.4-7)$$

where:

K = watts/cm-°C

T = °C.

#### 4.4.2.11.2 Radial Power Distribution in UO<sub>2</sub> Fuel Rods

An accurate description of the radial power distribution as a function of burnup is needed for determining the power level for incipient fuel melting and other important performance parameters such as pellet thermal expansion, fuel swelling and fission gas release rates.

This information on radial power distributions in UO<sub>2</sub> fuel rods is determined with the neutron transport theory code, LASER. The LASER Code has been validated by comparing the code predictions on radial burnup and isotopic distributions with measured radial microdrill data<sup>(60, 61)</sup>. A "radial power depression factor",  $f$ , is determined using radial power distributions predicted by LASER. The factor  $f$  enters into the determination of the pellet centerline temperature,  $T_c$ , relative to the pellet surface temperature,  $T_s$ , through the expression:

$$T_s \int_{T_s}^{T_c} k(T) dT = \frac{q'f}{4\eta} \quad (4.4-8)$$

where:

$K(T)$  = the thermal conductivity for UO<sub>2</sub> with a uniform density distribution

$q'$  = the linear power generation rate.

#### 4.4.2.11.3 Gap Conductance

The temperature drop across the pellet-clad gap is a function of the gap size and the thermal conductivity of the gap in the gap. The gap conductance model is selected such that when combined with the UO<sub>2</sub> thermal conductivity model, the calculated fuel centerline temperatures reflect the inpile temperature measurements.

The temperature drop across the gap is calculated by assuming an annular gap conductance model of the following form:

$$h = \frac{K_{\text{gas}}}{\frac{\delta}{2} + \delta_r} \quad (4.4-9)$$

where:

- $h$  = contact conductance, BTU/hr-ft<sup>2</sup>-°F  
 $K_{\text{gas}}$  = thermal conductivity of the gas mixture including a correction factor<sup>(62)</sup> for the accommodation coefficient for light gases (e.g. helium), BTU/hr-ft-°F.  
 $\delta$  = diametral gap size, ft.  
 $\delta_r$  = effective gap spacing due to surface roughness, ft.

or an empirical correlation derived from thermocouple and melt radius data.

The larger gap conductance value from these two equations is used to calculate the temperature drop across the gap for finite gaps.

For evaluations in which the pellet-clad gap is closed, a contact conductance is calculated. The contact conductance between UO<sub>2</sub> and Zircaloy has been measured and found to be dependent on the contact pressure, composition of the gas at the interface and the surface roughness<sup>(62, 63)</sup>. This information together with the surface roughness found in Westinghouse reactors leads to the following correlation:

$$h = 0.6P + \frac{K_{\text{gas}}}{\delta_r} \quad (4.4-10)$$

where:  $P$  = contact pressure, psi

#### 4.4.2.11.4 Surface Heat Transfer Coefficients

The fuel rod surface heat transfer coefficients during subcooled forced convection and nucleate boiling are presented in Section 4.4.2.7.1.

#### 4.4.2.11.5 Fuel Clad Temperatures

The outer surface of the fuel rod at the hot spot operates at a temperature of approximately 660<sup>0</sup>F for steady state operation at rated power throughout core life due to the onset of nucleate boiling. Initially (beginning-of-life), this temperature is that of the clad metal outer surface.

During operation over the life of the core, the buildup of oxides and crud on the fuel rod surface causes the clad surface temperature to increase. Allowance is made in the fuel center melt evaluation for this temperature rise. Since the thermal-hydraulic design basis limits DNB, adequate heat transfer is provided between the fuel clad and the reactor coolant so that the core thermal output is not limited by considerations of clad temperature.

#### 4.4.2.11.6 Treatment of Peaking Factors

The total heat flux hot channel factor,  $F_Q$ , is defined by the ratio of the maximum to core average heat flux. As presented in Table 4.3-2 and discussed in Section 4.3.2.2.6, the design value of  $F_Q$  for normal operation is 2.32. This results in a peak linear power of 12.6 kW/ft at full power conditions.

As described in Section 4.3.2.2.6 the peak linear power resulting from overpower transients/operator errors (assuming a maximum overpower of 118%) is 18.0 kW/ft. The centerline temperature kW/ft must be below the  $UO_2$  melt temperature over the lifetime of the rod, including allowances for uncertainties. The fuel temperature design basis is discussed in 4.4.1.2 and results in a maximum allowable calculated centerline temperature of 4700<sup>0</sup>F. The peak linear power for prevention of centerline melt is >18.0 kW/ft. The centerline temperature at the peak linear power resulting from overpower transients/overpower errors (assuming a maximum overpower of 118%) is below that required to produce melting.

#### 4.4.3 DESCRIPTION OF THE THERMAL AND HYDRAULIC DESIGN OF THE REACTOR COOLANT SYSTEM

##### 4.4.3.1 Plant Configuration Data

Plant configuration data for the thermal hydraulic and fluid systems external to the core are provided in the appropriate Chapters 5.0, 6.0, and 9.0 of the applicable FSAR. Implementation of the Emergency Core Cooling System (ECCS) is discussed in Chapter 15. Some specific areas of interest are the following:

1. Total coolant flow rates for the Reactor Coolant System (RCS) and each loop are provided in Table 5.1-1. Flow rates employed in the evaluation of the core are presented in Section 4.4.
2. Total RCS volume including pressurizer and surge line, RCS liquid volume including pressurizer water at steady state power conditions are given in Table 5.1-1.
3. The flow path length through each volume may be calculated from physical data provided in the above referenced tables.
4. The height of fluid in each component of the RCS may be determined from the physical data presented in Section 5.4. The components of the RCS are water filled during power operation with the pressurizer being approximately 60 percent water filled.
5. Components of the ECCS are to be located so as to meet the criteria for net positive suction head described in Section 6.3.
6. Line lengths and sizes for the Safety Injection System are determined so as to guarantee a total system resistance which will provide, as a minimum, the fluid delivery rates assumed in the safety analyses described in Chapter 15.0.

7. The parameters for components of the RCS are presented in Section 5.4, component and subsystem design.
8. The steady state pressure drops and temperature distributions through the RCS are presented in Table 5.1-1.

#### 4.4.3.2 Operating Restrictions on Pumps

The minimum Net Positive Suction Head (NPSH) and minimum seal injection flow rate must be established before operating the reactor coolant pumps. With the minimum labyrinth seal injection flow rate established, the operator will have to verify that the system pressure satisfies NPSH requirements.

#### 4.4.3.3 Power-Flow Operating Map (BWR)

Not applicable to Pressurized Water Reactors.

#### 4.4.3.4 Temperature-Power Operating Map

The relationship between Reactor Coolant System temperature and power is shown in Figure 4.4-9.

The effects of reduced core flow due to inoperative pumps is discussed in Sections 15.2.5, and 15.3.4. Natural circulation capability of the system is shown in Table 15.2-2.

#### 4.4.3.5 Load Following Characteristics

The Reactor Coolant System is designed on the basis of steady state operation at full power heat load. The reactor coolant pumps utilize constant speed drives as described in Section 5.4 and the reactor power is controlled to maintain average coolant temperature at a value which is a linear function of load, as described in Section 7.7. Operation with one pump out of service requires adjustment only in Reactor Trip System setpoints as discussed in Section 7.2 of the applicable FSAR.

#### 4.4.3.6 Thermal and Hydraulic Characteristics Summary Table

The thermal and hydraulic characteristics are given in Tables 4.3-1, 4.4-1, and 4.4-2.

#### 4.4.4 EVALUATION

##### 4.4.4.1 Critical Heat Flux

The critical heat flux correlation utilized in the core thermal analysis is explained in detail in Section 4.4.2.

##### 4.4.4.2 Core Hydraulics

###### 4.4.4.2.1 Flow Paths Considered in Core Pressure Drop and Thermal Design

The following flow paths or core bypass flow are considered:

1. Flow through the spray nozzles into the upper head for head cooling purposes.
2. Flow entering into the RCC guide thimbles to cool the control rods.
3. Leakage flow from the vessel inlet nozzle directly to the vessel outlet nozzle through the gap between the vessel and the barrel.
4. Flow introduced between the baffle and the barrel for the purpose of cooling these components and which is not considered available for core cooling.
5. Flow in the gaps between the fuel assemblies on the core periphery and the adjacent baffle wall.



The above contributions are evaluated to confirm that the design value of the core bypass flow is met. The design value of the core bypass flow is equal to 5.8% of the total vessel flow.

Of the total allowance, 2.0% is associated with the core and the remainder is associated with the internals (items 1, 3, 4 and 5 above). Calculations have been performed using drawing tolerances in the worst direction and accounting for uncertainties in pressure losses. Based on these calculations, the core bypass is no greater than the design values quoted above.

Flow model test results for the flow path through the reactor are discussed in Section 4.4.2.7.2.

#### 4.4.4.2.2 Inlet Flow Distributions

Data has been considered from several 1/7 scale hydraulic reactor model tests<sup>(24, 25, 64)</sup> in arriving at the core inlet flow maldistribution criteria to be used in the THINC analyses (see Section 4.4.4.5.1). THINC-I analyses made, using this data, have indicated that a conservative design basis is to consider 5 percent reduction in the flow to the hot assembly<sup>(65)</sup>. The same design basis of 5 percent reduction to the hot assembly inlet is used in THINC IV analyses.

The experimental error estimated in the inlet velocity distribution has been considered as outlined in Reference [20] where the sensitivity of changes in inlet velocity distributions to hot channel thermal performance is shown to be small. Studies<sup>(20)</sup> made with the improved THINC model (THINC-IV) show that it is adequate to use the 5 percent reduction in inlet flow to the hot assembly for a loop out of service based on the experimental data in References [24] and [25].

The effect of the total flow rate on the inlet velocity distribution was studied in the experiments of Reference [24]. As was expected, on the basis of the theoretical analysis, no significant variation could be found in inlet velocity distribution with reduced flow rate.

The above contributions are evaluated to confirm that the design value of the core bypass flow is met. The design value of the core bypass flow is equal to 7.5% of the total vessel flow.

Of the total allowance, 2.0% is associated with the core and the remainder is associated with the internals (items 1, 3, 4 and 5 above). Calculations have been performed using drawing tolerances in the worst direction and accounting for uncertainties in pressure losses. Based on these calculations, the core bypass is no greater than the design values quoted above.

Flow model test results for the flow path through the reactor are discussed in Section 4.4.2.7.2.

#### 4.4.4.2.2 Inlet Flow Distributions

Data has been considered from several 1/7 scale hydraulic reactor model tests<sup>(24, 25, 64)</sup> in arriving at the core inlet flow maldistribution criteria to be used in the THINC analyses (see Section 4.4.4.5.1). THINC-I analyses made, using this data, have indicated that a conservative design basis is to consider 5 percent reduction in the flow to the hot assembly<sup>(65)</sup>. The same design basis of 5 percent reduction to the hot assembly inlet is used in THINC IV analyses.

The experimental error estimated in the inlet velocity distribution has been considered as outlined in Reference [20] where the sensitivity of changes in inlet velocity distributions to hot channel thermal performance is shown to be small. Studies<sup>(20)</sup> made with the improved THINC model (THINC-IV) show that it is adequate to use the 5 percent reduction in inlet flow to the hot assembly for a loop out of service based on the experimental data in References [24] and [25].

The effect of the total flow rate on the inlet velocity distribution was studied in the experiments of Reference [24]. As was expected, on the basis of the theoretical analysis, no significant variation could be found in inlet velocity distribution with reduced flow rate.

#### 4.4.4.2.3 Empirical Friction Factor Correlations

Two empirical friction factor correlations are used in the THINC-IV computer code (described in Section 4.4.4.5.1).

The friction factor in the axial direction, parallel to the fuel rod axis, is evaluated using the Novendstern-Sandberg correlation<sup>(66)</sup>. This correlation consists of the following:

1. For isothermal conditions, this correlation uses the Moody<sup>(27)</sup> friction factor including surface roughness effects,
2. Under single-phase heating conditions a factor is applied based on the values of the coolant density and viscosity at the temperature of the heated surface and at the bulk coolant temperature, and
3. Under two-phase flow conditions the homogeneous flow model proposed by Owens<sup>(67)</sup> is used with a modification to account for a mass velocity and heat flux effect.

The flow in the lateral directions, normal to the fuel rod axis, views the reactor core as a large tube bank. Thus, the lateral friction factor proposed by Idel'chik<sup>(26)</sup> is applicable. This correlation is of the form:

$$F_L = A Re_L^{-0.2} \quad (4.4-11)$$

where:

A is a function of the rod pitch and diameter as given in Reference [26].

$Re_L$  is the lateral Reynolds number based on the rod diameter.

Extensive comparisons of THINC-IV predictions using these correlations to experimental data are given in Reference [51], and verify the applicability of these correlations in PWR design. 612 301

#### 4.4.4.3 Influence of Power Distribution

The core power distribution which is largely established at beginning-of-life by fuel enrichment, loading pattern, and core power level is also a function of variables such as control rod worth and position, and fuel depletion throughout lifetime. Radial power distributions in various planes of the core are often illustrated for general interest; however, the core radial enthalpy rise distribution as determined by the integral of power up each channel is of greater importance for DNB analyses. These radial power distributions, characterized by  $F_{\Delta H}^N$  (defined in Subsection 4.3.2.2.1) as well axial heat flux profiles are discussed in the following two sections.

##### 4.4.4.3.1 Nuclear Enthalpy Rise Hot Channel Factor, $F_{\Delta H}^N$

Given the local power density  $q'$  (kW/ft) at a point  $x, y, z$  in a core with  $N$  fuel rods and height  $H$ ,

$$F_{\Delta H}^N = \frac{\text{hot rod power}}{\text{average rod power}} = \frac{\text{MAX} \int_0^H q'(x_0, y_0, z) dz}{\frac{1}{N} \sum \int_0^H q'(x, y, z) dz} \quad (4.4-12)$$

where  $x_0, y_0$  are the position coordinates of the hot rod.

The way in which  $F_{\Delta H}^N$  is used in the DNB calculation is important. The location of minimum DNBR depends on the axial profile and the value of DNBR depends on the enthalpy rise to that point. Basically, the maximum value of the rod integral is used to identify the most likely rod for minimum DNBR. An axial power profile is obtained which when normalized to the value of  $F_{\Delta H}^N$ , recreates the axial heat flux along the limiting rod. The surrounding rods are assumed to have the same axial profile with rod average powers which are typical distributions found in hot assemblies. In this manner worst case axial profiles can be combined with worst case radial distributions for reference DNB calculations.

It should be noted again the  $F_{\Delta H}^N$  is an integral and is used as such in DNB calculations. Local heat fluxes are obtained by using hot channel and adjacent channel explicit power shapes which take into account variations in horizontal power shapes throughout the core. The sensitivity of the THINC-IV analysis to radial power shapes is discussed in Reference [20].

As mentioned earlier, the Integrated Protection System incorporated in this plant contains added measurement capability not found in the Byron-Braidwood plant. This makes possible the use of current values of plant parameters to determine protection setpoints, rather than relying on analytically calculated worst case values.

$F_{\Delta H}^N$  plays an important role in the calculation of the DNB limiting power level. As described in Section 4.3.2.2.6,  $F_{\Delta H}^N$  is a function of power level and rod position. The output from the instruments measuring the rod positions are processed by the  $F_{\Delta H}^N$  generator to yield the rod position dependent value of  $F_{\Delta H}^N$ , the algorithm used by this generator is shown graphically in Figure 4.3-46. For determining DNB protection setpoints, the variation of  $F_{\Delta H}^N$  with power level is accounted for by using a design  $F_{\Delta H}$  at part power given by:

$$F_{\Delta H} = F_{\Delta H}^{HFP} (RP) [1 + 0.1 (1-P)] \quad (4.4-13)$$

where P is fraction of full power

The value of  $F_{\Delta H}^N$  obtained from the generator is used along with factors representing the current axial heat flux shape, the system pressure and the core inlet fluid temperature to yield the DNB limiting power level. This power level, the value updated several times per second, is then incorporated into the protection system setpoints.

In addition, the value of  $F_{\Delta H}^{HFP} (RP)$  can be adjusted based on measured values of  $F_{\Delta H}$  on a monthly basis as described in the Technical Specification.

612 303

#### 4.4.4.3.2 Axial Heat Flux Distributions

As discussed in Section 4.3.2.2, the axial power, or heat flux, distribution can vary as a result of rod motion, power change, or due to a spatial xenon transients which may occur in the axial direction. The multi-excore detector system and its associated data processing equipment, is capable of constructing the average axial power distribution for use by the protection system.

The axial power distribution plays an important role in determining the DNB limiting power level since the minimum DNBR is a function of both the local heat flux at the point and the integrated heat flux to the point of interest. The parameter used to characterize the axial power distribution is denoted as MAXPIP and is defined by:

$$\text{MAXPIP} = \text{MAX}_{\text{on } Z} \left\{ P(Z) \int_0^Z p(\eta) d\eta \right\}, \quad (4.4-14)$$

Where  $Z$  is the elevation in the core,  $Z=0$  is the core inlet, and  $P(Z)$  is the normalized axial power distribution. MAXPIP, along with the current values of system pressure, core inlet fluid temperature, and  $F_{\Delta H}^N$  are input to the DNB calculator which computes the DNB limiting power level and assures that adequate margin is retained between the actual core power level and the DNB limiting power level. The protection system continuously monitors the margin, and trips the plant when minimum allowable margin is reached.

The axial power distribution is also used in conjunction with the rod position indicators to produce the value of the maximum Kw/ft present in the core for protection from fuel centerline melting and the  $F_{Qx}$  power vs. elevation plot is used for LOCA surveillance.

The DNB calculation incorporated in the plant protection system makes use of the DNB correlation and thermal design method and bases as described in Section 4.4.2.2.

It should be noted again the  $F_{\Delta H}^N$  is an integral and is used as such in DNB calculations. Local heat fluxes are obtained by using hot channel and adjacent channel explicit power shapes which take into account variations in horizontal power shapes throughout the core. The sensitivity of the THINC-IV analysis to radial power shapes is discussed in Reference [20].

For operation at a fraction  $P$  of full power, the design  $F_{\Delta H}^N$  used in DNB calculations is given by:

$$F_{\Delta H}^N = 1.49 [1 + 0.3 (1-P)]$$

where  $P$  is a fraction of full power.

The permitted relaxation of  $F_{\Delta H}^N$  is included in the DNB protection setpoints and allows radial power shape changes with rod insertion to the insertion limits<sup>(68)</sup>, thus allowing greater flexibility in the nuclear design.

#### 4.4.4.3.2 Axial Heat Flux Distributions

As discussed in Section 4.3.2.2, the axial heat flux distribution can vary as a result of rod motion, power change, or due to a spatial xenon transients which may occur in the axial direction. Consequently, it is necessary to measure the axial power imbalance by means of the excore nuclear detectors (as discussed in Section 4.3.2.2) and protect the core from excessive axial power imbalance.

The reference axial shape used in establishing core DNB limits (that is Overtemperature  $\Delta T$  protection system setpoints) is a chopped cosine with a peak to average value of 1.55. The Reactor Trip System provides automatic reduction of the trip setpoints on excessive axial power imbalance. To determine the magnitude of the setpoint reduction, the reference shape is supplemented by other axial shapes skewed to the bottom and top of the core.

The course of those accidents in which DNB is a concern is analyzed in Chapter 15 assuming that the protection setpoints have been set on the basis of these shapes. In many cases the axial power distribution in the hot channel changes throughout the course of the accident due to rod motion, coolant temperature and power level changes.

The initial conditions for accidents for which DNB protection is required are assumed to be those permissible within the constant axial offset control strategy for the load maneuvers described in Reference 69. In the case of the loss of flow accident the hot channel heat flux profile is very similar to the power density profile in normal operation preceding the accident. It is therefore possible to illustrate the calculated minimum DNBR for conditions representative of the loss of flow accident as a function of the flux difference initially in the core. A plot of this type is provided in Figure 4.4-11 for first core initial conditions without part length rods. As noted on this figure all power shapes were evaluated with a full power radial peaking factor  $F_{\Delta H}^N$  of 1.49. The radial contribution to the hot rod power shape is conservative both for the initial condition and for the condition at the time of minimum DNBR during the loss of flow transient. Also shown is the minimum DNBR calculated at the same conditions for the design power shape for non overpower/overtemperature DNB events. It can be seen that this design shape results in a calculated DNBR that bounds all the normal operation power shapes.

#### 4.4.4.4 Core Thermal Response

A general summary of the steady-state thermal-hydraulic design parameters including thermal output, flow rates, etc., is provided in Table 4.4-1 for all loops in operation, and in Table 4.2-2 for operation with one coolant loop out of service.

As stated in Subsection 4.4-1, the design bases of the application are to prevent DNB and to prevent fuel melting for condition I and II events. The protective systems described in Chapter 7.0 of the applicable FSAR are designed to meet these bases. The response of the core to Condition II transients is given in Chapter 15.0.

612-303



Using the THINC-IV code, (51) a correlation has been obtained between MAXPIP and  $Q/Q_{REF}$ , where  $Q$  is the DNB limiting power level permitted in the core for the current power shape (characterized by a value of MAXPIP), and  $Q_{REF}$  is the DNB limiting power level for a reference axial power shape and the current values of core thermal-hydraulic parameters, inlet fluid temperature, value of  $F_{\Delta H}^N$ , and cell type (typical or thimble). The  $Q/Q_{REF}$  vs. MAXPIP correlation is presented in the Technical Specifications for this plant. The DNB limiting power level  $Q$ , is obtained by multiplying the value of  $Q/Q_{REF}$  times the current value of  $Q_{REF}$ , determined from instrument output and from core limit relationships in the computer memory. The allowable power level is then compared to the actual core power level to determine if any protection is required. Note that since the MAXPIP vs  $Q/Q_{REF}$  correlation and the  $Q_{REF}$  functions have been determined with the same reference axial power shape, the DNB protection system is not dependent on any reference axial power distribution.

#### 4.4.4.4 Core Thermal Response

A general summary of the steady-state thermal-hydraulic design parameters including thermal output, flow rates, etc., is provided in Table 4.4-1 for all loops in operation, and in Table 4.4-2 for operation with one coolant loop out of service.

As stated in Subsection 4.4-1, the design bases of the application are to prevent DNB and to prevent fuel melting for Condition I and II events. The protective systems described in Chapter 7.0 of the applicable FSAR are designed to meet these bases. The response of the core to Condition II transients is given in Chapter 15.0.

612 307

#### 4.4.4.5 Analytical Techniques

##### 4.4.4.5.1 Core Analysis

The objective of reactor core thermal design is to determine the maximum heat removal capability in all flow subchannels and show that the core safety limits, as presented in the technical specifications are not exceeded while compounding engineering and nuclear effects. The thermal design considers local variations in dimensions, power generation, flow redistribution, and mixing. THINC-IV is a realistic three-dimensional matrix model which has been developed to account for hydraulic and nuclear effects on the enthalpy rise in the core<sup>(20, 51)</sup>. The behavior of the hot assembly is determined by superimposing the power distribution among the assemblies upon the inlet flow distribution while allowing for flow mixing and flow distribution between assemblies. The average flow and enthalpy in the hottest assembly is obtained from the core-wide, assembly by assembly analysis. The local variations in power, fuel rod and pellet fabrication, and mixing within the hottest assembly are then superimposed on the average conditions of the hottest assembly in order to determine the conditions in the hot channel.

##### 4.4.4.5.2 Steady-State Analysis

The THINC-IV computer program, as approved by the NRC<sup>(2)</sup>, is used to determine coolant density, mass velocity, enthalpy, vapor void, static pressure, and DNBR distributions along parallel flow channels within a reactor core under all expected operating conditions. The THINC-IV Code is described in detail in References [20] and [51], including models and correlations used. In addition, a discussion on experimental verification of THINC-IV is given in Reference [51].

612 308

PAGE 4.4-37 DOES NOT APPEAR  
FOR THE UHI/NON-IPS SCENARIO

GO TO PAGE 4.4-38

4.4-37

612 309

BLUE

The effect of crud on the flow and enthalpy distribution in the core is accounted for directly in the THINC-IV evaluations by assuming a crud thickness several times more than that which would be expected to occur. This results in slightly conservative evaluations of the minimum DNBR.

Estimates of uncertainties are discussed in Subsection 4.4.2.9.

#### 4.4.4.5.3 Experimental Verification

Extensive additional experimental verification is presented in Reference [51].

The THINC-IV analysis is based on a knowledge and understanding of the heat transfer and hydrodynamic behavior of the coolant flow and the mechanical characteristics of the fuel elements. The use of the THINC-IV analysis provides a realistic evaluation of the core performance and is used in the thermal analyses as described above.

#### 4.4.4.5.4 Transient Analysis

The THINC-IV thermal-hydraulic computer code does not have a transient capability. Since the third section of the THINC-I program(12) does have this capability, this code (THINC-III) continues to be used for transient DNB analysis.

The conservation equations needed for the transient analysis are included in THINC-III by adding the necessary accumulation terms to the conservation equations used in the steady-state (THINC-I) analysis. The input description must now include one or more of the following time dependent arrays:

1. Inlet flow variation,
2. Heat flux distribution, and
3. Inlet pressure history.

At the beginning of the transient, the calculation procedure is carried out as in the steady-state analysis. The THINC-III Code is first run in the steady-state mode to ensure conservatism with respect to THINC-IV and in order to provide the steady-state initial conditions at the start of the transient. The time is incremented by an amount determined either by the user or by the program itself. At each new time step the calculations are carried out with the addition of the accumulation terms which are evaluated using the information from the previous time step. This procedure is continued until a preset maximum time is reached.

At preselected intervals, a complete description of the coolant parameter distributions within the array as well as DNBR are printed out. In this manner the variation of any parameter with time can be readily determined.

At various times during the transient, steady-state THINC-IV is applied to show that the application of the transient version of THINC-I is conservative.

The THINC-III Code does not have the capability for evaluating fuel rod thermal response. This is treated by the methods described in Subsection 15.0.11.

#### 4.4.4.6 Hydrodynamic and Flow Power Coupled Instability

Boiling flows may be susceptible to thermohydrodynamic instabilities<sup>(70)</sup>. These instabilities are undesirable in reactors since they may cause a change in thermohydraulic conditions that may lead to a reduction in the DNB heat flux relative to that observed during a steady flow condition or to undesired forced vibrations of core components. Therefore, a thermohydraulic design criterion was developed which states that modes of operation under Condition I and II events shall not lead to thermohydrodynamic instabilities.

Two specific types of flow instabilities are considered for Westinghouse PWR operation. These are the Ledinegg or flow excursion type of static instability and the density wave type of dynamic instability.

A Ledinegg instability involves a sudden change in flow rate from one steady state to another. This instability occurs<sup>(70)</sup> when the slope of the reactor coolant system pressure drop-flow rate curve ( $\partial\Delta P/\partial G|_{\text{internal}}$ ) becomes algebraically smaller than the loop supply (pump head) pressure drop-flow rate curve ( $\partial\Delta P/\partial G|_{\text{external}}$ ). The criterion for stability is thus  $\partial\Delta P/\partial G|_{\text{internal}} > \partial\Delta P/\partial G|_{\text{external}}$ . The Westinghouse pump head curve has a negative slope ( $\delta\Delta P/\delta G|_{\text{external}} < 0$ ) whereas the reactor coolant system pressure drop-flow curve has a positive slope ( $\delta\Delta P/\delta G|_{\text{internal}} > 0$ ) over the Condition I and Condition II operational ranges. Thus, the Ledinegg instability will not occur.

The mechanism of density wave oscillations in a heated channel has been described by Lahey and Moody<sup>(71)</sup>. Briefly, an inlet flow fluctuation produces an enthalpy perturbation. This perturbs the length and the pressure drop of the single phase region and causes quality or void perturbations in the two-phase regions which travel up the channel with the flow. The quality and length perturbations in the two-phase region create two-phase pressure drop perturbations. However, since the total pressure drop across the core is maintained by the characteristics of the fluid system external to the core, then the two-phase pressure drop perturbation feeds back to the single phase region. These resulting perturbations can be either attenuated or self-sustained.

A simple method has been developed by Ishii<sup>(72)</sup> for parallel closed channel systems to evaluate whether a given condition is stable with respect to the density wave type of dynamic instability. This method had been used to assess the stability of typical Westinghouse reactor designs<sup>(73,74,75)</sup>, including Virgil C. Summer, under Condition I and II operation. The results indicate that a large margin to density wave instability exists, e.g., increases on the order of 200% of rated reactor power would be required for the predicted inception of this type of instability.

The application of the method of Ishii<sup>(72)</sup> to Westinghouse reactor designs is conservative due to the parallel open channel feature of Westinghouse PWR cores. For such cores, there is little resistance to

lateral flow leaving the flow channels of high power density. There is also energy transfer from channels of high power density to lower power density channels. This coupling with cooler channels has led to the opinion that an open channel configuration is more stable than the above closed channel analysis under the same boundary conditions. Flow stability tests<sup>(76)</sup> have been conducted where the closed channel systems were shown to be less stable than when the same channels were cross connected at several locations. The cross connections were such that the resistance to channel to channel cross flow and enthalpy perturbations would be greater than that which would exist in a PWR core which has a relatively low resistance to cross flow.

Flow instabilities which have been observed have occurred almost exclusively in closed channel systems operating at low pressure relative to the Westinghouse PWR operating pressures. Kao, Morgan and Parker<sup>(77)</sup> analyzed parallel closed channel stability experiments simulating a reactor core flow. These experiments were conducted at pressures up to 2200 psia. The results showed that for flow and power levels typical of power reactor conditions, no flow oscillations could be induced above 1200 psia.

Additional evidence that flow instabilities do not adversely affect thermal margin is provided by the data from the rod bundle DNB tests. Many Westinghouse rod bundles have been tested over wide ranges of operating conditions with no evidence of premature DNB or of inconsistent data which might be indicative of flow instabilities in the rod bundle.

In summary, it is concluded that thermohydrodynamic instabilities will not occur under Condition I and II modes of operation for Westinghouse PWR reactor designs. A large power margin, greater than doubling rated power, exists to predicted inception of such instabilities. Analysis has been performed which shows that minor plant to plant differences in Westinghouse reactor designs such as fuel assembly arrays, core power to flow ratios, fuel assembly length, etc. will not result in gross deterioration of the above power margins.

#### 4.4.4.7 Fuel Rod Behavior Effects from Coolant Flow Blockage

Coolant flow blockages can occur within the coolant channels of a fuel assembly or external to the reactor core. The effects of fuel assembly blockage within the assembly on fuel rod behavior is more pronounced than external blockages of the same magnitude. In both cases the flow blockages cause local reductions in coolant flow. The amount of local flow reduction, where it occurs in the reactor, and how far along the flow stream the reduction persists are considerations which will influence the fuel rod behavior. The effects of coolant flow blockages in terms of maintaining rated core performance are determined both by analytical and experimental methods. The experimental data are usually used to augment analytical tools such as computer programs similar to the THINC-IV program. Inspection of the DNB correlation (Section 4.4.2.2 and Reference 1) shows that the predicted DNBR is dependent upon the local values of quality and mass velocity.

The THINC-IV Code is capable of predicting the effects of local flow blockages on DNBR within the fuel assembly on subchannel basis, regardless of where the flow blockage occurs. In Reference [51], it is shown that for a fuel assembly similar to the Westinghouse design, THINC-IV accurately predicts the flow distribution within the fuel assembly when the inlet nozzle is completely blocked. Full recovery of the flow was found to occur about 30 inches downstream of the blockage. With the reactor operating at the nominal full power conditions specified in Table 4.4-1, the effects of an increase in enthalpy and decrease in mass velocity in the lower portion of the fuel assembly would not result in the reactor reaching the design DNBR specified in Section 4.4.1.1.

From a review of the open literature it is concluded that flow blockage in "open lattice cores" similar to the Westinghouse cores cause flow perturbations which are local to the blockage. For instance, A. Ohtsubo<sup>(78)</sup>, et al., show that the mean bundle velocity is approached asymptotically about 4 inches downstream from a flow blockage



in a single flow cell. Similar results were also found for 2 and 3 cells completely blocked. P. Basmer<sup>(79)</sup>, et al., tested an open lattice fuel assembly in which 41 percent of the subchannels were completely blocked in the center of the test bundle between spacer grids. Their results show the stagnant zone behind the flow blockage essentially disappears after 1.65 L/De or about 5 inches for their test bundle. They also found that leakage flow through the blockage tended to shorten the stagnant zone or, in essence, the complete recovery length. Thus, local flow blockages within a fuel assembly have little effect on subchannel enthalpy rise. The reduction in local mass velocity is then the main parameter which affects the DNBR. If the plants were operating at full power and nominal steady state conditions as specified in Table 4.4-1, a reduction in local mass velocity greater than 70% would be required to reduce the DNBR to the design DNBR. The above mass velocity effect on the DNB correlation was based on the assumption of fully developed flow along the full channel length. In reality a local flow blockage is expected to promote turbulence and thus would likely not effect DNBR at all.

Coolant flow blockages induce local crossflows as well as promote turbulence. Fuel rod behavior is changed under the influence of a sufficiently high crossflow component. Fuel rod vibration could occur, caused by this crossflow component, through vortex shedding or turbulent mechanisms. If the crossflow velocity exceeds the limit established for fluid elastic stability, large amplitude whirling results. The limits for a controlled vibration mechanism are established from studies of vortex shedding and turbulent pressure fluctuations. The crossflow velocity required to exceed fluid elastic stability limits is dependent on the axial location of the blockage and the characterization of the crossflow (jet flow or not). These limits are greater than those for vibratory fuel rod wear. Crossflow velocity above the established limits can lead to mechanical wear of the fuel rods at the grid support locations. Fuel rod wear due to flow induced vibration is considered in the fuel rod fretting evaluation (Section 4.2).

#### 4.4.5 TESTING AND VERIFICATION

##### 4.4.5.1 Tests Prior to Initial Criticality

A reactor coolant flow test is performed following fuel loading but prior to initial criticality. Coolant loop pressure drop data is obtained in this test. This data in conjunction with coolant pump performance information allows determination of the coolant flow rates at reactor operating conditions. This test verifies that proper coolant flow rates have been used in the core thermal and hydraulic analysis.

##### 4.4.5.2 Initial Power and Plant Operation

Core power distribution measurements are made at several core power levels (see Chapter 14.0). These tests are used to insure that conservative peaking factors are used in the core thermal and hydraulic analysis.

Additional demonstration of the overall conservatism of the THINC analysis was obtained by comparing THINC predictions to incore thermocouple measurements<sup>(80)</sup>. These measurements were performed on the Zion reactor. No further in-reactor testing is planned.

##### 4.4.5.3 Component and Fuel Inspections

Inspections performed on the manufactured fuel are delineated in Section 4.2.4. Fabrication measurements critical to thermal and hydraulic analysis are obtained to verify that the engineering hot channel factors in the design analyses (Section 4.4.2.2.4) are met.

#### 4.4.6 INSTRUMENTATION REQUIREMENTS

##### 4.4.6.1 Incore Instrumentation

Instrumentation is located in the core so that by correlating movable neutron detector information with fixed thermocouple information radial, axial, and azimuthal core characteristics may be obtained for all core quadrants.

The incore instrumentation system is comprised of thermocouples, positioned to measure fuel assembly coolant outlet temperatures at pre-selected positions, and fission chamber detectors positioned in guide thimbles which run the length of selected fuel assemblies to measure the neutron flux distribution. Figure 4.4-10 shows the number and location of instrumented assemblies in the core.

The core-exit thermocouples provide a backup to the flux monitoring instrumentation for monitoring power distribution. The routine, systematic, collection of thermocouple readings by the operator provides a data base. From this data base, abnormally high or abnormally low readings, quadrant temperature tilts, or systematic departures from a prior reference map can be deduced.

The movable incore neutron detector system would be used for more detailed mapping if the thermocouple system were to indicate an abnormality. These two complementary systems are more useful when taken together than either system alone would be. The incore instrumentation system is described in more detail in Section 7.7.1.9.

The incore instrumentation is provided to obtain data from which fission power density distribution in the core, coolant enthalpy distribution in the core, and fuel burnup distribution may be determined.

#### 4.4.6.2 Overtemperature and Overpower $\Delta T$ Instrumentation

As mentioned earlier, this plant contains the Integrated Protection System. Measurement capability exists, with this protection system, which allows the use of current values of plant parameters in determination of the protection system setpoints. The DNB and Overpower Protection Systems are discussed in Sections 4.4.4.3 and 4.4.6.3 respectively. More details on these protection systems are given in Chapter 7. Factors included in establishing the protection system setpoints include both axial and radial distributions of core power\*.

---

\*Discussed in RESAR-414.

The incore instrumentation system is comprised of thermocouples, positioned to measure fuel assembly coolant outlet temperatures at pre-selected positions, and fission chamber detectors positioned in guide thimbles which run the length of selected fuel assemblies to measure the neutron flux distribution. Figure 4.4-10 shows the number and location of instrumented assemblies in the core.

The core-exit thermocouples provide a backup to the flux monitoring instrumentation for monitoring power distribution. The routine, systematic, collection of thermocouple readings by the operator provides a data base. From this data base, abnormally high or abnormally low readings, quadrant temperature tilts, or systematic departures from a prior reference map can be deduced.

The movable incore neutron detector system would be used for more detailed mapping if the thermocouple system were to indicate an abnormality. These two complementary systems are more useful when taken together than either system alone would be. The incore instrumentation system is described in more detail in Section 7.7.

The incore instrumentation is provided to obtain data from which fission power density distribution in the core, coolant enthalpy distribution in the core, and fuel burnup distribution may be determined.

#### 4.4.6.2 Overtemperature and Overpower $\Delta T$ Instrumentation

The Overtemperature  $\Delta T$  trip protects the core against low DNBR. The Overpower  $\Delta T$  trip protects against excessive power (fuel rod rating protection).

As discussed in Chapter 7, factors included in establishing the Overtemperature  $\Delta T$  and Overpower  $\Delta T$  trip setpoints includes the reactor coolant temperature in each loop and the axial distribution of core power through the use of the two section excore neutron detectors.

#### 4.4.6.3 Instrumentation to Limit Maximum Power Output

Instrumentation is provided to limit the maximum power output of the reactor to preclude fuel damage or core power distributions which would result in peak clad temperatures in excess of design values should a design basis LOCA occur. The core is typically operated in a manner such that the design limiting power output is greater than the rated output of the plant. However, it is possible for unusual load change requirements or accident conditions to result in a core configuration such that operation at less than the rated power is required to maintain adequate margin between actual values and design limiting values of plant parameters. In either case, instrumentation must detect the relevant operating parameters and process the data into a form that can be compared with protection system setpoints.

Four different types of power level detectors are used in the plant. Two proportional counters for the source range are installed on the two opposing "flat" portions of the core containing the primary startup sources, and are located at an elevation approximately one quarter of the core height. Two compensated ionization chambers for the intermediate range, located in the same instrument walls and detector assemblies as the source range detectors, are positioned at an elevation corresponding to one half of the core height. Four sets of four-section uncompensated ionization chamber assemblies for the power range are installed vertically at the four corners of the core and are located equidistant from the reactor vessel at all points. Each power range detector element provides a signal corresponding to the neutron flux at that elevation in that quadrant. The three types of detectors, in combination, are capable of monitoring the neutron flux from a completely shutdown condition to 120% of full power, with the capability of recording overpower excursions up to 200% of full power.

The fourth type of power detection in the plant measures the nitrogen-16 (N-16) concentration in the coolant. N-16 is produced by neutron activation of the oxygen-16 in the coolant in a quantity proportional to the integrated fast flux, or power, throughout the core. The N-16 detectors are located on the hot leg of each loop of the reactor. The N-16 detector is further described in Section 7.1.

The neutron flux at each of the elevations in the core measured by the power range detectors are used as input to an analysis to determine the axial power distribution in the core. This axial heat flux distribution is then used for DNB, overpower, and LOCA power shape surveillance, as described in Section 4.4.4.3.2. The core power level as measured by the N-16 detectors is used to establish the absolute value of the core power. This absolute level, in conjunction with the normalized power shapes determined from other instrumentation, is compared to the appropriate setpoints to determine if trip action or power run back is required. Sections 7 and 15 contains further details on the protection system.

612 320

#### 4.4.6.3 Instrumentation to Limit Maximum Power Output

The output of the three ranges (source, intermediate, and power) of detectors, with the electronics of the nuclear instruments, are used to limit the maximum power output of the reactor within their respective ranges.

There are six radial locations containing a total of eight neutron flux detectors installed around the reactor in the primary shield, two proportional counters for the source range installed on opposite "flat" portions of the core containing the primary startup sources at an elevation approximately one quarter of the core height. Two compensated ionization chambers for the intermediate range, located in the same instrument wells and detector assemblies as the source range detectors, are positioned at an elevation corresponding to one half of the core height; four dual section uncompensated ionization chamber assemblies for the power range installed vertically at the four corners of the core and located equidistant from the reactor vessel at all points and, to minimize neutron flux pattern distortions, within one foot of the reactor vessel. Each power range detector provides two signals corresponding to the neutron flux in the upper and in the lower sections of a core quadrant. The three ranges of detectors are used as inputs to monitor neutron flux from a completely shutdown condition to 120 percent of full power with the capability of recording overpower excursions up to 200 percent of full power.

The output of the power range channels is used for:

1. The rod speed control function,
2. To alert the operator to an excessive power unbalance between the quadrants,
3. Protect the core against rod ejection accidents and

4. Protect the core against adverse power distributions resulting from dropped rods.

Details of the neutron detectors and nuclear instrumentation design and the control and trip logic are given in Chapter 7.0. The limits on neutron flux operation and trip setpoints are given in the Technical Specifications.



#### 4.4.7 REFERENCES

1. Motley, F. E., Hill, K. W., Cadek, F. F. and Shefcheck, J., "New Westinghouse Correlation WRB-1 for Predicting Critical Heat Flux in Rod Bundles with Mixing Vane Grids," WCAP-8762, July, 1976 (Proprietary) and WCAP-8763, July, 1976 (Non-Proprietary).
2. Letter from J. F. Stolz (NRC) to C. Eicheldinger (Westinghouse); Subject: Staff Evaluation of WCAP-7956, WCAP-8054, WCAP-8567 and WCAP-8762, April 19, 1978.
3. Chelemer, H., Boman, L. H. and Sharp, D. R., "Improved Thermal Design Procedure," WCAP-8567-P, July, 1975 (Proprietary) and WCAP-8568, July, 1975 (Non-Proprietary).
4. Christensen, J. A., Allio, R. J. and Biancheria, A., "Melting Point of Irradiated  $UO_2$ ," WCAP-6065, February, 1965.
5. Davidson, S. L., Motley, F. E., Lee, Y. C., Bogard, T., Bryan, W. J., "Verification Testing and Analyses of the 17x17 Optimized Fuel Assembly", WCAP-9401, March, 1979 (Proprietary) and WCAP-9402.
6. L. S. Torg, "Boiling and Critical heat Flux", TID-25887, 1972.
7. F. E. Motley, F. F. Cadek, "DNB Test Results for New Mixing Vane Grids (R), "WCAP-7695-P-A (Westinghouse Proprietary) July, 1972 and WCAP-7958-A (Non-Proprietary), January, 1975.
8. F. E. Motley, F. F. Cadek, "Application of Modified Spacer Factor to L. Grid Typical and Cold Wall Cell DNB", WCAP-7988 (Westinghouse Proprietary), and WCAP-8030-A (Non-Proprietary), October, 1972.
9. F. E. Motley, A. H. Wenzel, F. F. Cadek, "Critical Heat Flux Testing of 17 x 17 Fuel Assembly Geometry with 22 inch Grid Spacing", WCAP-8536, (Westinghouse Proprietary) and WCAP-8537 (Non-Proprietary), May, 1975.

10. K. W. Hill, F. E. Motley, F. F. Cadek, A. H. Wenzel, "Effect of 17 x 17 Fuel Assembly Geometry on DNB", WCAP-8296-P-A (Westinghouse Proprietary) and WCAP-8297-A (Non-Proprietary), February, 1975.
11. L. S. Tong, "Prediction of Departure from Nucleate Boiling for an Axially Non-Uniform Heat Flux Distribution," J. Nuclear Energy, 21, 241-248, 1967.
12. H. Chelemer, J. Weisman, and L. S. Tong, "Subchannel Thermal Analysis of Rod Bundle Cores," WCAP-7015, Revision 1, January 1969.
13. F. F. Cadek, F. E. Motley, and D. P. Dominicus, "Effect of Axial Spacing on Interchannel Thermal Mixing with the R Mixing Van Grid," WCAP-7941-P-A (Proprietary), January 1975 and WCAP-7959-A, January 1975.
14. D. S. Rowe and C. W. Angle, "Crossflow Mixing Between Parallel Flow Channels During Boiling, Part II Measurements of Flow and Enthalpy in Two Parallel Channels," BNWL-371, Part 2, December 1967.
15. D. S. Rowe and C. W. Angle, "Crossflow Mixing Between Parallel Flow Channels During Boiling, Part III Effect of Spacers on Mixing Between Two Channels, BNWL-371, Part 3, January 1969.
16. J. M. Gonzalez-Santalo and P. Griffith, "Two-Phase Flow Mixing in Rod Bundle Subchannels," ASME Paper 72-WA/NE-19.
17. F. E. Motley, A. H. Wenzel, and F. F. Cadek, "The Effect of 17 x 17 Fuel Assembly Geometry on Interchannel Thermal Mixing," WCAP-8298-P-A (Proprietary), January 1975 and WCAP 8299-A, January 1975.
18. Hill, K. W., Motley, F. E. and Cadek, F. F., "Effect of Local Heat Flux Spikes on DNB in Non-Uniform Heated Rod Bundles," WCAP-8174, August, 1973 (Proprietary) and WCAP-8202, August, 1973 (Non-Proprietary).

19. F. F. Cadek, "Interchannel Thermal Mixing with Mixing Vane Grids," WCAP-7667-P-A (Proprietary), January 1975 and WCAP-7755-A, January 1975.
20. L. E. Hochreiter, "Application of the THINC IV Program to PWR Design," WCAP-8054 (Proprietary), October 1973, and WCAP-8195, October 1973.
21. F. W. Dittus and L. M. K. Boelter, "Heat Transfer in Automobile Radiators of the Tubular Type," Calif. Univ. Publication in Eng., 2, No. 13, 443461, 1930.
22. J. Weisman, "Heat Transfer to Water Flowing Parallel to Tube Bundles," Nucl. Sci. Eng., 6, 78-79, 1959.
23. J. R. S. Thom, et al., "Boiling in Sub-cooled Water During Flowup Heated Tubes or Annuli," Proc. Instn. Mech. Engrs., 180, Pt. C 226-46, 1955-66.
24. G. Hetsroni, "Hydraulic Tests of the San Onofre Reactor Model," WCAP-3269-8, June 1964.
25. G. Hetsroni, "Studies of the Connecticut-Yankee Hydraulic Model," NYO-3250-2, June 1965.
26. I. E. Idel'chik, "Handbook of Hydraulic Resistance," AEC-TR-6630, 1960.
27. L. F. Moody, "Friction Factors for Pipe Flow," Transaction of the American Society of Mechanical Engineers, 66, 671-684, 1944.
28. G. W. Maurer, "A Method of Predicting Steady State Boiling Vapor Fractions in Reactor Coolant Channels," WAPD-BT-19, PP 59-70, June 1960.
29. P. Griffith, J. A. Clark, and W. M. Rohsenow, "Void Volumes in Sub-cooled Boiling Systems," ASME Paper No. 58-HT-19.

30. R. W. Bouring, Physical Model, Based on Bubble Detachment, and Calculation of Steam Voidage in the Subcooled Region of a Heated Channel," HPR-10, December 1962.
31. G. Kjaerheim and E. Rolstad, "In-Pile Determination of UO Thermal Conductivity, Density Effects and Gap Conductance," HPR-80, December 1967.
32. G. Kjaerheim, "In-Pile Measurements of Centre Fuel Temperatures and Thermal Conductivity Determination of Oxide Fuels," paper 1FA-175 presented at the European Atomic Energy Society Symposium on Performance Experience of Water-Cooled Power Reactor Fuel, Stockholm, Sweden, October 21-22, 1969.
33. I. Cohen, G. Lustman, and D. Eichenberg, "Measurement of the Thermal Conductivity of Metal-Clad Uranium Oxide Rods During Irradiation," WAPD-228, 1960.
34. D. J. Clough, and J. B. Sayers, "The Measurement of the Thermal Conductivity of UO<sub>2</sub> under Irradiation in the Temperature Range 150°-1600°C," AERE-R<sup>2</sup>4690, UKAEA Research Group, Harwell, December 1964.
35. J. P. Stora, et al., "Thermal Conductivity of Sintered Uranium Oxide under In-Pile Conditions," EURAEC-1095, 1964.
36. I. Devold, "A Study of the Temperature Distribution in UO Reactor Fuel Elements," AE-318, Aktiebolaget Atomenergi, Stockholm, Sweden, 1968.
37. M. G. Balfour, J. A. Christensen, and H. M. Ferrari, "In-Pile Measurement of UO<sub>2</sub> Thermal Conductivity," WCAP-2923, 1966.
38. V. C. Howard and T. G. Gulvin, "Thermal Conductivity Determinations on Uranium Dioxide by a Radial Flow Method," UKAEA IG-Report 51, November 1960.

39. C. F. Lucks and H. W. Deem, "Thermal Conductivity and Electrical Conductivity of  $UO_2$ ," in Progress Reports Relating to Civilian Applications, BMI-1448 (Rev.) for June 1960; BMI-1489 (Rev.) for December 1960 and BMI-1518 (Rev.) for May 1961.
40. J. L. Daniel, J. Matolich, Jr., H. W. Deem, "Thermal Conductivity of  $UO_2$ ," HW-69945, September 1962.
41. A. D. Feith, "Thermal Conductivity of  $UO_2$  by a Radial Heat Flow Method," TID-21668, 1962.
42. J. Vogt, L. Grandell, and U. Runfors, "Determination of the Thermal Conductivity of Unirradiated Uranium Dioxide," AB Atomenergi Report RMB-527, 1964, Quoted by IAEA Technical Report Series No. 59, "Thermal Conductivity of Uranium Dioxide,".
43. T. Nishijima, T. Kawada, and A. Ishihata, "Thermal Conductivity of Sintered  $UO_2$  and  $Al_2O_3$  at High Temperature," J. American Ceramic Society, 48, 31, 34, 1965.
44. J. B. Ainscough and M. J. Wheeler, "Thermal Diffusivity and Thermal Conductivity of Sintered Uranium Dioxide," in Proceedings of the Seventh Conference of Thermal Conductivity, p.467, National Bureau of Standards, Washington, 1968.
45. T. G. Godfrey, et al., "Thermal Conductivity of Uranium Dioxide and Armco Iron by an Improved Radial Heat Flow Technique," ORNL-3556, June 1964.
46. J. P. Stora, et al., "Thermal Conductivity of Sintered Uranium Oxide Under In-Pile Conditions," EURAEC-1095, August 1964.
47. A. J. Bush, "Apparatus of Measuring Thermal Conductivity to  $2500^{\circ}C$ ," Westinghouse Research Laboratories Report 64-1P6-401-43, (Proprietary) February 1965.

48. R. R. Asamoto, F. L. Anselin, and A. E. Conti, "The Effect of Density on the Thermal Conductivity of Uranium Dioxide," GEAP-5493, April 1968.
49. O. L. Kruger, "Heat Transfer Properties of Uranium and Plutonium Dioxide," Paper 11-N-68F presented at the Fall meeting of Nuclear Division of the American Ceramic Society, Pittsburgh, September 1968.
50. J. M. Hellman, (Ed.), "Fuel Densification Experimental Results and Model for Reactor Application," WCAP-8218-P-A (Proprietary) March 1975 and WCAP-8219-A, March 1975.
51. L. E. Hochreiter, H. Chelemer, and P. T. Chu, "THINC-IV An Improved Program for Thermal-Hydraulic Analysis of Rod Bundle Cores," WCAP-7956, June 1973.
52. R. N. Duncan, "Rabbit Capsule Irradiation of  $UO_2$ ," CVTR Project, CVNA-142, June 1962.
53. R. C. Nelson, et al., "Fission Gas Release from  $UO_2$  Fuel Rods with Gross Central Melting," GEAP-4571, July 1964.
54. J. A. Gyllander, "In-Pile Determination of the Thermal Conductivity of  $UO_2$  in the Range 500-2500°C," AE-411, January 1971.
55. M F. Lyons, et al., " $UO_2$  Powder and Pellet Thermal Conductivity During Irradiation," GEAP-5100-1, March 1966.
56. D. H. Coplin, et al., "The Thermal Conductivity of  $UO_2$  by Direct In-reactor Measurements," GEAP-5100-6, March 1968.
57. A. S. Bain, "the Heat Rating Required to Produce Center Melting in Various  $UO_2$  Fuels," ASTM Special Technical Publication, No. 306, pp. 30-46, Philadelphia, 1962.

58. J. P. Stora, "In-Reactor Measurements of the Integrated Thermal Conductivity of  $UO_2$  - Effect of Porosity," Trans. ANS, 13, 137-138, 1970.
59. International Atomic Energy Agency, "Thermal Conductivity of Uranium Dioxide," Report of the Panel held in Vienna, April 1965, IAEA Technical Reports Series, No. 59, Vienna, The Agency, 1966.
60. C. G. Poncelet, "Burnup Physics of Heterogeneous Reactor Lattices," WCAP-6069, June 1965.
61. R. J. Nodvick, "Saxton Core II Fuel Performance Evaluation," WCAP-3385-56, Part II, "Evaluation of Mass Spectrometric and Radio-chemical Analyses of Irradiated Saxton Plutonium Fuel," July 1970.
62. R. A. Dean, "Thermal Contact Conductance Between  $UO_2$  and Zircaloy-2, CVNA-127, May 1962.
63. A. M. Ross and R. L. Stoute, "Heat Transfer Coefficient Between  $UO_2$  and Zircaloy-2," AECL-1552, June 1962.
64. F. D. Carter, "Inlet Orificing of Open PWR Cores," WCAP-9004, January 1969 (Proprietary) and WCAP-7836, January 1972 (Non-Proprietary).
65. J. Shefcheck, "Application of the THINC Program to PWR Design," WCAP-7359-L (Proprietary), August 1969 and WCAP-7838, January 1972.
66. E. H. Novemdstern and R. O. Sandberg, "Single Phase Local Boiling and Bulk Boiling Pressure Drop Correlations," WCAP-2850 (Proprietary), April 1966 and WCAP-7916, June 1972.
67. W. L. Owens, Jr., "Two-Phase Pressure Gradient," in International Developments in Heat Transfer, Part II, pp. 363-368, ASME, New York, 1961.

68. A. F. McFarlane, "Power Peaking Factors," WCAP-7912-P-A (Proprietary), January 1975 and WCAP-7912-A, January 1975.
69. T. Morita, et al., "Topical Report, Power Distribution Control and Load Following Procedures," WCAP-8385 (Proprietary), September 1974 and WCAP-8403, September 1974.
70. J. A. Boure, A. E. Bergles, and L. S. Tong, "Review of Two-Phase Flow Instability," Nucl. Engr. Design 25 (1973) p. 165-192.
71. R. T. Lahey and f. J. Moody, "The Thermal Hydraulics of a Boiling Water Reactor," American Nuclear Society, 1977.
72. P. Saha, M. Ishii, and N. Zuber, "An Experimental Investigation of the Thermally Induced Flow Oscillations in Two-Phase Systems," J. of Heat Transfer, No. 1976, pp. 616-622.
73. Virgil C. Summer FSAR, Docket #50-395.
74. Byron/Braidwood FSAR, Docket #50-456.
75. South Texas FSAR, Docket #50-498.
76. S. Kakac, T. N. Vexiroglu, K. Akyuzlu, O. Berkol, "Sustained and Transient Boiling Flow Instabilities in a Cross-Connected Four-Parallel-Channel Upflow System." Proc. of 5th International Heat Transfer Conference, Tokyo, Sept. 3-7, 1974.
77. H. S. Kao, C. D. Morgan, and W. B. Parker, "Prediction of Flow Oscillation in Reactor Core Channel," Trans. AWS, Vol. 16, 1973, pp. 212-213.
78. A. Ohtsubo, and S. Uruwashi, "Stagnant Fluid due to Local Flow Blockage," J. Nucl. Sci. Technol., 9, No. 7, 433-434, 1972.



79. P. Basmer, D. Kirsh, and G. F. Schultheiss, "Investigation of the Flow Pattern in the Recirculation Zone Downstream of Local Coolant Blockages in Pin Bundles," Atomwirtschaft, 17, No. 8, 416-417, 1972. (In German).
80. T. M. Burke, C. E. Meyer, and J. Shefcheck, "Analysis of Data from the Zion (Unit 1) THINC Verification Test," WCAP-8453 (Proprietary), December 1974 and WCAP-8454, December 1974.
81. K. F. Graham and H. M. Forker, "An N-16 Transit Time Flow Measurement System (TTFM) Description and Performance", WCAP-9172 (Proprietary), October, 1977.

612 331

TABLE 4.4-1 (Sheet of 1 of 3)

THERMAL AND HYDRAULIC COMPARISON TABLE

| <u>DESIGN PARAMETERS</u>   | <u>BYRON AND BRAIDWOOD<br/>UNITS 1 &amp; 2</u> | <u>PRESENT DESIGN</u> |
|--|--|-----------------------|
| Reactor Core Heat Output (100%), Mwt                                 | 3411   | 3411                  |
| Reactor core Heat Output, $10^6$ But/hr                              | 11641.7  | 11641.7               |
| Heat Generated in Fuel, %  | 97.4   | 97.4                  |
| System Pressure, Nominal, psia <sup>(2)</sup>                        | 2250   | 2280                  |
| System Pressure, Minimum Steady-State, psia <sup>(2)</sup>           | 2220   | 2250                  |
| Minimum DNBR at Nominal Conditions <sup>(1)</sup>                    |  |                       |
| Typical Flow Channel   | 2.09   | 2.43                  |
| Thimble (Cold Wall) Flow Channel                                     | 1.74   | 2.29                  |
| Minimum DNBR for Design Transients <sup>(1)</sup>                    |  |                       |
| Typical Flow Channel   | $\geq 1.30$                                    | $\geq 1.85$           |
| Thimble Flow Channel   | $\geq 1.30$                                    | $\geq 1.82$           |
| DNB Correlation  | "R" (W-3 with<br>Modified Spacer Factor)       | WRB-1                 |
| <u>COOLANT FLOW</u>  |  |                       |
| Total Thermal Flow Rate, $10^6$ lb <sub>m</sub> /hr                  | 138.6  | 143.5                 |
| Effective Flow Rate for Heat<br>Transfer, $10^6$ lb <sub>m</sub> /hr | 132.4  | 137.3                 |
| Effective Flow Area for Heat<br>Transfer <sup>2</sup>                | 51.1   | 54.1                  |

4.4-58

612 332

TABLE 4.4-1 (Continued)

| <u>DESIGN PARAMETERS</u>  | <u>BYRON AND BRAIDWOOD<br/>UNITS 1 &amp; 2</u> | <u>PRESENT DESIGN</u> |
|---|--|-----------------------|
| Average Velocity Along Fuel<br>Rods, ft/sec                       | 16.4   | 16.1                  |
| Average Mass Velocity, $10^6$ lb <sub>m</sub> /hr-ft <sup>2</sup> | 2.59   | 2.54                  |
| <u>COOLANT TEMPERATURE</u>  |  |                       |
| Nominal Inlet, °F   | 556.9  | 562.5                 |
| Average Rise in Vessel, °F  | 61.1   | 58.3                  |
| Average Rise in Core, °F  | 63.6   | 60.6                  |
| Average in Core, °F   | 590.4  | 594.4                 |
| Average in Vessel, °F   | 587.4  | 593.1                 |
| <u>HEAT TRANSFER</u>  |  |                       |
| Active Heat Transfer, Surface Area, ft <sup>2</sup>               | 59,700   | 57,500                |
| Average Heat Flux, Btu/hr-ft <sup>2</sup>                         | 189,800  | 197,200               |
| Maximum Heat Flux for Normal<br>Operation, Btu/hr-ft <sup>2</sup> | 440,300  | 457,500               |
| Average Linear Power, kW/ft                                       | 5.44   | 5.44                  |
| Peak Linear Power for Normal<br>Operation, kW/ft <sup>(*)</sup>   | 12.6   | 12.6                  |

4.4-59

612  
333

TABLE 4.4-1 (Continued)

| <u>DESIGN PARAMETERS</u>  | <u>BYRON AND BRAIDWOOD<br/>UNITS 1 &amp; 2</u> | <u>PRESENT DESIGN</u> |
|---|--|-----------------------|
| Peak Linear Power Resulting from Overpower Transients/Operator Errors (assuming a maximum overpower of 118%), kW/ft <sup>(**)</sup> | 18.0   | 18.0                  |
| Peak Linear Power for Prevention of Centerline Melt, kW/ft <sup>(***)</sup>   | > 18.0   | > 18.0                |
| Power Density, kW per liter of core <sup>(+)</sup>  | 104.5  | 104.5                 |
| Specific Power, kW per kg Uranium <sup>(+)</sup>  | 38.4   | 41.9                  |
| <u>FUEL CENTRAL TEMPERATURE</u>   |  |                       |
| Peak at Peak Linear Power for Prevention of Centerline Melt, °F   | 4700   | 4700                  |
| Pressure Drop <sup>(++)</sup>   |  |                       |
| Across Core, psi  | 26.9 ± 2.7 <sup>+++</sup>                      | 26.2 ± 2.6            |
| Across Vessel, including nozzle psi   | 47.4 ± 4.7 <sup>+++</sup>                      | 46.4 ± 4.6            |

\* This limit is associated with the value of  $F_Q = 2.32$   
 \*\* See Subsection 4.3.2.2.6.  
 \*\*\* See Subsection 4.4.2.11.6.  
 + Based on cold dimensions and 95% of theoretical density fuel  
 ++ Based on best estimate reactor flow rate as discussed in Section 5.1  
 +++ Pressure Drops updated based on results from Reference 5.  
 (1) These numbers are not directly comparable for each plant design due to the incorporation of a different thermal design procedure and DNB correlation in the present core.  
 (2) Values used for thermal hydraulic core anal.

4.4-60

612 334

TABLE 4.4-2

THERMAL-HYDRAULIC DESIGN PARAMETERS FOR  
ONE OF FOUR COOLANT LOOPS OUT OF SERVICE

|  | <u>BYRON &amp; BRAIDWOOD</u><br><u>UNITS 1 &amp; 2</u> | <u>PRESENT DESIGN</u>        |
|--|--|------------------------------|
| Total Core Heat Output, Mwt  | 2560   | 2385                         |
| Total Core Heat Output, $10^6$ Btu/hr  | 8737.3   | 8153.7                       |
| Heat Generated in Fuel, %  | 97.4   | 97.4                         |
| Nominal System Pressure, psia  | 2250   | 2280                         |
| Coolant Flow   |  |                              |
| Effective Thermal Flow Rate for<br>Heat Transfer, $10^6$ lb <sub>m</sub> /hr | 105.2  | 99.6                         |
| Effective Flow Area for Heat<br>Transfer, ft <sup>2</sup>                    | 51.1   | 54.1                         |
| Average Velocity along Fuel<br>Rods, ft/sec                                  | 12.9   | 11.7                         |
| Average Mass Velocity, $10^6$<br>lb <sub>m</sub> /hr-ft <sup>2</sup>         | 2.06   | 1.84                         |
| Coolant Temperature, °F  |  |                              |
| Design Nominal Inlet   | 552.3  | 560.9                        |
| Average Rise in Core   | 61.3   | 59.0                         |
| Average in Core  | 584.4  | 591.9                        |
| Heat Transfer  |  |                              |
| Active Heat Transfer Surface Area ft <sup>2</sup>                            | 59,700   | 57,500                       |
| Average Heat Flux, Btu/hr-ft <sup>2</sup>                                    | 142,400  | 138,100                      |
| Minimum DNB Ratio at Nominal Conditions                                      | > 1.74   | > 2.7                        |
| Minimum DNB Ratio for Design and<br>Anticipated Transients                   | ≥ 1.30   | > 1.85 (TYP)<br>> 1.82 (THM) |

TABLE 4.4-3

VOID FRACTIONS AT NOMINAL REACTOR CONDITIONS  
WITH DESIGN HOT CHANNEL FACTORS

|                | <u>AVERAGE</u> | <u>MAXIMUM</u> |
|----------------|----------------|----------------|
| Core           | 0.3            | -              |
| Hot Subchannel | 4.0            | 15.4           |

612-336

TABLE 4.4-1 (Sheet of 1 of 3)

THERMAL AND HYDRAULIC COMPARISON TABLE

| <u>DESIGN PARAMETERS</u>   | <u>McGUIRE</u>                           | <u>PRESENT DESIGN</u> |
|--|--|-----------------------|
| Reactor Core Heat Output (100%), Mwt                                 | 3411                                     | 3411                  |
| Reactor core Heat Output, $10^6$ But/hr                              | 11641.7                                  | 11641.7               |
| Heat Generated in Fuel, %  | 97.4                                     | 97.4                  |
| System Pressure, Nominal, psia <sup>(2)</sup>                        | 2250                                     | 2280                  |
| System Pressure, Minimum Steady-State, psia <sup>(2)</sup>           | 2220                                     | 2250                  |
| Minimum DNBR at Nominal Conditions <sup>(1)</sup>                    |  |                       |
| Typical Flow Channel   | 2.05                                     | 2.4                   |
| Thimble (Cold Wall) Flow Channel                                     | 1.72                                     | 2.26                  |
| Minimum DNBR for Design Transients <sup>(1)</sup>                    |  |                       |
| Typical Flow Channel   | $\geq 1.3$                               | $\geq 1.49$           |
| Thimble Flow Channel   | $\geq 1.3$                               | $\geq 1.47$           |
| DNB Correlation  | "R" (W-3 with<br>Modified Spacer Factor) | WRB-1                 |
| <u>COOLANT FLOW</u>  |  |                       |
| Total Thermal Flow Rate, $10^6$ lb <sub>m</sub> /hr                  | 144.7                                    | 143.3                 |
| Effective Flow Rate for Heat<br>Transfer, $10^6$ lb <sub>m</sub> /hr | 133.9                                    | 134.7                 |
| Effective Flow Area for Heat<br>Transfer, ft <sup>2</sup>            | 51.1                                     | 54.1                  |

4.4-58

6.2 337

BLUE

TABLE 4.4-1 (Continued)

| <u>DESIGN PARAMETERS</u>  | <u>McGUIRE</u> | <u>PRESENT DESIGN</u> |
|---|----------------|-----------------------|
| Average Velocity Along Fuel Rods, ft/sec                          | 16.6           | 15.8                  |
| Average Mass Velocity, $10^6$ lb <sub>m</sub> /hr-ft <sup>2</sup> | 2.62           | 2.49                  |
| <u>COOLANT TEMPERATURE</u>  |                |                       |
| Nominal Inlet, °F   | 559.1          | 561.6                 |
| Average Rise in Vessel, °F  | 58.4           | 58.5                  |
| Average Rise in Core, °F  | 62.5           | 61.8                  |
| Average in Core, °F   | 590.4          | 594.2                 |
| Average in Vessel, °F   | 588.3          | 592.3                 |
| <u>HEAT TRANSFER</u>  |                |                       |
| Active Heat Transfer, Surface Area, ft <sup>2</sup>               | 59,700         | 57,500                |
| Average Heat Flux, Btu/hr-ft <sup>2</sup>                         | 189,800        | 197,200               |
| Maximum Heat Flux for Normal Operation, Btu/hr-ft <sup>2</sup>    | 440,300        | 457,500               |
| Average Linear Power, kW/ft                                       | 5.44           | 5.44                  |
| Peak Linear Power for Normal Operation, kW/ft <sup>(*)</sup>      | 12.6           | 12.6                  |

612 338

4.4-59

BLUE



TABLE 4.4-1 (Continued)

| <u>DESIGN PARAMETERS</u>  | <u>McGUIRE</u>            | <u>PRESENT DESIGN</u> |
|---|---------------------------|-----------------------|
| Peak Linear Power Resulting from Overpower Transients/Operator Errors (assuming a maximum overpower of 118%), kW/ft <sup>(**)</sup> | 18.0                      | 18.0                  |
| Peak Linear Power for Prevention of Centerline Melt, kW/ft <sup>(***)</sup>   | > 18.0                    | > 18.0                |
| Power Density, kW per liter of core <sup>(+)</sup>  | 104.5                     | 104.5                 |
| Specific Power, kW per kg Uranium <sup>(+)</sup>  | 38.4                      | 41.9                  |
| <u>FUEL CENTRAL TEMPERATURE</u>   |                           |                       |
| Peak at Peak Linear Power for Prevention of Centerline Melt, °F   | 4700                      | 4700                  |
| Pressure Drop <sup>(++)</sup>   |                           |                       |
| Across Core, psi  | 25.9 ± 2.6 <sup>+++</sup> | 25.7 ± 2.6            |
| Across Vessel including nozzle psi  | 45.3 ± 4.6 <sup>+++</sup> | 45.7 ± 4.6            |

\* This limit is associated with the value of  $F_Q = 2.32$

\*\* See Subsection 4.3.2.2.6.

\*\*\* See Subsection 4.4.2.11.6.

+ Based on cold dimensions and 95% of theoretical density fuel

++ Based on best estimate reactor flow rate as discussed in Section 5.1

+++ Pressure Drops updated based on results from Reference 5.

(1) These numbers are not directly comparable for each plant design due to the incorporation of a different thermal design procedure and DNB correlation in the present core.

(2) Values used for thermal hydraulic core analysis.

TABLE 4.4-2

THERMAL-HYDRAULIC DESIGN PARAMETERS FOR  
ONE OF FOUR COOLANT LOOPS OUT OF SERVICE

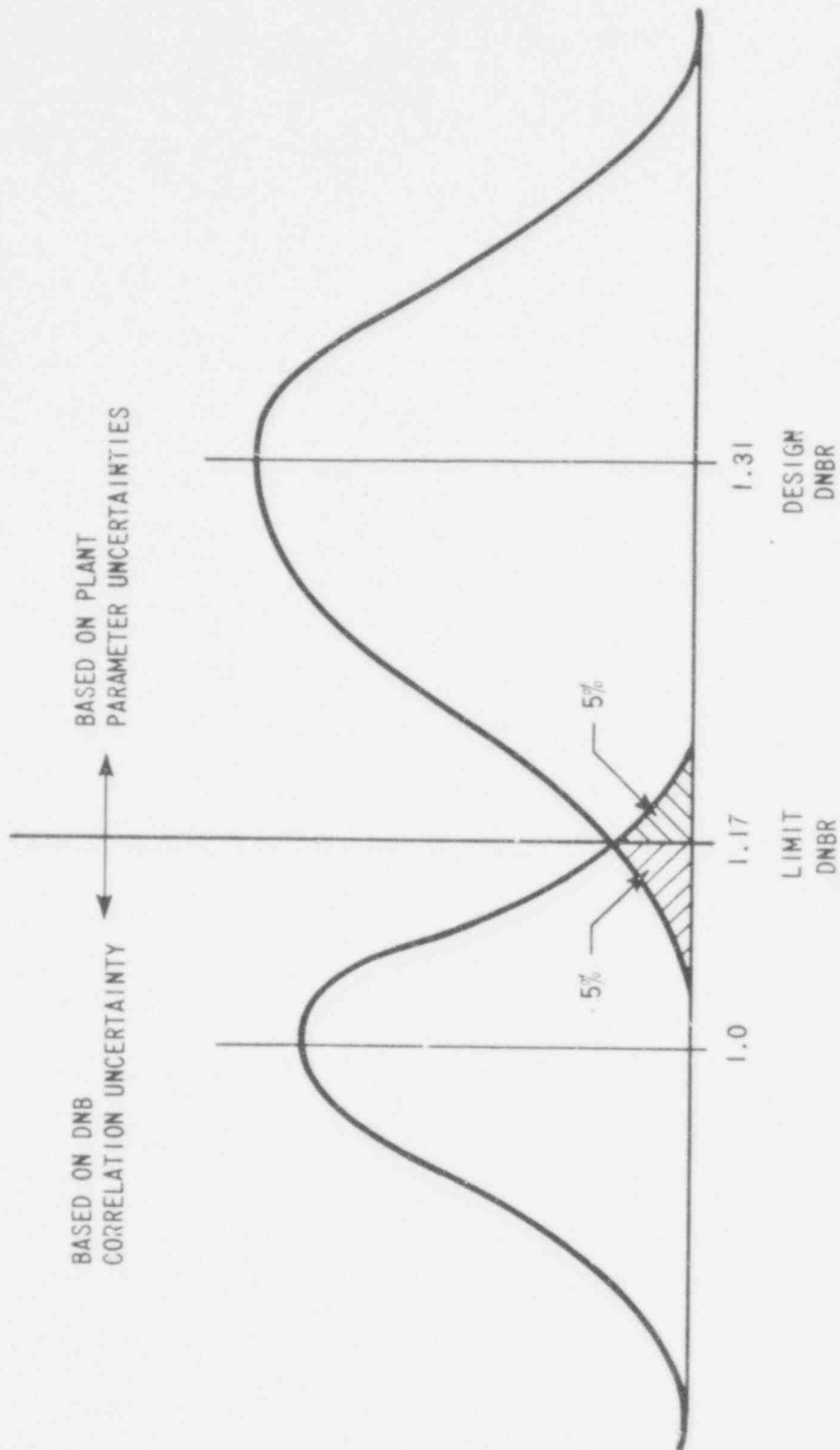
|  | <u>McGUIRE</u> | <u>PRESENT DESIGN</u>        |
|--|----------------|------------------------------|
| Total Core Heat Output, MWt  | 2389           | 2389                         |
| Total Core Heat Output, $10^6$ Btu/hr  | 8154           | 8154                         |
| Heat Generated in Fuel, %  | 97.4           | 97.4                         |
| Nominal System Pressure, psia  | 2250           | 2280                         |
| Coolant Flow   |                |                              |
| Effective Thermal Flow Rate for<br>Heat Transfer, $10^6$ lb <sub>m</sub> /hr | 96.4           | 98.7                         |
| Effective Flow Area for Heat<br>Transfer, ft <sup>2</sup>                    | 51.1           | 54.1                         |
| Average Velocity along Fuel<br>Rods, ft/sec                                  | 11.8           | 11.4                         |
| Average Mass Velocity, $10^6$<br>lb <sub>m</sub> /hr-ft <sup>2</sup>         | 1.89           | 1.82                         |
| Coolant Temperature, °F  | 551.7          | 554.5                        |
| Design Nominal Inlet   |                |                              |
| Average Rise in Core   | 62.3           | 60.7                         |
| Average in Core  | 584.4          | 586.3                        |
| Heat Transfer  |                |                              |
| Active Heat Transfer Surface Area ft <sup>2</sup>                            | 59,700         | 57,505                       |
| Average Heat Flux, Btu/hr-ft <sup>2</sup>                                    | 132,900        | 138,100                      |
| Minimum DNB Ratio at Nominal Conditions                                      | > 1.74         | > 2.79                       |
| Minimum DNB Ratio for Design and<br>Anticipated Transients                   | ≥ 1.3          | > 1.49 (TYP)<br>> 1.47 (THM) |

612 340

TABLE 4.4-3

VOID FRACTIONS AT NOMINAL REACTOR CONDITIONS  
WITH DESIGN HOT CHANNEL FACTORS

|                | <u>AVERAGE</u> | <u>MAXIMUM</u> |
|----------------|----------------|----------------|
| Core           | 0.4            | -              |
| Hot Subchannel | 4.4            | 16.6           |



WCAP - 9500

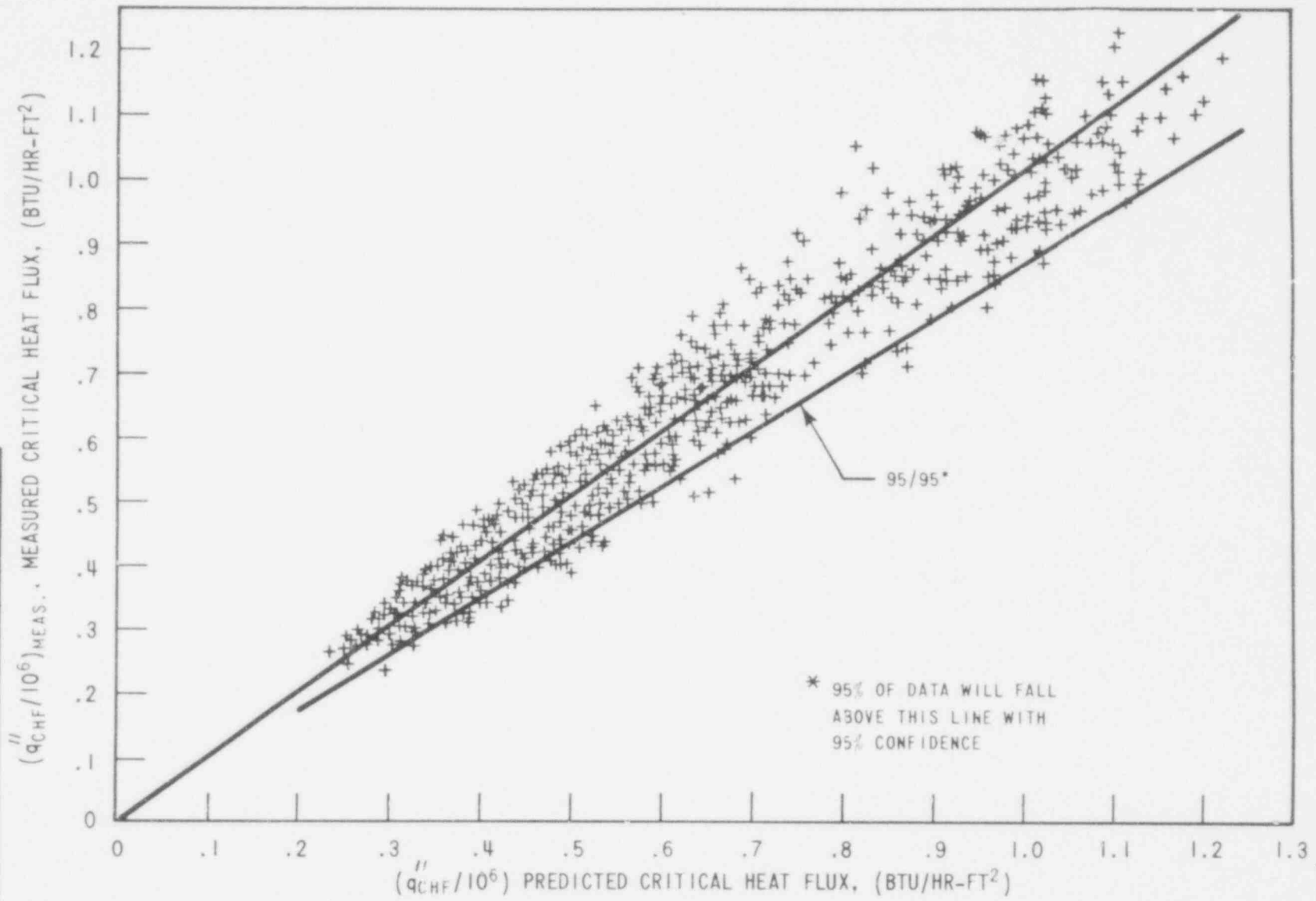
Figure 4.4-1.

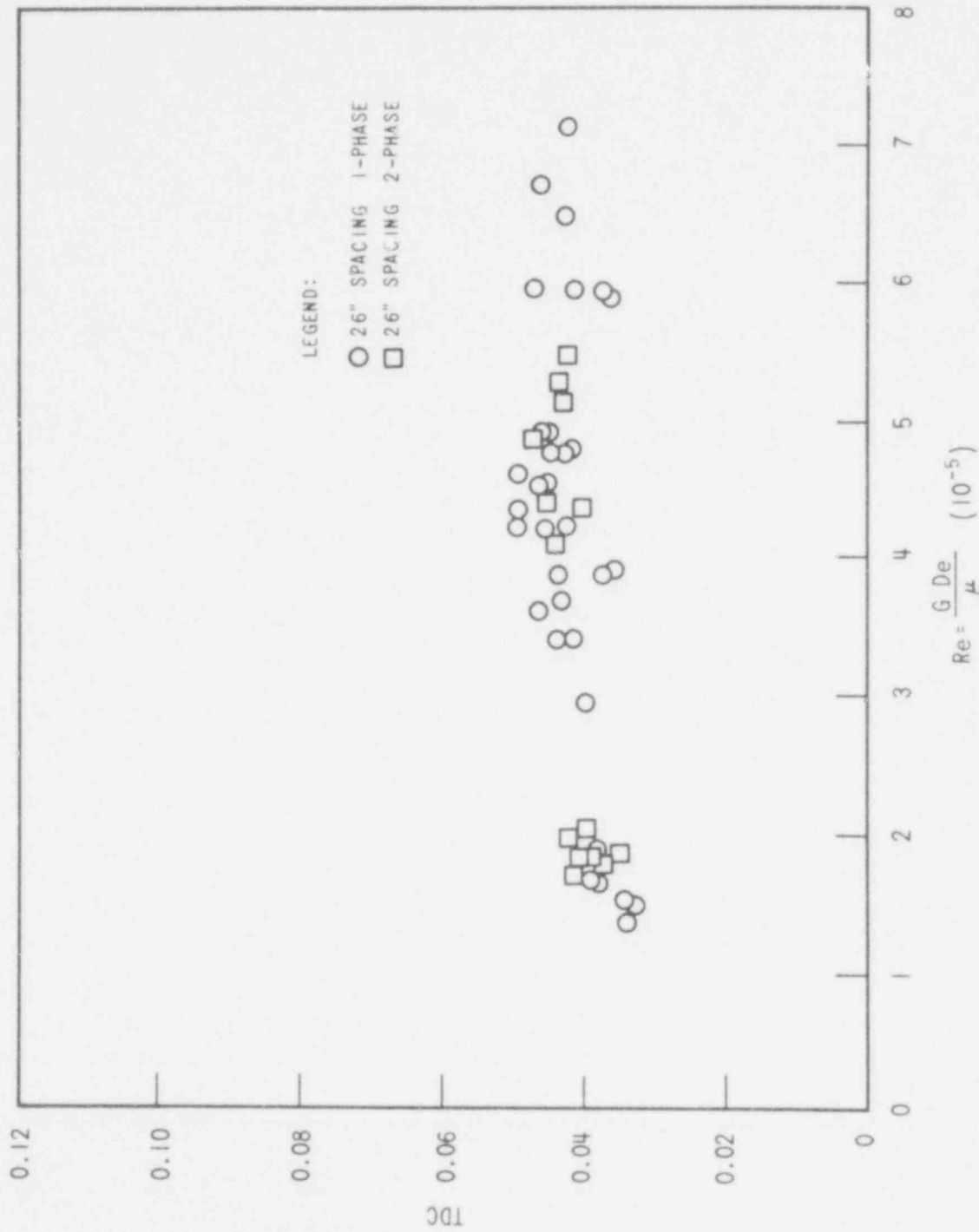
Improved Thermal Design Procedure Illustration

612 342

612 343

WCAP - 9500  
Figure 4.4-2.  
Measured versus Predicted Critical Heat Flux -  
WRB-1 Correlation





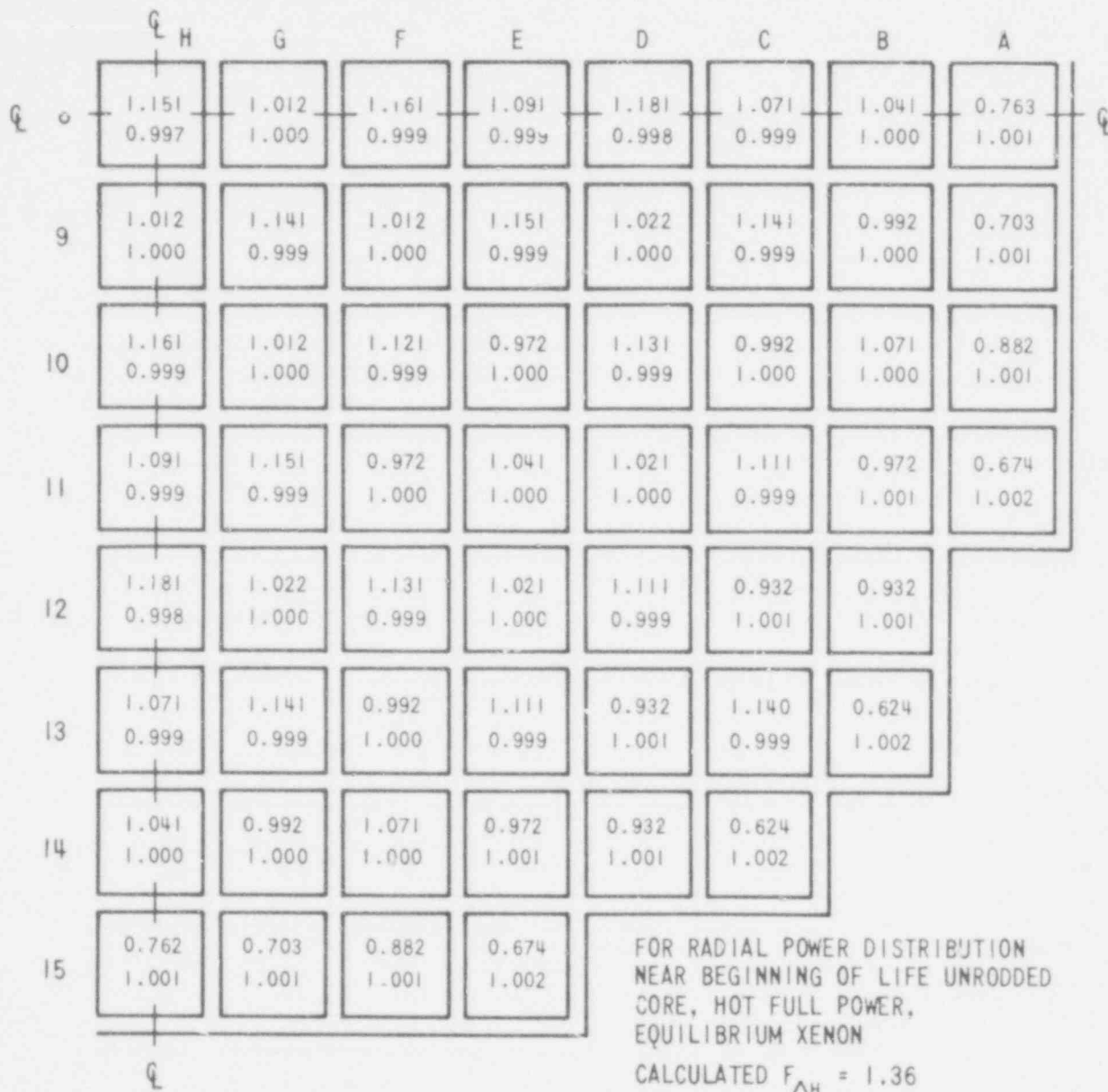
WCAP - 9500

Figure 4.4.3.

TDC versus Reynolds Number for  
26" Grid Spacing

612 344

KEY:  
 $\Delta H / \Delta \bar{H}$   
 $G / \bar{G}$



WCAP - 9500

Figure 4.4-4.

Normalized Radial Flow and  
 Enthalpy Rise Distribution at  
 4 FT Elevation

612 345

KEY:  
 $\frac{\Delta H / \Delta \bar{H}}{G / \bar{G}}$

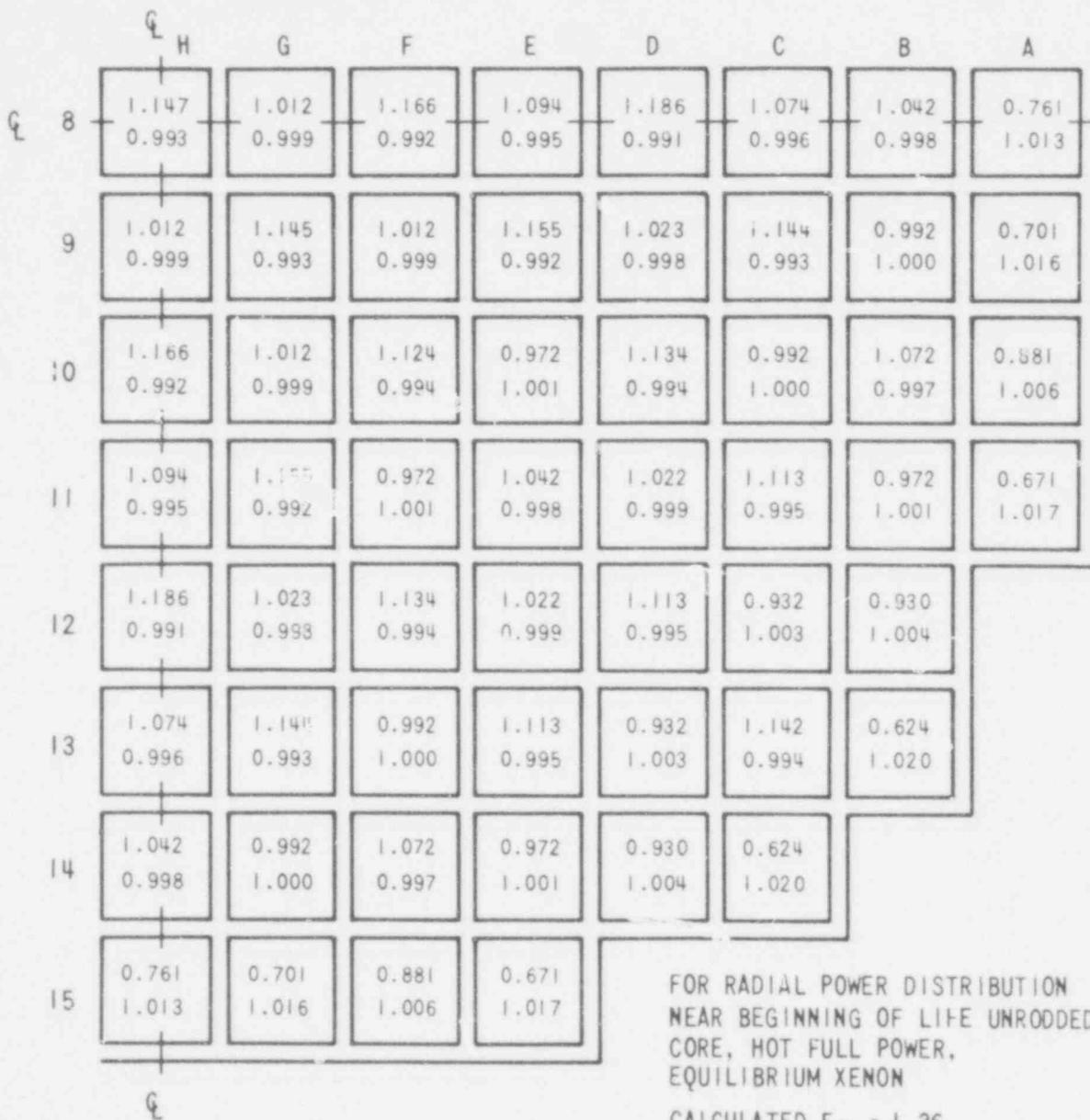
|    | H              | G              | F              | E              | D  | C              | B              | A              |
|----|----------------|----------------|----------------|----------------|--|----------------|----------------|----------------|
| 8  | 1.146<br>0.994 | 1.012<br>1.000 | 1.163<br>0.993 | 1.093<br>0.997 | 1.184<br>0.992   | 1.073<br>0.998 | 1.042<br>0.999 | 0.762<br>1.009 |
| 9  | 1.012<br>1.000 | 1.143<br>0.994 | 1.012<br>1.000 | 1.153<br>0.994 | 1.022<br>1.000   | 1.143<br>0.994 | 0.992<br>1.001 | 0.702<br>1.011 |
| 10 | 1.163<br>0.993 | 1.012<br>1.000 | 1.122<br>0.995 | 0.72<br>1.001  | 1.132<br>0.995   | 0.992<br>1.001 | 1.072<br>0.998 | 0.882<br>1.004 |
| 11 | 1.093<br>0.997 | 1.153<br>0.994 | 0.972<br>1.001 | 1.041<br>0.999 | 1.022<br>1.000   | 1.112<br>0.999 | 0.972<br>1.001 | 0.673<br>1.012 |
| 12 | 1.184<br>0.992 | 1.022<br>1.000 | 1.132<br>0.995 | 1.022<br>1.000 | 1.112<br>0.996   | 0.932<br>1.002 | 0.931<br>1.003 |                |
| 13 | 1.073<br>0.998 | 1.143<br>0.994 | 0.992<br>1.001 | 1.112<br>0.996 | 0.932<br>1.002   | 1.142<br>0.994 | 0.624<br>1.014 |                |
| 14 | 1.042<br>0.999 | 0.992<br>1.001 | 1.072<br>0.998 | 0.972<br>1.001 | 0.931<br>1.003   | 0.624<br>1.014 |                |                |
| 15 | 0.762<br>1.009 | 0.702<br>1.011 | 0.882<br>1.004 | 0.673<br>1.012 | FOR RADIAL POWER DISTRIBUTION<br>NEAR BEGINNING OF LIFE UNRODDED<br>CORE, HOT FULL POWER,<br>EQUILIBRIUM XENON<br><br>CALCULATED $F_{\Delta H} = 1.36$ |                |                |                |

WCAP - 9500  
 Figure 4.4-5.  
 Normalized Radial Flow and  
 Enthalpy Rise Distribution at  
 8 FT Elevation

612 346



KEY:  
 $\Delta H / \Delta \bar{H}$   
 $G / \bar{G}$

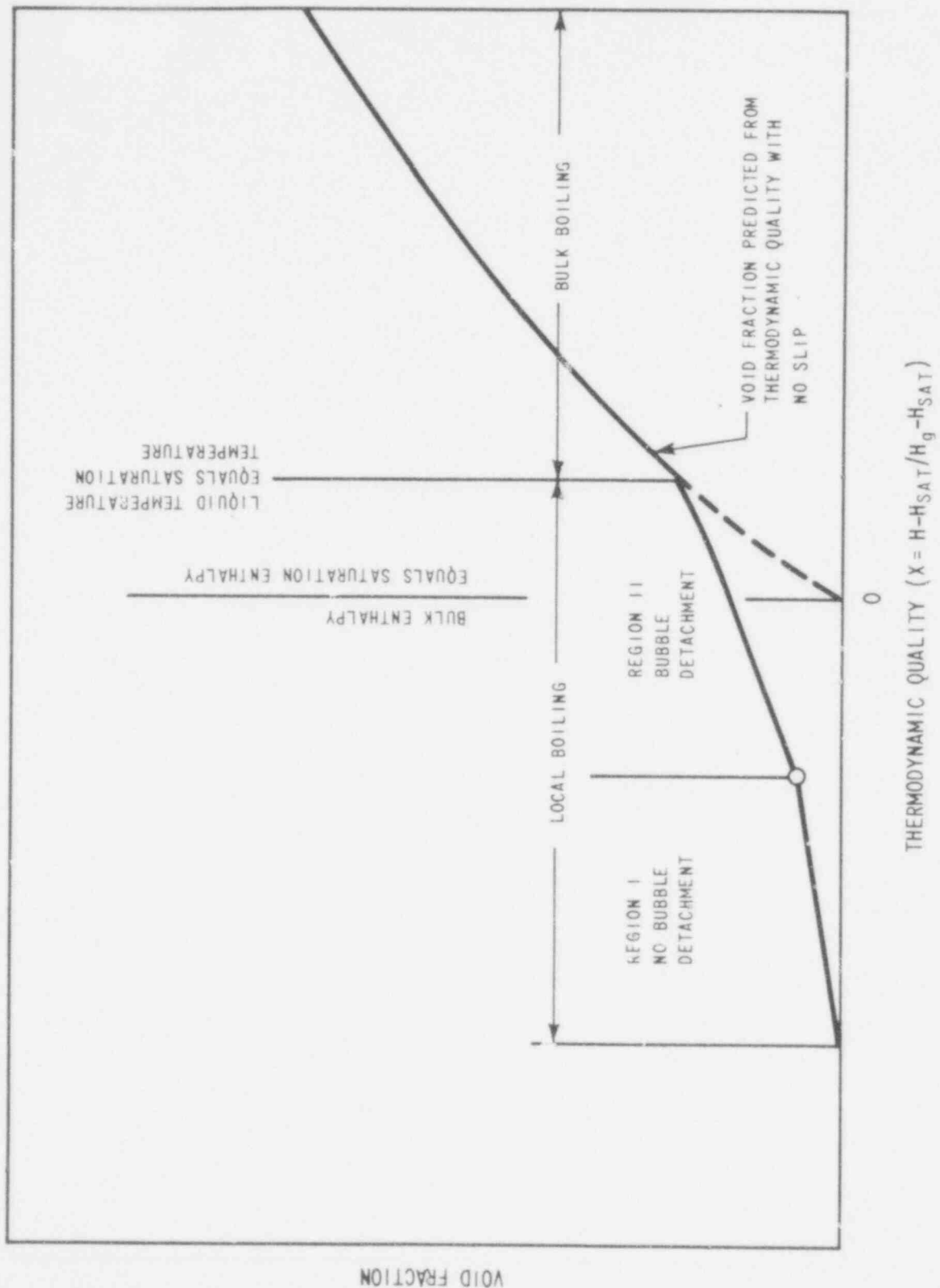


WCAP - 9500

Figure 4.4-6.

Normalized Radial Flow and  
 Enthalpy Rise Distribution at  
 12 FT Elevation

112 347



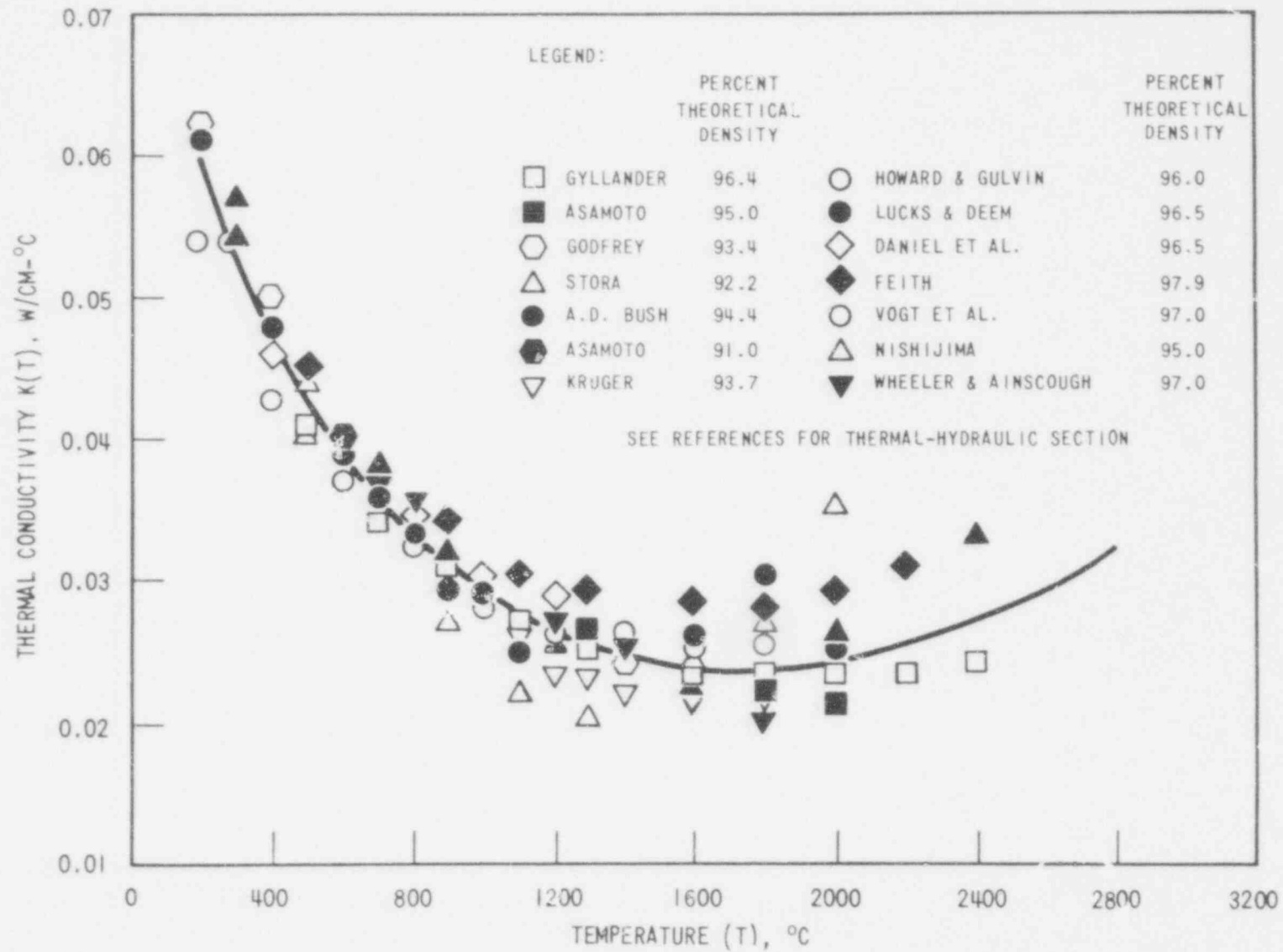
612 348

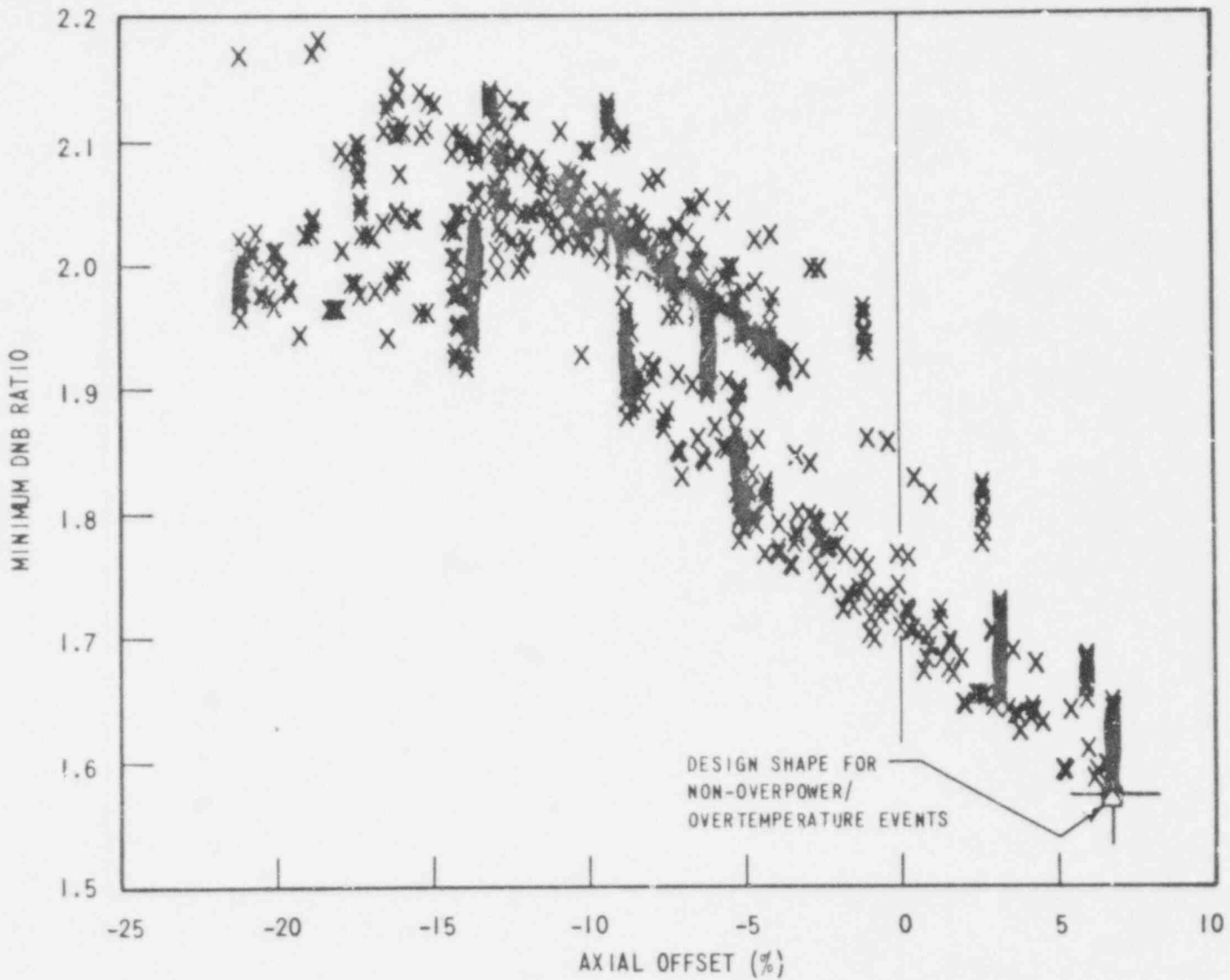
WCAP - 9500

Figure 4.4-7.  
 Void Fraction versus Thermodynamic Quality  
 $\frac{H - H_{SAT}}{H_g - H_{SAT}}$

612  
3A9

WCAP - 9500  
Figure 4.4.8.  
Thermal Conductivity of  $UO_2$   
(Data Corrected to 95%  
Theoretical Density)





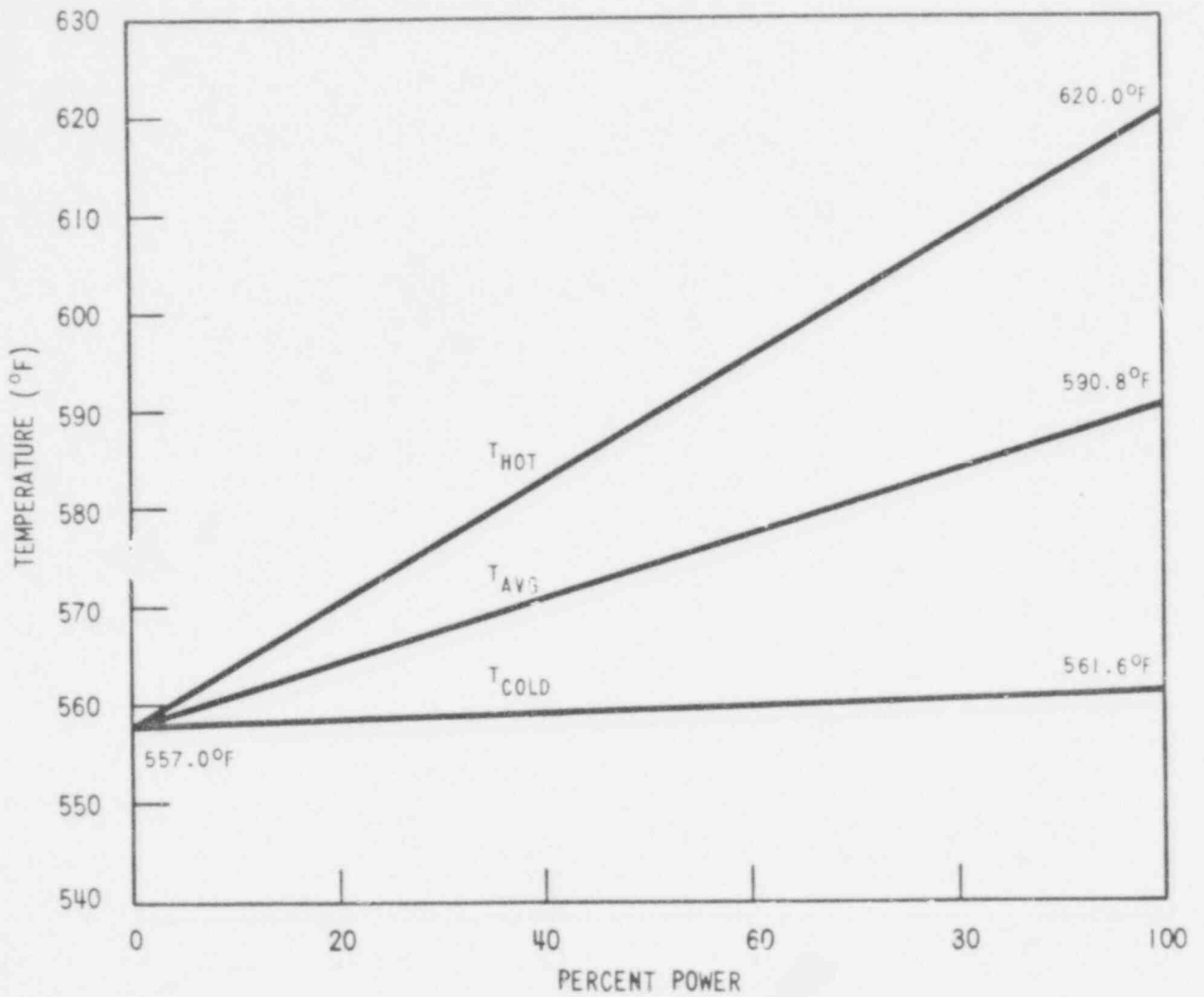
WCAP - 9500

Figure 4.4-11

100 Percent Power Shapes Evaluated at Conditions  
 Representative of Loss of Flow all Shapes  
 Evaluated with  $F_{NH} = 1.49$

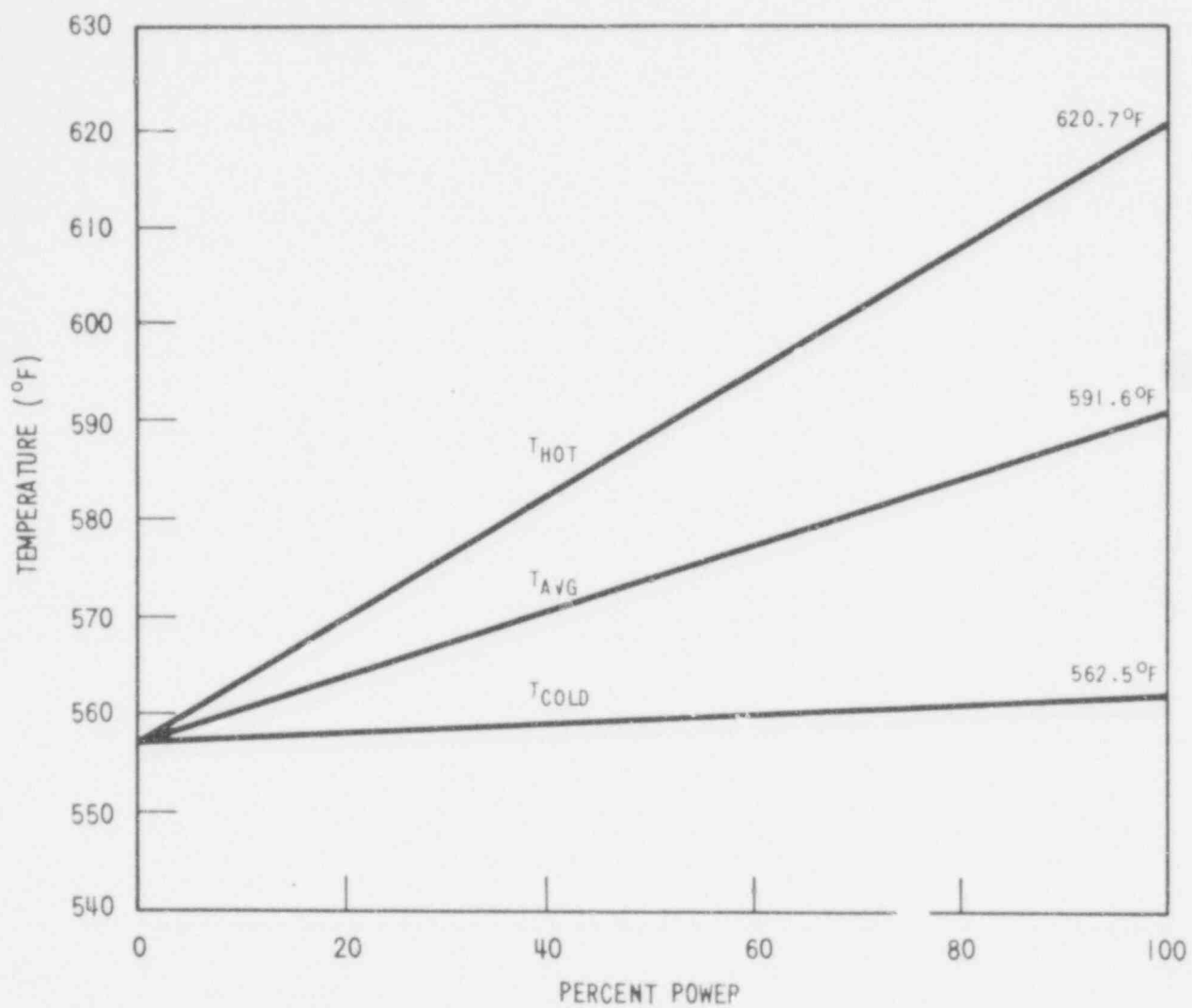
BLUE

612 350



612 351

|   |
|---|
| WCAP - 9500   |
| Figure 4.4-9  |
| Reactor Coolant System Temperature<br>Percent Power Map |
| BLUE  |

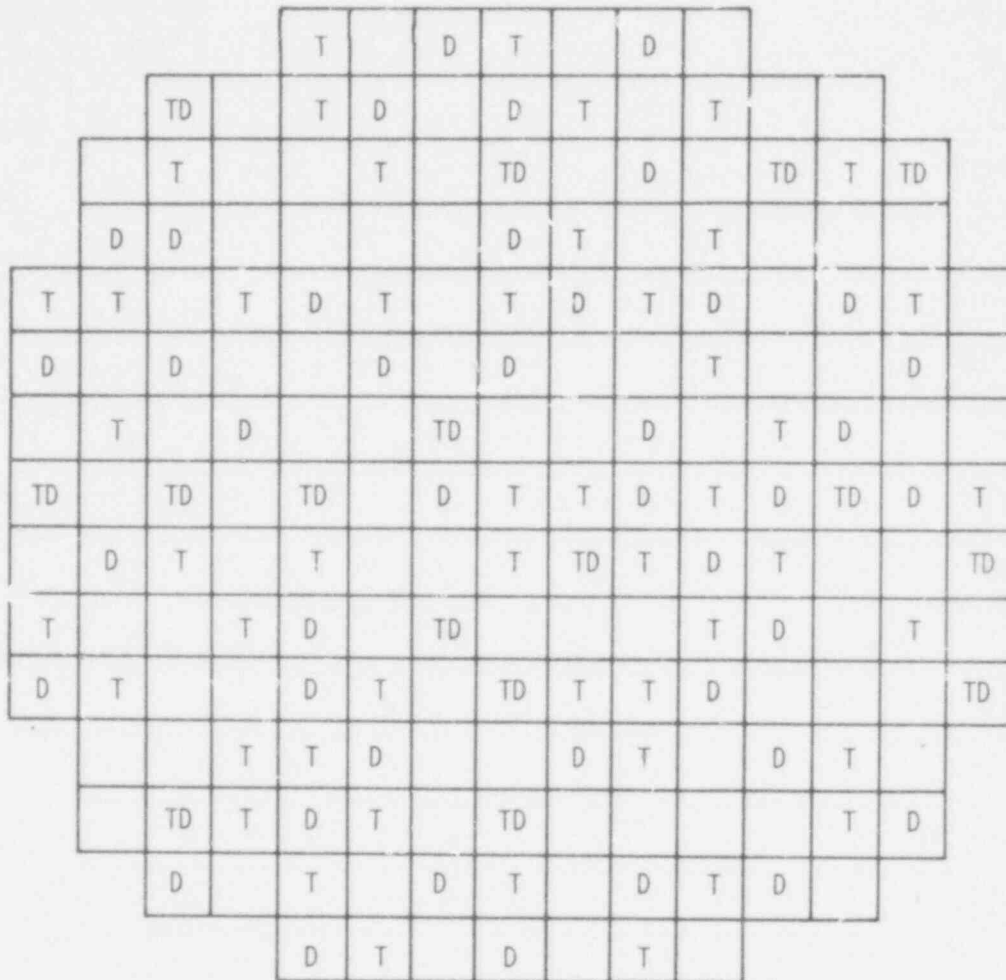


WCAP - 9500

Figure 4.4-9

Reactor Coolant System Temperature  
Percent Power Map

612 352



T = THERMOCOUPLE (65)

D = MOVABLE INCORE DETECTOR (58 LOCATIONS)

612 353

|   |
|---|
| WCAP - 9500   |
| Figure 4.4-10<br>Distribution of Incore Instrumentation |

4.5

612 354



## 4.5 REACTOR MATERIALS

### Note:

Sections 4.5 Reactor Materials and 4.6 Functional Design of Reactivity Control Systems have been incorporated to the present report to provide the complete information usually included in Chapter 4 of a Final Safety Analysis Report.

Each particular plant licensing application referencing the present report will include a more detailed evaluation of the reactor materials and reactivity control systems and will indicate the degree of conformance with the recommendations of the applicable Regulatory Guides. This information is usually presented in the Final Safety Analysis Report as follows:

- Control Rod Drive Mechanism and Reactor Internals: Chapter 3
- Control Rod Drive Mechanism Testing: Chapters 3, 14 and 16.
- Control Rod Drive Mechanism and Reactor Internals Materials: Chapter 5.
- Safety Injection System: Chapter 6
- Instrumentation for Reactor Control and Protection: Chapter 7
- Failure of the Control Rod Drive Mechanism Cooling System and Chemical and Volume Control System: Chapter 9.

### 4.5.1 CONTROL ROD SYSTEM STRUCTURAL MATERIALS

#### 4.5.1.1 Materials Specifications

All parts exposed to reactor coolant are made of metals which resist the corrosive action of the water. Three types of metals are used exclusively: stainless steels, nickel-chromium-iron, and cobalt based alloys. In the case of stainless steels, only austenitic and martensitic stainless steels are used. The martensitic stainless steels are

612 355

not used in the heat treated conditions which cause susceptibility to stress corrosion cracking or accelerated corrosion in the Westinghouse pressurized water reactor water chemistry.

1. Pressure vessel

All pressure containing materials comply with Section III of the ASME Boiler and Pressure Vessel Code, and are fabricated from austenitic (Type 304) stainless steel.

2. Coil stack assembly

The coil housings require a magnetic material. Both low carbon cast steel and ductile iron have been successfully tested for this application. The choice, made on the basis of cost and performance, indicates that ductile iron will be specified on the control rod drive mechanism (CRDM). The finished housings are zinc plated or flame sprayed to provide corrosion resistance.

Coils are wound on bobbins of molded Dow Corning 302 material, with double glass insulated copper wire. Coils are then vacuum impregnated with silicon varnish. A wrapping of mica sheet is secured to the coil outside diameter. The result is a well insulated coil capable of sustained operation at 200 C.

3. Latch assembly

Magnetic pole pieces are fabricated from Type 410 stainless steel. All nonmagnetic parts, except pins and springs, are fabricated from Type 304 stainless steel. Haynes 25 is used to fabricate link pins. Springs are made from nickel-chromium-iron alloy (Inconel-750). Latch arm tips are clad with Stellite-6 to provide improved wearability. Hard chrome plate and Stellite-6 are used selectively for bearing and wear surfaces.

612  
356

#### 4. Drive rod assembly

The drive rod assembly utilizes a Type 410 stainless steel drive rod and disconnect rod assembly. The coupling is machined from Type 403 stainless steel. Other parts are Type 304 stainless steel with the exception of the springs, which are nickel-chromium-iron alloy, and the locking button, which is Haynes 25; and the Belleville washers which are Inconel 718. Several small parts (screws and pins) are Inconel 600.

Material specifications for Class 1 components of the CRDM are as follows:

|                    |  |
|--------------------|--|
| CRDM, upper head   | SB-166 or SB-167 and SA-182<br>Grade F304  |
| Latch housing      | SA-182, Grade F304 or SA-351<br>Grade CF8  |
| Rod travel housing | SA-182, Grade F304 or SA-336<br>Class F8   |
| Cap                | SA-479, Type 304                           |
| Welding materials  | Stainless Steel Weld Metal<br>Analysis A-8 |

#### 4.5.1.2 Austenitic Stainless Steel Components

1. All austenitic stainless steel materials used in the fabrication of CRDM components are processed, inspected and tested to avoid sensitization and prevent intergranular stress corrosion cracking.

The rules covering these controls are stipulated in Westinghouse process specifications. As applicable, these process specifications

supplement the equipment specifications and purchase order requirements of every individual austenitic stainless steel component regardless of the ASME Code classification.

Westinghouse practice is that austenitic stainless steel materials of product forms with simple shapes need not be corrosion tested provided that the solution heat treatment is followed by water quenching. Simple shapes are defined as all plates, sheets, bars, pipe and tubes, as well as forgings, fittings and other shaped products which do not have inaccessible cavities or chambers that would preclude rapid cooling when water quenched. When testing is required the tests are performed in accordance with ASTM A 262, Practice A or E, as amended by Westinghouse Process Specification 84201 MW.

If, during the course of fabrication the steel is inadvertently exposed to the sensitization temperature range, 800 to 1500°F the material may be tested in accordance with ASTM A 262, as amended by Westinghouse Process Specification 84201 MW to verify that it is not susceptible to intergranular attack, except that testing is not required for:

- a. Cast metal or weld metal with a ferrite content of 5 percent or more,
- b. Material with a carbon content of 0.03 percent or less that is subjected to temperatures in the range of 800 to 1,500 F for less than 1 hour.
- c. Material exposed to special processing provided the processing is properly controlled to develop a uniform product and provided that adequate documentation exists of service experience and/or test data to demonstrate that the processing will not result in increased susceptibility to intergranular stress corrosion.

If it is not verified that such material is not susceptible to intergranular attack, the material will be re-solution annealed and water quenched or rejected.

2. The welding of austenitic stainless steel is controlled to mitigate the occurrence of microfissuring or hot cracking in the weld.

A minimum delta ferrite level, expressed in Ferrite Number (FN) between 0 FN and 3 FN percent delta ferrite, is specified for reducing the susceptibility of stainless steel welds to hot cracking. The undiluted weld deposits of the starting welding materials are required to contain a minimum of 5 FN.

#### 4.5.1.3 Other Materials

The CRDMs are cleaned prior to delivery in accordance with the guidance of ANSI 45.2.1. Westinghouse personnel do conduct surveillance to ensure that manufacturers and installers adhere to appropriate requirements.

Haynes 25 is used in small quantities to fabricate link pins. The material is ordered in the solution treated and cold worked condition. Stress corrosion cracking has not been observed in this application over the last 15 years.

The CRDM springs are made from nickel-chromium-iron alloy (Inconel-750) ordered to MIL-S-23192 or MIL N-24114 Class A #1 temper drawn wire. Operating experience has shown that springs made of this material are not subject to stress-corrosion cracking.

#### 4.5.1.4 Cleaning and Cleanliness Control

The CRDMs are cleaned prior to delivery in accordance with the guidance of ANSI 45.2.1. Measures are applied, as appropriate, to apply packaging requirements to procurement orders, to review supplier packaging

612 359

procedures, to apply proper cleaning requirements, marking and identification and to provide protection to equipment from physical or weather damage, to apply special handling precautions and to define storage requirements. Westinghouse quality assurance procedures are described in "Westinghouse Water Reactor Divisions Quality Assurance Plan," WCAP-8370, Revision 8A updated per letter NS-TMA-2039, from T. M. Anderson to W. P. Haass, February 8, 1979.

#### 4.5.2 REACTOR INTERNALS MATERIALS

##### 4.5.2.1 Materials Specifications

All the major material for the reactor internals is Type 304 stainless steel. Parts not of fabricated from Type 304 stainless steel include bolts and dowel pins, which are fabricated from Type 316 stainless steel, and radial support key bolts, which are fabricated from Inconel-750.

Material specifications for reactor vessel internals for emergency core cooling systems are as follows:

|          |   |
|----------|---|
| Forgings | SA-182, Grade F304  |
| Plates   | SA-240, Type 304  |
| Pipes    | SA-312, Grade TP304 Seamless<br>or SA-376, Grade TP304  |
| Tubes    | SA-213, Grade TP304   |
| Bars     | SA-479, Type 304 and 410  |
| Castings | SA-351, Grade CF8 and CF8A  |
| Bolting  | SA-193, Grade B8M (65 MYS/90 MTS)<br>Code Case 1618, SA-479, Type 316,<br>strain hardened (code core 1618),<br>Inconel-750; SA-637, Grade 688, Type 2 |

|                   |                               |
|-------------------|-------------------------------|
| Nuts              | SA-194, Grade 1 or 8A         |
| Locking devices   | SA-479, Type 304              |
| Welding Materials | Stainless steel, analysis A-8 |

There are no other materials used in the reactor internals or core support structures which are not otherwise included in ASME Code, Section III, Appendix I.

#### 4.5.2.2 Controls on Welding

The discussions provided in Section 4.5.1 are applicable to the welding of reactor internals and core support components.

#### 4.5.2.3 Nondestructive Examination of Wrought Seamless Tubular Products and Fittings

The nondestructive examination of wrought seamless tubular products and fittings is in accordance with Section III of the ASME Code.

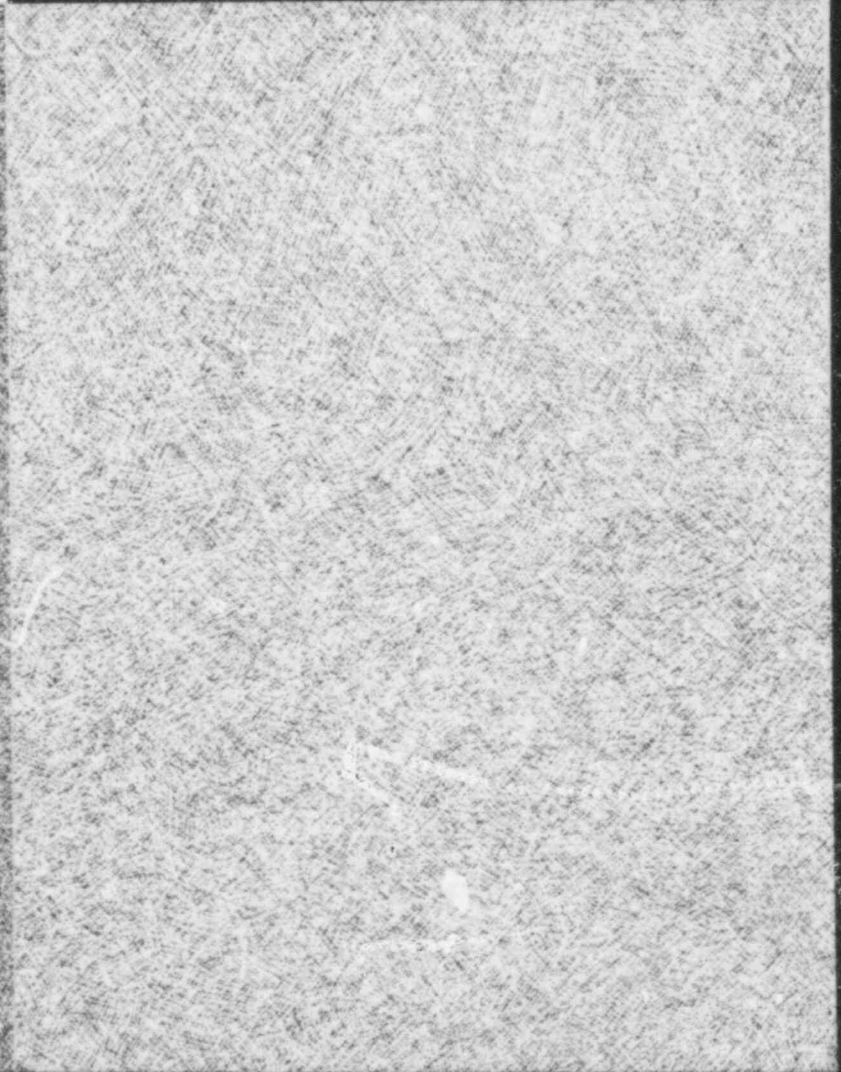
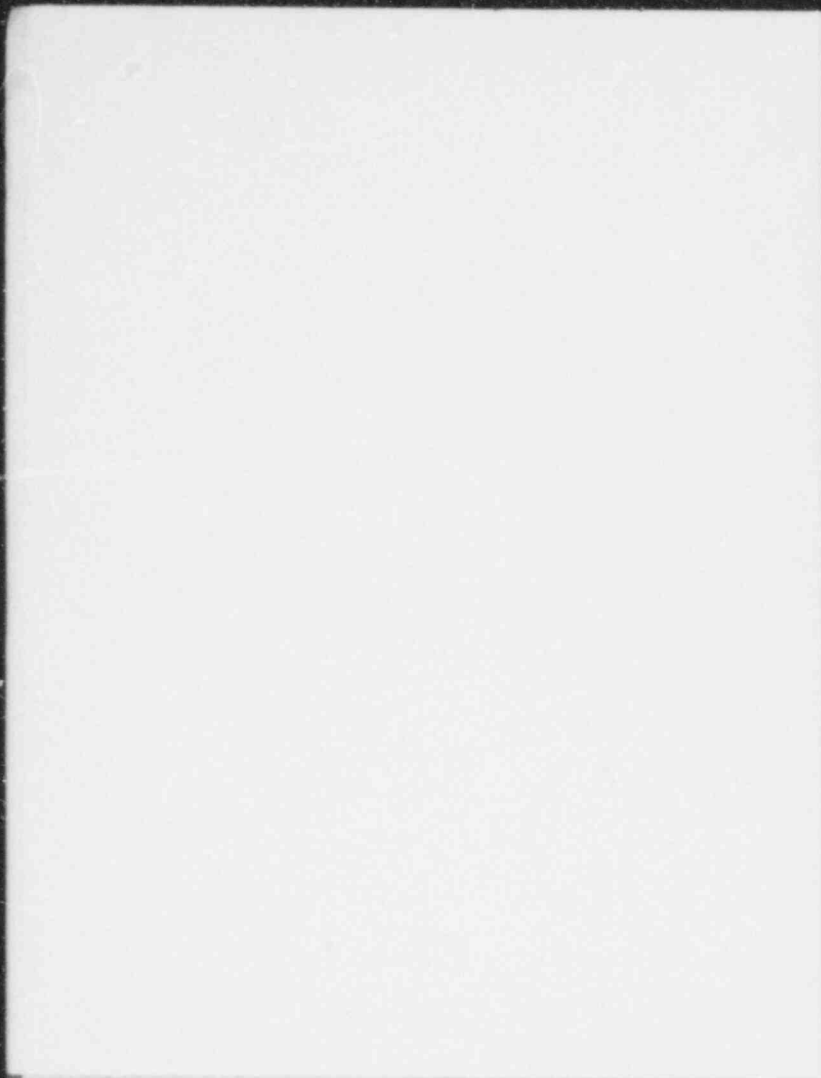
#### 4.5.2.4 Fabrication and Processing of Austenitic Stainless Steel Components

The discussions provided in Section 4.5.1 are applicable to the fabrication and processing of austenitic stainless steel reactor internals components.

#### 4.5.2.5 Contamination Protection and Cleaning of Austenitic Stainless Steel

The discussions provided in Section 4.5.1 are applicable to the cleaning of reactor internals and core support structures.

612 361





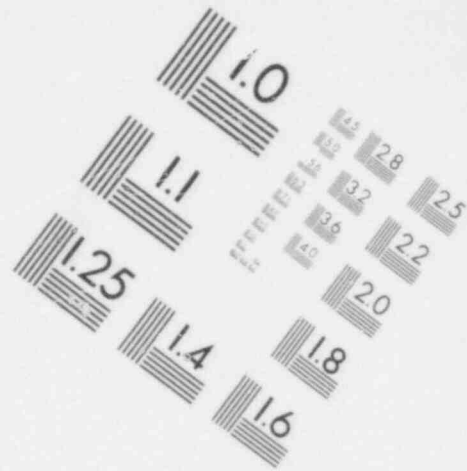
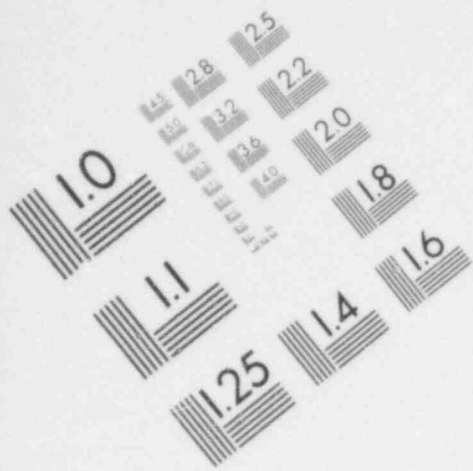
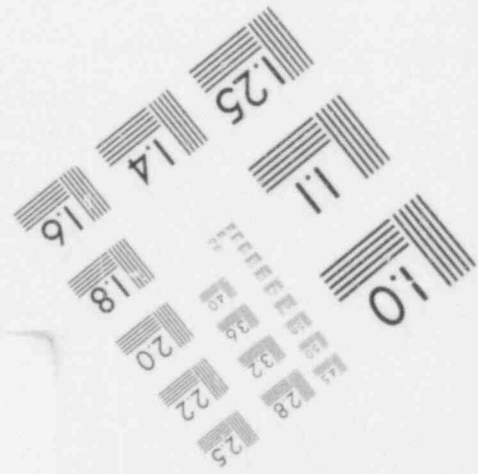
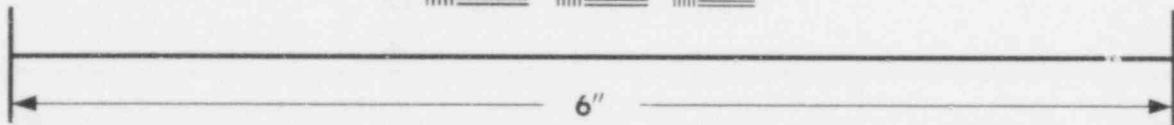
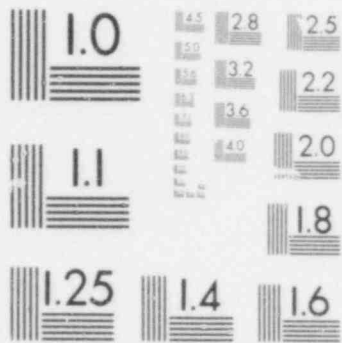


IMAGE EVALUATION  
TEST TARGET (MT-3)



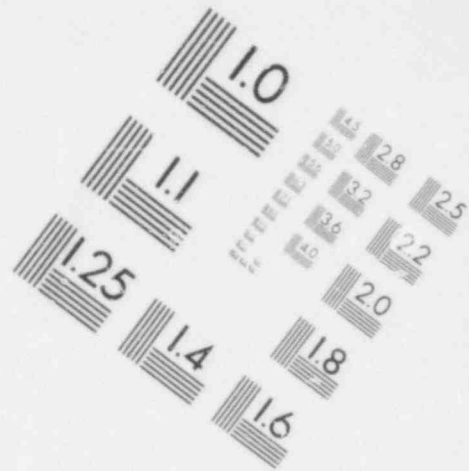
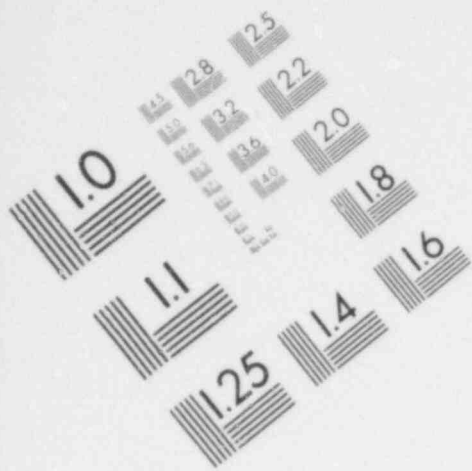
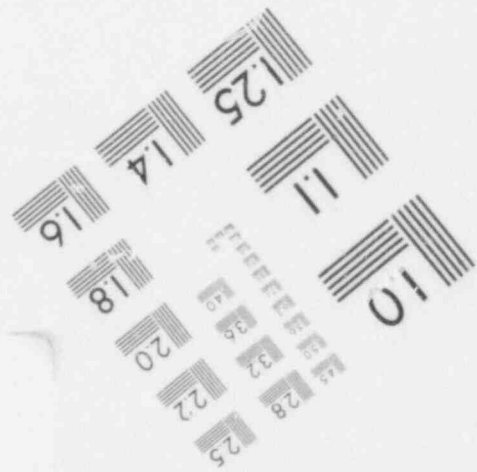
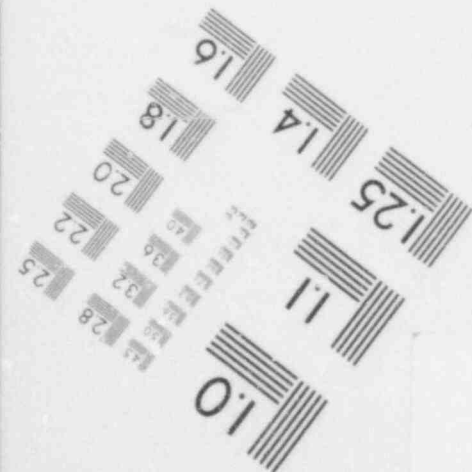
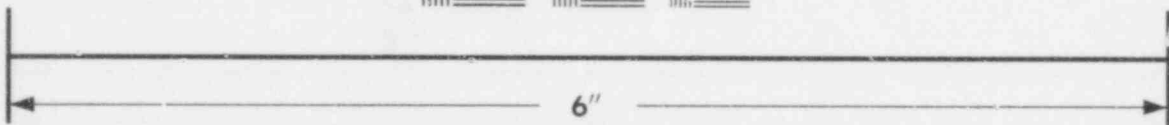


IMAGE EVALUATION  
TEST TARGET (MT-3)



613 001

## 4.6 FUNCTIONAL DESIGN OF REACTIVITY CONTROL SYSTEMS

### 4.6.1 INFORMATION FOR CONTROL ROD DRIVE SYSTEM (CRDS)

Figure 4.2-8 provides the layout of the CRDS. The CRDS is a magnetic-ally operated jack with no hydraulic system associated with its functioning. The control rod drive mechanism consists of four separate subassemblies.

1. The pressure vessel which includes the latch and rod travel housings.
2. The coil stack assembly which includes three operating coils: stationary gripper coil, movable gripper coil and lift coil.
3. The latch assembly which includes the guide tube, the stationary and the movable pole pieces and the stationary and movable gripper latches.
4. The drive rod assembly which includes the RCC coupling system and the drive rod.

### 4.6.2 EVALUATION OF THE CRDS

The CRDS has been analyzed in detail in a failure mode and effects analysis (Ref. 1). This study, and the analyses presented in Chapter 15.0, demonstrates that the CRDS performs its intended safety function, reactor trip, by putting the reactor in a subcritical condition when a safety system setting is approached, with any assumed credible failure of a single active component. The essential elements of the CRDS (those required to ensure reactor trip) are isolated from nonessential portions of the CRDS (the rod control system).

Despite the extremely low probability of a common mode failure impairing the ability of the reactor trip system to perform its safety function, analyses have been performed in accordance with the requirements of

WASH-1270. These analyses, documented in References [2 and 3], have demonstrated that acceptable safety criteria would not be exceeded even if the CRDS were rendered incapable of functioning during a reactor transient for which their function would normally be expected.

The design of the control rod drive mechanism is such that failure of the control rod drive mechanism cooling system will, in the worst case, result in an individual control rod trip or a full reactor trip.

#### 4.6.3 TESTING AND VERIFICATION OF THE CRDS

The CRDS is extensively tested prior to its operation. These tests may be subdivided into five categories: 1) prototype tests of components, 2) prototype CRDS tests, 3) production tests of components following manufacture and prior to installation and 4) onsite preoperational and initial startup tests. In addition, the CRDS is subject to periodic inservice tests. These tests, are conducted to verify the operability of the CRDS when called upon to function.

#### 4.6.4 INFORMATION FOR COMBINED PERFORMANCE OF REACTIVITY SYSTEMS

As is indicated in Chapter 15.0, the only postulated events which assume credit for reactivity control systems other than a reactor trip to render the plant subcritical are the steam line break, feedwater line break, and loss-of-coolant accident. The reactivity control systems for which credit is taken in these accidents are the reactor trip system and the safety injection system (SIS). Note that no credit is taken for the boration capabilities of the chemical and volume control system (CVCS) as a system in the analysis of transients presented in Chapter 15. The adverse boron dilution possibilities due to the operation of the CVCS are investigated in Chapter 15. Prior proper operation of the CVCS has been presumed as an initial condition to evaluate transients, and appropriate Technical Specifications have been prepared to ensure the correct operation or remedial action.

613 003

#### 4.6.5 EVALUATION OF COMBINED PERFORMANCE

The evaluations of the steam line break, feedwater line break, and the loss-of-coolant accident, which presume the combined actuation of the reactor trip system to the CRDS and the SIS, are presented in Chapter 15. Reactor trip signals and safety injection signals for these events are generated from functionally diverse sensors and actuate diverse means of reactivity control, i.e., control rod insertion and injection of soluble poison.

Nondiverse but redundant types of equipment are utilized only in the processing of the incoming sensor signals into appropriate logic, which initiates the protective action. In particular, note that protection from equipment failures is provided by redundant equipment and periodic testing. Effects of failures of this equipment have been extensively investigated as reported in Reference [4]. The failure mode and effects analysis described in this reference verifies that any single failure will not have a deleterious effect on the engineered safety features actuation system.

#### 4.6.6 REFERENCES

1. Shopsy, W. E., "Failure Mode and Effects Analysis (FMEA) of the Solid State Full Length Rod Control System," WCAP-8976, August 1977.
2. "Westinghouse Anticipated Transients Without Trip Analysis," WCAP-8330, August 1974.
3. Gangloff, W. C. and Loftus, W. D., "An Evaluation of Solid State Logic Reactor Protection in Anticipated Transients," WCAP-7706-L (Proprietary) and WCAP-7705 (Non-Proprietary), July 1971.
4. Eggleston, F. T., Rawlins, D. H. and Petrow, J. R., "Failure Mode and Effects Analysis (FMEA) of the Engineering Safeguard Features Actuation System," WCAP-8584 (Proprietary) and WCAP-8760 (Non-Proprietary), April 1976.